

Spatial and temporal patterns of liana infestation across a primary and selectively logged tropical forest in Sabah, Malaysia

Chris J. Chandler BSc (Hons), MRes

Thesis submitted to the University of Nottingham
for the degree of Doctor of Philosophy

June 2020

Acknowledgements

I am hugely grateful for all the support I have received over the course of my PhD. First and foremost, I would like to thank my supervisors, Geertje van der Heijden, Giles Foody and Doreen Boyd, who have guided me through this process and have consistently provided me with their knowledge, advice, support and encouragement.

I am also grateful to all the research assistants and staff at Danum Valley Field Centre and within the South East Asia Rainforest Research Partnership (SEARRP) for all their help and support in the field. Also to the many other researchers who I met at the field centre during fieldwork that have either assisted in some way or simply helped to provide an enjoyable experience during these times. Particular thanks go to Reuben Nilus for his support with research permits and visas. Also the many supporting agencies including; Sabah Biodiversity Center, Danum Valley Management Committee, Sabah Forestry Department and the Chief Minister's Department Office of Internal Affairs & Research for their logistical support.

My thanks to the National Environmental Research Centre (NERC) and the ENVISION Doctoral Training Programme (DTP) for awarding, and funding, my PhD studentship. Not only has this funding supported the research herein, but has greatly enhanced my personal academic progression. I would also like to recognise the support of many people within the School of Geography, the Ecological Reading Group, the Advanced UseRs Group and many other colleagues within, and outside, the University of Nottingham who have provided numerous helpful discussions and have contributed towards a fulfilling and enjoyable experience. Thanks also go to Twinings for ensuring a constant supply of tea.

Lastly, a special thank you must go to my parents for everything they have done for me; their continual encouragement, support and love in every aspect of this journey!

List of Figures

Figure 1.1 An example of a liana tangle on the forest floor (left) and a large liana climbing to the canopy (right).	9
Figure 1.2 Thesis structure	23
Figure 2.1 Location of the Danum Valley Conservation Area (DVCA) in Sabah, Malaysia, showing the position of the 50 ha plot and remotely sensed imagery..	30
Figure 2.2 Spectral reflectance of liana-free trees and trees highly infested with liana leaves using ground-based training data..	36
Figure 2.3 Relationship between predicted and ground reference liana canopy cover.	37
Figure 2.4 Predicted liana infestation showing a) the frequency of predicted values across the primary forest using b) a pixel-based classification (Output P), and c) an object-based classification (Output O).	38
Figure 2.5 Estimated uncertainty for both model outputs. Panel (a) shows the relationship between estimated uncertainty and predicted liana infestation, (b) and (c) show the scaled and unscaled frequency of uncertainty values across the study area, respectively.....	39
Figure 3.1 Location of the Danum Valley Conservation Area (DVCA) and 50 ha permanent plot in relation to the airborne remote sensing data, in Sabah, Borneo.....	47
Figure 3.2 Frequency distribution (scaled between 0 and 1) of predicted liana infestation within each forest type showing the values in gap (orange) and non-gap areas (blue).....	55
Figure 3.3 Relationship between liana infestation and a) the proportion of canopy gap area per 50x50 m pixel and b) gap size frequency distribution expressed as λ within each forest type.....	55
Figure 3.4 Differences in forest structure between the a) primary, b) active restoration and c) natural regeneration forests. Differences were assessed using d) median and e) standard deviation of canopy height with f) Cliff's <i>delta</i> , as an indication of effect size for comparisons of canopy height (red; panel d) and standard deviation of canopy height (blue; panel e) values across the three forest areas.	57
Figure 3.5 Relationship between liana infestation and aboveground carbon stocks (Mg C ha^{-1}) within each forest type.....	58
Figure 4.1 Location of the study area in Sabah, Malaysia, showing the extent of the air- and space-borne remotely sensed imagery across a primary and selectively logged tropical forest. .	67
Figure 4.2 Satellite-derived predicted mean greenness a) combined for all years (2016-2019) across forest types (black) and within the primary (blue) and selectively logged (orange) forests	

in response to airborne-derived liana infestation classes and b) for each year in response to airborne-derived liana infestation percent cover.....	71
Figure 4.3 Relationship between airborne- and satellite-derived liana infestation using a, d) Greenness Index, b, e) all Sentinel-2 bands and c, f) Greenness Index and all Sentinel-2 bands as input variables in the primary and selectively logged forests, respectively..	73
Figure 4.4 Predicted liana infestation in two classes, Low [$\leq 25\%$] (purple) and Severe [$\geq 75\%$] (yellow), derived from Sentinel-2 satellite imagery in 2016 and 2019..	74
Figure S 1.1 Relationship between liana canopy cover (%) and canopy height (m) for a) pixel- and b) object-based data.....	121
Figure S 1.2 Relationship between predicted and ground reference liana canopy cover for a) a pixel-based approach and b) an object-based approach on a continuous scale.....	122
Figure S 1.3 Relationship between predicted and ground reference liana canopy cover for 168 trees inside the 50 ha plot for the first 10 of the 100 iterations of the modelling process..	123
Figure S 2.1 An extract from predicted a) liana infestation and b) aboveground carbon stocks in Mg C ha ⁻¹	126
Figure S 2.2 Relationship between predicted and ground reference a) liana canopy cover and b) aboveground carbon stocks (Mg C ha ⁻¹).....	127
Figure S 2.3 Height – Diameter models and their relationship with 50 trees (D>140 cm) of known D and H as well as ‘Menara’ the World’s tallest tropical tree at 98.9m.....	129
Figure S 2.4 Relationship between three airborne laser scanning (ALS)-derived metrics: 1) height of median energy (HOME), 2) waveform distance (WFD) and 3) the top-of-canopy height derived from the canopy height model (CHM).	130
Figure S 2.5 Predicted aboveground carbon stocks (Mg C ha ⁻¹) within the three forest types..	132
Figure S 2.6 Relationship between canopy gap size and liana infestation.....	133
Figure S 2.7 The gap-size frequency distributions represented by the power-law exponent (λ) within the primary (blue), actively restored (orange) and naturally regenerating (green) forests using five different parameter combinations.....	135
Figure S 2.8 Relationship between liana infestation and aboveground carbon stocks (Mg C ha ⁻¹) within each forest type.....	136
Figure S 2.9 The effect of different gap definitions on the change in aboveground carbon stocks in relation to areas that were completely liana-infested or liana-free.....	139
Figure S 3.1 Airborne-derived standardised ($\mu = 0, \sigma = 1$) hyperspectral reflectance of liana-free trees and trees severely infested with liana leaves.....	140

Figure S 3.2 Satellite-derived predicted mean greenness in response to airborne-derived liana infestation classes for a) 2016, b) 2017, c) 2018 and d) 2019.....	147
Figure S 3.3 Predicted liana infestation across primary and selectively logged forests, showing the extent of the predictions in relation to the airborne lidar data (greyscaled).	148
Figure S 3.4 Difference in greenness between the primary and logged forest for imagery collected from 2016 to 2019.....	149
Figure S 3.5 Predicted greenness in response to liana infestation for each year (2016-2019) showing the distribution of data points..	151
Figure S 4.1 Neural network architecture showing the input layer with nine variables, one hidden layer with four neurons and one output layer corresponding to each class to be predicted.	153
Figure S 4.2 A sigmoid function (blue) and its derivative (orange).	154

List of Tables

Table 1.1 Summary of papers	24
Table 1.2 Author contributions to each chapter	25
Table 2.1 Data used for the training of neural network models and validation of predicted liana infestation maps.	33
Table 2.2 Accuracy assessment of pixel- and object-based model outputs.	38
Table 4.1 Pairwise comparison of linear regression slope coefficients (in Figure 4.2b)..	72
Table S 1.1 The first and second grid searches with meanshift parameters.	115
Table S 1.2 All parameter combinations ($n=64$) within the first grid search and corresponding Segmentation Evaluation Index (SEI).	116
Table S 1.3 All parameter combinations ($n=27$) within the second grid search and corresponding Segmentation Evaluation Index (SEI).	118
Table S 1.4 Neural network model parametrisation and assessment of best performing model.. ...	120
Table S 1.5 Pairwise comparison of linear regression slope coefficients in Figure S1.3.	124
Table S 2.1 Accuracy assessment for predicted liana infestation in three and two classes.	128
Table S 2.2 Results from a ten-fold cross validation to identify the best model for the prediction of aboveground carbon stocks (AGC).	131
Table S 2.3 Tukey Honest Significant Differences between predicted levels of aboveground carbon (AGC) in the primary (PR), actively restored (AR) and naturally regenerating (NR) forests..	132
Table S 2.4 Different parameter combinations used for the detection of canopy gaps and the resulting power-law exponent (λ -value) representing the gap size frequency distribution.	134
Table S 2.5 Summary table showing the coefficients (log scale) from multiple regressions using a generalised linear model for each forest type and for all forests combined.	137
Table S 3.1 Comparison of vegetation indices for the separation of low ($\leq 25\%$) and severe ($\geq 75\%$) liana infestation classes within the primary and logged forests and across the full landscape for each of the four satellite-derived images (2016-2019).	141
Table S 3.2 Accuracy assessment for predicted liana infestation in satellite-based multispectral imagery using three different sets of input variables: 1) all Sentinel 2-bands, 2) Greenness Index 3) all Sentinel 2-bands and Greenness Index within the primary and selectively logged forests..	145

Table S 3.3 Change in the percentage of pixels classified as having low ($\leq 25\%$) and severe ($\geq 75\%$) liana infestation from 2016 to 2019 in the primary forest, Danum Valley.	150
Table S 4.1 Example of neural network output conducting a hard or soft classification.....	156

List of abbreviations

AGB	Aboveground Biomass
AGBD	Aboveground Biomass Density
AGC	Aboveground Carbon
AIC	Akaike Information Criterion
ALS	Airborne Laser Scanning
AR	Active Restoration
ARF	Airborne Research Facility
AUC	Area Under the Curve
C	Carbon
CHM	Canopy Height Model
CO ₂	Carbon Dioxide
D	Diameter
DBH	Diameter at Breast Height
DEM	Digital Elevation Model
DR	Discrete Return
DSM	Digital Surface Model
DVCA	Danum Valley Conservation Area
EM	Endmember
EnMAP	Environmental Mapping and Analysis Program
EO-1	Earth Observing one
Eq.	Equation
FLAASH	Fast Line-of-sight Atmospheric Analysis of Hypercubes
FW	Full Waveform
GI	Greenness Index
GLAS	Geoscience Laser Altimeter System
GPS	Global Positioning System
GSFD	Gap Size-Frequency Distribution
H	Height
H:D	Height:Diameter [relationship]
HOME	Height of Median Energy
INFAPRO	Innoprise-Forest Absorbing carbon emission foundation rainforest rehabilitation PROject

ITC	Individual Tree Crown
LAI	Leaf Area Index
LiDAR	Light Detection and Ranging
Mg C ha ⁻¹	Mega grams of Carbon per Hectare
NDVI	Normalised Difference Vegetation Index
NERC	Natural Environmental Research Council
NIR	Near-Infrared
NPP	Net Primary Productivity
NR	Natural Regeneration
OTB	Orfeo ToolBox
P	Primary
Pg	Petagram (1 Pg = 10 ¹⁵ g)
RGB	Red Green Blue
RIL	Reduced-impact logging
RMSD	Root Mean Squared Deviation
RMSE	Root Mean Squared Error
SEI	Segmentation Evaluation Index
SFMA	Sabah Forest Management Area
SPCA	Standardised Principal Component Analysis
SWIR	Shortwave Infrared
TCH	Top-of-Canopy Height
UAV	Unoccupied Aerial Vehicle
USGS	United States Geological Survey
VIS	Visible [light]
VNIR	Visible-to-Near Infrared
WD	Wood Density
WFD	Waveform Distance
χ^2	Chi-squared

Table of Contents

Acknowledgements.....	ii
List of Figures	iii
List of Tables	vi
List of abbreviations.....	viii
Table of Contents.....	x
Abstract.....	1
Chapter 1: Introduction	5
1.1. Tropical forests in a changing world	5
1.2. Forest loss	6
1.3. Active restoration vs. natural regeneration.....	7
1.4. Lianas	8
1.4.1. Liana-induced effect on trees and carbon storage	9
1.4.2. Increasing liana biomass and abundance	11
1.4.3. Spatial distribution of liana infestation.....	11
1.4.4. Spatial distribution of liana infestation at multiple scales.....	13
1.5. Remote sensing of tropical forests	14
1.5.1. LiDAR	15
1.5.2. Optical imagery	16
1.5.3. Information extraction	17
1.5.4. Remote sensing of liana infestation.....	19
1.6. Study location: Sabah, Borneo.....	21
1.7. Thesis aims and objectives.....	22
1.7.1. Thesis aim.....	22
1.7.2. Thesis objectives	22
1.8. Thesis structure.....	23
1.9. Summary of papers	24
1.10. Author contributions.....	25
Chapter 2: Remote sensing liana infestation in an aseasonal tropical forest: addressing mismatch in spatial units of analyses	27
2.1. Abstract.....	27
2.2. Introduction	28
2.3. Methods.....	29
2.3.1. Study area	29
2.3.2. Occupied airborne data collection.....	30

2.3.3.	Liana canopy cover survey	31
2.3.4.	Tree crown segmentation	32
2.3.5.	Hyperspectral data extraction	32
2.3.6.	Neural network	33
2.3.7.	Neural network classification for mapping liana infestation	34
2.3.8.	Accuracy assessment of predicted outputs	35
2.4.	Results	36
2.4.1.	Spectral difference between liana-free and highly liana-infested trees	36
2.4.2.	Predicted and observed liana canopy cover	37
2.4.3.	Model outputs and uncertainty	38
2.5.	Discussion.....	39
2.6.	Conclusion.....	41
Chapter 3: Lianas are strongly associated with areas of low carbon stocks at the landscape scale		43
3.1.	Abstract.....	43
3.2.	Introduction	44
3.3.	Methods.....	47
3.3.1.	Study site.....	47
3.3.2.	Airborne hyperspectral and LiDAR data.....	48
3.3.3.	Landscape-level liana assessment	48
3.3.4.	Landscape-scale above ground carbon stocks assessment	50
3.3.5.	Relating liana infestation to above ground carbon stocks.....	53
3.4.	Results.....	54
3.5.	Discussion.....	58
3.6.	Conclusion.....	62
Chapter 4: Detection of spatial and temporal patterns of liana infestation using satellite-derived imagery		63
4.1.	Abstract.....	63
4.2.	Introduction	64
4.3.	Methods.....	66
4.3.1.	Study area	66
4.3.2.	Airborne-derived liana infestation assessment	67
4.3.3.	Satellite-derived liana infestation assessment	68
4.3.4.	Accuracy assessment	70
4.4.	Results.....	71
4.5.	Discussion.....	74

4.6.	Conclusion.....	78
Chapter 5: Conclusions	79
5.1.	Thesis synthesis.....	79
5.1.1.	Mapping liana infestation at a landscape-scale.....	79
5.1.2.	Association of liana infestation with aboveground carbon stocks	80
5.1.3.	Detection of liana infestation in satellite-imagery	80
5.2.	Research Implications	81
5.2.1.	Relating liana infestation to aboveground carbon stocks	81
5.2.2.	Increasing liana abundance in the Palaeotropics: implications for the tropical forest carbon cycle	82
5.2.3.	Consequences of detecting liana infestation in satellite imagery	84
5.2.4.	Limitations of remote sensing: implications and solutions for assessing liana infestation over multiple scales	84
5.3.	Summary	87
References.....	89
Appendix 1: Paper 1	115
Appendix 2: Paper 2	126
Appendix 3: Paper 3	140
Appendix 4	152

Abstract

Lianas are woody vines that use the physical support of other plants to reach the forest canopy. They are a dominant and widespread feature of tropical forests and play an important role in tree and carbon dynamics. By strongly affecting the growth and survival of their host trees, lianas can significantly limit the ability of tropical forests to store and sequester carbon. Any increases in liana dominance, as has been observed predominantly in the Neotropics, may therefore further reduce the carbon sink function of tropical forests. However, studies assessing liana ecology and the impact on carbon storage have typically been conducted 1) in the Neotropics and 2) using ground-based measurements. This may limit our understanding of liana ecology for two reasons. Firstly, patterns of liana infestation and the effects on carbon storage may not be synonymous with that of the Neotropics. Secondly, ground-based measurements are restricted in the total area they can feasibly sample and are potentially biased towards areas which are more accessible and therefore they may not be representative of the wider landscape.

Remote sensing may provide a solution to assess liana infestation over multiple spatial and temporal scales, based on differences in the spectral reflectance of trees and lianas. However, as liana chemistry and the spectral response converges with that of trees as precipitation increases, it remains unclear whether remote sensing technologies can assess the distribution of liana infestation, particularly in aseasonal forests. This thesis, therefore, aims to assess whether air- and satellite-based remote sensing can accurately detect liana infestation in order to 1) assess patterns of liana infestation at varying spatial and temporal scales and 2) quantify the relationship between liana infestation and aboveground carbon stocks at a landscape-level.

This research was carried out across a primary and selectively logged aseasonal tropical forest (~7500 ha) in Danum Valley, Sabah, Malaysia. In the selectively logged forest, certain areas have been actively restored, whilst the remaining area has been allowed to naturally regenerate over time. The research in this thesis uses a combination of airborne laser scanning (ALS) and hyperspectral data, satellite-based multispectral imagery and ground-based data sets of liana canopy cover and plot-level carbon estimates. Satellite-derived imagery were collected annually from 2016 to 2019. Imagery collected from 2016 also aligned with the end of an El-Niño induced drought which was used to test the detectability of liana infestation under different climatic conditions. Neural network classifications were used to predict patterns of liana infestation in space and time.

Chapter 2 aims to assess whether liana infestation can be detected using ALS and hyperspectral data in an aseasonal primary forest. Furthermore, this chapter focuses on overcoming discrepancies in spatial units in order to accurately map liana infestation at a landscape-level. Data

derived using remote sensing technologies are characterised by pixels, which are artificial units that do not correspond to natural features (*i.e.* tree crowns) on the ground. An object-based approach can be achieved by segmenting the hyperspectral data on a tree crown-level. Alternatively, liana infestation can be predicted at a pixel-level by spectrally unmixing pixels from a pure class, *i.e.* from either a completely-infested or liana-free tree crown. A pixel-based approach revealed a stronger relationship between predicted and observed liana infestation, most likely due to difficulties in the ability to accurately segment tree crowns in dense, closed canopy forests. This work therefore suggests that a pixel-based approach is more suitable for assessing liana infestation at a landscape-level.

Using the pixel-based approach devised in **Chapter 2**, liana infestation was predicted across the primary and selectively logged forest and related to estimates of aboveground carbon stocks (**Chapter 3**). Liana infestation was widespread across the landscape, however particularly dominant in canopy gaps. After accounting for variation in the size and frequency of canopy gaps, completely liana-infested areas were found to store, on average, $59.6 \pm 11 \text{ Mg C ha}^{-1}$ less than areas that were liana-free. However, the degree of carbon stock reduction relative to liana infestation varied within forest types, whereby completely liana-infested areas stored 14.8 ± 6.4 , 32.8 ± 16.2 and $85.1 \pm 12.8 \text{ Mg C ha}^{-1}$ less compared to liana-free areas in the actively restored, naturally regenerating and primary forests, respectively. This implies that liana infestation is a strong predictor of AGC, and that this relationship can be observed across forest types and after accounting for variability in carbon stocks across the landscape.

In **Chapter 4**, satellite-based imagery were used to predict liana infestation across the landscape and over time using a neural network classification trained with the airborne-derived liana infestation output. This study is the first to show that liana infestation can be accurately detected across a closed-canopy forest using satellite-based multispectral imagery. Furthermore, evidence of the detectability of lianas across forest types and under different climatic conditions, suggests that these findings should apply to other tropical forest locations. Assessing liana infestation in imagery over time showed an increase in the percentage of severely ($\geq 75\%$) liana-infested pixels from $12.9\% \pm 0.63$ in 2016 to $17.3\% \pm 2$ in 2019. Liana infestation was also dynamic, with $2.66\% \pm 0.76$ of pixels changing from low to severe and $1.22\% \pm 0.2$ changing from severe to low liana infestation over the same three-year time period. These results show for the first time a potential forest-wide increase in liana infestation in a Palaeotropical forest and therefore suggests that an increase in liana dominance may not be confined to the Neotropics.

The findings of this thesis suggest that 1) remote sensing approaches are effective at accurately detecting liana infestation and 2) lianas exert a strong control on carbon storage, in an aseasonal forest. This thesis also shows that liana infestation can be detected across forest types, under

different climatic conditions and over time, demonstrating that remote sensing techniques are a useful tool to assess patterns of liana infestation across tropical forests. This is likely to provide unique insights into the mechanisms that drive their distribution at multiple spatial and temporal scales. Furthermore, this will assist in predicting where liana infestation is likely to change and what global consequences this may have for carbon sequestration and storage.

Chapter 1: Introduction

1.1. Tropical forests in a changing world

Tropical forests are highly productive (Phillips *et al.* 1998; Malhi *et al.* 2004; Beer *et al.* 2010), biologically rich (Dirzo & Raven 2003; Gibson *et al.* 2011) and carbon dense (Luyssaert *et al.* 2008; Keith, Mackey & Lindenmayer 2009; Pan *et al.* 2011; Grace, Mitchard & Gloor 2014; McAlpine *et al.* 2018), thus their protection is a fundamental aim of international strategies for conserving biodiversity and ecosystem services (Convention on Biological Diversity 2015). Tropical forests play an important role in the delivery of many important ecosystem services including biodiversity richness, water purification, climate regulation, disease control and carbon storage (Myers *et al.* 2000; Ter Steege *et al.* 2003; Foley *et al.* 2005; Bradshaw, Sodhi & Brook 2009; Neary, Ice & Jackson 2009; Giam 2017; Brock *et al.* 2019; Hubau *et al.* 2020). It is estimated that tropical forests store around 200-300 Petagrams (Pg) ($1 \text{ Pg} = 10^{15} \text{ g}$) of carbon (C) (Pan *et al.* 2011; Saatchi *et al.* 2011; Baccini *et al.* 2012; Avitabile *et al.* 2016) corresponding to around 118, 65 and 47 Pg C in tropical America, Africa and Asia, respectively (Baccini *et al.* 2012). Tropical forests are also very dynamic, with average levels of net primary productivity (NPP) estimated at around 17.8 Pg C per year (Field *et al.* 1998; see also, Malhi *et al.* 2009).

However, tropical forests are undergoing significant modifications to their structure, diversity, function and extent (Lewis *et al.* 2004a; Phillips *et al.* 2008; Hansen *et al.* 2013; Lewis, Edwards & Galbraith 2015; Cusack *et al.* 2016; Baccini *et al.* 2017; Qie *et al.* 2017; Esquivel-Muelbert *et al.* 2019; McDowell *et al.* 2020). Human-driven land-use change is one of the greatest threats to terrestrial biodiversity and ecosystem functioning globally, and nowhere is this more ubiquitous than across the tropics (Pimm & Raven 2000; Bunker *et al.* 2005; Lewis, Edwards & Galbraith 2015; Barlow *et al.* 2016; Venter *et al.* 2016; Cushman *et al.* 2017). Tropical forests are particularly vulnerable due to the high availability of suitable land for conversion combined with poor policies and weak governance (Laurance 1999; Geist & Lambin 2002; Lawson *et al.* 2014). The rapid conversion of tropical forests for agriculture, timber production and other natural resources has significantly increased the extent of human-modified landscapes (Tilman *et al.* 2001; Achard *et al.* 2002; Davis *et al.* 2020).

In addition, large areas of intact tropical forest, free from significant anthropogenic influence, are also showing signs of impact from broad environmental changes as a direct or indirect response to increased CO₂ concentrations. These include, higher temperatures, increased frequency of droughts and changes in precipitation (Malhi & Grace 2000; Malhi & Phillips 2004; Malhi & Wright 2004; Phillips *et al.* 2008; Gloor *et al.* 2009; Lewis *et al.* 2009; Phillips *et al.* 2009; Sullivan *et al.* 2020).

This is of particular concern given the unique and important role intact forests play in the global carbon cycle (Watson *et al.* 2018; Maxwell *et al.* 2019). Long-term monitoring of field-plots has revealed an increase in above-ground biomass (Phillips *et al.* 1998; Baker *et al.* 2004a; Chave *et al.* 2008a; Phillips *et al.* 2008; Lewis *et al.* 2009; Malhi 2010) and an increase in tree turnover rates (Phillips & Gentry 1994; Lewis *et al.* 2004a; Phillips *et al.* 2004), as assessed by tree recruitment and mortality. Such changes to forest growth and productivity may have profound implications on species diversity and tree community composition (Feeley *et al.* 2011).

1.2. Forest loss

Deforestation occurs globally and results in the complete removal of forest cover. As such, forest loss can be easily detected and monitored through earth-observing satellites (Asner *et al.* 2005; Peres, Barlow & Laurance 2006). Using space-borne imagery it has been estimated that around 1.1 million km² of tropical forest were lost from 2000 to 2012 (Hansen *et al.* 2013) corresponding to an annual gross deforestation rate of ~0.09 million km² yr⁻¹ (Hansen *et al.* 2013; Achard *et al.* 2014). Subsequent global carbon emissions from tropical deforestation are estimated within the range of 0.8 to 2.8 Pg C yr⁻¹ (Pan *et al.* 2011; Harris *et al.* 2012; Rosa *et al.* 2016). However, the proportion of tropical forest disturbance may be underestimated as less intensive logging (*i.e.* selective logging) may be difficult to distinguish with satellite-borne imagery (Asner *et al.* 2004; Peres, Barlow & Laurance 2006).

Selective logging is a common practice in tropical forests where only large trees (typically >40-60 cm DBH), often from a particular tree species, are removed, whilst disturbance to the rest of the forest is minimised (Asner *et al.* 2009a). Subsequently, studies have shown that selectively logged forests can retain similar levels of biodiversity and carbon stocks as unlogged forests (Cannon, Peart & Leighton 1998; Berry *et al.* 2010; Putz *et al.* 2012; Edwards *et al.* 2014). Tropical forests may be able to maintain high species diversity following selective logging due to the positive effects of disturbance. Species diversity has shown to be higher when disturbances are intermediate on the scales of frequency and intensity – similar to the ‘intermediate disturbance’ hypothesis (Connell 1978) - owing to an increase in shade intolerant species (Bongers *et al.* 2009).

Selective logging in tropical forests is spatially diffuse with around 20.3% of humid tropical forests allocated to selective timber harvests (Asner *et al.* 2009b). However, logging densities are known to vary considerably with the volume logged typically ranging between 5 and 180 m³ ha⁻¹ (Pinard & Putz 1996; Bertault & Sist 1997; Pereira Jr *et al.* 2002; Feldpausch *et al.* 2005; Medjibe, Putz

& Romero 2013; Bicknell *et al.* 2014; Pfeifer *et al.* 2015; Putz *et al.* 2019). Sist *et al.* (1998) reported average logging intensities of 86.9 m³ ha⁻¹ (nine trees ha⁻¹) in East Kalimantan (Indonesia), although volumes ranged between 9-247 m³ ha⁻¹ (1-17 trees ha⁻¹) (Sist *et al.* 1998). Subsequently, total carbon emissions from selective logging vary, however, are suggested to average around 35% of emissions resulting from deforestation (Maxwell *et al.* 2019). Additional estimates have suggested selective logging to be equivalent to around 12-25% of carbon emissions from deforestation (Huang & Asner 2010; Pearson, Brown & Casarim 2014; Pearson *et al.* 2017), with emissions ranging from 6% to 68%, depending on logging densities (Pearson, Brown & Casarim 2014) and practices (Pinard & Putz 1996; Putz *et al.* 2008a; Laurance & Edwards 2014; Martin *et al.* 2015).

Improved logging practices have also been shown to minimize forest damage and reduce carbon emissions, while maintaining timber production (Ellis *et al.* 2019). Reduced-impact logging (RIL) is one such technique which may help curtail the negative effects of logging (Putz *et al.* 2008a; Bicknell *et al.* 2014). While the techniques used may vary considerably, RIL typically includes: liana cutting prior to logging, maximum slope gradients on which to operate, felling trees in a direction that minimises damage to surrounding trees and effective planning and construction of roads and skid trails to minimize ground disturbance (Putz *et al.* 2008a). While the major source of carbon losses results from the felling of large trees, forests that employed RIL techniques were capable of retaining higher levels of biodiversity and carbon stocks (Pinard & Putz 1996; Cannon, Peart & Leighton 1998; Putz *et al.* 2008b; Putz *et al.* 2012; Edwards *et al.* 2014). On the other hand, forests subjected to conventional logging can lose much silvicultural value due to the impacts on the quality of soil (Pinard, Putz & Tay 2000; Asner, Keller & Silva 2004) and future crop trees (Pinard & Putz 1996; Bertault & Sist 1997; West, Vidal & Putz 2014). In such cases, active restoration practices post logging have been employed to help recover carbon stocks and ecosystem functioning.

1.3. Active restoration vs. natural regeneration

Ecological restoration can be a critical strategy for reversing biodiversity and carbon losses following logging and degradation of tropical forests (Lamb, Erskine & Parrotta 2005; Shimamoto *et al.* 2018). Restoration can be achieved through either active (more intensive) or passive (less intensive) interventions to recover degraded forests (Chazdon & Guariguata 2016). Passive restoration simply involves protecting the forest from future degradation and allowing it to recover naturally through secondary succession. Active restoration may include the planting of trees, fertilisation or/and the removal of lianas in order to restore heavily degraded areas (Shono, Cadaweng & Durst 2007; Holl & Aide 2011; Chazdon & Guariguata 2016). While the role of active

restoration during recovery can significantly increase canopy cover and aboveground carbon storage (Lamb, Erskine & Parrotta 2005; Osuri *et al.* 2019), the restoration of biodiversity and vegetation structure has shown to be more successful in naturally regenerating systems (Berry *et al.* 2010; Crouzeilles *et al.* 2017; Shimamoto *et al.* 2018). However, naturally regenerating land is prone to arrested succession due to poor soil conditions (Chazdon 2014), increased fire frequencies (Cochrane 2003) and increased liana infestation (Putz 1991; Gerwing 2006; Schnitzer & Carson 2010), which all hamper tree growth and carbon storage potential (Cochrane & Schulze 1999; van der Heijden, Powers & Schnitzer 2015). In such cases, active restoration, such as enrichment planting, has shown to be a promising method to increase vegetation cover and carbon stocks (Wu *et al.* 2020). Furthermore, liana cutting has been employed as a method to increase carbon storage and uptake in tropical forests (Pérez-Salicrup 2001; Marshall *et al.* 2017; Mangueira, D. Holl & Rodrigues 2019). For example, a liana removal experiment conducted in Panama found that lianas significantly affected tree growth and reduced forest-level aboveground carbon uptake by 2.43 Mg C ha⁻¹ yr⁻¹ (van der Heijden, Powers & Schnitzer 2015). Therefore, restoration efforts may provide a useful strategy for reversing biodiversity loss and enhancing carbon stocks in degraded tropical forests (Osuri *et al.* 2019).

1.4. Lianas

Lianas (woody vines) are a dominant plant functional type in tropical forests, contributing up to 44% of the woody species (Appanah, Gentry & LaFrankie 1993; Pérez-Salicrup, Sork & Putz 2001; Schnitzer & Bongers 2002) and 40% of the woody stems (Gerwing & Farias 2000; Chave, Riéra & Dubois 2001). Lianas share a common growth strategy; exploiting trees for physical support in order to reach the canopy for light (Putz 1984; Schnitzer 2005) (Figure 1.1). They differ from other parasites (such as epiphytes and hemiepiphytes) by remaining rooted in the ground throughout their life cycle (Schnitzer & Bongers 2002). By using the support of host trees to reach the canopy, lianas can focus energy into leaf production (Gerwing & Farias 2000; van der Heijden *et al.* 2013) and therefore can produce a disproportionately large canopy in comparison to the size of their stem (Cox *et al.* 2019). For example, it has been shown that lianas commonly constitute less than 5% of tropical forest biomass (DeWalt & Chave 2004), but up to 40% of leaf productivity (Hegarty & Cabelle 1991).



Figure 1.1 An example of a liana tangle on the forest floor (left) and a large liana climbing to the canopy (right).

1.4.1. Liana-induced effect on trees and carbon storage

Liana infestation within tree crowns can have a strong negative effect on tree growth (Grauel & Putz 2004; van der Heijden & Phillips 2009; van der Heijden, Powers & Schnitzer 2015; Estrada-Villegas *et al.* 2020), reproduction (Nabe-Nielsen, Kollmann & Peña-Claros 2009; García León *et al.* 2018) and survival (Putz 1984; Phillips *et al.* 2005; Ingwell *et al.* 2010; Martínez-Izquierdo *et al.* 2016). Additionally, lianas within canopy gaps have been shown to suppress the regeneration of trees (Schnitzer & Carson 2010; Schnitzer *et al.* 2014b) and even halt ecological succession following disturbance (Schnitzer, Dalling & Carson 2000; Tymen *et al.* 2016). The competitive effect of lianas can be experienced both above- and below-ground (Dillenburg *et al.* 1993; Pérez-Salicrup & Barker 2000; Andrade *et al.* 2005; Schnitzer, Kuzee & Bongers 2005; Rodríguez-Ronderos *et al.* 2016). Once lianas reach the canopy, they can produce a layer of foliage above the tree crown, thereby reducing the amount of light available to their host tree (Clark & Clark 1990; Avalos *et al.* 2007; Rodríguez-Ronderos *et al.* 2016). For example, van der Heijden and Phillips (2009) found that lianas, mainly by competing above-ground, were responsible for a 10% reduction in relative annual tree aboveground biomass growth. Meanwhile, below-ground, lianas reduce tree growth via competition for shared resources such as nutrients and water (Pérez-Salicrup & Barker 2000).

Lianas and trees differ in their response to water availability, such as during drought conditions, with lianas showing unimpeded growth whilst trees are temporarily stumped (Schnitzer 2005; Cai, Schnitzer & Bongers 2009; Doughty *et al.* 2015; O'Brien *et al.* 2019; Schnitzer & van der Heijden 2019; Marimon *et al.* 2020). The ability of lianas to access and use water more efficiently than co-occurring trees (Chen *et al.* 2015; Maréchaux *et al.* 2017; Smith-Martin *et al.* 2019; van der Sande *et al.* 2019) during dry periods gives them a seasonal growth advantage (Álvarez-Cansino *et al.* 2015; Schnitzer & van der Heijden 2019). Therefore, it is expected that liana abundance may be greater in dry forests due to a greater availability of light (DeWalt *et al.* 2010) and higher evapotranspirative demand (Schnitzer 2005) resulting from a shorter forest stature and lower leaf area index (Kalácska, Calvo-Alvarado & Sánchez-Azofeifa 2005). However, despite the great abundance of lianas in dry forests, a stronger negative effect of lianas on carbon stocks has been observed in moist tropical forests (Durán *et al.* 2015) and in wet seasons (van der Heijden, Powers & Schnitzer 2019). This may be attributed to the ability of trees and lianas to more effectively partition resources in dry forests. Whereas, in wet tropical forests, and during wet seasons, where water availability is not as limited, competition for light may be more intense (Schnitzer & Bongers 2011; van der Heijden *et al.* 2013; Durán *et al.* 2015; van der Heijden, Powers & Schnitzer 2019).

As liana-tree competition is much stronger than tree-tree competition (Tobin *et al.* 2012), lianas can have a significant impact on the ability of tropical forests to store and sequester carbon (DeWalt & Chave 2004; van der Heijden & Phillips 2009; Ingwell *et al.* 2010; Durán & Gianoli 2013; Schnitzer *et al.* 2014b; van der Heijden, Powers & Schnitzer 2015; Tymen *et al.* 2016). Several studies have highlighted the negative relationship between liana abundance and aboveground biomass (AGB) and carbon (AGC) stocks in Neotropical forests (van der Heijden *et al.* 2013; Schnitzer *et al.* 2014b; van der Heijden, Powers & Schnitzer 2015; Ledo *et al.* 2016; Tymen *et al.* 2016). For example, using a large-scale liana removal experiment in Panama, van der Heijden *et al.* (2015) demonstrated that lianas significantly reduced net AGC uptake, by as much as 76% per year, mostly due to suppressed tree growth. Durán & Gianoli (2013) revealed a negative association between liana abundance and carbon stocks of large trees using a large pantropical dataset. Results revealed that areas with high liana abundance stored on average 146 Mg C ha⁻¹ less than areas with low liana abundance. Other studies have also revealed a negative relationship between liana abundance and AGB (Laurance *et al.* 2001; Laurance *et al.* 2014). For example, Laurance *et al.* (2014) showed that an increase in liana abundance was associated with a reduction of ~60 Mg ha⁻¹ in aboveground tree biomass. Further concern for the impact lianas on tropical forest carbon dynamics has also be intensified by evidence of increasing liana dominance (Schnitzer & Bongers 2011).

1.4.2. Increasing liana biomass and abundance

Lianas may be favoured competitively by: ongoing disturbance (Lewis, Edwards & Galbraith 2015), an increase in atmospheric CO₂ concentrations (Condon, Sasek & Strain 1992; Granados & Körner 2002; Zotz, Cueni & Körner 2006), an increase in forest turnover and dynamism (Phillips & Gentry 1994; Phillips *et al.* 1994; Bongers *et al.* 2009), and longer and more intense drought periods (Cai, Schnitzer & Bongers 2009; DeWalt *et al.* 2010; Schnitzer & van der Heijden 2019). There is now compelling evidence that liana biomass and abundance are increasing in many seasonal forests in the Neotropics (Phillips *et al.* 2002; Benítez-Malvido & Martínez-Ramos 2003; Wright *et al.* 2004; Wright & Calderón 2006; Chave *et al.* 2008b; Foster, Townsend & Zganjar 2008; Ingwell *et al.* 2010; Laurance *et al.* 2014). Phillips *et al.* (2002) reported an increase in the abundance of large lianas (>10 cm diameter) that nearly doubled over the 20-year period. Similarly, in an old-growth forest in French Guiana, Chave *et al.* (2008b) found that liana abundance increased by 1.8%, and tree abundance decreased by 4.8% over a 10-year period. However, there is little evidence to suggest that the same is true of aseasonal forests (although see, Schnitzer & Bongers 2011). Furthermore, evidence suggests that the pattern of increasing liana dominance may be restricted to old-growth forests (Yorke *et al.* 2013) and may also not be a pantropical phenomenon. For example, studies have reported declining liana abundance in African forests (Caballé & Martin 2001; Bongers *et al.* 2020), and similar levels of liana infestation in tree canopies over time in Malaysian forests (Wright *et al.* 2015). Nevertheless, evidence that lianas may be favoured by future climate change scenarios has driven an expansion of studies in recent years (Marshall *et al.* 2020) which have focused on understanding the mechanisms that drive spatial patterns of liana infestation and the impact on tropical forest functioning and carbon storage.

1.4.3. Spatial distribution of liana infestation

Lianas respond strongly to light availability and disturbance (Schnitzer, Dalling & Carson 2000; Laurance *et al.* 2001; Schnitzer & Bongers 2011). They may therefore be more abundant in logged forests (Martin, Sherman & Fahey 2004; Magrach *et al.* 2016) and proliferate rapidly in treefall gaps and at forest edges (Laurance *et al.* 2001; Schnitzer & Carson 2001; Schnitzer & Carson 2010; Schnitzer *et al.* 2014b; Campbell *et al.* 2018; Rocha *et al.* 2020) by forming highly clumped distributions by clonal stem recruitment (Schnitzer *et al.* 2012; Yorke *et al.* 2013; Ledo & Schnitzer 2014).

Studies have found a decrease in liana stem density from gaps to intact forests (Putz 1984) and with increasing stature (Gerwing & Farias 2000) related to lower light availability (DeWalt,

Schnitzer & Denslow 2000). As a result, lianas may become more dependent on tree fall gaps for establishment (Appanah, Gentry & LaFrankie 1993; Schnitzer, Dalling & Carson 2000; Schnitzer & Carson 2001). Liana proliferation in canopy gaps may also be associated with their ability to survive tree falls as well as the speed to which they can recruit via lateral growth along the forest floor from the intact understory (Schnitzer, Dalling & Carson 2000; Schnitzer, Parren & Bongers 2004; Yorke *et al.* 2013; Umaña, Manzané-Pinzón & Comita 2020). Lianas dragged down in gaps during tree fall can quickly root and colonise the gap area taking advantage of the high light conditions, disturbed soil and reduced competition (Kennard 1998; Schnitzer & Bongers 2002; Schnitzer *et al.* 2014a). Indeed in larger canopy gaps, formed by multiple tree falls, liana abundance is often greater (Thompson *et al.* 1998; Schnitzer, Dalling & Carson 2000; Gerwing & Uhl 2002; Londré & Schnitzer 2006), potentially due to the fact that light availability typically increases with increasing gap size (Babweteera, Plumptre & Obua 2000). Therefore, in small gaps, light levels may not be sufficient to promote the establishment and high growth rate of lianas (Denslow, Ellison & Sanford 1998).

While lianas often show highly-aggregated distributions driven by treefall gaps (Schnitzer & Carson 2001; Schnitzer *et al.* 2012), they also often infest tree crowns in search of light (Ingwell *et al.* 2010). In some Neotropical forests lianas are more frequently observed within tall, well-lit trees (Malizia & Grau 2006; van der Heijden, Healey & Phillips 2008; Sfair *et al.* 2016), suggesting in some habitats lianas require physical support in order to escape lower light conditions on the forest floor (Meyer *et al.* 2019). However, while the distribution of host trees is a key factor in controlling liana growth in the forest understory (Putz 1984), host trees show differential susceptibility and responses to liana infestation. For example, it has been shown that trees within the Dipterocarpaceae have a lower susceptibility to lianas (Campbell & Newbery 1993; Wright *et al.* 2015). Some species of dipterocarps (*Parashorea tomentella* and *P. malaanonan*) are known to have rapid growth rates which approach that of pioneer species (Ghazoul 2016). Other characteristics of dipterocarps include high branch-free bole heights, branch shedding, via monopodial growth, and smooth bark, which can all contribute towards a reduced susceptibility to liana infestation (Campbell & Newbery 1993; van der Heijden, Healey & Phillips 2008; Wright *et al.* 2015). Indeed the ability of trees to shed and/or tolerate lianas are important components in explaining variation in liana prevalence among tree species (Visser *et al.* 2018a). In addition, where the forest canopy is high and small-diameter branches (*i.e.* trellises) are scarce, lianas have been found to enter their host trees horizontally from neighbouring trees (Balfour & Bond 1993). However, large, emergent dipterocarp trees typically have more separated crowns which can reduce infestation by lianas from nearby trees (Campbell & Newbery 1993; Wright *et al.* 2015).

Trees may also differ in their response to liana infestation, but there is some debate. On one hand, it has been suggested that lianas have a stronger negative impact on slow-growing, shade-tolerant tree species with high wood density, whilst not affecting or even indirectly promoting pioneer species (Campbell & Newbery 1993; Schnitzer, Dalling & Carson 2000; Laurance *et al.* 2001; van der Heijden, Healey & Phillips 2008). On the other hand, liana infestation may be more harmful for fast-growing tree species (Visser *et al.* 2018b). Visser *et al.* (2018b) proposed that this relationship is likely due to survivorship bias such that the observable sample is biased towards those trees that survived and are liana-free. If host trees were to have differential responses to liana infestation, then this could lead to changes in tree community composition with potential impacts on the forest-wide ability to store and sequester carbon (van der Heijden, Powers & Schnitzer 2015; di Porcia E Brugnara *et al.* 2019; Estrada-Villegas *et al.* 2020).

1.4.4. Spatial distribution of liana infestation at multiple scales

The biomass and abundance of lianas have also been shown to relate with multiple abiotic variables which vary at different scales. For example, liana abundance has been shown to increase with decreasing precipitation and increasing seasonality at global- (Schnitzer 2005; DeWalt *et al.* 2010) and regional-scales (Parolari *et al.* 2020) but not across the Neotropics (van der Heijden & Phillips 2008). Similarly, while some studies have shown a relationship between liana abundance and soil fertility on a local scale (Proctor *et al.* 1983; Putz & Chai 1987; DeWalt *et al.* 2006), there has been no compelling evidence for this across the Neotropics (DeWalt & Chave 2004; van der Heijden & Phillips 2008).

Differences in the relationship between forest variables and liana abundance may be associated with a number of factors. Firstly, the numerous complex and often confounded variables that operate at multiple scales. For example, liana abundance may covary with soil fertility in areas of greater disturbance (Denslow, Ellison & Sanford 1998; Yee *et al.* 2019) or higher elevation (de Castilho *et al.* 2006; John *et al.* 2007; Körner 2007; Unger, Homeier & Leuschner 2012). Therefore, studies that are conducted at a local- versus a continental-scale may capture less variation relating to disturbance or elevation which could make it easier to assess the direct effect of soil fertility on liana abundance (*cf.* Sullivan *et al.* 2017).

Similarly, studies which attempt to assess the relationship between liana abundance and carbon stocks may be challenged by high variability in carbon stocks driven by multiple scale-dependant variables. For example, an increase in AGB has been related to an increase in soil fertility

(Slik *et al.* 2010; Quesada *et al.* 2012), decrease in temperature (Durán *et al.* 2015; Sullivan *et al.* 2020) an increase in elevation (de Castilho *et al.* 2006), topography (Ferry *et al.* 2010; Taylor *et al.* 2015; Muscarella *et al.* 2020), geologic substrate (Asner *et al.* 2010) and species composition (Baker *et al.* 2004b). Thus, studies at continental- or global-scales which do not account for variables that drive patterns in AGC stocks may make it difficult to disentangle the direct effect of liana abundance on carbon stocks.

Secondly, differences in the relationships between forest variables and liana abundance may be related to the size of plots, which capture different levels of spatial heterogeneity (DeWalt *et al.* 2010). For example, assessing the level of aboveground biomass density (AGBD) using small (0.1 ha) plots may result in large AGBD variability depending on whether large diameter trees, which explain much of the variation in AGB (Slik *et al.* 2013; Bradford & Murphy 2019), are present or absent within the plot. However, AGBD variability is likely to decrease with an increasing plot area (Zolkos, Goetz & Dubayah 2013; Rejou-Mechain *et al.* 2014) and may provide a more representative 1) estimation of forest-wide AGB and 2) relationship with liana abundance. Durán & Gianoli (2013) revealed a negative association between liana abundance and carbon stocks of large trees using a large pantropical dataset. However this study was confined to small (0.1 ha) forest plots which makes it difficult to disentangle the multitude of contributing processes at varying spatial scales. While some ground-based studies may not be limited in their geographical extent (*e.g.* Durán & Gianoli 2013), they are limited 1) to areas which are more easily accessible and 2) by the total area they can feasibly sample. As a result, ground-based studies may be biased (Powers *et al.* 2011) and are unlikely to be able to capture sufficient variation to fully assess the forest-wide relationship between liana abundance and carbon stocks. Assessing the distribution of lianas over large areas may provide unique insights into the mechanisms that drive their spatial patterns and the impact on carbon storage.

1.5. Remote sensing of tropical forests

Given the extent and complexity of tropical forests, remote sensing can provide a synoptic view and cover a much larger area than possible using field-based methods alone (Foody 2003). A variety of forest metrics have been obtained using remote sensing data, including canopy height (Lefsky *et al.* 2005; Lefsky 2010; Simard *et al.* 2011; Mielcarek, Stereńczak & Khosravipour 2018), forest structure (Drake *et al.* 2002; Palace *et al.* 2008; Bastin *et al.* 2018), tree density (Foody & Curran 1994), species composition/richness (Foody & Cutler 2006; Higgins *et al.* 2014) and functional diversity (Jetz *et al.* 2016; Durán *et al.* 2019). While remote sensing instruments cannot directly

measure AGB, properties of the forest canopy, such as radiance or canopy height, can be used as predictors of forest AGB. For biomass estimation, studies have utilised optical, radar and light detection and ranging (LiDAR) data acquired from space- (Foody *et al.* 2001; Castro, Sanchez-Azofeifa & Rivard 2003; Foody, Boyd & Cutler 2003; Lefsky *et al.* 2005; Cutler *et al.* 2012; Avtar *et al.* 2013; Bastin *et al.* 2014; Hu *et al.* 2016; Pfeifer *et al.* 2016), air- (Drake *et al.* 2003; Clark *et al.* 2011; Hernández-Stefanoni *et al.* 2014; Laurin *et al.* 2014b) and terrestrial-based sensors (Palace *et al.* 2016; Gonzalez de Tanago *et al.* 2018). Each product presents advantages and disadvantages with respect to spatial extent, sensitivity to clouds and varying spatial, spectral and temporal resolutions (Lechner, Foody & Boyd 2020). Thus, fusion of two or more of each sensor have often been employed (Reiche *et al.* 2016) to produce detailed maps at regional (Saatchi *et al.* 2007; Asner *et al.* 2010; Asner *et al.* 2018; Bazezew, Hussin & Kloosterman 2018; Urbazaev *et al.* 2018) and global scales (Saatchi *et al.* 2011; Baccini *et al.* 2012; Hansen *et al.* 2013; Avitabile *et al.* 2016; Hu *et al.* 2016). Previous studies have shown that LiDAR data improves estimates of vegetation structure in comparison to optical remote sensed imagery which tend to saturate and therefore produce unreliable estimates of biomass and carbon stocks (Lu *et al.* 2012).

1.5.1. LiDAR

LiDAR is an active sensor (*i.e.* it transmits and receives its own signal). The signal emitted is capable of penetrating clouds and small openings in forest canopies to finely obtain tree dimensions and canopy structural properties at multiple scales. LiDAR data derived from space- or air-borne sensors will differ in the width of the laser beam (large or small footprint). Large footprint satellite LiDAR data (~65m), such as that provided by the Geoscience Laser Altimeter System (GLAS) (Abshire *et al.* 2005), have the potential to assess vegetation at local (Popescu *et al.* 2011), regional (Lefsky *et al.* 2005; Rosette, North & Suarez 2008) and global scales (*cf.* Saatchi *et al.* 2011, Baccini *et al.* 2012). Airborne LiDAR with a small footprint, also referred to as airborne laser scanning (ALS), can provide detailed measurements of vegetation structure and elevation, particularly useful in tropical forests with dense closed canopies and steeply sloping terrain. Forest structural characteristics derived from airborne LiDAR with larger (10-25m) footprints have also shown to be well correlated with field-derived metrics (Drake *et al.* 2002).

Most commercial airborne LiDAR systems deliver discrete return (DR) point data. In this system, each point is associated with high intensities in the back-scattered laser pulse and record multiple returns per laser pulse (1-5 returns). However, DR systems can only detect the surfaces which are separated sufficiently in space (Cao *et al.* 2016). In between each detected return there

are gaps in which no other surfaces can be detected. More recent developments in LiDAR technology can resolve this issue by using the full waveform (FW) which records the entire backscattered laser pulse. This can improve the detection of weak return echoes and also allows other metrics to be extracted from the waveform height and energy (Cao *et al.* 2014; Crespo-Peremarch & Ruiz 2020). The use of FW LiDAR and waveform metrics have been shown to provide more detailed information on vegetation structure (Alexander *et al.* 2015) and more accurate biomass estimates (Drake *et al.* 2002; Nie *et al.* 2017; Shen *et al.* 2018; Luo *et al.* 2019) in comparison to traditional DR metrics. However, estimates of canopy height, elevation or the spatial arrangement of canopy gaps may not be significantly improved as the additional points from FW LiDAR mainly contribute to the internal structure of the forest (Chauve *et al.* 2009).

The size and spatial arrangement of canopy gaps can describe the disturbance regime of a forest and may be particularly useful for understanding forest structural characteristics, spatial variation in AGC and other ecological processes (Hubbell 1986; Brokaw & Scheiner 1989; Asner, Keller & Silva 2004). ALS data have been used to distinguish canopy gaps at large spatial scales (Kellner, Clark & Hubbell 2009; Kent *et al.* 2015) which can be used to understand spatial and temporal patterns of gap dynamics. However, recognising that the size of canopy gaps may influence ecological processes in different ways (Denslow 1987), canopy-gap size-frequency distributions (GSFD) have been used to account for variation in size and frequency (Asner *et al.* 2013; Boyd *et al.* 2013). The frequency distribution of gap sizes often follows a power-law probability distribution and the exponent of this relationship (λ) can be used to provide a single metric to quantify the GSFD (Hubbell 1986; Asner *et al.* 2013).

1.5.2. Optical imagery

In contrast to LiDAR, optical remote-sensing can be defined as a passive technique that measures the solar energy reflected from the Earth's surface. The intercepted spectral reflectance typically ranges from 400 to 2500nm which includes the visible, near-infrared and shortwave infrared wavelengths. Satellite-derived optical imagery are attractive for their ability to cover large extents and provide repeated measurements. However, spatial and spectral resolutions can be relatively coarse which can restrict their use at local- or fine-scales. Furthermore, optical data are sensitive to cloud cover which can be a challenge when acquiring imagery in tropical regions. Despite this, optical imagery has been used successfully in tropical forests to predict AGB (Steininger 2000; Foody, Boyd & Cutler 2003; Mutanga, Adam & Cho 2012; Singh, Malhi & Bhagwat 2014) and species diversity (Carlson *et al.* 2007; Féret & Asner 2014; Laurin *et al.* 2014a; Rocchini *et al.* 2016; Jha *et al.* 2019).

Chapter 1: Introduction

Variation in remotely sensed spectral reflectance (spectral heterogeneity, or spectral variability) has also shown to relate with environmental heterogeneity; which is considered to be a key factor associated with species diversity as heterogeneous environments have a greater number of available niches to support more species (Rocchini, Chiarucci & Loiselle 2004). Thus, variation in spectral reflectance can be a useful proxy of species diversity whereby an increase in spectral heterogeneity corresponds to areas that have the capacity to harbour greater levels of biodiversity (Spectral Variation Hypothesis) (Palmer *et al.* 2000; Rocchini *et al.* 2010).

Advances in remote sensing technology, now include high spectral-resolution sensors, which can detect reflectance across a continuous spectrum, typically 200 or more spectral bands. Hyperspectral imagery can be used to detect fine spectral differences between species (Shen & Cao 2017). However, the ability to discriminate plant species relies on 1) differences in their biochemistry and whether this difference is manifested in their spectral reflectance (Asner 1998) and 2) whether the spectral variability within species is lower than the variability among species (Price 1994; Cochrane 2000; Zhang *et al.* 2006; Ferreira *et al.* 2013).

1.5.3. Information extraction

Spectral reflectance derived from remotely sensed data can be extracted for land cover classification. Clark *et al.* (2005) performed a classification of seven species of emergent trees in Costa Rica. Classifications were performed at the leaf-, pixel- and crown-level and were able to detect species, based on differences in their spectral reflectance (Clark, Roberts & Clark 2005). At a leaf-scale, Clark *et al.* were able to classify species with 100% overall accuracy. However, at a pixel- or crown-scale the accuracy was reduced ($\leq 87\%$) as spectral reflectance is known to be influenced by multiple properties including; branches, understory trees, fruits, flowers and lianas (Spanner *et al.* 1990; Schlerf & Atzberger 2006; Zhang *et al.* 2006). Despite the high floristic diversity, studies have demonstrated the feasibility of mapping tree species in tropical forests (Carlson *et al.* 2007; Papeş *et al.* 2010; Féret & Asner 2012; Baldeck *et al.* 2015; Ferreira *et al.* 2016). However, the ability to generate observations from remotely sensed data at scales that align with ecological processes is often a challenge.

Delineation of individual tree crowns (ITCs), referred to as segmentation, can afford the extraction of spectra from individual objects (tree crowns) (Zhang *et al.* 2016). Accurate ITC delineation can improve the classification of tree species as intraspecific spectral variation can be reduced (Marceau *et al.* 1994) and additional attributes such as texture and shape can be included

(Franklin *et al.* 2000; Warner, McGraw & Landenberger 2006; Yan *et al.* 2006; Voss & Sugumaran 2008; Dalponte *et al.* 2012; Féret & Asner 2012; Immitzer, Atzberger & Koukal 2012; Ferreira *et al.* 2016). However, an object-based approach may be compromised by errors caused by over- and under-segmentation (Chen *et al.* 2018). In dense tropical forests, tree crowns are often overlapping or lack a clear boundary. Similarly, logged forests are typically less structurally diverse which poses a significant challenge for the accurate detection and delineation of tree crowns.

In contrast, a pixel-based approach does not require the detection of crowns and has been used effectively to map biodiversity (Féret & Asner 2014), species invasions (Amaral *et al.* 2015), species composition (Laurin *et al.* 2014a) and biomass (Laurin *et al.* 2014b). The choice of whether to adopt a pixel- or object-based approach may therefore depend on the resulting map. For example, mapping tree species, growth or mortality may benefit from an object-based approach as change is interpreted at the crown-level; whereas stand-level aboveground biomass or biodiversity must be mapped at the pixel-level. Other ecological processes such as liana infestation can be performed using either approach. Both approaches are able to generate results with spatial units that can provide meaningful interpretation for ecologists or forest managers.

For an object-based approach, ground data on liana canopy cover can be associated with the spectral response of the same object. However, for a pixel-based approach, estimates of liana infestation cannot be collected at the same scale of the hyperspectral pixels when assessed from the ground. To overcome this, pixel-level endmember spectra can be derived from trees without lianas in their canopy (therefore 'tree') and trees with highly liana-infested canopies (therefore 'liana') (Bateson & Curtiss 1996). As such, each pixel represents a pure class of either tree or liana leaves. Then, by spectral unmixing of endmember spectra (Keshava & Mustard 2002) it is possible to obtain a percent estimate of liana infestation indicated by the strength of class membership to each endmember (Foody 1996; Foody 2002; Foody & Doan 2007). Alternatively, Unoccupied Aerial Vehicles (UAVs) can provide an approach to advance the remote sensing of individual plants (*cf.* Kellner *et al.* 2019). Optical sensors on UAVs can capture data at ultra-fine spatial resolutions (mm) which can provide spatially detailed imagery to clearly differentiate liana leaves from tree leaves in the canopy (Waite *et al.* 2019). Thus, UAVs may provide a useful tool to generate estimates of liana infestation at the pixel-level (airborne-derived data) which can then be scaled over larger areas.

1.5.4. Remote sensing of liana infestation

Lianas and trees can be discriminated based on differences in their spectral response (Sánchez-Azofeifa *et al.* 2009). Many studies have shown that spectral differences are most pronounced in the visible- (400-690 nm) followed by the near infrared (NIR)-region (700-1340nm) (Castro-Esau, Sánchez-Azofeifa & Caelli 2004; Sánchez-Azofeifa & Castro-Esau 2006; Foster, Townsend & Zganjar 2008; Sánchez-Azofeifa *et al.* 2009; Marvin, Asner & Schnitzer 2016). Higher reflectance within the visible spectra and particularly in the green region has shown to be strongly related to the level of chlorophyll content, which is lower in liana leaves (Castro-Esau, Sánchez-Azofeifa & Caelli 2004). Furthermore, NIR features are expressed more strongly in canopies with high leaf area (Asner 1998; Sims & Gamon 2002; Delegido *et al.* 2015). As lianas have greater leaf area in comparison to trees (Putz 1983; Sánchez-Azofeifa *et al.* 2009; Campanello *et al.* 2016), this can result in higher reflectance in the NIR region as well as in greenness indices (Sánchez-Azofeifa *et al.* 2009; Delegido *et al.* 2015).

Subsequently, studies have shown that lianas can be spectrally distinguished from trees using hyperspectral imagery (Castro-Esau, Sánchez-Azofeifa & Caelli 2004). Studies have found that the spectral properties of lianas and trees were distinguishable at the leaf-level (Castro-Esau, Sánchez-Azofeifa & Caelli 2004; Sánchez-Azofeifa & Castro-Esau 2006; Kalacska *et al.* 2007; Hesketh & Sánchez-Azofeifa 2012; Guzman, Rivard & Sánchez-Azofeifa 2018) and crown-level, when liana infestation was greater than 40% (Kalacska *et al.* 2007). Studies have also used UAVs to clearly differentiate liana leaves from tree leaves in the canopy (Waite *et al.* 2019). UAVs fitted with thermal sensors have also been able to discriminate liana-infested and non-infested areas (Yuan *et al.* 2019) based on differences in the temperature of liana and tree leaves (Sánchez-Azofeifa *et al.* 2011; Guzmán *et al.* 2018). Furthermore, multispectral sensors combined with machine learning approaches have been utilised to effectively predict liana-infested and non-liana-infested trees in Costa Rica (Li *et al.* 2018). Liana infestation has also been detected in large canopy gaps using satellite imagery (Foster, Townsend & Zganjar 2008) and within tree canopies using airborne hyperspectral imagery in seasonal (Marvin, Asner & Schnitzer 2016) and aseasonal (Chandler *et al.* in review) forests.

The approach by Marvin *et al.* (2016) benefitted from the fusion of hyperspectral and LiDAR data to detect liana canopy cover at the landscape-level. However, while the LiDAR data were used to mask canopy gaps, shadows, water and bare soil for accurate spectral data extraction, only the spectral data were used to train and predict the percentage cover of liana infestation in tree canopies. Lianas have shown to be significantly associated with both lower (Dalling *et al.* 2012) and

taller canopy heights (Meyer *et al.* 2019) suggesting that vertical vegetation structure could be a key driver of liana infestation. As a result, canopy height may provide a useful variable to assist in the prediction of liana infestation.

In addition, a disagreement between the spatial units of remotely sensed data, characterized by pixels, with field estimates of liana canopy cover, characterised by individual tree crowns, may have led to a reduction in classification accuracy. In an attempt to overcome this, Marvin *et al.* (2016) removed all isolated groups of less than three pixels with predicted liana infestation. While this may have reduced the so called 'salt and pepper' effect, whereby individual pixels are classified differently from their neighbours, it is unlikely to have improved the accuracy of predicted liana infestation (Yu *et al.* 2006; Blaschke 2010; Liu & Xia 2010; Pu, Landry & Yu 2011). The ability to generate remotely sensed data with spatial units that align with ground observations is essential for the accurate prediction of liana infestation.

Previous research on detecting lianas from trees has been mainly limited to dry forest sites where lianas and host tree spectra can be more easily separated (Castro-Esau, Sánchez-Azofeifa & Caelli 2004; Kalacska *et al.* 2007; Guzman, Rivard & Sánchez-Azofeifa 2018). As precipitation increases chlorophyll content is observed to simultaneously increase in liana leaves and decrease in tree leaves (Sánchez-Azofeifa *et al.* 2009). This change is also observed in their spectral response and therefore in wet, or aseasonal tropical forests, a low spectral contrast between lianas and trees (Castro-Esau, Sánchez-Azofeifa & Caelli 2004; Sánchez-Azofeifa *et al.* 2009) poses a significant challenge for detecting and mapping liana infestation. While trees and lianas have been discriminated across seasons at the leaf-level (Hesketh & Sánchez-Azofeifa 2012), currently no study has mapped liana infestation across an aseasonal tropical forest at a landscape-level. Furthermore, previous studies have heavily focused in the Neotropics and therefore our understanding of the spatial patterns of liana infestation in the Palaeotropics and the impact on carbon storage is currently lacking.

Tree and liana biogeography differ markedly in the Palaeotropics, with low liana densities and a complex forest structure (Gentry 1991; Appanah, Gentry & LaFrankie 1993; Schnitzer & Bongers 2002; Banin *et al.* 2012). Differences in the spatial distribution of liana infestation and aboveground carbon may be driven by the high proportion of dipterocarp trees (Ashton & Kettle 2012) which make these forest structurally unique and give rise to high aboveground carbon densities (Sullivan *et al.* 2017). Therefore, assessing whether the negative relationship between liana infestation and aboveground carbon (AGC) stocks holds in south-east Asian forests requires further attention.

1.6. Study location: Sabah, Borneo

South East Asia has the highest rate of lowland forest loss of any tropical region with deforestation for conversion to plantations as the primary driver (Flint 1994; Sodhi *et al.* 2004). As a result, mapping logged forests and their impact on carbon stocks has become a primary conservation concern. In recent years LiDAR has been heavily utilised for state-wide assessments of forest biomass and carbon stocks in the Neotropics and Africa (Asner *et al.* 2012; Asner & Mascaro 2014). However, the forests of south-east Asia are structurally and compositionally distinct from others pantropically (Banin *et al.* 2012). As a result, this structural anomaly fails to conform with generalised functions to predict carbon within tropical forests. To address this, regional calibration of models were required (Coomes *et al.* 2017; Jucker *et al.* 2018) in order to estimate carbon stocks from ALS in Sabah, Borneo (Asner *et al.* 2018).

The Malaysian state of Sabah occupies an area of 73,371 km² which constitutes around 10% of the island of Borneo (Marsh & Greer 1992). Sabah is still considered to be well forested by regional standards, however only a small percentage of primary lowland forest remains (Reynolds *et al.* 2011). In 1990, it was estimated that Sabah retained ca 500, 000 ha of primary lowland forest (Marsh & Greer 1992), however in 2010 this was reduced to less than 70,000 ha (Reynolds *et al.* 2011) with almost none outside protected areas. Over half (43,800 ha) of this is accounted for by the Danum Valley Conservation Area (DVCA) under the management of the Yayasan Sabah (Sabah Foundation) forest concession (Reynolds *et al.* 2011). Given the high levels of past and current deforestation, some of these degraded forests are now part of active restoration projects such as the Innoprise-Forests Absorbing Carbon Emission (FACE) Foundation Rainforest Rehabilitation Project (INFAPRO). Rehabilitation projects such as these aim to improve the capacity of the forest to sequester carbon by enrichment planting of dipterocarps, liana cutting and fertilisation (Future 2011). The DVCA and surrounding landscape is therefore characterised by a mosaic of primary and recovering forests. These forests have been exposed to varying intensities of logging and post-logging restoration treatments and therefore provide an ideal location to study the distribution of liana infestation and the relationship with carbon stocks.

1.7. Thesis aims and objectives

1.7.1. Thesis aim

Assess spatial and temporal patterns of liana infestation and the relationship with aboveground carbon stocks across a primary and selectively logged tropical forest in Sabah, Malaysia.

1.7.2. Thesis objectives

Firstly, I will focus on whether airborne-derived hyperspectral and ALS data can be used to accurately detect liana infestation across an aseasonal primary tropical forest (Objective 1). Secondly, using this methodology, I will assess spatial patterns of liana infestation across primary and selectively logged forests and the relationship with aboveground carbon stocks at a landscape-scale (Objective 2). Lastly, using predicted landscape-level liana infestation, I will explore the ability to detect liana infestation in satellite-based multispectral imagery (Objective 3). Specifically this thesis aims to achieve the following objectives:

Objective 1: *Produce a methodology that is capable of accurately detecting liana infestation across an aseasonal primary forest*

- 1.1. Predict the spatial distribution of liana infestation across primary forest using airborne hyperspectral and LiDAR data;
- 1.2. Utilise both pixel- and object-based approaches to overcome challenges associated with differences in spatial units, and compare the accuracies of predicted liana infestation outputs.

Objective 2: *Explore the relationship between liana infestation and carbon stocks at a landscape-scale*

- 2.1. Assess spatial patterns of liana infestation across primary and selectively logged forest;
- 2.2. Quantify the liana-induced impact on aboveground carbon stocks after accounting for variation in topography and the size and frequency of canopy gaps.

Objective 3: *Assess whether liana infestation can be detected in satellite-based multispectral imagery*

- 3.1. Determine whether liana infestation can be detected in satellite imagery;
- 3.2. Quantify change in liana infestation over time using a time series of satellite imagery;
- 3.3. Assess whether there is a larger contrast in spectral reflectance between lianas and trees in 2016 in comparison to other years (2017-2019), as a result of the 2015/2016 El-Niño.

1.8. Thesis structure

The chapters in this thesis have all been written for publication in the peer-reviewed literature. The structure of this work is therefore made up of individual, stand-alone chapters (Figure 1.2, Table 1.1). **Chapter 2** is a methodological paper and is under review at *Remote Sensing in Ecology and Conservation*. **Chapter 3** utilises the methodology from Chapter 2 to predict liana infestation across the full landscape and assess the relationship with carbon stocks at a landscape-level. This chapter is being prepared for submission to the *Journal of Ecology*. **Chapter 4** uses the predicted liana infestation output from Chapter 3 to assess whether liana infestation can be detected in satellite-based imagery and how liana infestation varies over time. This chapter is being prepared as a submission to *Remote Sensing of Environment*. **Chapter 5** provides a synthesis on the research conducted and discusses the implications of this research within a wider context. To avoid repetition of some common material, such as the methodology and references, each chapter has been slightly adapted.

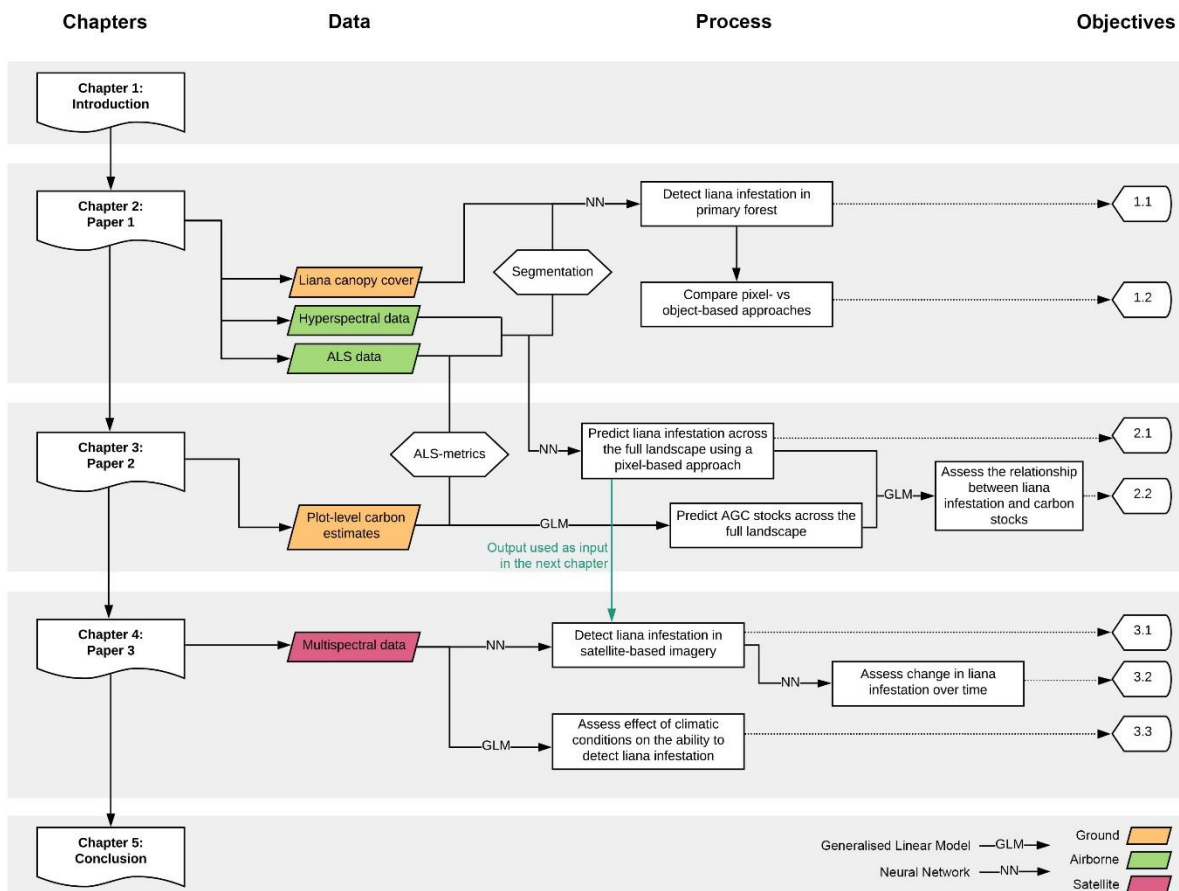


Figure 1.2 Thesis structure

1.9. Summary of papers

Table 1.1 Summary of papers

Paper No.	Chapter No.	Title	Status	Journal/Target Journal	Page No.
1	2	Remote sensing liana infestation in an aseasonal tropical forest: addressing mismatch in spatial units of analyses	In review	<i>Remote Sensing in Ecology and Conservation</i>	27
2	3	Lianas are strongly associated with areas of low carbon stocks at the landscape scale	Final edits in progress	<i>Journal of Ecology</i>	43
3	4	Spatial and temporal patterns of lianas detected in satellite-derived imagery	Final edits in progress	<i>Remote Sensing of Environment</i>	63

1.10. Author contributions

This work was only possible due to the support of numerous people involved in the funding, collection and sharing of ground- and airborne-derived data. Contributions were made by authors for specific chapters which are presented in Table 1.2.

Table 1.2 Author contributions to each chapter

Chapter 2: Remote sensing liana infestation in an aseasonal tropical forest: addressing mismatch in spatial units of analyses	
Ground-derived liana canopy cover	Chris J. Chandler
Airborne-derived remote sensing data	NERC Airborne Research Facility (Mark E.J. Cutler, Giles M. Foody, Doreen S. Boyd, Geertje M.F. van der Heijden)
Image segmentation	Hugo Costa
Data Analysis	Chris J. Chandler
Permit and logistical support	Reuben Nilus
Writing/Edits	Chris J. Chandler led the writing, all authors contributed critically to the manuscript
Chapter 3: Lianas are strongly associated with areas of low carbon stocks at the landscape scale	
Ground-derived liana canopy cover	Chris J. Chandler
Plot data for AGB estimation	Chris J. Chandler, Geertje M.F. van der Heijden, Doreen S. Boyd, Mark E.J. Cutler, Giles M. Foody, David F.R.P. Burslem
Airborne-derived remote sensing data	NERC Airborne Research Facility (Mark E.J. Cutler, Giles M. Foody, Doreen S. Boyd, Geertje M.F. van der Heijden)
Data Analysis	Chris J. Chandler
Permit and logistical support	Reuben Nilus
Writing/Edits	Chris J. Chandler led the writing, Geertje M.F. van der Heijden, Doreen S. Boyd and Giles M. Foody contributed critically to the manuscript
Chapter 4: Spatial and temporal patterns of lianas detected in satellite-derived imagery	
Airborne-derived remote sensing data	NERC Airborne Research Facility (Mark E.J. Cutler, Giles M. Foody, Doreen S. Boyd, Geertje M.F. van der Heijden)
Data Analysis	Chris J. Chandler
Writing/Edits	Chris J. Chandler led the writing, Geertje M.F. van der Heijden, Doreen S. Boyd and Giles M. Foody contributed critically to the manuscript
Funding	
NE/P004806/1 to MEJC, DSB, GMF, GMFvdH	
NE/I528477/1 (ARSF MA14/11) to MEJC, DSB, GMF	
NERC ENVISION NE/L002604/1 to CJC, GMF, GMFvdH	
Anne McLaren Research Fellowship to GMFvdH	

Chapter 2: Remote sensing liana infestation in an aseasonal tropical forest: addressing mismatch in spatial units of analyses¹

2.1. Abstract

1. The ability to accurately map liana (woody vine) infestation at the landscape-level is essential to quantify their impact on carbon dynamics and help inform targeted forest management and conservation action. Remote sensing techniques provide potential solutions for mapping liana infestation. However, their use so far has been limited to seasonal forests, where there is a high spectral contrast between lianas and trees. Additionally, a number of methodological issues require addressing, particularly the difference in spatial units between remotely sensed data and canopy observations of liana infestation.
2. Airborne hyperspectral and LiDAR data were combined with a neural network machine learning classification to assess the distribution of liana infestation at the landscape-level across an aseasonal primary forest in Sabah, Malaysia. I tested whether an object-based classification was more effective at predicting liana infestation when compared to a pixel-based classification.
3. A stronger relationship was found between predicted and observed liana infestation when using a pixel-based approach (RMSD = 18.4%) in comparison to an object-based approach (RMSD = 20.4%). However, there was no significant difference in accuracy for object- versus pixel-based classifications when predicted liana infestation was grouped into three classes; Low [0-30%], Medium [31-69%] and High [70-100%] (McNemar's $\chi^2 = 0.211$, $p = 0.65$).
4. I demonstrate, for the first time, that remote sensing approaches are effective in accurately mapping liana infestation at a landscape scale in aseasonal tropical forests. These results indicate potential limitations in object-based approaches which require refinement in order to accurately segment imagery across contiguous closed-canopy forests. I conclude that the decision on whether to use a pixel- or object-based approach may still depend on the structure of the forest and the ultimate application of the resulting map. Both approaches will provide a valuable tool to monitor liana infestation and inform effective conservation and forest management.

¹ Chandler *et al.* (in review). Remote sensing liana infestation in an aseasonal tropical forest: addressing mismatch in spatial units of analyses. *Remote sensing in Ecology and Conservation*.

2.2. Introduction

Lianas (woody vines) are a dominant plant functional type in tropical forests. Lianas use the structural composition of trees to reach the forest canopy, where they strongly compete with trees for light (Putz 1984; Schnitzer 2005). Recent studies have indicated that the presence of lianas may have a strong negative effect on tree diversity (Schnitzer & Carson 2010), growth (van der Heijden & Phillips 2009), recruitment (Stevens 1987; Tymen *et al.* 2016), survival (Putz 1984) and the ability of these forests to store and sequester carbon (Durán & Gianoli 2013; van der Heijden, Powers & Schnitzer 2015). This is particularly relevant as tropical forests represent around 55% (471 ± 93 Pg C) of global carbon stocks (Pan *et al.* 2011) and thus are highly valued for their role in the global carbon cycle. Therefore, liana proliferation, such as that observed in Neotropical forests (Phillips *et al.* 2002; Schnitzer & Bongers 2011), may have global consequences for climate change.

Growing concern for the impact of lianas on tropical forest carbon balance has led to an expansion of studies in recent years. However, the impact on tropical carbon budgets are usually studied from the ground (Ingwell *et al.* 2010; van der Heijden, Powers & Schnitzer 2015; Wright *et al.* 2015) with spatial extents limited to the order of plot size (typically, 0.1 ha to 50 ha) (Ingwell *et al.* 2010; Schnitzer *et al.* 2012). As the abundance and distribution of lianas may be influenced by processes that operate at multiple scales, field measurements that are constrained to small plots may restrict our understanding of the distribution and impact of lianas over larger areas. The ability to accurately assess liana infestation at a landscape-level is therefore essential to quantify their impact on carbon dynamics and monitor change over time, which will assist in targeting conservation and management actions focussing on climate change mitigation in tropical forests.

Remote sensing may provide a solution to map liana infestation over larger areas than possible using field-based methods alone. Studies have shown clear differences in the spectral response of trees and lianas at the leaf- (Castro-Esau, Sánchez-Azofeifa & Caelli 2004; Hesketh & Sánchez-Azofeifa 2012; Guzman, Rivard & Sánchez-Azofeifa 2018) and canopy-levels (Kalacska *et al.* 2007). Based on differences in the spectral response of trees and lianas, airborne-derived hyperspectral and LiDAR data have been used to effectively map liana canopy cover at a landscape-level (Marvin, Asner & Schnitzer 2016). However, the use of remote sensing methodologies to map liana infestation at the landscape-level have so far been limited to seasonal forests in the Neotropics (Foster, Townsend & Zganjar 2008; Marvin, Asner & Schnitzer 2016). In aseasonal forests, a low spectral contrast between lianas and trees (Castro-Esau, Sánchez-Azofeifa & Caelli 2004; Sánchez-Azofeifa *et al.* 2009) may pose an additional challenge for mapping liana infestation. Moreover, in the study by Marvin *et al.* (2016) a disagreement between liana infestation predictions at the pixel-level

(*i.e.*, determined by the hyperspectral data) with field estimates at the object-level (*i.e.*, per tree-crown) may have led to a reduction in classification accuracy. Such discrepancies in spatial units have been noted in multiple studies that have suggested the need to account for meaningful image objects in order to produce accurate land cover maps (Yu *et al.* 2006; Blaschke 2010; Li & Shao 2014).

The ability to align ground observations of liana infestation with remotely sensed data is essential for accurate classification. Liana infestation estimates at the pixel-level may be achieved by spectral unmixing of endmember pixels (Adam, Csaplovics & Elhaja 2016; Shao & Lan 2019). Alternatively, LiDAR data may be used to delineate individual tree crowns (Jakubowski *et al.* 2013; Jing *et al.* 2014; Nunes *et al.* 2017), which can be used to segment hyperspectral imagery for object-based classification. However, the effectiveness of an object-based approach may be compromised by errors caused by over- and under-segmentation (Liu & Xia 2010; Chen *et al.* 2018).

Here, I examine, for the first time, whether a combination of airborne hyperspectral and LiDAR data can be used to accurately map liana infestation across an aseasional primary forest in Sabah, Borneo. By employing a neural network machine learning classification, I aim to predict liana infestation using both pixel- and object-based approaches and compare differences in their accuracies. I also discuss the potential benefits of pixel- versus object-based liana infestation maps and their suitability for informing effective conservation and land management.

2.3. Methods

2.3.1. Study area

The study area is situated within the Danum Valley Conservation Area (DVCA), a primary lowland dipterocarp forest within the Yayasan Sabah (Sabah Foundation) forest concession (Reynolds *et al.* 2011) (Figure 2.1). The DVCA (117°48'15.641"E, 4°57'54.822"N) remains a large and intact lowland forest (438 km²). The climate is typical of the aseasional tropics with an annual rainfall of >2800 mm (Marsh & Greer 1992) and a mean annual temperature of 26.7°C (Walsh 1990).

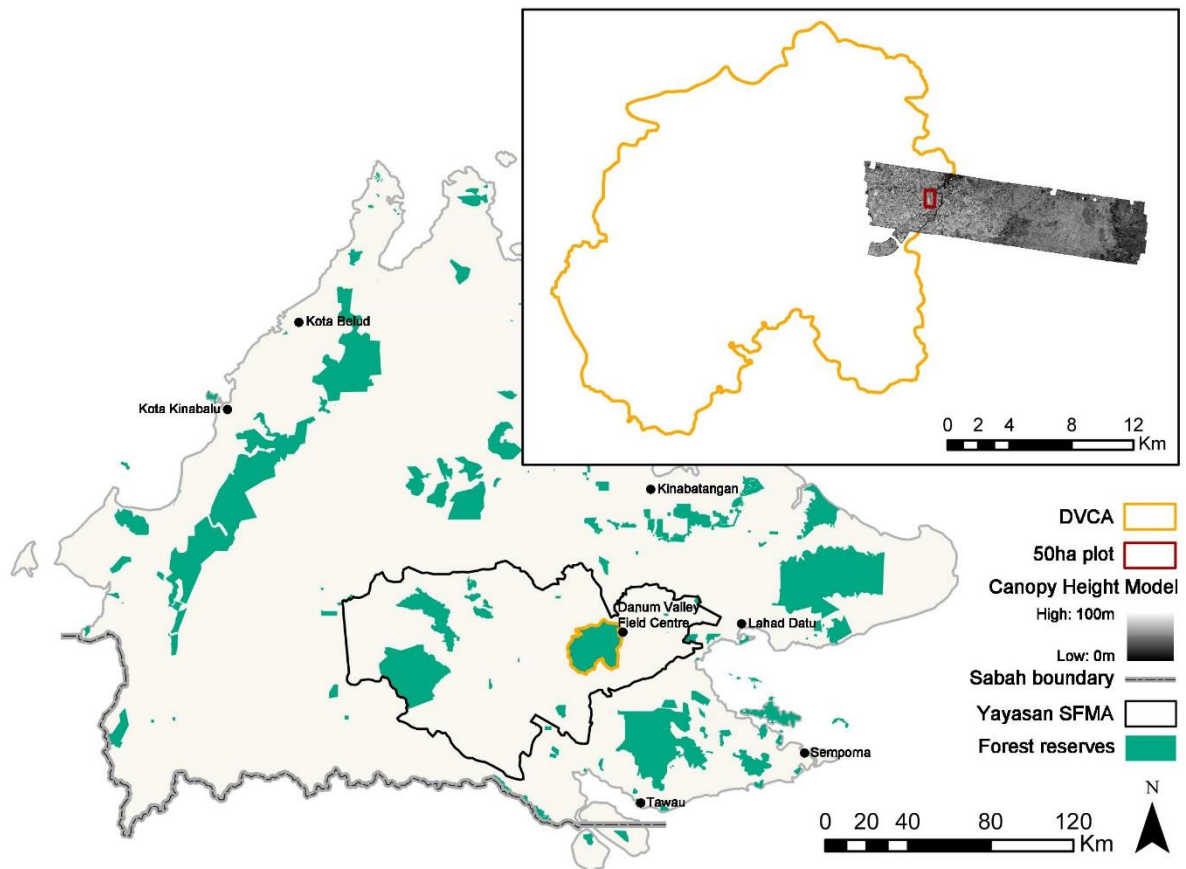


Figure 2.1 Location of the Danum Valley Conservation Area (DVCA) in Sabah, Malaysia, showing the position of the 50 ha plot and remotely sensed imagery. SFMA, Sabah Forest Management Area.

2.3.2. Occupied airborne data collection

Occupied (or manned) airborne hyperspectral and LiDAR data were collected concurrently by the UK Natural Environmental Research Council’s Airborne Research Facility (NERC-ARF) in November 2014. The data were captured from a Dornier 228-201, flying at 127-139 knots at an altitude of 2335-2429m. In total 10 flightlines were flown, on bearings of 100 or 280 degrees, surveying an area of ~2083ha of primary forest (Figure 2.1).

LiDAR data were captured using a Leica ALS50-II with the capacity to record both Discrete (DR) and Full Waveform (FW) data. The dataset has a point density ranging between 2.80-3.16 per m² and a spatial resolution of 1 m². The DR data were processed to produce a top-of-Canopy Height Model (CHM) based on the difference between the Digital Surface Model (DSM) and the Digital Elevation Model (DEM) using LAStools software (Isenburg 2014).

Hyperspectral imagery were collected using a FENIX sensor (Specim Spectral Imaging, Finland), which acquired high resolution data from a large spectral range (380-2500 nm). Data were collected across 448 contiguous channels at a spatial resolution of 3 m². Spectral radiance measured in the visible-to-near infrared (VNIR) ranged from 380-970 nm with a spectral resolution of 3.5 nm; in the shortwave infrared (SWIR) spectra ranged from 970-2500 nm with a spectral resolution of 12 nm. Radiometric corrections were applied to the full hyperspectral dataset. Bands without data or those which were overly-saturated were removed. Data were atmospherically corrected using ENVI FLAASH (Fast Line-of-sight- Atmospheric Analysis of Spectral Hypercube) Atmospheric Correction (ENVI version 4.8, Exelis Visual Information Solutions, Boulder, Colorado). Post-correction quality checks revealed reflectance values varied between flightlines for the same individual pixels. As a result, all spectral values for individual flightlines were adjusted based on the difference in reflectance between overlapping pixels of adjacent flightlines (Taylor 2001). An average of all pixels from one flight line were compared with an average of all overlapping pixels from the adjacent flightline. The average difference was calculated and adjusted for each band across the full flightline. All flightlines were combined and the dimensions of the data were reduced using a Standardised Principal Component Analysis (SPCA). SPCA uses a correlation matrix which has the same effect as using normalised bands of unit variance (Chang & Yoon 2003). The first 8 principal components were retained, which explained more than 99% of the variation. Lastly, all values were scaled using a min-max normalisation:

$$z = \frac{x - \min(x)}{\max(x) - \min(x)} \quad (1)$$

2.3.3. Liana canopy cover survey

Data on liana canopy cover were collected in 2017 and 2018 for training of a neural network classification ($n=454$ trees). The LiDAR data were uploaded to a tablet computer (Apple, California, USA) connected to a GPS receiver (Garmin GLO 2; GARMIN, USA) so individual tree crowns could be visually delineated in the field using the GeoEditor application (MapTiler). Thus error associated with GPS accuracies can be avoided. To minimise error associated with estimating liana canopy cover, effort was taken to ensure each tree crown was thoroughly and accurately assessed by; 1) only recording tree crowns that were identified on the canopy height model with a high degree of certainty, 2) making sure tree crowns were fully sun-lit and completely unobscured from above and 3) having a minimum of two people independently estimating the percentage of a tree crown infested with liana to the nearest 5% and then mutually agreeing on a final estimate (*sensu* Marvin, Asner & Schnitzer 2016).

2.3.4. Tree crown segmentation

The CHM was segmented using the meanshift in the Orfeo Toolbox (OTB) within QGIS v3.6.0 (QGIS Development Team 2018). The segmentation output consisted of a set of contiguous and non-overlapping objects. The meanshift algorithm was controlled by three main parameters: scale, radius and threshold. A grid-search was performed using four different values for each parameter (Table S1.1). A total of 64 segmentations were produced using each parameter combination (Table S1.2). It is not possible to know, prior to segmentation, which combination of values will produce the optimal segmentation, therefore a large range of values were chosen for each parameter to ensure the optimal parameter combination was captured. Following this, a second grid search was performed which inspected an additional 27 combinations (Table S1.3). Each segmentation result was submitted to a supervised accuracy assessment. Among the many methods available (Costa, Foody & Boyd 2018) the Segmentation Evaluation Index (SEI) (Yang *et al.* 2015) was selected to provide an estimate of the accuracy of the segmentation. SEI is a strict measure as it requires a one-to-one correspondence between the segments and reference polygons. This is a desirable feature in the context of this study as one object should correspond to just one tree and vice versa. If not, the segmentation accuracy is penalised (Costa, Foody & Boyd 2018). The 91 segmentations were compared against a reference set of 124 tree boundaries across the study area manually delineated using the CHM. SEI values ranged from 0.276 to 0.818, corresponding to the best and worse results, respectively. The smallest SEI value was derived from the parameter combination: scale=15, radius=5 and threshold=0.005 (Table S1.3). The segmentation produced with this parameter combination was used in the subsequent analysis.

2.3.5. Hyperspectral data extraction

When assessing liana canopy cover from the ground, it is only possible to estimate liana infestation for entire tree-crowns (objects). A more detailed assessment of liana infestation within a tree crown can be achieved by visually dividing the crown into quadrants (*cf.* Marvin *et al.* 2015). In either case, estimates of liana infestation when assessed from the ground cannot be achieved at the same scale of the hyperspectral pixels. To overcome this, end-member spectra were derived from trees without lianas in their canopy (therefore 'tree') and trees with highly liana-infested ($\geq 75\%$) canopies (therefore 'liana') to explain the spectral range (Plaza *et al.* 2012). As such, each hyperspectral pixel within the object relates to a pure cover of either tree or liana leaves. To allow comparison with the object-based approach, end-member spectra were derived for both approaches. For the object-based classification, end-member spectra were extracted from the

segmented hyperspectral imagery for the same trees used in the pixel-based classification ($n=267$ trees/8827 pixels; Table 2.1). This yielded a total of 7826 hyperspectral pixels (226 trees) with no liana infestation and 1001 hyperspectral pixels (41 trees) with highly liana-infested canopies (see, Table 2.1).

Where the crown delineation derived from the CHM overlapped more than one object in the segmented hyperspectral imagery, a weight was assigned based on the proportion of each segmented object that made up the area as defined by the delineated crown boundaries. All weights were normalised to add up to one and used to calculate a weighted mean by multiplying the spectral values of a segmented object with the associated weight.

Table 2.1 Data used for the training of neural network models and validation of predicted liana infestation maps. EMs, Endmembers; values within [] indicate proportional coverage of liana infestation in the tree crown. Balanced EMs contain an equal number of data points within each class.

Approach	Spatial Unit	Training Data	Total EMs	EMs [0%]	EMs [$\geq 75\%$]	Balanced EMs [0, $\geq 75\%$]	EMs (80%) training [0, $\geq 75\%$]	EMs (20%) verification [0, $\geq 75\%$]	Valid. data (#trees)
Pixel Output P	9m ² Pixel	14552	8827	7826	1001	2002	1602	200	168
Object Output O	Tree crown	454	267	226	41	82	66	16	168

2.3.6. Neural network

Machine learning classifications such as neural networks often perform well when dealing with large datasets that include variables with non-linear, complex relationships. Unlike many other prediction techniques, they can learn hidden relationships without imposing restrictions such as fixed relationships in the data. A neural network model with resilient backpropagation and weight backtracking was used, which means that parameters such as learning rate are not required to achieve optimal convergence time (Yu & Liu 2002).

The input variables consisted of the eight principal components and canopy height. Tree height was used as an input variable as it has shown to be a key driver in the spatial distribution of lianas (Dalling *et al.* 2012; Meyer *et al.* 2019). Each input class contained an equal number of data points, with pixels or objects removed in a random manner from those that had additional data

points (Table 2.1). Each input class was then split 80% for training and 20% for verification (Olson, Wyner & Berk 2018). The number of hidden layers and neurons were defined subjectively based on trial runs and the model's performance with verification data (see Table S1.4.). The hidden layers refer to the internal structure of the network where the learning process is performed in order to separate classes non-linearly. The neurons within the hidden layer multiply the input data by a weight, add bias, execute an activation function and transfer to the next layer. The optimal model consisted of one hidden layer with 4 neurons, thus the architecture took the form of 9 : 4 : 2 for input : hidden : output units, respectively. A sigmoid activation function was applied and therefore predicted values were restricted to a range between 0 and 1, *i.e.* $\sigma(x) \in (0, 1)$.

I accounted for error in liana canopy cover estimates which may have changed during the time lag (2.5 – 3.5 years) between airborne data acquisition and liana canopy cover survey. Ingwell *et al.* (2010) showed that 5% of trees changed from no liana infestation to severely ($\geq 75\%$) liana-infested; and 11% of trees changed from severely liana-infested to no liana infestation over a nine year period. I estimated 6% of trees to change over a three and a half year period (approximately a third of the degree of change recorded by Ingwell *et al.* (2010) over nine years). Subsequently, I suggest 3% of all trees may have become severely ($\geq 75\%$) liana-infested and vice versa. Taking 3% of the endmember data for each class used for training (see, Table 2.1) equates to 24 pixels, or one tree, (*i.e.* 3% of 801 pixels, or 33 trees). As a result, I randomly selected 24 pixels, or one tree, from each class and replaced them with 24 pixels, or one tree, from the other class. One hundred neural networks were trained and applied to the study area. Averaging multiple models improves generalisation and also allows the calculation of uncertainty estimates based on the standard deviation of all predictions (Lu *et al.* 2008). To assess the level of uncertainty across predictions, I regressed the standard deviation for predicted values, from 100 iterations of the neural network, against liana infestation.

2.3.7. Neural network classification for mapping liana infestation

To predict liana infestation using data from end-members, a soft, or fuzzy, classification was employed. The neural network model was applied to the entire study landscape during each iteration at both an object- and pixel-level, to predict the occurrence of a 'liana' or 'tree'. The output from the neural network represents a measure of the strength of class membership, and so may be used to generate a soft classification output, in this case, the proportion of liana infestation cover (Foody 1997; Foody 2000). A final predicted map was produced by averaging all 100 iterations.

2.3.8. Accuracy assessment of predicted outputs

The final predicted liana infestation map was validated using a random selection of trees ($n=168$) from within the 50 ha plot (Figure 2.1; Table 2.1). A weighted mean approach was used (see section 2.3.5) to account for cases where tree crown boundaries of segmented objects did not match perfectly with crown boundaries delineated using the CHM in the field. To validate the pixel-based classification, predicted liana infestation values for individual pixels inside the delineated crown boundaries were averaged to derive liana canopy cover estimates at the tree-level.

To assess the accuracy of predicted liana infestation maps, the root mean squared deviation (RMSD) was estimated as:

$$RMSD = \sqrt{\frac{1}{n-1} \sum_{i=1}^n (\hat{y}_i - y_i)^2} \quad (2)$$

which represents the mean deviation of predicted \hat{y}_i from observed values y_i (*i.e.* with respect to the 1:1 line) (Piñeiro *et al.* 2008). Assessing the accuracy of model predictions imposes special interest in the 1:1 line of equality, $Y = X$. Unlike the root mean squared error (RMSE) which estimates the mean deviation of predicted values from the regression line of predicted vs observed values, the RMSD calculates the deviation of each predicted value against the 1:1 line (Gauch, Hwang & Fick 2003). Subsequently, RMSE will always be smaller and thus an underestimation of the error between observed and predicted values (Piñeiro *et al.* 2008). The units of RMSD correspond to the same units as the model variable under evaluation, in this case the percentage of liana infestation. The final RMSD was an average of all RMSD values for each of the 100 iterations.

I accounted for error associated with observational uncertainty in liana canopy cover estimates as well as temporal change applied in model training. Firstly, I quantified observational error such that 90% of trees contained a small error of 5% and 4% of trees were assigned a large error of 30%. Error derived from temporal change was also applied whereby 6% of trees had an error of 50%. Observed liana canopy cover values were entered into Monte Carlo simulations. Random values were generated with a variation that encompassed the three levels of error (*i.e.* 5%, 30% and 50%). Using this approach 100 random values were generated which could be used to calculate mean and standard deviation values of liana canopy cover.

Outputs were also degraded to an ordinal scale by partitioning predicted liana infestation into three groups as follows: neural network membership values equal to or below 0.3 were set to 'low', values between 0.31 and 0.69 were set to 'medium' and values equal to or greater than 0.7 were set to 'high'. A confusion matrix was produced using predicted and reference liana infestation

grouped in three classes. Overall accuracy, specificity and Area Under the Curve (AUC) were used to assess the accuracy of predicted values. To test for significant differences between pixel- and object-based approaches a McNemar test was used to assess the level of consistency between the two model outputs. A 0.05 significance level was used. All analyses were conducted in R v3.5.1 (R Core Team 2019).

2.4. Results

2.4.1. Spectral difference between liana-free and highly liana-infested trees

Spectral differences were found between liana-free trees and trees severely infested with lianas for both pixel- (Figure 2.2a) and object-based approaches to the classification (Figure 2.2b). The spectral reflectance for severely liana-infested trees was greater across all spectral bands in comparison to liana-free trees (Figure 2.2c and d).

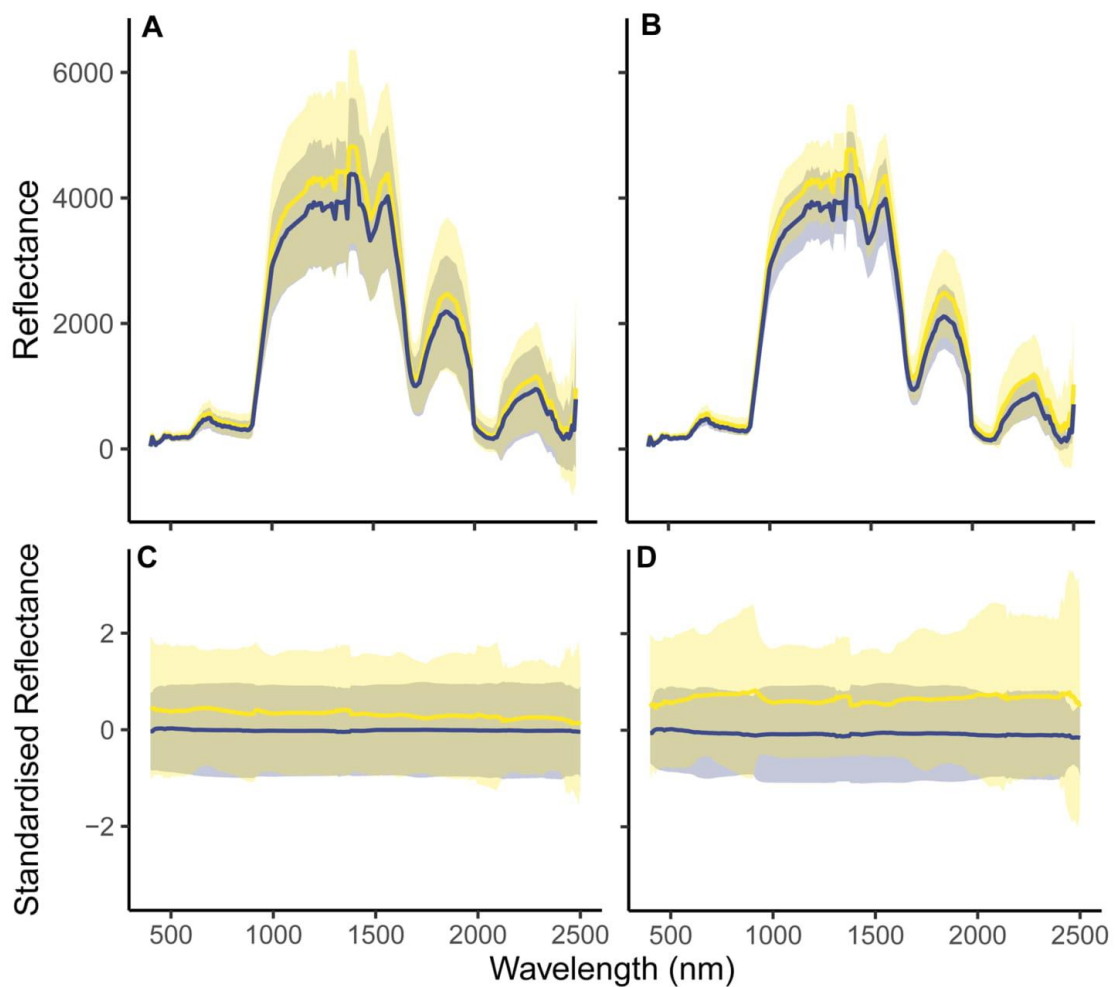


Figure 2.2 Spectral reflectance of liana-free trees and trees severely ($\geq 75\%$) infested with liana leaves using ground-based training data. **a, b)** Average reflectance values for pixel- and object-based

approaches, respectively. **c, d**) Standardised reflectance values for pixel- and object-based approaches, respectively. Standardised ($\mu = 0, \sigma = 1$) reflectance shows the difference across all bands by removing the magnitude of reflectance. Lines are mean reflectance values for all trees (shading ± 1 SD). Blue lines represent liana-free trees ($n_{\text{trees}} = 226, n_{\text{pixels}} = 7826$), yellow lines represent trees highly infested with liana leaves ($n_{\text{trees}} = 41, n_{\text{pixels}} = 1001$).

2.4.2. Predicted and observed liana canopy cover

A scatterplot of observed and predicted liana infestation revealed a better fit with a pixel-based approach (RMSD = 18.4%; Figure 2.3a; Figure S1.2a) compared to an object-based approach (RMSD = 20.4%; Figure 2.3b; Figure S1.2b). However, the accuracy of predicted liana infestation when partitioned into three classes [$\leq 30\%$, 31-69%, $\geq 70\%$] did not differ between pixel- and object-based approaches (McNemar's $\chi^2 = 0.211, p = 0.65$, Table 2.2).

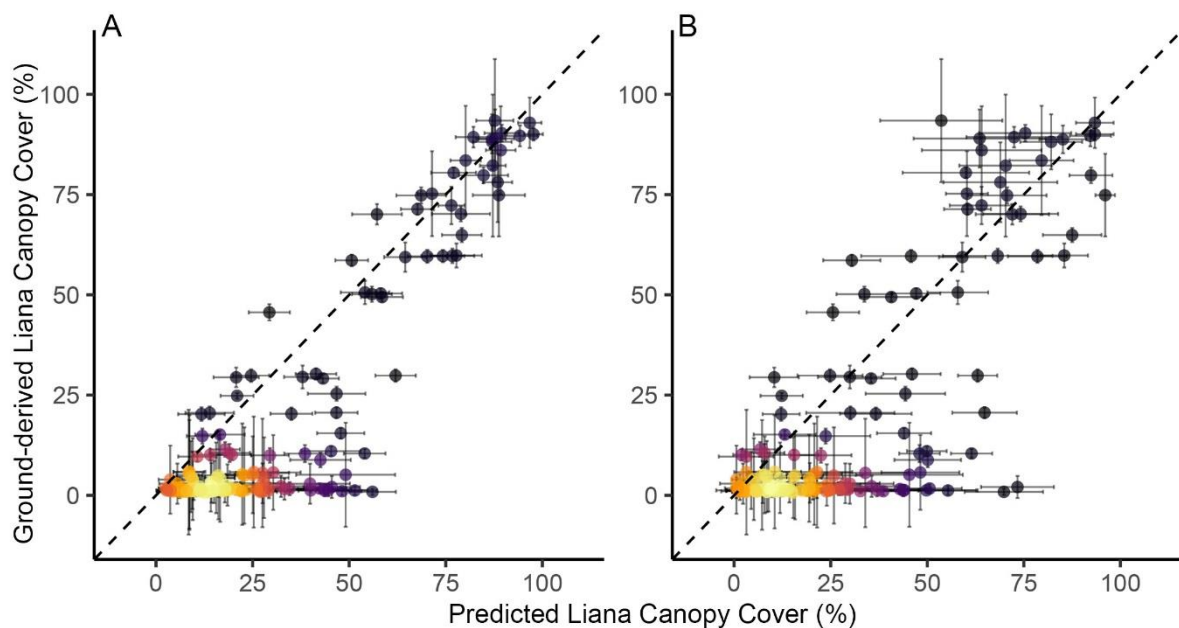


Figure 2.3 Relationship between predicted and ground reference liana canopy cover for **a)** a pixel-based approach and **b)** an object-based approach on a continuous scale. Black dashed line represents a 1:1 line. Coloured points correspond to the density of overlapping points. Horizontal error bars represent the standard deviation of 100 predicted values generated from multiple iterations of the neural network model. Vertical error bars represent the standard deviation of 100 randomly generated liana canopy cover values using Monte Carlo simulations.

2.4.3. Model outputs and uncertainty

Table 2.2 Accuracy assessment of pixel- and object-based model outputs. AUC = area under the curve; RMSD = root mean squared deviation

Model Output	Classification	AUC	Accuracy (95% CI)	Kappa	Specificity	RMSD
Output P	Pixel	0.88	0.79 (0.72-0.85)	0.54	0.92	18.4
Output O	Object	0.85	0.77 (0.70-0.83)	0.51	0.91	20.4

Both pixel- and object-based approaches produced similar patterns of predicted liana infestation across the landscape (Figure 2.4). An increase in liana infestation was generally associated with a decrease in canopy height (Figure S1.1). The use of multiple neural network models allowed for a calculation of uncertainty around overall predictions (Figure 2.5). A pixel-based classification was found to predict liana infestation with less uncertainty in comparison to an object-based classification (Figure 2.5).

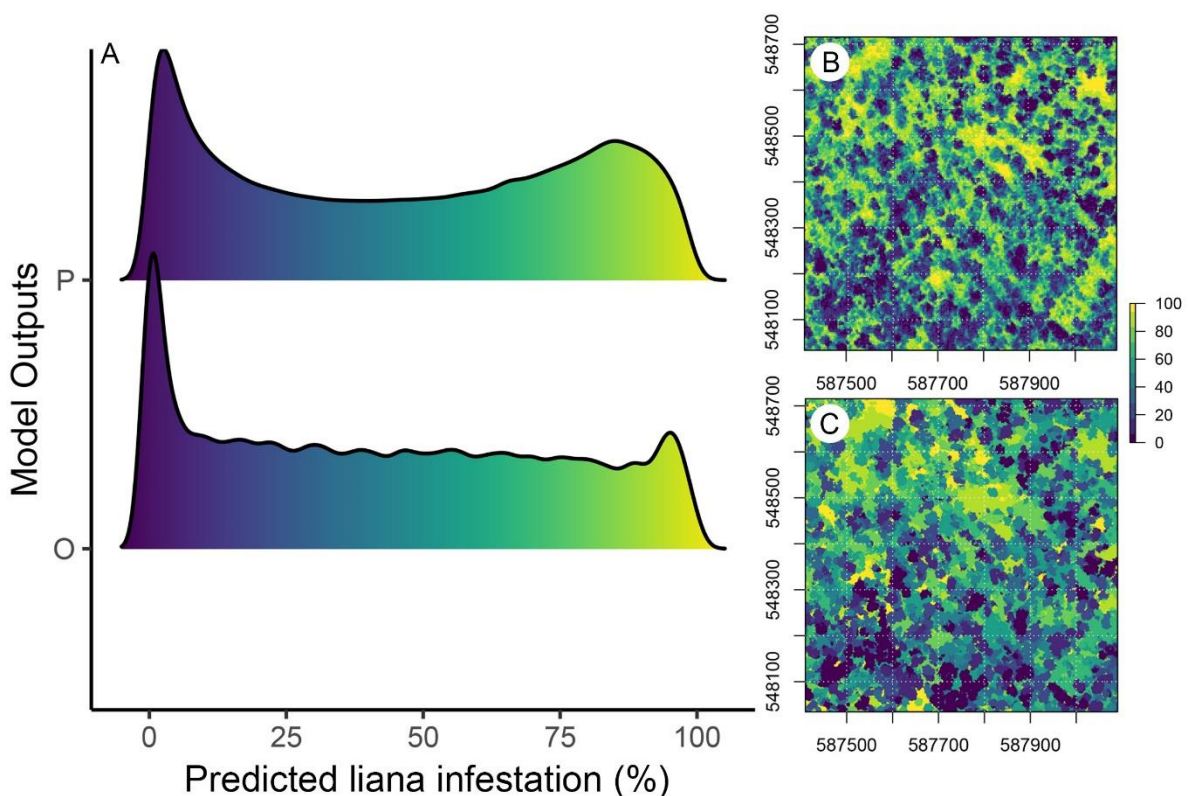


Figure 2.4 Predicted liana infestation showing **a**) the frequency of predicted values across the primary forest using **b**) a pixel-based classification (Output P), and **c**) an object-based classification (Output O). Predicted liana infestation maps **(b,c)** are extracts from a small area within the primary forest. Change in colour from purple to yellow represents an increase in liana infestation percent (0-100%) as shown by the scale bar.

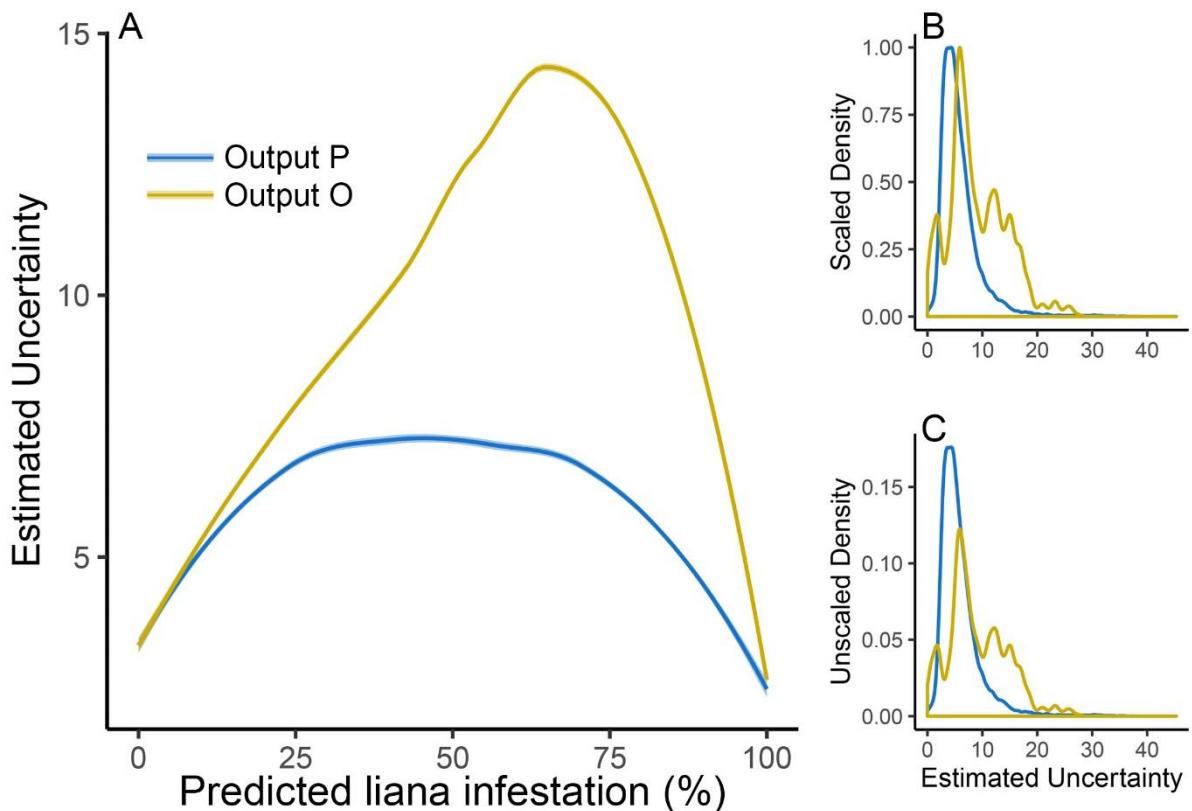


Figure 2.5 Estimated uncertainty for both model outputs. Panel (a) shows the relationship between estimated uncertainty and predicted liana infestation, (b) and (c) show the scaled and unscaled frequency of uncertainty values across the study area, respectively. Estimated uncertainty was calculated based on the standard deviation of predicted values over 100 neural network models. Fitted lines are produced using a local regression (loess) with 95% confidence intervals. Output P, pixel-based classification; Output O, object-based classification.

2.5. Discussion

Here, I show, for the first time, that despite a lower spectral contrast between liana-free and highly liana-infested tree crowns compared to seasonally dry forests (Castro-Esau, Sánchez-Azofeifa & Caelli 2004; Sánchez-Azofeifa *et al.* 2009; Marvin, Asner & Schnitzer 2016), airborne remotely sensed data and a neural network machine learning classification can be used to assess liana infestation at a landscape-level across an aseasonal tropical forest. This work therefore extends previous research using similar methodologies to predict liana infestation in seasonally dry forests (Foster, Townsend & Zganjar 2008; Marvin, Asner & Schnitzer 2016).

Additionally, two different approaches were utilised in an attempt to overcome some of the methodological issues associated with a difference in scale between remotely sensed data and

canopy observations of liana infestation. A pixel-based classification approach revealed a stronger relationship with reference data (RMSD = 18.4%) in comparison with an object-based approach (RMSD = 20.4%; Figure 2.3; Figure S1.2). Furthermore, a pixel-based approach revealed less variation in predictions compared to an object-based approach (Figure 2.5).

While the change in spatial units from pixels to objects reduced within-class spectral variation (Figure 2.2), error associated with under-segmentation, that is objects that cover more than one class, may have resulted in large differences in predictions for segmented objects (Liu & Xia 2010). The overall effects of both over- and under-segmentation present a key limitation for object-based classifications (Lee *et al.* 2016). Therefore, while utilising the entire tree canopy may offer a more attractive approach in theory, the success of this approach in dense tropical forests depends greatly on the segmentation process to accurately define objects.

Several factors may have influenced the accuracy of predicted liana infestation in this study. Firstly, a noticeable over-prediction of liana canopy cover was found for observed estimates below 50% infestation (Figure 2.3). I often observed tall, emergent dipterocarps to be liana-free. However, the accuracy of liana infestation estimates may be reduced when assessing tall canopy and emergent trees from the ground (Waite *et al.* 2019) due to the greater distance between the observer and tree crown. In such cases, or when trees are obscured, unoccupied aerial vehicles have proven to be an effective tool for accurate liana infestation assessment (Waite *et al.* 2019).

Secondly, hyperspectral data were collected in 2014 whereas ground-based estimates of liana canopy cover were collected between 2017-2019. Data from Wright *et al.* (2015) indicated around 2% of all trees that had no liana infestation had become severely ($\geq 75\%$) liana-infested, and vice versa, over a 12-year period. I therefore suggest liana canopy cover estimates may not have varied considerably over a 3.5-year period. Nevertheless, I propagated errors associated with temporal change and field estimates of liana canopy cover to quantify uncertainty in predictions of liana infestation. Accounting for this error did not substantially alter predicted liana infestation (Figure S1.3 and Table S1.5).

This method shows that it is possible to identify tree crowns and pixels with liana infestation greater than 50% with a high degree of accuracy (Figure 2.3). Accurately identifying trees with more than 50% of their crown covered is essential as previous research has indicated that the impact of lianas on growth, survival and fecundity is greatest for those trees that have more than 50% of their crown covered by liana leaves (Ingwell *et al.* 2010; Wright *et al.* 2015). Information on the spatial distribution of high liana infestation may be particularly important for targeted conservation and restoration efforts, especially when geared toward increasing the carbon storage and sequestration

potential of tropical forests for climate change mitigation (Bongers, Schnitzer & Traore 2002; Addo-Fordjour, Rahmad & Shahrul 2014). For example, one of the methods deployed to increase carbon storage and uptake in tropical forests is liana removal (van der Heijden *et al.* 2015, Marshall *et al.* 2017). However, blanket liana cutting can be expensive, particularly when it needs to be carried out over large areas or more than once to be effective (Parren & Bongers 2001; Gerwing & Vidal 2002; Schnitzer & Bongers 2005). Being able to accurately locate areas with high liana infestation may therefore help target liana cutting to areas where it is most beneficial and inform efficient forest management and conservation action.

These findings have demonstrated that remote sensing technologies are capable of accurately detecting liana infestation across an aseasonal tropical forest. As the spectral response of lianas in comparison to trees (Figure 2.2) closely resembled results derived from seasonal forests (Marvin, Asner & Schnitzer 2016), this method may be broadly applicable to other forest locations.

The approaches used in this study also revealed limitations, suggesting certain approaches may be more suited to one environment over another. For example, the accuracy of segmentation is critical for an object-based approach, which may only be achievable in a primary forest, where there is greater heterogeneity in the canopy in comparison to logged forests (Numata *et al.* 2006). On the other hand, in selectively logged forests, where tree and canopy dimensions are typically more homogenous, a pixel-based approach may be more suitable.

In addition, the requirement for a liana infestation map may guide the decision to adopt a pixel- or object-based approach. The use of an object-based liana infestation map may be more relatable for forest managers or conservationists that are interested in locating specific trees which are liana-free or heavily liana-infested. Similarly, monitoring change in liana infestation over time, or assessing tree mortality as a result of liana infestation, may favour an object-based approach as change is interpreted at the tree-level. However, relating liana infestation to an aboveground biomass map or species diversity may benefit from a pixel-based approach, to allow estimates to be generated at scales which can be aligned for meaningful comparisons.

2.6. Conclusion

The assessment of liana infestation at the landscape scale is essential to understand the mechanisms that drive spatial patterns of liana coverage, monitor changes over time and quantify the impact on carbon storage and sequestration. By combining airborne hyperspectral and LiDAR data with a neural network classification approach, I have demonstrated the ability to detect and

Chapter 2: Remote sensing liana infestation in an aseasonal tropical forest

map liana infestation in an aseasonal tropical environment, where the spectral contrast between lianas and trees is low. Due to potential limitations in the accurate segmentation of tree canopies required for an object-based approach, a pixel-based classification revealed a higher accuracy in predicting liana infestation at a landscape-level. This study advances our ability to assess spatial patterns of liana infestation at the landscape-level, particularly for high (>50%) liana infestation where the impact on carbon storage and sequestration is more pronounced. Being able to detect liana infestation in a tropical forest landscape provides a valuable tool for targeted conservation action and effective forest management focused on liana assessment and control.

Chapter 3: Lianas are strongly associated with areas of low carbon stocks at the landscape scale²

3.1. Abstract

1. Lianas are a dominant component of many tropical forests, where they can dramatically reduce carbon uptake and storage. The negative effect of lianas on carbon stocks has been well documented at the plot-level and in the Neotropics. However, plot-based studies may not capture sufficient variation in forest variables to be able to fully assess the relationship between liana infestation and aboveground carbon (AGC) stocks. It is therefore essential to i) quantify the liana-induced effect on AGC stocks at a landscape-level and ii) understand whether this pattern is representative of Palaeotropical forests.
2. Here, remote sensing techniques were used to assess the impact of liana infestation on AGC stocks across aseasonal primary and either actively restored or naturally regenerating selectively logged forests in Sabah, Malaysia. Full waveform airborne laser scanning (ALS) data were used to predict carbon stocks across the study area and related this to a landscape-level liana infestation map derived from airborne hyperspectral and ALS data.
3. Liana infestation was widespread across the landscape, although average levels of infestation were greater within the logged forests ($63.9\% \pm 7.9$) in comparison to the primary forest ($44.3\% \pm 7.9$). Canopy gaps were particularly dominated by lianas, with $86.8\% \pm 4.2$ of gaps being severely ($\geq 75\%$) liana-infested. Across the landscape, areas completely infested with lianas stored, on average, $59.6 \pm 11 \text{ Mg C ha}^{-1}$ less than areas that were liana-free after accounting for the effect of canopy gaps. However, the degree of carbon stock reduction relative to liana infestation varied within forest types, whereby severely liana-infested areas stored 14.8 ± 6.4 , 32.8 ± 16.2 and $85.1 \pm 12.8 \text{ Mg C ha}^{-1}$ less compared to liana-free areas in the actively restored, naturally regenerating and primary forests, respectively.
4. *Synthesis.* These findings show that severely liana-infested areas store less carbon at a landscape-level. This implies that an increase in liana infestation in the future may reduce the carbon storage potential of tropical forests. Therefore, in order to provide effective climate change mitigation in the future, liana control may be required in areas with severe infestation. To this end, it is imperative that lianas and their effects are included in global vegetation models to accurately predict the effects of changing climatic conditions on the carbon sink function of tropical forests.

² Chandler *et al.* (in prep). Lianas are strongly associated with areas of low carbon stocks at the landscape scale.

3.2. Introduction

Tropical forests play a critical role in the storage and sequestration of carbon and therefore structural changes within them may have large implications on the global carbon cycle (Pan *et al.* 2011). Lianas (woody vines) are an important component of tropical forests, contributing up to 40% of the woody stems (Gerwing & Farias 2000; Chave, Riéra & Dubois 2001). Lianas are non-self-supporting structural parasites that use the physical support of trees in order to reach the forest canopy. Once in the canopy, lianas can produce extensive foliage above the tree canopy, thereby reducing the amount of light available to their host tree. Competition between lianas and trees is often more direct, and therefore stronger, than tree-tree competition (Tobin *et al.* 2012) and can severely reduce the growth and survival of their hosts (van der Heijden & Phillips 2009; Ingwell *et al.* 2010). Lianas are therefore able to significantly limit the ability of tropical forests to store and sequester carbon (DeWalt & Chave 2004; van der Heijden & Phillips 2009; Ingwell *et al.* 2010; Durán & Gianoli 2013; Schnitzer *et al.* 2014b; van der Heijden, Powers & Schnitzer 2015; Tymen *et al.* 2016). Furthermore, changes in the biomass and abundance of lianas may impact the capacity of tropical forests to act as carbon sinks in the future.

Several studies, predominantly based in the Neotropics, have reported a negative relationship between liana abundance and aboveground tree biomass (Laurance *et al.* 2001; Durán & Gianoli 2013; Laurance *et al.* 2014; Durán *et al.* 2015; Ledo *et al.* 2016). However, tree and liana biogeography differ markedly in the Palaeotropics, with liana densities reported to be lower and forest heights significantly higher compared to Neotropical forests (Gentry 1991; Appanah, Gentry & LaFrankie 1993; Schnitzer & Bongers 2002; Banin *et al.* 2012). Differences in patterns of liana infestation and forest structure may be related in part to the high proportion of dipterocarp trees which are typically tall, slender and support lianas less often than other tree species (Ashton & Kettle 2012; Wright *et al.* 2015; Shenkin *et al.* 2019). Assessing whether the negative relationship between liana infestation and aboveground carbon (AGC) stocks holds in Palaeotropical forests therefore requires further attention.

The relationship between lianas and AGC storage has often been explored using ground-based plots (Laurance *et al.* 2001; Durán & Gianoli 2013; van der Heijden, Powers & Schnitzer 2015). However, ground-based studies are limited 1) to areas which are more easily accessible and 2) by the total area they can feasibly sample. Subsequently, plot-based censuses may not cover a sufficiently large area to be able to disentangle the impact of lianas on carbon stocks.

For example, liana abundance has been shown to increase with decreasing precipitation and increasing seasonality at global- (Schnitzer 2005; DeWalt *et al.* 2010) and regional-scales (Parolari *et*

al. 2020) but not across the Neotropical continent (van der Heijden & Phillips 2008). Differences may be attributed to the high variation in rainfall among and within regions (Malhi & Wright 2005). Furthermore, differences may also be attributed to the complex and often confounded forest variables (Currie, Pétrin & Boucher-Lalonde 2019). For example, an increase in AGB has also been related to an increase in soil fertility (Slik *et al.* 2010; Quesada *et al.* 2012; Vicca *et al.* 2012) an increase in elevation (de Castilho *et al.* 2006) and topography (Ferry *et al.* 2010; Taylor *et al.* 2015). However, liana abundance may covary with soil fertility (DeWalt *et al.* 2006) or above ground biomass (Durán *et al.* 2015; Ledo *et al.* 2016), in areas of greater disturbance (Denslow, Ellison & Sanford 1998; Yee *et al.* 2019) and higher elevation (de Castilho *et al.* 2006; John *et al.* 2007; Körner 2007; Unger, Homeier & Leuschner 2012). Additionally, variation in soil type may affect species distribution patterns and the structure of forest communities (Russo *et al.* 2005; John *et al.* 2007) which in turn may affect the distribution and abundance of lianas (Poulsen *et al.* 2017).

Furthermore, the distribution of lianas is highly aggregated and often associated with disturbed or open-canopy patches within forests (Schnitzer, Dalling & Carson 2000; Laurance *et al.* 2001; Schnitzer & Carson 2001; Schnitzer & Bongers 2002; van der Heijden & Phillips 2008; Schnitzer & Carson 2010). As forest plots that contain open canopy areas are likely to have lower values of AGB as well as higher liana abundance, the presence of gaps may therefore artificially amplify the relationship between liana abundance and tree carbon stocks, which may not be representative of the wider landscape. Ultimately, the variables that influence spatial patterns of both lianas and carbon stocks may be scale-dependant and vary across the landscape in response to forest type, topography and canopy gaps. Therefore, a landscape-level evaluation may allow variation in forest variables to be captured in order to fully assess the relationship between liana infestation and AGC stocks.

Remote sensing techniques offer solutions to investigate AGC storage and liana infestation concurrently at multiple spatial and temporal scales (Lechner, Foody & Boyd 2020). However the ability to generate estimates of liana infestation at scales which align with estimates of carbon stocks may limit the use of certain systems. For example, the detection of lianas in satellite-based imagery has only been possible in large canopy gaps (Foster, Townsend & Zganjar 2008) where the relationship between liana infestation and carbon stocks is evident. Lianas have also been detected using UAVs (Waite *et al.* 2019), however UAV-derived data is captured at ultra-fine resolutions, *i.e.* at the scale of individual leaves, and therefore provides overly detailed information to assess the relationship between liana infestation and carbon stocks at a landscape level.

Airborne-derived data, on the other hand, can provide a middle ground to predict liana infestation at a scale which aligns with predictions of AGC stocks. Advances in technology now include high spectral-resolution sensors which can be used to detect fine spectral differences between species. Studies have shown that lianas and trees are distinguishable as groups based on their spectral response (Castro-Esau, Sánchez-Azofeifa & Caelli 2004; Sánchez-Azofeifa & Castro-Esau 2006). As a result, studies have been able to detect lianas over landscape-scale areas from airborne platforms with hyperspectral and LiDAR sensors in seasonal (Marvin, Asner & Schnitzer 2016) and aseasonal tropical forests (Chandler *et al.* in review). So far, however, spatial patterns of liana infestation have not been linked to carbon dynamics at a landscape-level.

The ability to assess the relationship between liana infestation and AGC stocks at a landscape-level may reveal patterns which do not emerge at the scale of field-based measurements. On the other hand, patterns revealed at the plot-level may be lost when assessed over larger areas. For example, at a landscape-level, variables relating to forest structure and topography are likely to affect the distribution of liana infestation and carbon stocks. Therefore, at a landscape-level, a more representative forest-wide effect of lianas on carbon stocks can be assessed and may also provide unique insights into the mechanisms that drive spatial patterns in the distribution and abundance of lianas.

Here, I therefore assess the relationship between liana infestation and aboveground carbon storage in Sabah, Borneo using landscape-level predictions based upon full waveform airborne laser scanning and hyperspectral data. I relate carbon stocks to liana infestation across three areas of tropical forests, 1) unlogged primary forest and selectively logged forests that have been 2) actively restored or 3) allowed to naturally regenerate. More specifically, focusing within and across forest types, I aim to:

- 1) Assess the distribution of liana infestation;
- 2) Determine the relationship between liana infestation and the size and frequency of canopy gaps;
- 3) Investigate the effect of liana infestation on carbon stocks after accounting for variation in canopy gaps and topography

3.3. Methods

3.3.1. Study site

The study was carried out in an aseasonal tropical forest in Danum Valley, Malaysia (117°48'15.641"E, 4°57'54.822"N). The climate is typical of the aseasonal tropics with an annual rainfall of >2800 mm (Marsh & Greer 1992) and a mean annual temperature of 26.7°C (Walsh 1990). The study area contains a mix of primary and selectively logged lowland dipterocarp forest. Logging took place between 1972 and 1993, followed by a second round of logging from 1999-2010. The amount of timber extracted varied, but averaged 117 m³ ha⁻¹. Active restoration was also implemented in some areas between 1993 and 2004 in the form of climber cutting and enrichment planting of indigenous dipterocarps, fast growing pioneers and fruit trees (Face the Future 2011). The remaining forest was left to regenerate naturally. The location of these three forest types in relation to the airborne-derived imagery are shown in Figure 3.1.

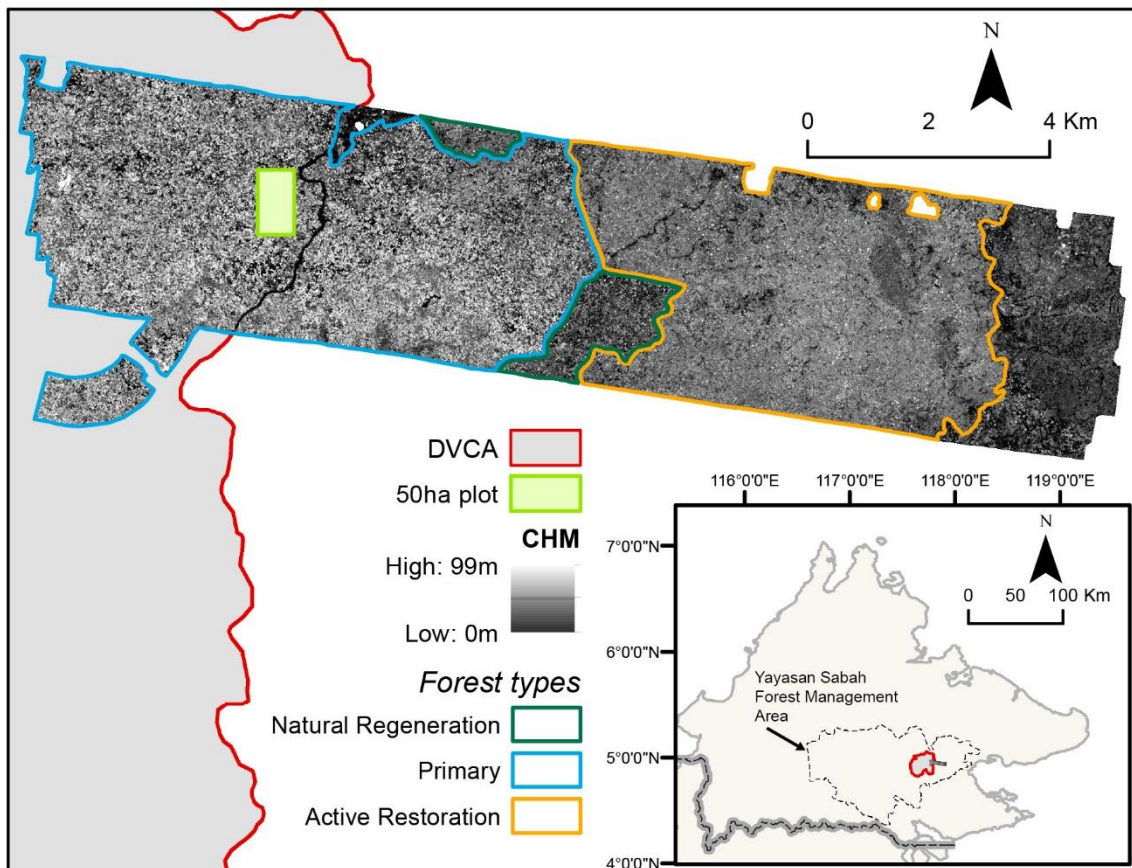


Figure 3.1 Location of the Danum Valley Conservation Area (DVCA) and 50 ha permanent plot in relation to the airborne remote sensing data, in Sabah, Borneo. CHM, Canopy Height Model. Inset: the state of Sabah showing the location of the DVCA within the Yayasan Sabah Foundation Management Area.

3.3.2. Airborne hyperspectral and LiDAR data

Hyperspectral and LiDAR data were captured in November 2014 by a Dornier 228-201 aircraft from the Natural Environmental Research Council (NERC) Airborne Research Facility (ARF). An inbuilt AisaFENIX sensor (Specim Spectral Imaging, Finland) was used to capture hyperspectral data and a Leica ALS50-II system to capture small footprint airborne laser scanning (ALS) data. In total data were collected along 10 flightlines, flown at an altitude of 2335-2429 m and surveying an area covering *ca.* 7500 ha.

The Leica ALS50-II sensor captured both Discrete (DR) and Full Waveform (FW) ALS data, with a point density ranging between 2.80 – 3.16 per m² and a footprint of approximately 22 cm at 1000 m altitude. The DR data were processed using LASTools software (Isenburg 2014) to produce a canopy height model (hereafter referred to as CHM) corresponding to the top-of-Canopy Height (TCH) with a spatial resolution of 1 m.

Hyperspectral imagery were collected using a AisaFENIX sensor (Specim Spectral Imaging, Finland) which uses two parallel sensors to collect continuous spectral reflectance from the visible to short wave infrared (380-2,500 nm) with a spatial resolution of 3 m. The full hyperspectral dataset was radiometrically corrected and an ENVI FLAASH Atmospheric Correction (ENVI version 4.8, Exelis Visual Information Solutions, Boulder, Colorado) was applied. All flightlines were combined and the dimensions of the data were reduced to 10 principal components using a Standardised Principal Component Analysis (SPCA) in an attempt to reduce the computational demand. SPCA uses a correlation matrix which has the same effect as using normalised bands of unit variance (Chang & Yoon 2003). All values were scaled using a min-max normalisation thus ranging between 0 and 1.

3.3.3. Landscape-level liana assessment

Data on the degree of liana infestation in individual tree crowns, which were fully exposed from above, were collected during three field seasons from March 2017 to July 2019. The Canopy Height Model (CHM), pre-loaded on a tablet computer with a GPS connection (GARMIN GLO), was used to locate individual tree crowns to visually assess for liana infestation. If lianas were present, the infestation was classified as the proportion of the tree crown covered by lianas, to the nearest 5%, otherwise, liana cover was set at 0%. The field team consisted of two people, with each person independently estimating the percentage of liana infestation in a tree crown. Each estimate was then discussed and a final estimate mutually agreed (*sensu* Marvin, Asner & Schnitzer 2016). Tree crowns were also manually delineated in the field on the CHM using the GeoEditor application (MapTiler).

A total of 724 trees were delineated with liana canopy cover estimates ranging from 0 to 100%. The spectral values of pixels that were fully inside tree crown boundaries were extracted from the hyperspectral imagery, which yielded a total of 21822 pixels. However, hyperspectral data at the pixel-level do not correspond with liana canopy cover values collected at the tree-level. To overcome this, spectra from trees without liana canopy cover (*i.e.* tree) and trees with canopies severely infested ($\geq 75\%$) with liana leaves (*i.e.* liana) were used. Therefore, each pixel reflects a pure cover of either tree or liana leaves and the spectra associated with either class represents either ends of the liana infestation range (also referred to as end-members). This yielded a total of 7832 pixels from tree crowns without liana infestation and 1979 pixels from those with severe liana infestation.

Prior to training the neural network model, the liana-free and severely liana-infested data were balanced by randomly removing pixels without liana infestation to ensure there was an equal number of data points within each input class (*i.e.* 1979 pixels for each class). The pixels for each class were then randomly split into 80% for training (1583 pixels) and 20% for verification (396 pixels) of the model (*cf.* Olson, Wyner & Berk 2018). I accounted for error in liana canopy cover estimates which may have changed during the time lag (2.5 – 3.5 years) between airborne data acquisition and the ground survey of liana canopy cover estimates. Following the methodology used in Chandler *et al.* (in review), I reclassified 3% of all pixels selected for model training (47 pixels) from the liana-free class to the severely ($\geq 75\%$) liana-infested class and vice versa.

To predict liana infestation across the landscape, a neural network model with resilient backpropagation was used. Resilient backpropagation is often faster than regular backpropagation and doesn't require parameters such as learning rate to be specified (see Appendix 4 for details on neural networks). The model architecture consisted of an input layer with 9 units, corresponding to the discriminating variables (*e.g.* principal components), one hidden layer with 6 units (neurons) and an output layer with 2 units which correspond to either a tree or liana class. The number of hidden layers and neurons are defined subjectively based on trial runs. A sigmoid activation function was used and therefore the predicted values were restricted to a range between 0 and 1, *i.e.* $\sigma(x) \in (0, 1)$. However, rather than producing a single output value, the output from the neural network represents a strength of class membership that a pixel has to each class (Foody 1996). Therefore, the membership value can be used to generate a soft classification output, in this case, the proportion of liana infestation cover for each pixel. The neural network model was run 100 times and after each iteration the model was applied to the entire study landscape. With each iteration I randomly: 1) removed pixels from the no liana infestation class to ensure each input class was balanced, 2) split data for training and verification and 3) permuted 47 pixels into an incorrect class (as above). The final landscape scale liana infestation output is an average of all 100 neural network iterations.

This final liana infestation output (Figure S2.1a) was validated using ground reference liana canopy cover data assessed from a random selection of trees ($n=168$) inside a permanent 50 ha forest plot located in the DVCA (Figure S2.2a). I accounted for error in ground reference data associated with observational uncertainty and the fact ground data were collected 3.5 years after airborne data collection as follows. Firstly, I quantified observational error such that 90% of trees contained a small error of 5% and 4% of trees contained a large error of 30%. Secondly, I allowed 6% of trees to have an error of 50% which represents potential change in liana infestation during the time between the airborne and ground data surveys. Finally, I conducted a Monte Carlo simulation on the ground reference liana canopy cover data to generate random data with a level of variation that encompassed the three degrees of error (*i.e.* 5%, 30% and 50%). Using this approach 100 random values were generated for each of the 168 trees which were used to compare with the 100 predicted liana infestation outputs.

As validation data were at the tree-level, predicted liana infestation values for individual pixels inside the delineated crown boundaries were averaged to derive tree-level estimates of liana canopy cover. To assess the accuracy of the predicted liana infestation outputs, the root mean squared deviation (RMSD) (Eq. 2) was estimated. The final RMSD was an average of all RMSD values for each of the 100 iterations.

3.3.4. Landscape-scale above ground carbon stocks assessment

Tree-level data were collected from a total of 68 permanent forest plots ranging in size from 0.07 to 1 ha (mean size: 0.34 ha) across all three forest types to encompass the wide range of biomass and forest structure. While 1 ha plots may achieve highest accuracies for LiDAR model performance (Zolkos, Goetz & Dubayah 2013; Rejou-Mechain *et al.* 2014), a widely distributed array of plots were required in order to gain a better representation of the full landscape. Therefore, in addition to the use of already established plots of varying sizes, I settled on a plot size of 50x50 m for all new forest plots. Plot censuses were carried out between 2015 and 2018. In each plot, I measured the diameter and identified all trees >10 cm diameter at breast height (1.3 m or above the buttress). Trees were identified in the field where possible and, if not, voucher specimens were collected for identification at a later date. The locations of the plot corners and mid-point were recorded on a GPS (Garmin, Etrex). In addition, I walked the perimeter of a plot two times with tracking enabled on the GPS, because I observed that with this approach a decrease in positional accuracy did not impact the overall boundary to the same degree as by just recording individual corner points.

Using this GPS data, polygons were then drawn in ArcGIS and visually aligned to fit as best as possible to the corner points and tracked boundaries. For each plot, aboveground biomass (AGB, in Mg ha^{-1}) was calculated using the BIOMASS package in R (Réjou-Méchain *et al.* 2017), which provides a workflow to estimate AGB as well as a level of uncertainty in AGB estimates based on the error in allometric models and field measurements. AGB was calculated using the pantropical allometric model: $\text{AGB} = 0.067 * (H * D^2 * WD)^{0.976}$ (Chave *et al.* 2014). Wood density (WD) values for individual trees were obtained from their taxonomy using the global wood density database (Chave *et al.* 2009; Zanne *et al.* 2009). For each taxon, a species-level average was obtained (39% of trees) where possible, or genus- (36% of trees) or family-level (3% of trees) averages when not. If no taxonomic information for the tree was available, a stand-level average (22% of trees) was applied. Tree height (H) was not measured in the field and was therefore estimated using tree diameter (D) and a region-specific H - D model (Feldpausch *et al.* 2012). Using estimates of H and three different H - D models, three additional H - D curves were estimated. All H - D curves were compared and a 'log1' method *i.e.*, $\log(H) = a + b * \log(D)$, (equivalent to a power model) was chosen as the best fit based on the relationship with 50 trees of known D ($D > 140$ cm) and H (Figure S2.3).

In addition, I propagated uncertainty in tree AGB estimates using Monte Carlo simulations (*cf.* Réjou-Méchain *et al.* 2017), which uses, (i) uncertainty in the H - D allometric model (*i.e.* residual standard error of the model associated to tree height), (ii) error associated with the WD estimate (*i.e.* standard deviation at a given taxonomic level), which is known to influence the accuracy of carbon estimates (Phillips *et al.* 2019), and (iii) measurement error in D , where 95% of stems have a typical error of 0.27 cm and 5% of stems have a gross error of 4.63 cm (Chave *et al.* 2004). From this, I obtained 100 estimates of tree AGB for each plot following error propagation over 100 iterations, which represents uncertainty in plot-level AGB. Plot-level AGB was converted into aboveground tree carbon (AGC) stocks by applying a conversion factor of 0.47 (IPCC 2006). Lastly, I applied a correction factor estimated by Jucker *et al.* (2018) to compensate for carbon stored in tree stems with $D < 10$ cm that were not recorded (Jucker *et al.* 2018).

To predict AGC stocks using ALS data, two metrics, in addition to the canopy height model (CHM), were obtained which may provide useful information on the vertical structure of the canopy and therefore beneficial for the accurate prediction of AGC stocks. I obtained i) height of median energy (HOME), which is the distance from the waveform centroid to the ground, and ii) waveform distance (WFD), which is the distance from the beginning of the waveform to the ground (Drake *et al.* 2002). While the WFD metric is often well correlated with LiDAR canopy height (Sun *et al.* 2008), I show variation in WFD values in comparison to CHM and HOME values which may provide additional information on the structural complexity of the forest (Figure S2.4).

From all three datasets (CHM, HOME and WFD), eight landscape-level variables at the plot scale (*i.e.* 50 x 50 m) were produced which can be used to predict AGC stocks at a spatial resolution of 2500 m². Variables included: minimum, maximum, mean, median and standard deviation. I also derived variables relating to canopy cover, defined as the percentage of pixels above or below a given height within each 50 x 50 m area: canopy cover above 20 m ($Cover_{20}$), canopy cover above 40 m ($Cover_{40}$) and canopy cover below 10 m ($Cover_{10}$). Canopy cover above a given height is an effective metric for capturing variation in forest volume (Ni-Meister *et al.* 2010; Coomes *et al.* 2017). In particular, studies have found that canopy cover above *ca.* 20 m was the optimal height for estimating plot-level basal area (Coomes *et al.* 2017; Jucker *et al.* 2018). In contrast to other ALS-derived metrics which have complex nonlinear relations with AGC, that between canopy cover and AGC is linear, irrespective of forest type (Meyer *et al.* 2018).

I accounted for the accuracy of field plot locations by allowing their position to vary by 5 m in any given direction. This process was repeated 100 times and ALS metrics were extracted from each new plot location to derive a geospatial uncertainty (δa). Data were used from 56 of the 68 field plots to fit a model for the prediction of AGC, with the remaining 12 plots used for model validation. Of the 24 variables derived from ALS data, an automated stepwise algorithm was used to identify the best input variables based on their Akaike Information Criterion (AIC) value. To identify variables which are also capable of forming a model that generalises well, I randomly chose 80% of the data to run the stepwise algorithm. This process was repeated ten times to obtain ten top-ranked variable selections. These variables were used in a multiple regression and assessed for their predictive performance by using a ten-fold cross validation (Table S2.2). The optimal model was then used to generate 100 predictions of AGB across the full landscape using the 100 estimates of plot-level AGB to derive uncertainty in predicted AGB (δb).

To validate the model I used the 12 validation plots that were positioned across the landscape using an entirely random distribution in order to comply with good practices for accuracy assessment (Olofsson *et al.* 2014; Stehman & Foody 2019). The model used for the prediction of AGC was applied to ALS-derived variables for each of the 12 plots. Uncertainty derived from the geospatial error of forests plots (δa), plot-level AGB estimates (δb) as well as error in the model used to predict AGC stocks (δc) were propagated, *i.e.* $\delta Q_a = \sqrt{(\delta a)^2 + (\delta b)^2 + (\delta c)^2}$ to estimate an overall uncertainty (δQ_a) in predicted AGC stocks (Figure S2.1b). The relationship between predicted and observed AGC was assessed using the RMSD (Eq. 2) (Figure S2.2b). I also calculated the relative bias, expressed as a percentage

$$\frac{1}{n} \sum_{i=1}^n \frac{Pred-Obs}{Obs} * 100 \quad (3)$$

whereby, *Obs* and *Pred* denote observed and predicted AGC stocks. This gives an indication of the degree to which predicted AGC stocks may be over- or under- predicted relative to ground-derived plot-level AGC stocks.

3.3.5. Relating liana infestation to above ground carbon stocks

Predicted liana infestation across the full landscape was divided into the three forest types in order to compare differences in the degree of liana infestation. I also compared differences in the median and standard deviation of canopy heights to assess differences in forest structure between forest types. Statistical significance can often be an artefact of large sample sizes, such as when using remotely sensed imagery collected over large areas (Lin, Lucas Jr & Shmueli 2013). I therefore used Cliff's *delta*, which is considered a robust measure of effect size (Cliff 2014; Marfo & Okyere 2019), to compare the magnitude of difference between groups. Cliff's *delta* computes the probability that a randomly selected observation from one group is larger than a randomly selected observation from another group, minus the reverse probability, $\frac{\sum[x>y]-[x<y]}{mn}$ where x and y are pixel values from each group and m and n are the number of observations within each group (Cliff 2014). The magnitude of difference between groups is assessed using the thresholds provided in (Romano *et al.* 2006), *i.e.* Cliff's *delta* values >0.474 are considered significant (Torchiano 2017).

To assess the relationship between liana infestation and canopy gaps, the LiDAR-derived CHM and the R package *ForestGapR* (Silva *et al.* 2019) was used to detect canopy gaps across the landscape. Gap definitions vary widely, often due to differences in forest structure and techniques used to detect gaps (van der Meer *et al.* 1994). As the vegetation remaining within gaps after large tree falls can be up to 7 m tall (Lieberman *et al.* 1985), I defined a canopy gap as an area >10 m² and a canopy height <10 m (*cf.* Hunter *et al.* 2015). I overlaid the CHM with a 2500 m² pixel grid as this aligns with spatial resolution of predicted carbon stocks. I calculated the proportion of gap area, the frequency of gaps and the gap size frequency distribution (GSFD) within each 50x50 m pixel. The proportion of gap area was calculated as the number of pixels within a canopy gap divided by the total number of pixels within each 50x50 m area (*i.e.* 2500 pixels), expressed as a percentage. The GSFD was quantified using the parameter λ which relates to the negative slope (exponent) of the relationship between gap size and frequency on a log-log scale (*cf.* Asner *et al.* 2013).

The relationship between liana infestation and AGC was also evaluated whilst accounting for variation derived from the size and frequency of canopy gaps. A generalised linear model was used to predict AGC as a function of liana infestation and the interaction between the proportion of gap area

and the frequency of canopy gaps. I subsequently used this model to predict values of AGC for each forest type allowing liana infestation to vary whilst holding gap area and frequency constant. Additional uncertainty in AGC due to error in the prediction of liana infestation (δd) was estimated by using the 100 predictions of liana infestation obtained in Chandler *et al.* (in review). Here, predictions of liana infestation were obtained over 100 neural network model iterations accounting for error associated with observational uncertainty in liana canopy cover estimates (Chandler *et al.* in review). Uncertainty derived from error in liana infestation (δd), error in the model used to predict AGC stocks (δe) as well as overall uncertainty (δQ_a) in predicted AGC stocks (calculated previously) were combined using summation in quadrature (Bell 2001).

3.4. Results

I found average levels of liana infestation across the full landscape to be significantly higher in the logged forest ($63.9\% \pm 8$ SD) than the primary forest ($44.3\% \pm 7.9$). Furthermore, levels of liana infestation were significantly greater within the naturally regenerating forest ($68.9\% \pm 8.1$) than the actively restored forest ($58.9\% \pm 7.8$), suggesting active restoration, such as liana cutting, may have reduced the degree of infestation (Figure 3.2). Across the landscape, the areas most dominated by lianas were canopy gaps, with $86.8\% \pm 4.2$ of gaps being severely ($\geq 75\%$) liana-infested. Indeed, severe liana infestation in canopy gaps was observed across all forest types, with $85.8\% \pm 4.5$, $90.7\% \pm 3.5$ and $83.9\% \pm 6.3$ of gaps being severely liana-infested in the primary, actively restored and naturally regenerating forests, respectively. However, canopy gaps explained less than half of the total distribution of severe liana infestation pixels, with only $40.7\% \pm 1.5$, $16.5\% \pm 1.2$ and $50.8\% \pm 1.9$ of the severely liana-infested pixels falling within canopy gaps in the primary, actively restored and naturally regenerating forests, respectively. I found that liana infestation was strongly positively related to the proportion of canopy gap area (Figure 3.3a). Furthermore, liana infestation was negatively related to the gap size frequency distribution (λ : Figure 3.3b), indicating that liana infestation is more severe in larger gaps (Figure S2.6).

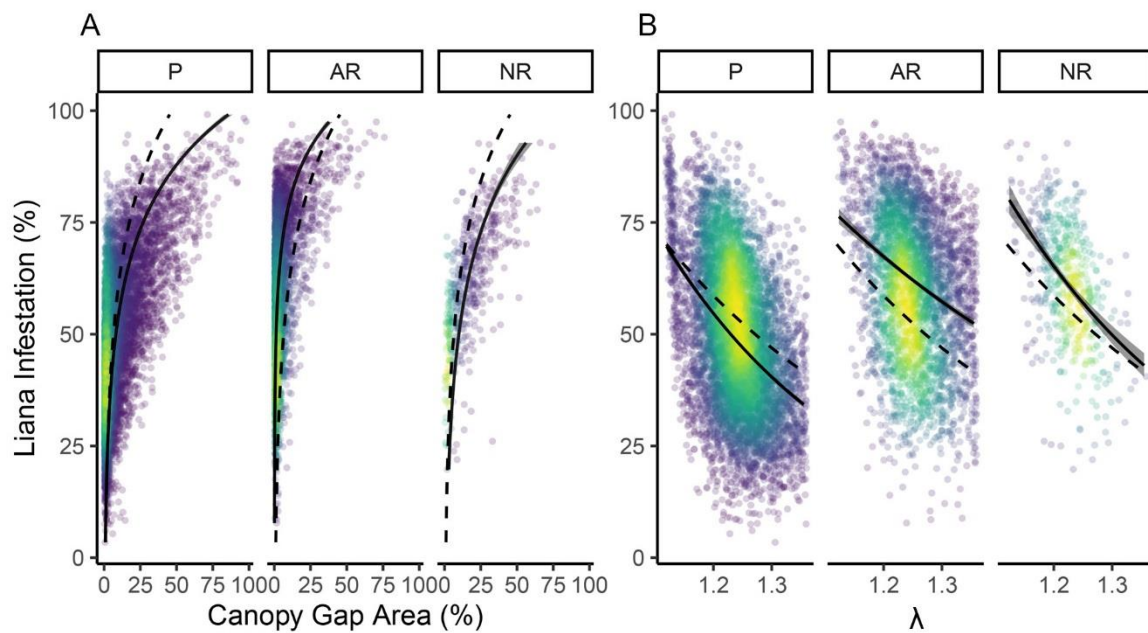
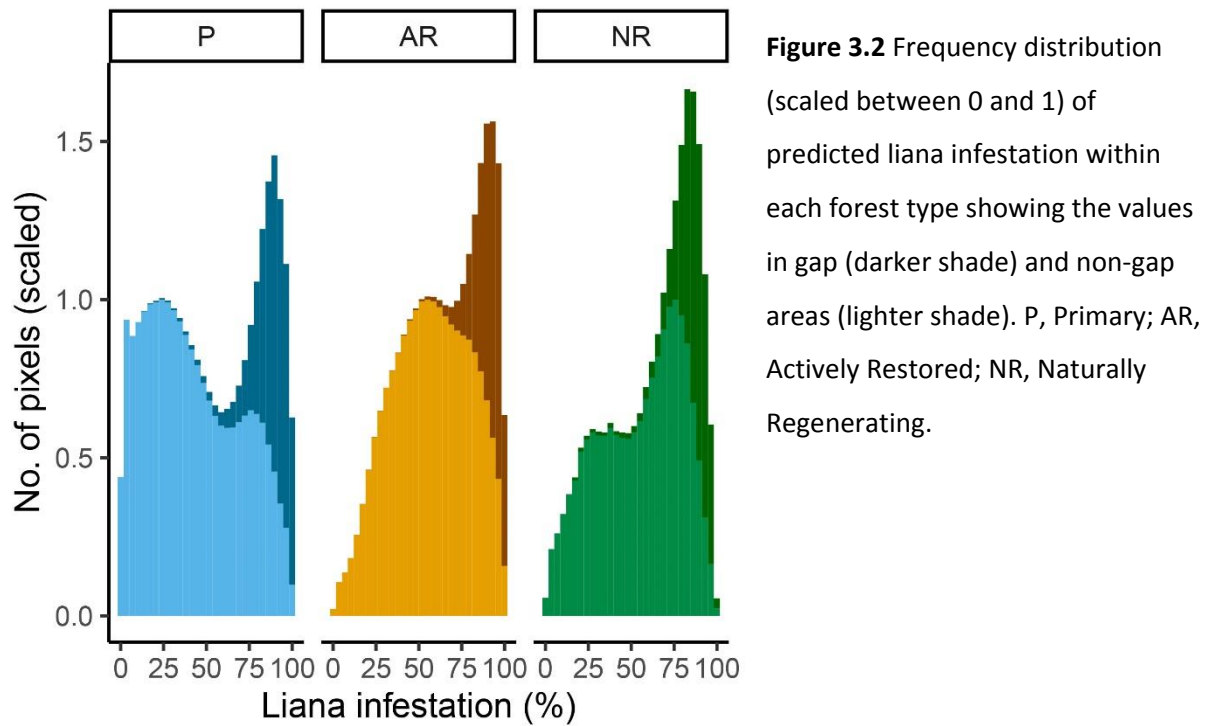


Figure 3.3 Relationship between liana infestation and **a)** the proportion of canopy gap area per 50x50 m pixel and **b)** gap size frequency distribution expressed as λ within each forest type. Solid black lines correspond to generalised linear models for each forest type. Grey shaded bands refer to 95% confidence intervals. Black dashed lines correspond to models fit on the data across all forest types. P, Primary; AR, Actively Restored; NR, Naturally Regenerating.

The optimal model for the prediction of AGC across the landscape included the variables; median of canopy height (TCH_{med}), canopy cover at 20 m canopy height ($TCHcover_{20}$) and canopy cover at 20 m waveform distance ($WFDcover_{20}$):

$$AGC = 13.89 + 6.81 * TCH_{med} + 0.59 * TCHcover_{20} - 1.81 * WFDcover_{20} \quad (4)$$

Predicted and observed AGC stocks showed good correspondence as indicated by an RMSD of 33.5 Mg C ha⁻¹. In addition, I found no systematic over or under prediction of AGC stocks in relation to observed values (bias: 1.8%) (Figure S2.2b). Mean AGC stocks were significantly greater in the primary forest (164.2 Mg C ha⁻¹ ± 40.1) than in the actively restored (141.6 Mg C ha⁻¹ ± 12.3; Cliff's $d=0.44$) or naturally regenerating (108.3 Mg C ha⁻¹ ± 22.8; Cliff's $d=0.78$) forests (Figure S2.5; Table S2.3). There was also a significant difference in mean AGC stocks between the actively restored and naturally regenerating forests (Cliff's $d=0.83$) due to the lower variation in canopy height and a higher gap size frequency (*i.e.* smaller canopy gaps) in the actively restored forest (Figure 3.4, Figure S2.7, Table S2.4). Indeed, canopy height and variation in canopy height varied substantially between forest types (Figure 3.4d,e), with variation in canopy height being significantly greater in the primary forest (median σ : 14.5 m) in comparison to both selectively logged forest types (median σ : 11.3 m and 8.5 m, for naturally regenerating and actively restored forests respectively) (Figure 3.4e,f). Furthermore, canopy height (H) was significantly greater in the primary forest (median H : 33.2 m) than the naturally regenerating (median H : 20.5 m) but not the actively restored (median H : 29.7 m) forest (Figure 3.4d,f).

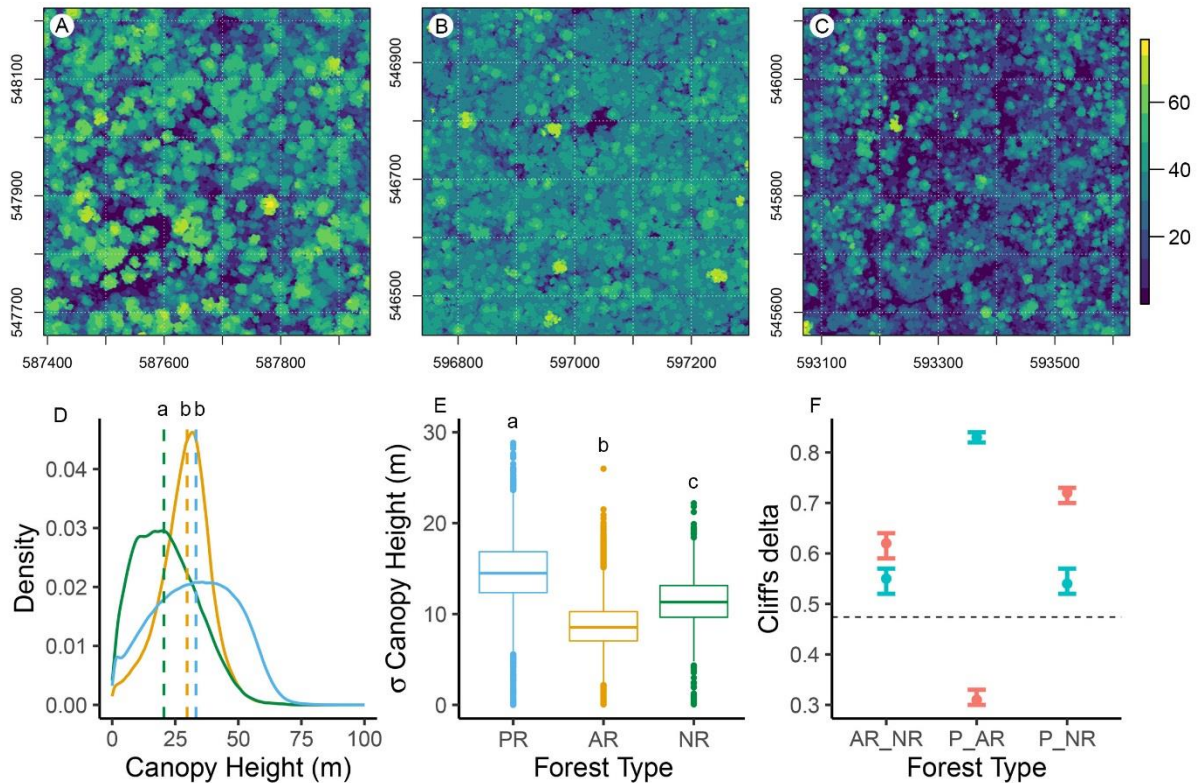


Figure 3.4 Differences in forest structure between the **a**) primary, **b**) active restoration and **c**) natural regeneration forests. Differences were assessed using **d**) median and **e**) standard deviation of canopy height with **f**) Cliff's *delta*, used as an indication of effect size, for comparisons of canopy height (red; panel **d**) and standard deviation of canopy height (blue; panel **e**) values across the three forest areas. Dashed black line corresponds to a Cliff's *d* of 0.474, which is considered significant. Forest areas: AR, active restoration; NR, natural regeneration, and P, primary. Letters in **(d,e)** indicate statistically significant differences between forest types as assessed using Cliff's *delta* effect sizes **(f)**.

Liana infestation was negatively related to carbon stocks across all three forest types (Figure S2.8). After controlling for variation in canopy gaps and topography across the landscape, areas which were completely liana-infested stored on average $59.6 \pm 11 \text{ Mg C ha}^{-1}$ less than areas that were liana-free (Figure 3.5). The effect of liana infestation on AGC differed between forest types. In the primary forest, areas which were completely liana-infested stored on average $85.1 \pm 12.8 \text{ Mg C ha}^{-1}$ less than areas that were liana-free. This difference was smaller in the actively restored ($14.8 \pm 6.4 \text{ Mg C ha}^{-1}$) and naturally regenerating forests ($32.8 \pm 16.2 \text{ Mg C ha}^{-1}$). However, carbon stocks in the severely liana-infested ($\geq 75\%$) areas in the actively restored forest were significantly higher compared to both the primary and naturally regenerating forests (Figure 3.5). Changing the way in which canopy gaps were defined (Table S2.4) did not have a significant impact on the relationship between liana infestation and forest carbon stocks (Figure S2.9).

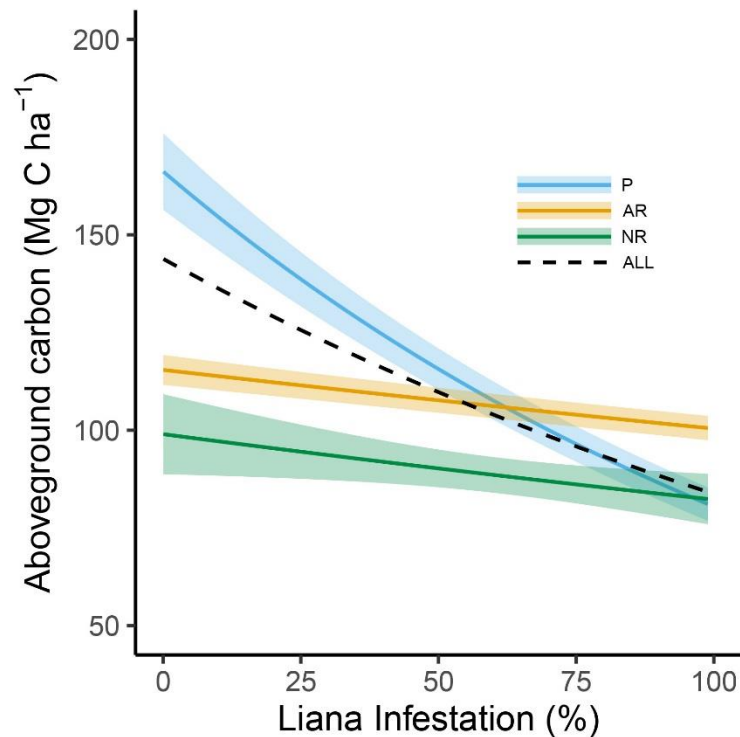


Figure 3.5 Relationship between liana infestation and aboveground carbon stocks (Mg C ha^{-1}) within each forest type. Solid coloured lines refer to predicted carbon stocks derived using a generalised linear model controlling for variation in canopy gaps and topography in the primary (blue), actively restored (orange) and naturally regenerating (green) forests. Black dashed line corresponds to a model fit on all the data. Colour filled bands refer to 95% confidence intervals derived from propagating error at all stages of carbon estimation.

3.5. Discussion

This is the first landscape-level study assessing the impact of liana infestation on aboveground carbon stocks. These results indicate that within Danum Valley, Malaysia, areas of forest completely infested with lianas store on average $59.6 \pm 11 \text{ Mg C ha}^{-1}$ less than areas that are liana-free after accounting for variation in canopy gaps and topography. This corroborates with other studies that have shown a negative relationship between lianas and carbon stocks in tropical forests, whereby an increase in liana abundance is associated with a reduction in carbon stocks that ranged from $\sim 30 \text{ Mg C ha}^{-1}$ to 146 Mg C ha^{-1} across central Amazonia (Laurance *et al.* 2014) and the pantropics (Durán & Gianoli 2013), respectively.

The liana-induced impact on forest-level carbon storage is caused by the effect of lianas on tree growth and mortality which reduces carbon uptake and increases carbon losses (van der

Heijden, Powers & Schnitzer 2015) thus reducing forest-level carbon storage. For example, the probability of mortality for liana-infested trees is two to three times greater than for trees that are liana-free (Phillips *et al.* 2005; Ingwell *et al.* 2010). However, there is also an alternative explanation for this relationship. Liana densities are known to increase in canopy gaps (Schnitzer & Carson 2001; Fig. 3.3) and therefore can be abundant in areas with low carbon stocks, whilst dipterocarp trees, which are tall and carbon-dense (Slik *et al.* 2010), are less often infested by lianas (Wright *et al.* 2015). Subsequently, the negative relationship between liana infestation and carbon stocks may be driven by lianas and/or by other processes. It may therefore be difficult to separate cause and effect when assessing the relationship between lianas and carbon stocks on a landscape level.

Here, variation in canopy gaps was accounted for in the analyses and the results indicate that this negative relationship between lianas and carbon storage holds even in the absence of large mortality event (i.e. canopy gaps; Fig. 3.5). Furthermore, this relationship is still observed in areas where the targeted removal of large dipterocarps has occurred (Fig. 3.5). This provides some indication that lianas are responsible for the reduction in carbon storage on a landscape-scale.

This work also demonstrates for the first time that lianas are negatively associated with carbon stocks in a Palaeotropical forest; a finding which supports previous studies in the Neotropics (Durán & Gianoli 2013; Laurance *et al.* 2014; van der Heijden, Powers & Schnitzer 2015). Furthermore, despite the greater abundance of lianas in dry forest sites, the negative effects of lianas on carbon storage has shown to be stronger in aseasonal forests (Durán *et al.* 2015). Therefore, these findings that lianas are associated with a reduction in tree carbon stocks in an aseasonal tropical forest suggests that lianas are likely to have global consequences for carbon storage and sequestration.

Although average levels of liana infestation were higher within the naturally regenerating ($68.9\% \pm 8.1$) and actively restored ($58.9\% \pm 7.8$) than the primary forest ($44.3\% \pm 7.9$), lianas seem to have a more pronounced effect on carbon storage in the primary forest ($85.1 \pm 12.8 \text{ Mg C ha}^{-1}$) compared to the actively restored ($14.8 \pm 6.4 \text{ Mg C ha}^{-1}$) and naturally regenerating ($32.8 \pm 16.2 \text{ Mg C ha}^{-1}$) forests. There may be two, not necessarily mutually exclusive, explanations for this result.

Firstly, the primary forest is characterised by a relatively high abundance of large emergent dipterocarp trees, which are carbon-dense (Slik *et al.* 2010) but less often infested by lianas due to branch shedding (Wright *et al.* 2015). This may have amplified the difference in AGC stocks between liana-free and severely liana-infested areas in the primary forests, compared to selectively logged forests where dipterocarps have been specifically targeted for removal (Reynolds *et al.* 2011).

Secondly, these tall dipterocarp trees typically have large, emergent crowns which mask liana infestation in tree canopies directly beneath. Liana infestation of the upper canopy, as assessed by an airborne platform, may therefore underestimate the amount of liana infestation in the forest canopy as a whole and artificially enhance the relationship between low liana infestation and high carbon stocks. The greater effect of liana infestation on carbon storage in the primary forest may therefore be driven by differences in the spatial distribution of carbon stocks and an underestimation of forest-level liana infestation enhanced by the presence of emergent dipterocarps.

Nevertheless, these results clearly show that, after removing the effect of canopy gaps, severe liana infestation has the potential to reduce tree above ground carbon. Furthermore, this relationship was examined across primary and selectively logged forests. Given the large alterations to the spatial distribution of aboveground carbon as a result of selective logging, it would be expected that a negative relationship between liana infestation and carbon stocks may be lost in selectively logged areas. Indeed, many variables which are responsible for driving spatial patterns in carbon stocks may have been influenced during selective logging such as a reduction in nutrient availability (Bowd *et al.* 2019; Swinfield *et al.* 2020). However, I show that, within each forest type, a significant reduction in carbon stocks in relation to an increase in liana infestation is still observed, which implies that liana infestation is a strong predictor of AGC (Table S2.5).

These findings also indicate that liana infestation was particularly dominant in canopy gaps across the landscape. Liana infestation is often associated with disturbed or open-canopy patches within forests (Schnitzer, Dalling & Carson 2000; Laurance *et al.* 2001; Schnitzer & Carson 2001; Schnitzer & Bongers 2002; van der Heijden & Phillips 2008; Schnitzer & Carson 2010) and can significantly reduce tree growth and carbon storage potential (Toledo-Aceves & Swaine 2008; Schnitzer & Carson 2010; Schnitzer *et al.* 2014b). While I found that lianas were positively associated with the presence of canopy gaps (Figure 3.3a), I also found that the severity of liana infestation increased with the size of canopy gaps (Figure 3.3b and Figure S2.6). Light availability typically increases with increasing gap size (Babweteera, Plumptre & Obua 2000) and therefore light levels may not be sufficient in smaller gaps to promote the establishment or high growth rate of lianas (Denslow, Ellison & Sanford 1998). Similarly, Gerwing & Uhl (2002) found liana cover to be substantially greater in conventional logging gaps in comparison to reduced impact logging gaps that had average gap areas of 260 m² and 160 m², respectively. Additionally, Schnitzer, Dalling and Carson (2000) found that low canopy height, liana-dominated gaps had almost four times greater total stem density in comparison to higher-canopy height gaps.

There are a number of limitations to the current study. Firstly, limitations in predicting liana infestation across the landscape may have contributed towards differences in the relationship between liana infestation and AGC stocks observed in the primary and logged forests. A large proportion of the training data used in the neural network modelling was based on data collected within the primary forest. Generally, spectral reflectance in primary forests is lower than in logged forests (Huete *et al.* 2008; Tangki & Chappell 2008). The structure of logged forests is often characterised by a single canopy layer, with relatively few canopy gaps, whereas undisturbed forests are characterised by a mix of tree sizes with multiple canopy layers and larger canopy gaps (Lamb 2011; Baccini *et al.* 2012) (Figure S2.7, Table S2.4). Therefore, the greater structural heterogeneity in the primary forest increases tree shadow which decreases reflectance (Tangki & Chappell 2008), particularly in the SWIR bands (Cohen & Spies 1992; Baccini *et al.* 2004). This effect may also be more pronounced due to the higher proportion of tall, emergent dipterocarps. Subsequently, the application of the model across the logged forest may have over-predicted liana infestation, which, in turn, may have affected the strength of the relationship between liana infestation and forest carbon stocks. However, despite this, I show that predicted liana infestation in low ($\leq 25\%$) and severe ($\geq 75\%$) classes was 100% accurate in relation to ground reference data (Table S2.1). Therefore, even with a decrease in the accuracy of predicted liana infestation, it is unlikely that the difference in carbon stocks in relation to areas that are liana-free and severely liana-infested will have changed significantly.

Secondly, as airborne-derived data contain both atmospheric and surface information, atmospheric corrections must be applied in order to allow accurate inference of Earth surface properties. However, atmospheric corrections are typically homogenous despite the fact that conditions vary across the landscape. As the spectral reflectance between trees and lianas varies only in the magnitude of reflectance and not within the shape of the spectra, differences in atmospheric conditions may lead to classification inaccuracies. However, I show good accuracy in predicted liana infestation in comparison to ground reference liana canopy cover. Therefore the severity of liana infestation appears to have a stronger effect than any potential atmospheric correction inaccuracies.

Lastly, while airborne surveys can provide high spatial and spectral resolution data which may be unmatched in terms of their ability to capture the spectral and structural properties of the forest, a major limitation is the cost. This can be particularly prohibitive for monitoring where repeated surveys are required. Our ability to monitor change in liana infestation over time will be essential to accurately quantify the liana-induced effect on carbon storage as well as to target appropriate conservation action and prevent excessive losses to carbon and biological diversity.

3.6. Conclusion

The ability to assess the relationship between liana infestation and above ground carbon stocks over large areas is essential to fully understand the impact of liana infestation on carbon storage. Data collected with field-based measurements may be biased by local conditions and may not capture sufficient variation to assess the forest-wide relationship between liana infestation and carbon stocks. However, all studies on liana-carbon relationships have been conducted at the plot-level and the majority of these have been conducted in the Neotropics. Using remote sensing technologies I show that it is possible to accurately assess the distribution of liana infestation at a landscape-level. My findings show that liana infestation is a strong predictor of carbon stocks across primary and selectively logged forests in Sabah, Malaysia. I found that areas severely infested by lianas stored on average $59.6 \pm 11 \text{ Mg C ha}^{-1}$ less than areas that were liana-free. Understanding the distribution of lianas over large areas, and across areas which may be inaccessible on the ground, can provide unique insights into the mechanisms that drive their distribution, help to quantify the forest-wide liana-induced effect on carbon storage, and provide a useful tool for conservation and forest management focused on liana control. It is currently unclear whether an increase in liana biomass and abundance is occurring pantropically (Schnitzer & Bongers 2011; Bongers *et al.* 2020). However, the strong control that lianas seem to exert on the carbon storage potential of aseasonal Palaeotropical forests, as well as Neotropical forests, indicates that any change in liana proliferation pantropically may impact on the storage of carbon with potential global implications for the rate of climate change.

Chapter 4: Detection of spatial and temporal patterns of liana infestation using satellite-derived imagery³

4.1. Abstract

1. Lianas (woody vines) play a key role in tropical forest dynamics because of their strong influence on tree growth, mortality and regeneration. Assessing liana infestation over large areas is critical to understand the mechanisms that drive their spatial distribution and to monitor change over time. However, it currently remains unclear whether satellite-based imagery can be used to detect liana infestation across closed-canopy forests and therefore if satellite-observed changes in liana infestation can be detected over time and in response to climatic conditions.
2. Here, I aim to determine the efficacy of satellite-based remote sensing for the detection of spatial and temporal patterns of liana infestation across a primary and selectively logged aseasonal forest in Sabah, Borneo. I used predicted liana infestation derived from airborne hyperspectral data to train a neural network classification for prediction across four Sentinel-2 satellite-based images from 2016 to 2019.
3. Results showed that liana infestation was positively related to an increase in Greenness Index (GI), a simple metric relating to the amount of photosynthetically active green leaves. Furthermore, this relationship was observed in different forest types and during (2016), as well as after (2017-2019), an El Niño-induced drought.
4. Using a neural network classification, I assessed liana infestation over time and showed an increase in the percentage of severely ($\geq 75\%$) liana-infested pixels from $12.9\% \pm 0.63$ (95% CI) in 2016 to $17.3\% \pm 2$ in 2019. This implies that reports of increasing liana abundance may be more wide-spread than currently assumed.
5. This is the first study to show that liana infestation can be accurately detected across closed-canopy tropical forests using satellite-based imagery. Furthermore, the detection of liana infestation during both dry and wet years and across forest types suggests this method should be broadly applicable across tropical forests. This work therefore advances our ability to explore the drivers responsible for patterns of liana infestation at multiple spatial and temporal scales and to quantify liana-induced impacts on carbon dynamics in tropical forests globally.

³ Chandler, C.J., van der Heijden, G.M.F., Boyd, D.S & Foody, G.M. (in prep). Detection of spatial and temporal patterns of liana infestation using satellite-derived imagery.

4.2. Introduction

Lianas (woody vines) are a pervasive component of tropical forests (Pérez-Salicrup 2001; Schnitzer *et al.* 2012). They are non-self-supporting structural parasites that use the architecture of trees to extend their leaves to the forest canopy (Schnitzer & Bongers 2002). As competition between lianas and trees is stronger than tree-tree competition (Tobin *et al.* 2012), lianas can negatively impact the growth (Grauel & Putz 2004; van der Heijden & Phillips 2009) and survival of their host (Phillips *et al.* 2005; Ingwell *et al.* 2010) and therefore suppress the ability of tropical forests to sequester and store carbon (van der Heijden, Powers & Schnitzer 2015).

Lianas have been proliferating in some tropical forests (Phillips *et al.* 2002; Schnitzer & Bongers 2011), which may lead to a stronger negative impact on carbon storage and sequestration in these areas. Several putative mechanisms have been suggested for this increase, such as elevated atmospheric CO₂, an increase in forest disturbance and an increase in the frequency and severity of droughts (Schnitzer & Bongers 2011). However, it is currently still unknown which driver(s) may be responsible for changes in liana biomass and abundance over time. Additionally, while there is compelling evidence that lianas are increasing in many Neotropical forests (Laurance *et al.* 2001; Phillips *et al.* 2002), this may not be a global phenomenon (Bongers *et al.* 2020). This suggests that liana proliferation over time may be driven by regional rather than global drivers. However, in order to provide insights into the mechanisms responsible for changes in liana abundance and to test whether these differ geographically, wide-spread monitoring of lianas over time and across large areas is essential.

Most previous studies which have assessed temporal changes in liana abundance, biomass or infestation have been based on ground data collected from permanent sampling plots (Phillips *et al.* 2002; Wright *et al.* 2004; Laurance *et al.* 2014). However, while field-based studies may not be limited in their geographical extent, they are limited by the total area that can be feasibly sampled. This may be particularly problematic if plot-based research is unable to capture sufficient variation in environmental variables through space and time to disentangle the driving forces behind change (*cf.* Di Vittorio *et al.* 2014; Espírito-Santo *et al.* 2014).

Remote sensing technologies may provide a solution to extend field-based knowledge to larger spatial and temporal scales. However, they are dependent on the ability to detect liana infestation. Many studies have shown that lianas, as a plant group, can be distinguished from trees based on their spectral reflectance, particularly in the visible- (400–690 nm) and Near Infrared (NIR)-region (700–1340 nm) (Castro-Esau, Sánchez-Azofeifa & Caelli 2004; Sánchez-Azofeifa & Castro-Esau 2006; Kalacska *et al.* 2007; Hesketh & Sánchez-Azofeifa 2012; Guzman, Rivard & Sánchez-Azofeifa

2018), as well as thermal properties (Sanchez-Azofeifa *et al.* 2011; Guzmán *et al.* 2018).

Subsequently, recent research has successfully detected lianas using data acquired from; UAVs, fitted with RGB (Li *et al.* 2018; Waite *et al.* 2019) and thermal (Yuan *et al.* 2019) sensors, satellite imagery (Foster, Townsend & Zganjar 2008) and airborne hyperspectral imagery in seasonal (Marvin, Asner & Schnitzer 2016) and aseasonal forests (Chandler *et al.* in review). While airborne sensors have the potential to provide high spatial and spectral resolution imagery which can be used to detect liana infestation at landscape-scales, satellite-based sensors can typically afford more frequent measurements across much larger geographical extents. However, there are a number of limitations which may pose challenges for assessing liana infestation with satellite-based remote sensing.

Firstly, spectral reflectance derived from multispectral satellites can be limited in scope as data represent non-contiguous regions of the light spectrum. Thus, a single value for each band is associated with the spectral reflectance from large regions of the spectrum (Asner 1998). Crucially, however, some bands cover smaller regions than others and may align with areas of the spectrum that are important for the discrimination of lianas and trees. However, this may limit the accurate detection of liana infestation to specific satellite sensors, which have spectral bands that represent similar regions of the spectrum. For example, research by Foster *et al.* (2008) assessed the spatial distribution of liana infestation in large canopy gaps using satellite-based hyperspectral imagery (EO-1 Hyperion: 220 10-nm bands covering 400-2500 nm). However, while Hyperion imagery was used to detect liana-dominated patches for training purposes, the prediction of liana infestation across Landsat imagery was achieved by using minimum values of brightness and greenness. The use of a simple vegetation index, such as greenness, which relates to the amount of photosynthetically active green leaves, is attractive for its ability to transfer across different sensors. However, as the study by Foster *et al.* (2008) was conducted in the dry season and the detection of lianas was limited to severely liana-dominated patches, it remains unclear whether multispectral satellite-based imagery, or a simple vegetation index, could be used to successfully detect liana infestation across a dense, closed-canopy aseasonal forest.

Secondly, variation in spectral reflectance between forest types may restrict the detection of lianas over broad geographical-scales if the difference is greater than that of trees and lianas. For example, logged forests typically have higher spectral reflectance compared to primary forests (Huete *et al.* 2008; Tangki & Chappell 2008). Differences in spectral reflectance may be driven by the fact that the canopies of logged forests are typically more homogenous whereas those of primary forests contain a mix of tree sizes and multiple canopy layers (Lamb 2011; Baccini *et al.* 2012). This greater structural heterogeneity can result in an increase in tree shadow and a decrease in overall

reflectance in primary forests (Tangki & Chappell 2008) which in turn may affect predictions of liana infestation (*cf.* Pinter Jr *et al.* 1985).

Thirdly, liana chemistry tends to converge with that of trees in aseasonal tropical forests or those with high annual precipitation (Asner & Martin 2012) and therefore reflectance spectra for lianas and trees are not as clearly separable (Castro-Esau, Sánchez-Azofeifa & Caelli 2004; Sánchez-Azofeifa *et al.* 2009). Higher reflectance of liana leaves has been shown to be strongly related to the level of chlorophyll content (Castro-Esau, Sánchez-Azofeifa & Caelli 2004), which is known to be more similar in wet conditions or within aseasonal forests (Sánchez-Azofeifa *et al.* 2009). As a result, differences in satellite-derived spectral reflectance between lianas and trees is likely to be more difficult in aseasonal forests, particularly if spectral resolution is limited to relatively few wavebands. It is therefore essential to test whether lianas can be detected in aseasonal tropical forests using satellite-based remote sensing in order to advance our ability to assess the spatial distribution of liana infestation globally.

Here, I therefore aim to determine the efficacy of satellite-based remote sensing for the detection of liana infestation across an aseasonal tropical forest in Sabah, Borneo. Additionally, I assess the detectability within primary and selectively logged forests as well as during and after a period of El Niño-induced drought. I therefore aim to test whether 1) liana infestation can be detected in satellite-based imagery using a neural network classification trained by airborne-derived liana infestation, 2) one single vegetation index is capable of detecting liana infestation, 3) a response to drought facilitates the differentiation in spectral reflectance for lianas versus trees and 4) temporal changes in liana infestation can be observed using a time-series of satellite-based imagery.

4.3. Methods

4.3.1. Study area

This study was based in an aseasonal tropical forest in Danum Valley, Malaysia which contains a mix of primary and selectively logged lowland dipterocarp forest (Figure 4.1). The Danum Valley Conservation Area (DVCA) represents a large swathe (438 km²) of intact primary tropical forest. The area surrounding the DVCA has been selectively logged at varying intensities between 1972 and 1993 (Reynolds *et al.* 2011). The climate is typical of the aseasonal tropics with a mean annual temperature of 26.7°C and an average yearly rainfall of 2,900 mm (O'Brien *et al.* 2019). Borneo has one of the most aseasonal climates of any tropical region (Whitmore 1984), although droughts do occur infrequently and usually in association with an El Niño event (Walsh & Newbery

1999; Chapman *et al.* 2020). The vegetation within the primary forest is dominated by dipterocarps (Kettle, Maycock & Burslem 2012), whereas the logged forest has received targeted removal of larger dipterocarps and now has a higher proportion of fast-growing, early successional species (O'Brien *et al.* 2019).

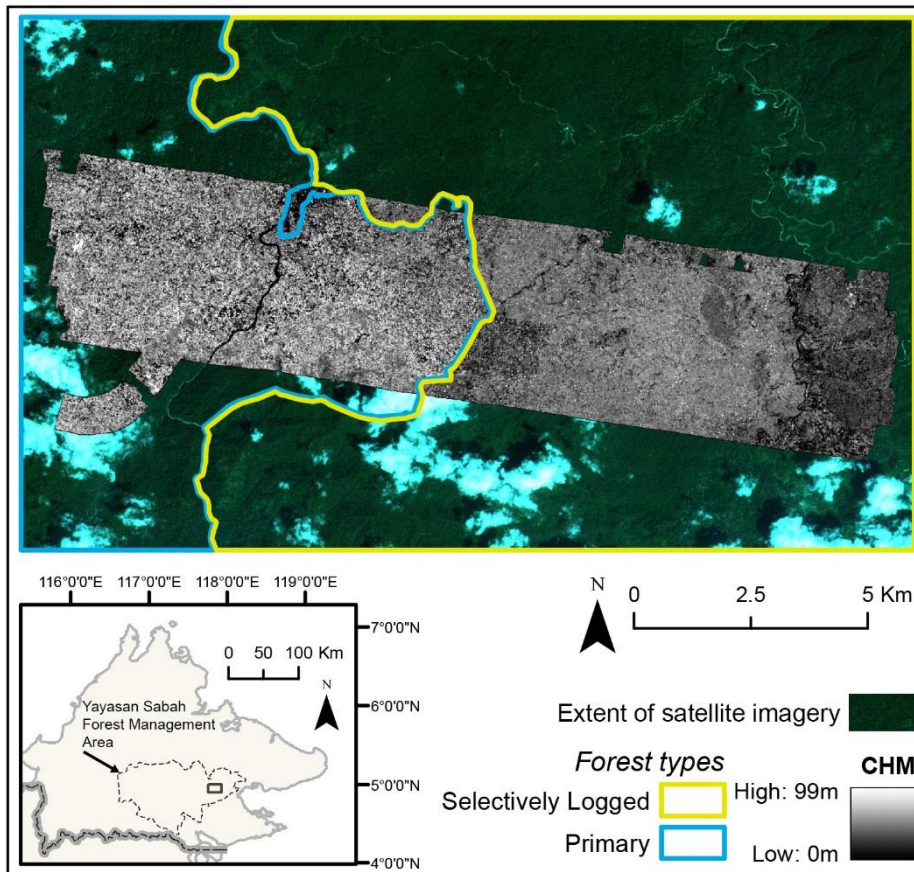


Figure 4.1 Location of the study area in Sabah, Malaysia, showing the extent of the air- and space-borne remotely sensed imagery across a primary and selectively logged tropical forest.

4.3.2. Airborne-derived liana infestation assessment

Hyperspectral and LiDAR data were captured in November 2014 by the Natural Environmental Research Council (NERC) Airborne Research Facility (ARF). An inbuilt AisaFENIX sensor (Specim Spectral Imaging, Finland) was used to capture hyperspectral data from the visible to short wave infrared (380-2,500 nm) with a spatial resolution of 3 m. A Leica ALS50-II system was used to capture both Discrete (DR) and Full Waveform (FW) airborne laser scanning (ALS) data with a spatial resolution of 1 m. Full details on the airborne data collection is provided in Chapter 2, Section 2.3.2.

Liana canopy cover data were collected in the field over a three-year time period (2017-2019). Individual tree crowns, which were fully exposed from above, were identified using a tablet computer connected to a GPS with a Canopy Height Model (CHM) preloaded. Tree crowns were then visually assessed, by a minimum of two people, to estimate the degree of liana infestation to the nearest 5%. Each estimate was discussed and a final estimate mutually agreed (*sensu*. Marvin, Asner

& Schnitzer 2016). Tree crowns were then manually delineated on the CHM using the GeoEditor application (MapTiler).

A total of 724 trees were delineated with liana canopy cover estimates ranging from 0 to 100%. This corresponded to 21,822 pixels from the hyperspectral imagery that were fully inside tree crown boundaries. Airborne hyperspectral data were used to train a neural network classification to predict liana infestation across the full extent of the airborne survey. I accounted for error in liana canopy cover estimates which may have changed during the time lag (2.5 – 3.5 years) between airborne data acquisition and the ground survey of liana canopy cover estimates. Following the methodology used in Chandler *et al.* (in review), I reclassified 3% of all pixels selected for model training from the liana-free class to the severely ($\geq 75\%$) liana-infested class and vice versa. The neural network model was run 100 times and after each iteration the model was applied to the entire study landscape. The average of the 100 neural network outputs was used to produce a final landscape scale liana infestation map. Full details on the landscape-level liana assessment can be found in Chapter 2, Section 2.3.2.

4.3.3. Satellite-derived liana infestation assessment

Freely available bottom of atmosphere reflectance Sentinel-2 imagery were downloaded from the United States Geological Survey (USGS) Earth Explorer (<https://earthexplorer.usgs.gov/>). The earliest image with limited cloud cover to use in combination with airborne imagery (2014), was obtained in May 2016. This also aligned with the end of an El Niño-induced drought period in which there were higher temperatures (Thirumalai *et al.* 2017) and a significant reduction in precipitation between November 2015 and April 2016 in Danum Valley Conservation Area (DVCA) (Nunes *et al.* 2019). Additional imagery were collected in approximately one-year time intervals, depending on when cloud-free images could be obtained (*i.e.* November 2017, June 2018 and April 2019). Areas contaminated by cloud and cloud shadow were manually delineated and removed from each image. As the spatial resolution of Sentinel-2 bands range from 10 m to 60 m all bands were resampled to a spatial resolution of 10 m so they could be aligned at the same scale. These images were then used to produce a time series in order to assess whether changes in liana infestation can be observed over time.

To identify which spectral bands from Sentinel-2 imagery may be most important for discriminating lianas from trees, the difference in spectra derived from airborne hyperspectral imagery for liana-free and liana-infested ($\geq 75\%$) trees specifically within the Sentinel-2 spectral band regions were assessed. I calculated the average difference in reflectance between the two infestation

classes for all hyperspectral bands that aligned with Sentinel-2 spectral regions. This revealed that the green band was most important for discriminating between trees and lianas (Figure S3.1).

A variety of vegetation indices were also calculated to assess whether one simple metric is capable of discriminating between liana-free and liana-infested pixels. As the green band was the most effective, I specifically calculated indices that may promote signals in the green spectrum such as, Greenness Index (GI) which has shown to outperform other indices when discriminating vegetation using the visible spectra (Woebbecke *et al.* 1995). I assessed which vegetation index was most effective at separating severely ($\geq 75\%$) and low ($\leq 25\%$) liana-infested pixels by comparing their effect size (Table S3.1). Cliff's *delta*, which is considered to be a robust measure of effect size, was used to calculate the magnitude of difference between the two groups (Cliff 2014). Cliff's *delta* computes the probability that a randomly selected observation from one group is larger than an observation from another group, $\frac{\sum[x>y]-[x<y]}{mn}$ whereby x and y are liana-free and severely liana-infested pixels and m and n are the number of pixels within each group.

To assess whether a single vegetation index could be used to detect liana infestation in satellite imagery over broad spatial scales I tested whether the vegetation index varied in response to forest type (*i.e.* primary and selectively logged forests) as well as during and after a period of El Niño-induced drought (*i.e.* across years). Subsequently, a linear regression model with an interaction term was used to allow the effect of airborne-derived liana infestation on the vegetation index to vary by forest type or year. A linear mixed effects model was also used to account for variation in forest type. I tested whether the relationship between the vegetation index and liana infestation differed across the four years by using a pairwise comparison of the slope coefficients.

To predict liana infestation in satellite imagery a neural network classification was performed, trained using the airborne liana infestation output. To accurately predict liana infestation in satellite-based imagery as well as to test the efficacy of a single vegetation index liana infestation was modelled using three different sets of input variables: 1) vegetation index only, 2) all Sentinel 2-bands and 3) all Sentinel 2-bands and the vegetation index.

The same model construction and process was applied (as in the airborne-derived liana infestation assessment). As the spatial resolutions of the satellite (10 m) and airborne (3 m) imagery do not match, I degraded the resolution of the airborne imagery so both products had a resolution of 10 m. Pixels from the airborne-derived liana infestation output classified as having no infestation or completely liana-infested were used as training data. Values greater than 95% were therefore classified as a 'liana' and values less than 5% were classified as a 'tree'. This yielded a total of 3622 pixels with no (<5%) liana infestation and 6128 pixels completely (>95%) liana-infested. Data were

balanced to ensure there was an equal number of data points within each input class (*i.e.* 3622 pixels). Data were split 80% for training and 20% for verification. The neural network model was run 100 times and after each iteration the model was applied to the entire study landscape. I propagated error associated with uncertainty in the airborne liana infestation assessment (Chapter 2, section 2.3.6) by using each of the 100 airborne-derived liana infestation outputs to train the satellite-based models. With each iteration I repeated the following steps; 1) removed pixels that were completely liana-infested to ensure each input class was balanced and 2) split data for training and verification. A final satellite-derived liana infestation map was calculated by averaging all of the 100 neural network outputs.

To reliably assess a degree of change in predicted liana infestation over time, I focused on change between low [$\leq 25\%$] and severe [$\geq 75\%$] liana infestation classes within the primary forest. Individual neural network models were trained for each of the four years. The percentage of pixels classified as having either low or severe liana infestation were calculated for each year to indicate a level of change over time. Additionally, the percentage of pixels that changed from low to severe and vice versa from 2016 to 2019 were calculated. This process was repeated for each of the 100 satellite-derived liana infestation outputs. This allowed for a calculation of uncertainty around estimates of change in liana infestation over the four years.

4.3.4. Accuracy assessment

To assess the accuracy of the satellite-derived liana infestation output a random selection of pixels ($n=200$) from both the airborne- and satellite-derived liana infestation outputs were used. This process was repeated 10 times and the relationship between the predictions were assessed after each iteration. To assess the accuracy of the predicted liana infestation outputs the root mean squared deviation (RMSD) (Eq. 2) and relative bias (Eq. 3) were calculated.

To increase the level of confidence around estimates of liana infestation I also degraded outputs to an ordinal scale by partitioning predicted liana infestation into four groups as follows: neural network membership values equal to or below 0.25 were set to 'low', values between 0.26 and 0.50 were set to 'medium', values between 0.51 and 0.74 were set to 'high' and values equal to or greater than 0.75 were set to 'severe'. To assess the accuracy of liana infestation classes, I produced a confusion matrix using satellite-derived liana infestation (predicted) and airborne-derived liana infestation (observed) and calculated the overall accuracy, specificity, sensitivity, balanced accuracy and area under the curve (AUC). The accuracy assessment for the airborne-derived liana infestation output is detailed in Chapter 2, Section 2.3.8.

4.4. Results

Satellite-based spectral reflectance in the visible spectrum, and predominantly in the green reflectance region, was most effective at separating low ($\leq 25\%$) and severe liana infestation ($\geq 75\%$) classes derived from airborne-hyperspectral data (Figure S3.1). Subsequently, I found Greenness Index (GI) to be the most effective vegetation index for discriminating between low and severe liana infestation (Table S3.1). I also found that average predicted greenness values derived from satellite imagery increased significantly in response to an increase in liana infestation and were significantly greater in the logged forest in comparison to the primary forest (Figure 4.2a, Figure S3.4). In addition, average predicted greenness values were positively related to liana infestation in all four years (Figure 4.2b; Figure S3.2). However, there was a greater increase in greenness relative to an increase in liana infestation in 2016 (drought year) in comparison to other years, as shown by significant differences in slope coefficients (Table 4.1). Slopes did not differ between the three non-drought years, except for a weak significant difference between 2017 and 2018 (Table 4.1).

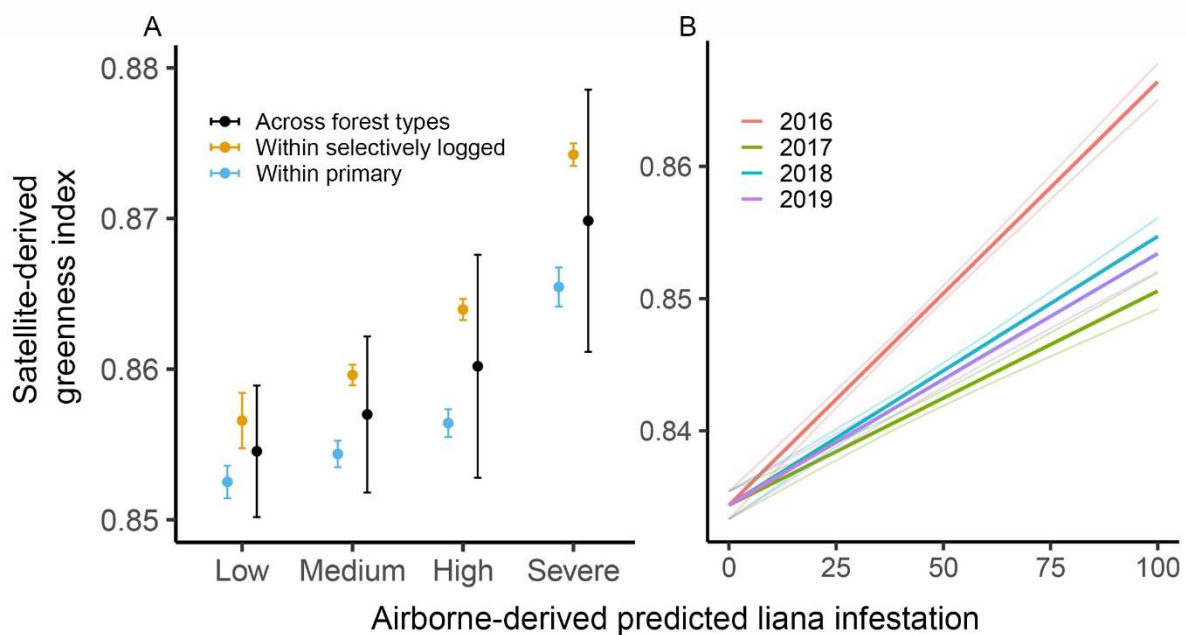


Figure 4.2 Satellite-derived predicted mean greenness **a)** combined for all years (2016-2019) across forest types (black) and within the primary (blue) and selectively logged (orange) forests in response to airborne-derived liana infestation classes and **b)** for each year in response to airborne-derived liana infestation percent cover. Liana infestation classes are defined as: Low [$\leq 25\%$], Medium [26-50%], High [51-74%] and Severe [$\geq 75\%$]. Error bars are 95% confidence intervals based on error in model fit as well as uncertainty derived from error in airborne-derived liana infestation estimates.

Table 4.1 Pairwise comparison of linear regression slope coefficients (in Figure 4.2b). *P* values adjusted using Bonferroni correction. Significance level set at 0.05.

Contrast (years)	Estimate	SE	df	t	<i>p</i>
2016 – 2017	0.01583	0.00158	34852	10.038	<.0001
2016 – 2018	0.01170	0.00158	34852	7.415	<.0001
2016 – 2019	0.01300	0.00158	34852	8.240	<.0001
2017 – 2018	-0.00414	0.00158	34852	-2.623	0.0524
2017 – 2019	-0.00284	0.00158	34852	-1.798	0.4330
2018 – 2019	0.00130	0.00158	34852	0.825	1.0000

A neural network classification using GI as the only input variable was not capable of accurately predicting liana infestation in satellite-based imagery (Figure 4.3a,d). While predicted mean greenness values showed a clear increasing trend in response to an increase in liana infestation (Figure 4.2), large variation in greenness values ultimately limited its use as a single predictor variable (Figure 4.3a,d; Table S3.2). Using all Sentinel-2 bands without GI increased the accuracy of satellite-based predictions in the primary (AUC: 0.76) and logged (AUC: 0.7) forests (Figure 4.3b,e; Table S3.2). Furthermore, combining all Sentinel-2 bands and GI provided a further increase in accuracy within the primary (AUC: 0.8) and logged (AUC: 0.71) forests (Figure 4.3c,f; Table S3.2). In addition, I found a larger underestimation of satellite-derived liana infestation, relative to liana infestation obtained from airborne data, in the logged forest (bias = -15.5% and -14.8%) in comparison to the primary forest (bias = -9.5% and -6.2%) for the model using only Sentinel-2 bands and the model using Sentinel-2 bands and GI, respectively.

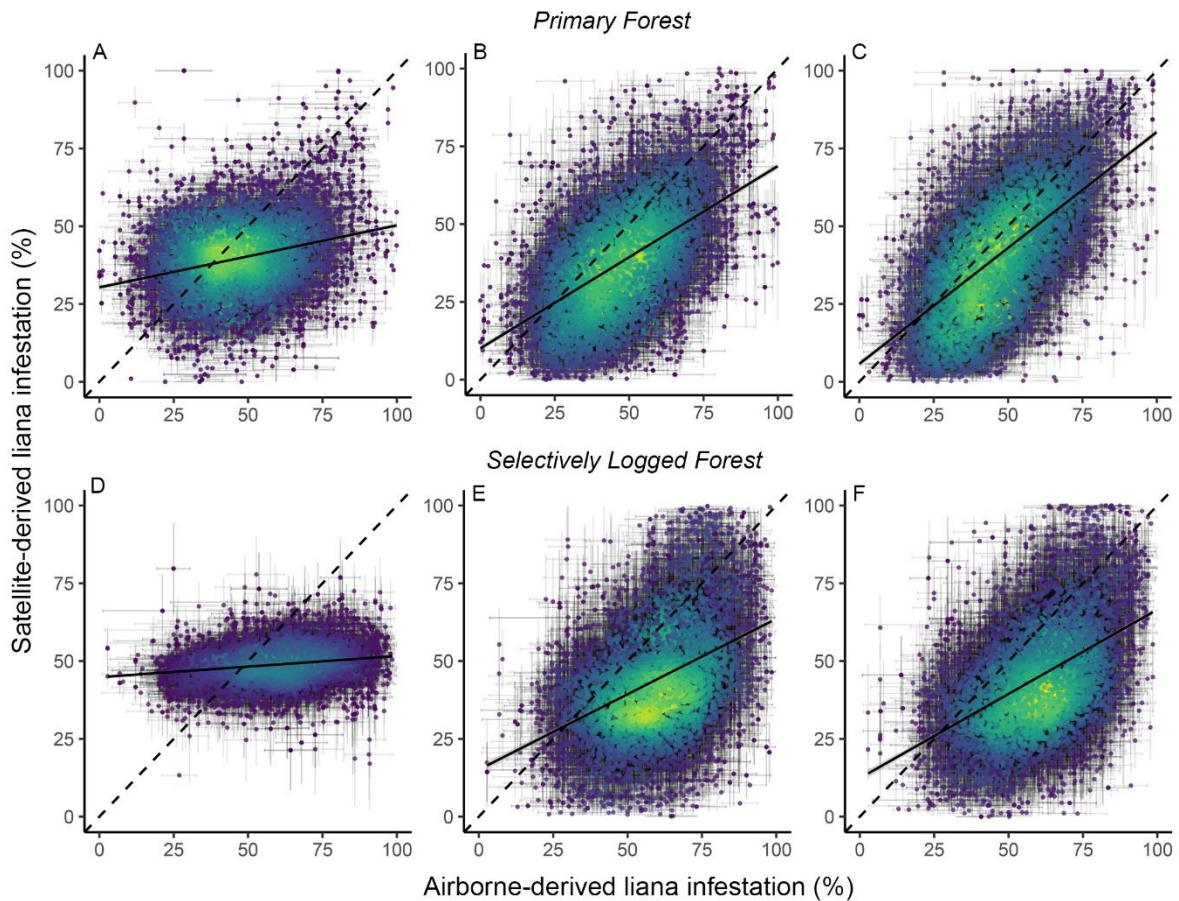


Figure 4.3 Relationship between airborne- and satellite-derived liana infestation using **a, d)** Greenness Index, **b, e)** all Sentinel-2 bands and **c, f)** Greenness Index and all Sentinel-2 bands as input variables in the primary and selectively logged forests, respectively. Dashed lines represent a 1:1 lines. Solid black lines correspond to linear models. Coloured points correspond to the density of overlapping points ranging from purple to yellow with increasing density. Error bars represent ± 1 standard deviation.

To assess change in liana infestation over time I used the output from the model using Sentinel-2 bands and GI which revealed the greatest accuracy (AUC: 0.99) (Table S3.2). The percentage of pixels classified as severe liana infestation showed a sustained and significant increase over time, from $12.9\% \pm 0.63$ (95% CI) in 2016 to $17.3\% \pm 2$ in 2019 (Figure 4.4; Table S3.3). However, the low liana-infested pixels did not show a similarly consistent downward trend and instead remained more or less constant over the three year period ($35.4\% \pm 3.6$ in 2016 to $33.6\% \pm 3.2$ in 2019). Liana infestation at a pixel level was dynamic, with $2.66\% \pm 0.76$ of pixels having changed from low to severe and $1.22\% \pm 0.2$ having changed from severe to low liana infestation from May 2016 to

April 2019. Taken together, these results indicate a potential forest-wide increase in severe liana infestation.

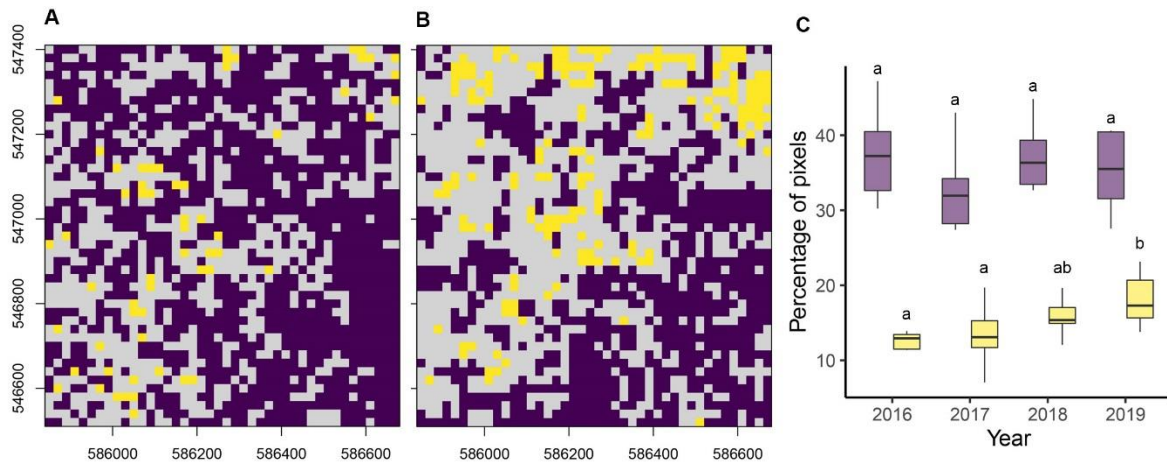


Figure 4.4 Predicted liana infestation in two classes, Low [$\leq 25\%$] (purple) and Severe [$\geq 75\%$] (yellow), derived from Sentinel-2 satellite imagery showing an extract from **a)** 2016, **b)** 2019. Grey areas correspond to liana infestation values not within low or severe classes (*i.e.* 26-74%). Panel **(c)** the percentage of pixels within each class for all four years (2016-2019). Letters in **(c)** indicate statistically significant differences between years as assessed using a least significant difference test with Bonferroni adjusted p values. Significance level was set at 0.05.

4.5. Discussion

This study provides evidence, for the first time, that liana infestation can be detected in a closed-canopy tropical forest using multispectral satellite-based imagery. Furthermore, satellite-derived Greenness Index showed clear separation in response to airborne-derived liana infestation classes within both primary and selectively logged forests as well as during periods of wet and dry conditions (Figure 4.2). These results indicate that reflectance in the visible spectra (546-574 nm) was most efficient in distinguishing lianas from trees (Figure S3.1) and in particular Greenness Index (GI) was found to be an effective metric (Table S3.1). This corroborates results from other studies that found the visible spectral region to be the most important for spectrally discriminating between lianas and trees (Sánchez-Azofeifa & Castro-Esau 2006; Sánchez-Azofeifa *et al.* 2009; Marvin, Asner & Schnitzer 2016). Previous studies have shown higher reflectance of liana leaves in the visible region consistent with lower levels of chlorophyll content in lianas than in trees (Sánchez-Azofeifa & Castro-Esau 2006; Sánchez-Azofeifa *et al.* 2009). Subsequently, an increase in liana canopy cover will result in higher values of greenness.

A significant positive relationship between GI and liana infestation was found across all four years for which imagery was obtained, however there was a greater increase in greenness relative to an increase in liana infestation for the year in which the El Niño-induced drought occurred (Figure 4.2b). A greater increase in greenness in the drought year may be attributed to: 1) a reduction in tree greenness (*i.e.* at 0% liana infestation), 2) an increase in liana greenness, or 3) a combination of both. Lianas generally seem to experience less water stress due to their ability to access and use water more efficiently than co-occurring trees during seasonal or periodic droughts (Chen *et al.* 2015; Maréchaux *et al.* 2017; van der Sande *et al.* 2019). Evidence from dry forests show that the chlorophyll concentration of liana leaves is lower than for trees, and this difference results in an increase in reflectance in the visible spectra (Sánchez-Azofeifa *et al.* 2009). However, in wetter forests chlorophyll concentration is observed to simultaneously increase in liana leaves and decrease in tree leaves (Sánchez-Azofeifa *et al.* 2009), which leads to a lower spectral contrast between trees and lianas.

A strong relationship between greenness and liana infestation also indicates that interpretation of forest-wide responses to environmental or climatic changes using satellite imagery may be problematic, if lianas are interpreted as tree canopies. Lianas are a particularly dominant and wide-spread feature of tropical canopies (Pérez-Salicrup, Sork & Putz 2001; Ingwell *et al.* 2010) and therefore their presence may obscure or distort satellite-derived spectral reflectance of tree canopies. Furthermore, as the effect of increased liana infestation on greenness differed under different climatic conditions (Figure 4.2b), satellite-observed changes in spectral reflectance in response to climatic changes (*e.g.* Saleska *et al.* 2007) may be complicated (*cf.* Anderson *et al.* 2010) by the differential responses of lianas and trees. This highlights the importance of accounting for the effect of liana infestation on satellite-derived reflectance metrics to ensure the accurate interpretation of remotely sensed multispectral data, especially given evidence of increasing liana biomass and abundance.

Based on a time-series of satellite-derived imagery, severely liana-infested pixels ($\geq 75\%$ infested by lianas) increased significantly over time from $12.9\% \pm 0.63$ in May 2016 to $17.3\% \pm 2$ in April 2019, whilst low ($\leq 25\%$) liana infestation remained relatively constant $35.4\% \pm 3.6$ to $33.6\% \pm 3.2$ over the same three-year period (Figure 4.4c). This degree of change is minimal compared to change in seasonal forests, where lianas show more rapid growth and have a significant growth advantage over trees compared with aseasonal forests (Schnitzer & van der Heijden 2019). For example, in a seasonal forest, an increase of 65% of trees with severe liana infestation was observed over a ten-year period (Ingwell *et al.* 2010) in contrast to an increase of around 3% of trees with severe liana infestation in Peninsula Malaysia over the same time period (Wright *et al.* 2015). In this

study we found an increase of 4.4% over three years, proportional to an increase of around 14.7% over a ten-year period. However, low liana infestation remained relatively constant over the same time period. This suggests that increases are limited to severe liana infestation which may not necessarily represent an increase in the overall percentage of infested trees. Furthermore, assessing the level of change in the severe liana infestation class over time is subject to error. While the accuracy of predicted liana infestation in low ($\leq 25\%$) and severe ($\geq 75\%$) classes revealed good accuracy (AUC: 0.99), accuracy was reduced when liana infestation was predicted across all infestation classes (Figure 4.3c; Table S3.2). Subsequently, error in the classification of severe liana infestation, due to misclassification of pixels in the high (50-74%) liana infestation class, may have led to an under- or over-estimation of change in liana infestation over time. Although I do not have ground data to support this, these results imply that, despite the proportion of low liana-infested pixels remaining relatively constant, severely liana-infested pixels may have increased by 4.4% over the three-year time period. If indeed true, this suggests that an increase in liana abundance may not be confined to the Neotropics, as indicated by previous studies (*e.g.* Schnitzer & Bongers, 2011; Wright *et al.* 2015). A possible driver of the increase in liana infestation may be that lianas tend to favour dry conditions and exhibit a dry season growth advantage over trees (Schnitzer & van der Heijden 2019). Whilst Borneo has one of the most aseasonal climates of any tropical region (Whitmore 1984), recent evidence has suggested that Borneo may be experiencing hotter and drier conditions driven by continued deforestation (McAlpine *et al.* 2018; Gaveau *et al.* 2019; Chapman *et al.* 2020), which is likely to provide favourable conditions for liana growth (Schnitzer & van der Heijden 2019; Marimon *et al.* 2020).

However, similar to studies that assessed individual tree crowns (Ingwell *et al.* 2010; Wright *et al.* 2015), these results also indicate that liana infestation is dynamic, with $2.66\% \pm 0.76$ of pixels changing from low to severe and $1.22\% \pm 0.2$ changing from severe to low liana infestation over the three-year time period. This represents a total of 3.9% change between classes over a 3-year period. Available data from aseasonal and seasonal forests show that changes between low and severe liana infestation classes over time scales longer than three years range from 4% – 16.2% (Ingwell *et al.* 2010; Wright *et al.* 2015). This represents around 1% - 4.8% over a three-year period. Results from this study imply that change in liana infestation is dynamic and is more closely related to the degree of change observed in a seasonal forest. A possible explanation for this relatively high change in liana infestation could be related to the El Niño-induced drought which occurred in 2016 (Nunes *et al.* 2019). During this time, trees may have been temporarily stumped and lianas may have had a growth advantage which may have resulted in more dynamic changes in liana infestation over this period. A longer time-series is therefore needed to provide conclusive results of whether there is a temporal

increase in liana infestation and how this may impact on the ability of these forests to store and sequestration carbon.

Evidence that lianas can be detected across closed-canopy forest using satellite imagery provides a substantial advance in our ability to monitor change in liana infestation over time. Furthermore, evidence of this relationship under different climatic conditions and across forest types suggests that this methodology should apply broadly. However, there are a number of limitations to the current study. First, satellite-based liana infestation predictions on a continuous scale seemed to underestimate liana infestation compared to airborne predictions. Although there was a small bias in predictions in the primary forests, underprediction was a particular problem in the selectively logged forests. However, a high classification accuracy (0.88) for predicted liana infestation for low ($\leq 25\%$) and severe ($\geq 75\%$) classes in the selectively logged forest was found (Table S3.2). Therefore, prediction within classes may be required in order to compare liana infestation between forest types.

Second, satellite-based images were trained with the same airborne-derived liana infestation output, to assess temporal changes in liana infestation over time. This may be problematic given the dynamic nature of liana infestation (Ingwell *et al.* 2010; Wright *et al.* 2015). For example, changes across the landscape, such as the formation of canopy gaps, may have led to changes in liana infestation over time which are not reflected in the training data. This would have led to certain areas across the landscape being trained incorrectly, and therefore may result in an increase in error around liana infestation predictions over time. However, as change was assessed over a relatively short time period, it is unlikely that this would have affected a large area of the forest. Furthermore, a small degree of error in training data has shown to have little impact on the accuracy of predictions (Chandler *et al.* in review). Ultimately, I therefore think it is unlikely that these results are severely confounded by using the same training data.

Third, the level of exposure to sun light may affect spectral reflectance, which, in turn, may make it more difficult to detect liana infestation. For example, large canopy gaps will be more exposed to light whereas smaller canopy gaps and some tree crowns may be affected by shadow from nearby tall trees. While the effect of shadow has shown to impact some vegetation indices, the effect has shown to be less on NDVI and Greenness Index (Zhang *et al.* 2015). Therefore, while Greenness Index, as a sole input variable, was unable to accurately predict liana infestation (Figure 4.3a,d), it is possible that including Greenness Index assists in the detection of liana infestation in areas affected by shadow. Indeed, the inclusion of Sentinel-2 bands which cover the NIR- and SWIR- regions appear to be essential in order to discriminate between trees and lianas (Kalacska *et al.* 2007; Guzman, Rivard & Sánchez-Azofeifa 2018). The similarity of spectral coverage and resolution across

products including, Sentinel, Landsat and Aster suggests that the detection of liana infestation should be achievable across a variety of multispectral sensors.

Lastly, while this methodology appears to provide an accurate assessment of liana infestation for the region to which it was trained, it may be limited in its broad applicability across forests in different regions. The accuracy of satellite-derived liana infestation is obtained relative to airborne-derived predictions. However, this represents the same area in which the model was trained upon. It is therefore likely that there could be a reduction in classification accuracy for areas outside the training extent. The use of this current model with no additional training data may therefore only be accurately applied to nearby areas and may require a classification to be restricted to classes of low and high/severe liana infestation if being applied further afield. Future work should consider the feasibility to obtain a generalised model to predict liana infestation over regional- or continental-scales.

4.6. Conclusion

I have shown, for the first time, that satellite-based imagery can be used to accurately predict liana infestation across a closed canopy tropical forest. Greenness Index showed a clear increase in response to airborne-derived liana infestation classes both during wet and drought years and across forest types, which suggests remote sensing methodologies should be capable of detecting liana infestation in tropical forests in other locations. The use of satellite remote sensing therefore advances our ability to assess the distribution of liana infestation over time and across forests globally. This in turn will assist in providing insights into the drivers responsible for the distribution and change in liana infestation at multiple spatial and temporal scales as well as quantify the liana-induced impacts on carbon dynamics in tropical forests.

Chapter 5: Conclusions

5.1. Thesis synthesis

This thesis investigates spatial patterns of liana infestation and the relationship with forest structure and aboveground carbon (AGC) storage across a primary and selectively logged tropical forest in Sabah, Borneo. I show, for the first time, that airborne and satellite-based remote sensing technologies can be used to accurately assess spatial and temporal patterns of liana infestation in an aseasonal tropical forest. Liana infestation can be detected using satellite-based multispectral imagery across forest types, under different climatic conditions and over time, which indicates that this remote sensing methodology may apply to tropical forests in other locations. My results also indicate an increase in severely ($\geq 75\%$) liana-infested areas over time in Danum Valley. This is an important finding as completely liana-infested areas stored on average $59.6 \pm 11 \text{ Mg C ha}^{-1}$ less than areas that were liana-free. This implies that if this increase in liana infestation persists, lianas may cause a reduction in the carbon sequestered and stored in this area. Below I synthesize the key findings and conclusions of this thesis.

5.1.1. Mapping liana infestation at a landscape-scale

Chapter 2, Objectives 1.1 & 1.2

This study is the first to successfully assess the spatial distribution of liana infestation in an aseasonal tropical forest at a landscape-scale. Despite liana chemistry and their spectral response converging with those of trees as precipitation increases (Castro-Esau, Sánchez-Azofeifa & Caelli 2004; Sánchez-Azofeifa *et al.* 2009), liana infestation was accurately detected in a primary tropical forest by combining a neural network classification with hyperspectral and LiDAR data. The use of spectra derived from pure classes, *i.e.* tree crowns that were either liana-free or completely liana-infested, allowed the accurate detection of liana infestation at a pixel-level. The model over-predicted liana infestation for tree crowns with liana canopy cover below 25%. However, as the impact of lianas on tree growth and survival increases exponentially for those trees with more than 50% of their crown infested with lianas (Ingwell *et al.* 2010; Wright *et al.* 2015), it is most essential to accurately detect high (>50%) liana infestation for its application in conservation and forest management. Furthermore, a pixel-based approach revealed a stronger relationship between predicted and observed liana infestation compared to an object-based approach potentially due to the difficulties of successfully segmenting tree crowns in imagery across dense, closed-canopy tropical forests. This suggests that a pixel-based approach is more suited to tropical forest

environments and is therefore able to produce more accurate predictions of liana infestation at a landscape-level.

5.1.2. Association of liana infestation with aboveground carbon stocks

Chapter 3, Objectives 2.1 & 2.2

My results show that although liana infestation was widespread across the landscape, it was particularly severe in canopy gaps. Accounting for the size and frequency of canopy gaps, I found that aboveground carbon (AGC) stocks were negatively related to liana infestation both across primary as well as naturally regenerating and actively restored selectively logged forests. Areas that were completely liana-infested stored on average $59.6 \pm 11 \text{ Mg C ha}^{-1}$ less than areas that were liana-free, however lianas had a more pronounced effect on carbon storage in the primary forest ($85.1 \pm 12.8 \text{ Mg C ha}^{-1}$) compared to the actively restored ($14.8 \pm 6.4 \text{ Mg C ha}^{-1}$) and naturally regenerating forests ($32.8 \pm 16.2 \text{ Mg C ha}^{-1}$). These findings show that the negative effects of liana infestation can be observed across forest types including selectively logged forests which have experienced large alterations to the spatial distribution of carbon stocks. Liana infestation therefore affects AGC stocks at a landscape-level, which implies that any increases in liana infestation may have a significant impact on the carbon storage potential of these forests in the future.

5.1.3. Detection of liana infestation in satellite-imagery

Chapter 4, Objectives 3.1, 3.2 & 3.3

I show for the first time that satellite-based imagery is effective in detecting the spatial distribution of liana infestation across closed canopy tropical forest. The Greenness Index, a simple vegetation index derived from satellite imagery, in particular, was an effective metric for the separation of liana infestation classes. Results show a clear increase in the Greenness Index as a response to increases in liana infestation across forest types as well as during and after a period of El-Niño induced drought. Furthermore, assessing satellite imagery over time showed a significant increase in the percentage of severely ($\geq 75\%$) liana-infested pixels, from $12.9\% \pm 0.63$ in 2016 to $17.3\% \pm 2$ in 2019. This study provides a first indication that liana infestation may have increased over a three-year period, although long-term studies are required to assess whether this trend continues over a longer time period. These results suggest that satellite-based remote sensing could be employed to detect liana infestation across tropical forests globally which will advance our ability to explore the drivers responsible for patterns of liana infestation at multiple spatial and temporal

scales as well as assist in quantifying the liana-induced impacts on carbon dynamics in tropical forests.

5.2. Research Implications

Tropical forests of South-East Asia comprise a significant proportion of the World's biodiversity and carbon stocks. The dominance of dipterocarp species, particularly in Borneo, make these forests structurally unique and give rise to greater aboveground carbon densities than anywhere else in the tropics (Slik *et al.* 2013; Avitabile *et al.* 2016; Sullivan *et al.* 2017). However, structural changes, such as the distribution and abundance of lianas, may have severe implications on the diversity and carbon balance of tropical forests (Schnitzer & Carson 2010; van der Heijden, Powers & Schnitzer 2015). The remote sensing advances presented in this thesis extend field-based knowledge spatially and temporally and enhance our understanding of liana ecology as a whole, but particularly in the Palaeotropics. More specifically, this work 1) advances our ability to assess the spatial distribution of liana infestation across the wider landscape, 2) provides the first landscape-level evaluation of their relationship with carbon stocks and 3) gives a first indication of the changes in the distribution and severity of liana infestation over time in Sabah, Malaysia.

5.2.1. Relating liana infestation to aboveground carbon stocks

Our knowledge of liana ecology has expanded substantially in recent years (Marshall *et al.* 2020). However, typically, liana studies have been conducted at a plot-level (Ingwell *et al.* 2010; van der Heijden, Powers & Schnitzer 2015; Wright *et al.* 2015). While these studies have helped increase our understanding of the liana-induced impacts on tropical forest dynamics (Phillips *et al.* 2005; van der Heijden, Powers & Schnitzer 2015), their limited coverage and potential bias towards more easily accessible areas, restricts their ability to apply results over spatially large areas. This is particularly important as across forests worldwide, lianas exert a strong control over aboveground carbon storage and sequestration (Schnitzer *et al.* 2014b; van der Heijden, Powers & Schnitzer 2015; Chapter 3). Being able to extend this relationship across space and time will assist in predicting which tropical forests are likely to be limited in the amount of carbon they can store and sequester and the implications that predicted changes in liana biomass and abundance may have on the ability of tropical forests to serve as carbon sinks in the future.

Indeed, there is evidence of a long-term decreasing trend of carbon accumulation throughout the Amazon (Brienen *et al.* 2015) and a carbon sink saturation across the African

continent related to an increase in temperature and CO₂ (Hubau *et al.* 2020). However, climate-driven vegetation model simulations have not predicted a similar saturation in carbon uptake (Huntingford *et al.* 2013). Such discrepancies, in the Amazon, may be partly related to the pervasive increase of liana infestation and their negative effect on tree survival (Phillips *et al.* 2002; Schnitzer & Bongers 2011). However, evidence of a decline in liana infestation on the African continent (Caballé & Martin 2001; Bongers *et al.* 2020) suggests other changes may be response for the carbon sink saturation, such as changes in precipitation, frequency of drought events and changes in species composition (Malhi & Wright 2004; Malhi *et al.* 2013; Bonal *et al.* 2016).

5.2.2. Increasing liana abundance in the Palaeotropics: implications for the tropical forest carbon cycle

Compelling evidence exists for increasing liana dominance in seasonal forests in the Neotropics (Benítez-Malvido & Martínez-Ramos 2003; Wright *et al.* 2004; Wright & Calderón 2006; Chave *et al.* 2008b; Foster, Townsend & Zganjar 2008; Ingwell *et al.* 2010). However, so far, there is little evidence to suggest that the same is true of aseasonal forests or that this is a pantropical phenomenon (Caballé & Martin 2001; Wright *et al.* 2015; Bongers *et al.* 2020). Several mechanistic explanations have been suggested for the observed patterns of increasing liana biomass and abundance.

Firstly, lianas may grow more rapidly under elevated CO₂ concentration in comparison to trees (Granados & Körner 2002), and therefore continued increases in atmospheric CO₂ should favour liana growth. Indeed, comparing tree and liana growth under experimental increases in CO₂ have shown lianas to respond faster than trees (Zotz, Cueni & Körner 2006). However, as increasing liana abundance has not been observed pantropically (Schnitzer & Bongers 2011), this mechanism does not explain continental differences in liana proliferation over time.

Secondly, lianas are known to increase in abundance, biomass and diversity in areas of greater disturbance (DeWalt, Schnitzer & Denslow 2000; Laurance *et al.* 2001; Schnitzer & Carson 2001). As a result, lianas are particularly abundant in canopy gaps, forest edges and within selectively logged and secondary forests (Schnitzer & Carson 2001; Martin, Sherman & Fahey 2004; Addo-Fordjour *et al.* 2009; Schnitzer & Carson 2010; Magrath *et al.* 2016; Rocha *et al.* 2020). As secondary forests, and the total area of old-growth forests impacted by selective logging, are increasing in area (Asner *et al.* 2005), lianas are also likely to increase in abundance due to their propensity to capitalise on disturbed areas. Furthermore, evidence suggests tropical forests are now more productive and have higher tree mortality and turnover (Phillips & Gentry 1994; Phillips 1996; Phillips *et al.* 2004;

Wright 2010), which may also provide favourable conditions for liana growth. In Phillips (1996), turnover rates were significantly higher in Neo- versus Palaeotropical sites. However, when census intervals were corrected, average turnover rates were not significantly different (Lewis *et al.* 2004b). Therefore, evidence of a pantropical increase in forest turnover does not explain the rapid increases in liana biomass and abundance in Neotropical old-growth forest sites.

Lastly, liana abundance is reported to increase with decreasing rainfall (DeWalt *et al.* 2010; Parolari *et al.* 2020) and increasing temperature (Durán *et al.* 2015), therefore lianas are likely to experience a growth advantage over trees during dry seasons or drought periods (Schnitzer & van der Heijden 2019). Throughout the tropics there has been an overall decrease in rainfall and an increase in the extent and frequency of drought events driven by ongoing deforestation (Lean & Warrilow 1989; Shukla, Nobre & Sellers 1990; Malhi & Wright 2005; Hasler, Werth & Avissar 2009; Phillips *et al.* 2009; Lee & McPhaden 2010; Spracklen, Arnold & Taylor 2012; Spracklen & Garcia-Carreras 2015; McAlpine *et al.* 2018), which may lead to an increase in liana abundance globally. However, while changes in temperature may be relatively consistent over large areas, changes in rainfall are known to vary significantly among and within regions (Malhi & Wright 2005). For example, in contrast to others (*e.g.* Chapman *et al.* 2020) an increase in local rainfall has been observed over deforested areas (Negri *et al.* 2004). These site-specific changes in rainfall and the intensity of dry seasons may explain regional differences in patterns of liana infestation over time.

Differences in rainfall and drought events at a continental-level may also provide some explanation for observed increases in liana abundance which have been confined to the Neotropics. In general, Amazonian forests are exposed to stronger climate impacts, including faster temperature increases and more regular and severe droughts, than African forests (Saatchi *et al.* 2013; Boisier *et al.* 2015; Jiménez-Muñoz *et al.* 2016; Garcia, Libonati & Nunes 2018). Precipitation changes have also been predicted to decrease in tropical Americas and increase in Africa and Asia in response to a warming climate (Zelazowski *et al.* 2011; Kooperman *et al.* 2018). These climatic changes may therefore favour liana proliferation in the Neotropics. Future research on long-term liana dynamics from tropical forests covering a range of environmental variation worldwide is required to determine the generality of increasing liana dominance as well as to assess which mechanisms may be responsible for change over time.

The results from Chapter 4 provide some indication that the degree of liana infestation may be increasing over time across the landscape. Results revealed 1) a significant increase in the percentage of pixels classified as severely ($\geq 75\%$) liana-infested and 2) that a significantly greater number of pixels had changed from low to severe infestation ($2.66\% \pm 0.76$) than vice versa ($1.22\% \pm$

0.2), over a three year period (2016-2019). These findings imply therefore that an increase in lianas may not be confined to seasonal forests in the Neotropics. However, these results only cover a three-year period and as liana infestation is dynamic temporally, may not prove unequivocally that liana infestation is increasing in these forests. Nonetheless, this study (Chapter 4) makes an important contribution in highlighting that satellite-based remote sensing can be used to detect liana infestation and will provide a useful methodology to track changes in liana infestation in Danum Valley as well as other locations.

5.2.3. Consequences of detecting liana infestation in satellite imagery

The results from Chapter 4 suggest that the detectability of lianas in satellite imagery may be broadly applicable to other forests globally. While this can benefit our understanding of liana ecology, it may also be of concern for studies that utilise vegetation indices without accounting for the effect of lianas. As lianas can distort the reflectance of tree canopies, interpretation of popular vegetation indices such as the normalized difference vegetation index (NDVI) and leaf area index (LAI) could be erroneous if lianas are interpreted as trees. For example, it has been shown that lianas typically have higher values of LAI in comparison to trees (Putz 1983; Cai, Schnitzer & Bongers 2009; Sánchez-Azofeifa *et al.* 2009). Furthermore, higher reflectance of liana leaves is strongly related to the level of chlorophyll content (Castro-Esau, Sánchez-Azofeifa & Caelli 2004). As NDVI is sensitive to chlorophyll (Pettorelli *et al.* 2005) and canopy architectural features (Pinter Jr *et al.* 1985) it is likely that significant differences in NDVI will be observed for trees and lianas (see also Table S3.1). Therefore the use of spectral indices to assess ecological functions may be problematic if lianas are not accounted for. Future work should look to explore the impact of liana infestation in canopy-level trees on the relationship between spectral indices and ecological properties.

5.2.4. Limitations of remote sensing: implications and solutions for assessing liana infestation over multiple scales

Remote sensing techniques offer a solution to assess both changes in liana infestation and aboveground carbon stocks over larger areas than possible using field-based methods alone. However, there are a number of limitations which must be addressed or accounted for when using remotely sensed data.

5.2.4.1. Discrepancies in spatial units

The ability to generate remotely sensed data with spatial units that align with ground observations is essential for the accurate prediction of liana infestation. However, as liana infestation is typically not homogeneous across a tree crown, data collected using airborne sensors that have high spatial resolutions (*i.e.* at a sub-canopy level), pose a challenge for assessing liana infestation at a pixel-level. Results from Chapter 2 indicate that, the prediction of liana infestation in airborne-derived imagery can be achieved at the pixel-level by spectral unmixing of endmembers derived from tree crowns that were either severely ($\geq 75\%$) liana-infested or liana-free. All pixels within a tree crown therefore represent the same class of infestation. This methodology highlights that the collection of ground data for training purposes need only focus on identifying the distribution of trees within either class of liana infestation. This can therefore reduce time and cost associated with ground surveys and potentially allow a greater sample size over a larger area.

The use of Unoccupied Aerial Vehicles (UAVs) may also provide an approach to assess the degree of liana infestation for each pixel in airborne-derived imagery. UAVs can capture data at ultra-fine spatial resolutions (mm) which can provide spatially detailed imagery to clearly separate liana leaves from tree leaves in the canopy (Waite *et al.* 2019). However, the success of this approach is entirely dependent on the ability to align airborne- and UAV-derived imagery (Hsu 2012; Lucier 2018), whereby a slight misalignment could result in vastly different estimates of liana infestation at the pixel-level.

Alternatively, an object-based approach can be achieved by the use of LiDAR data to segment hyperspectral imagery at the tree-crown level. However, the accuracy of an object-based classification revealed potential limitations (Chapter 2), which requires refinement in order to accurately segment imagery in dense, closed-canopy tropical forests. Accurate segmentation is critical for an object-based approach, however this may only be achievable in a primary forest, where there is greater heterogeneity in canopy structure in comparison to logged forests (Numata *et al.* 2006). Therefore, as an object-based approach may be restricted to certain forest types, and require the use of airborne-derived LiDAR in order to accurately segment tree crowns, it may not be broadly applicable over larger areas.

The use of satellite-derived imagery also poses a challenge for the accurate alignment with ground observations. As the spatial resolution of popular sensors such as Landsat and Sentinel are typically in the order of 10-30 m, training data collected on the ground at the tree crown-level may not align with the pixel size of satellite imagery. In Chapter 4, the predicted liana infestation output derived from airborne hyperspectral data was used to generate estimates of liana infestation at the

scale of a satellite image pixel. However, in the absence of airborne-derived data, plot-level average liana infestation data (for example per 1 ha) may provide a solution to relate with satellite-image pixels. An extensive and available global network of plot-level liana canopy infestation data (forestpots.net; Lopez-Gonzalez *et al.* 2011) will likely provide a key step in our ability to assess liana infestation over larger areas. Future work should therefore focus on assessing whether plot-level data could be used to predict liana infestation over continental- or global-scales. Furthermore, while the prediction of liana infestation in Sentinel-2 imagery can be achieved at a resolution of 10 m (Chapter 4), assessing the relationship between liana infestation and variables relating to climate or carbon stocks at global- or continental-scales will most likely be conducted at resolutions ranging from 500m to 1km (*e.g.* Saatchi *et al.* 2011; Baccini *et al.* 2012; Fréjaville & Benito Garzón 2018). Future work should therefore consider whether estimates of liana infestation produced at coarse resolutions can be effective (*cf.* Belward & Lambin 1990) in order to provide insights into the mechanisms that shape patterns of liana infestation at multiple scales.

5.2.4.2. Future of remote sensing for assessing liana infestation

The use of UAVs as a remote sensing tool for liana assessment is strengthened by new technologies which may improve the detection of liana infestation. For example, UAVs fitted with thermal sensors have found significant differences in the temperature of liana-infested and non-infested areas (Yuan *et al.* 2019) based on differences in the temperature of liana and tree leaves (Sanchez-Azofeifa *et al.* 2011; Guzmán *et al.* 2018). Furthermore, UAVs fitted with multispectral (Li *et al.* 2018) as well as hyperspectral and LiDAR sensors (Sankey *et al.* 2018; Thomson *et al.* 2018) represent a powerful solution to provide spectral and structural characteristic at high resolutions for individual plant species identification. However, while imagery acquired from UAVs can cover a larger spatial extent than what can be achieved from ground-based data collection within the same time period, they do not provide a solution for regional- or state-wide assessments. Therefore, it's critical that UAV- or ground-derived estimates can be combined with satellite-derived imagery to assess liana infestation over larger spatial, as well as temporal, scales.

Advances in satellite hyperspectral sensors are likely to provide effective tools for the detection of liana infestation in space and time. For example, the Environmental Mapping and Analysis Program (EnMAP) satellite is capable of imaging the earth's surface at a spatial resolution of 30 m with a spectral range between 420 and 2450 nm (Guanter *et al.* 2015). Furthermore, EnMAP's revisit time is in the order of 27 days and therefore can provide repeated yearly measurements. In Chapter 4, the Greenness Index was shown to be an effective metric for discriminating between

lianas and trees, however the inclusion of all Sentinel-2 bands was required to accurately assess the distribution of liana infestation. With a high spectral resolution (between 5 and 12 nm) across a large spectral range, EnMAP offers another solution to assess the distribution of liana infestation over large spatial extents. Additional advances in satellite-based remote sensing include four hyperspectral satellites as part of a new constellation (Zhuhai-1). Each satellite is able to obtain imagery at a spatial resolution of 10 m with 32 bands covering a spectral range from 400 to 1000 nm (Jiang *et al.* 2019). These satellites also sample a large area on the ground and therefore can achieve global coverage within 5 days. However, the broad use of such products is ultimately limited by their cost (Turner 2013). Therefore, evidence that liana infestation can be detected in freely available multispectral imagery (Chapter 4) provides an approach with broad applicability. Future work should focus on the use of Sentinel-2 and EnMAP as well as new satellites including Landsat 9 in combination with plot-level canopy infestation data to advance our understanding of liana infestation over large spatial and temporal scales.

5.3. Summary

This study shows for the first time that lianas are a strong forest-wide predictor of aboveground carbon stocks at a landscape-level, which, by confirming this pattern in the Palaeotropics, indicates that lianas exert a strong control on carbon storage in tropical forests worldwide. Both airborne and satellite-based remote sensing technologies are capable of accurately detecting liana infestation across primary and selectively logged aseasonal tropical forests. Furthermore, the accurate detection of liana infestation by satellite-based remote sensing technologies across forest types and under different climatic conditions suggests the methodologies employed in this thesis should apply broadly and can be used to assess liana infestation in other forests across the world. This will allow patterns of liana infestation to be assessed at multiple scales, which is imperative to explore the mechanisms that shape their distribution both spatially and temporally. Under predicted climate change scenarios it is likely that the severity of liana infestation will increase globally and therefore remote sensing will provide an effective tool to monitor change over time and assess the impact these changes may have on the functioning and dynamics of tropical forests.

References

- Abshire, J.B., Sun, X., Riris, H., Sirota, J.M., McGarry, J.F., Palm, S., Yi, D. & Liiva, P. (2005) Geoscience laser altimeter system (GLAS) on the ICESat mission: on-orbit measurement performance. *Geophysical research letters*, **32**.
- Achard, F., Beuchle, R., Mayaux, P., Stibig, H.J., Bodart, C., Brink, A., Carboni, S., Desclée, B., Donnay, F. & Eva, H.D. (2014) Determination of tropical deforestation rates and related carbon losses from 1990 to 2010. *Global Change Biology*, **20**, 2540-2554.
- Achard, F., Eva, H.D., Stibig, H.-J., Mayaux, P., Gallego, J., Richards, T. & Malingreau, J.-P. (2002) Determination of deforestation rates of the world's humid tropical forests. *Science*, **297**, 999-1002.
- Adam, H., Csaplovics, E. & Elhaja, M. (2016) A comparison of pixel-based and object-based approaches for land use land cover classification in semi-arid areas, Sudan. *IOP Conference Series: Earth and Environmental Science*, 012061. IOP Publishing.
- Addo-Fordjour, P., Obeng, S., Addo, M. & Akyeampong, S. (2009) Effects of human disturbances and plant invasion on liana community structure and relationship with trees in the Tinte Bepo forest reserve, Ghana. *Forest Ecology and Management*, **258**, 728-734.
- Addo-Fordjour, P., Rahmad, Z. & Shahrul, A. (2014) Impacts of forest management on community assemblage and carbon stock of lianas in a tropical lowland forest, Malaysia. *Tropical Conservation Science*, **7**, 244-259.
- Alexander, C., Deak, B., Kania, A., Mücke, W. & Heilmeyer, H. (2015) Classification of vegetation in an open landscape using full-waveform airborne laser scanner data. *International Journal of Applied Earth Observation and Geoinformation*, **41**, 76-87.
- Álvarez-Cansino, L., Schnitzer, S.A., Reid, J.P. & Powers, J.S. (2015) Liana competition with tropical trees varies seasonally but not with tree species identity. *Ecology*, **96**, 39-45.
- Amaral, C.H., Roberts, D.A., Almeida, T.I. & Souza Filho, C.R. (2015) Mapping invasive species and spectral mixture relationships with neotropical woody formations in southeastern Brazil. *ISPRS journal of photogrammetry and remote sensing*, **108**, 80-93.
- Anderson, L.O., Malhi, Y., Aragão, L.E., Ladle, R., Arai, E., Barbier, N. & Phillips, O. (2010) Remote sensing detection of droughts in Amazonian forest canopies. *New Phytologist*, **187**, 733-750.
- Andrade, J.L., Meinzer, F.C., Goldstein, G. & Schnitzer, S.A. (2005) Water uptake and transport in lianas and co-occurring trees of a seasonally dry tropical forest. *Trees*, **19**, 282-289.
- Appanah, S., Gentry, A. & LaFrankie, J. (1993) Liana diversity and species richness of Malaysian rain forests. *Journal of Tropical Forest Science*, 116-123.
- Ashton, P. & Kettle, C.J. (2012) Dipterocarp biology as a window to the understanding of tropical forest structure: where are we looking now? *Biotropica*, **44**, 575-576.
- Asner, G.P. (1998) Biophysical and biochemical sources of variability in canopy reflectance. *Remote Sensing of Environment*, **64**, 234-253.
- Asner, G.P., Brodrick, P.G., Philipson, C., Vaughn, N.R., Martin, R.E., Knapp, D.E., Heckler, J., Evans, L.J., Jucker, T. & Goossens, B. (2018) Mapped aboveground carbon stocks to advance forest conservation and recovery in Malaysian Borneo. *Biological Conservation*, **217**, 289-310.
- Asner, G.P., Keller, M., Lentini, M., Merry, F. & Souza Jr, C. (2009a) Selective logging and its relation to deforestation. *Geophys. Monogr. Ser.*, **186**, 25-42.
- Asner, G.P., Keller, M., Pereira, J., Rodrigo, Zweede, J.C. & Silva, J.N. (2004) Canopy damage and recovery after selective logging in Amazonia: field and satellite studies. *Ecological Applications*, **14**, 280-298.
- Asner, G.P., Keller, M. & Silva, J.N. (2004) Spatial and temporal dynamics of forest canopy gaps following selective logging in the eastern Amazon. *Global Change Biology*, **10**, 765-783.

- Asner, G.P., Kellner, J.R., Kennedy-Bowdoin, T., Knapp, D.E., Anderson, C. & Martin, R.E. (2013) Forest canopy gap distributions in the southern Peruvian Amazon. *PLoS one*, **8** (4): e60875. <https://doi.org/10.1371/journal.pone.0060875>.
- Asner, G.P., Knapp, D.E., Broadbent, E.N., Oliveira, P.J., Keller, M. & Silva, J.N. (2005) Selective logging in the Brazilian Amazon. *Science*, **310**, 480-482.
- Asner, G.P. & Martin, R.E. (2012) Contrasting leaf chemical traits in tropical lianas and trees: implications for future forest composition. *Ecology letters*, **15**, 1001-1007.
- Asner, G.P. & Mascaro, J. (2014) Mapping tropical forest carbon: Calibrating plot estimates to a simple LiDAR metric. *Remote Sensing of Environment*, **140**, 614-624.
- Asner, G.P., Mascaro, J., Muller-Landau, H.C., Vieilledent, G., Vaudry, R., Rasamoelina, M., Hall, J.S. & Van Breugel, M. (2012) A universal airborne LiDAR approach for tropical forest carbon mapping. *Oecologia*, **168**, 1147-1160.
- Asner, G.P., Powell, G.V., Mascaro, J., Knapp, D.E., Clark, J.K., Jacobson, J., Kennedy-Bowdoin, T., Balaji, A., Paez-Acosta, G. & Victoria, E. (2010) High-resolution forest carbon stocks and emissions in the Amazon. *Proceedings of the National Academy of Sciences*, **107**, 16738-16742.
- Asner, G.P., Rudel, T.K., Aide, T.M., DeFries, R. & Emerson, R. (2009b) A contemporary assessment of change in humid tropical forests. *Conservation Biology*, **23**, 1386-1395.
- Avalos, G., Mulkey, S.S., Kitajima, K. & Wright, S.J. (2007) Colonization strategies of two liana species in a tropical dry forest canopy. *Biotropica*, **39**, 393-399.
- Avitabile, V., Herold, M., Heuvelink, G.B., Lewis, S.L., Phillips, O.L., Asner, G.P., Armston, J., Ashton, P.S., Banin, L. & Bayol, N. (2016) An integrated pan-tropical biomass map using multiple reference datasets. *Global Change Biology*, **22**, 1406-1420.
- Avtar, R., Suzuki, R., Takeuchi, W. & Sawada, H. (2013) PALSAR 50 m mosaic data based national level biomass estimation in Cambodia for implementation of REDD+ mechanism. *PLoS one*, **8**, e74807.
- Babaeizadeh, M., Smaragdis, P. & Campbell, R.H. (2016) A simple yet effective method to prune dense layers of neural networks. *ICLR Conference paper*
- Babweteera, F., Plumptre, A. & Obua, J. (2000) Effect of gap size and age on climber abundance and diversity in Budongo Forest Reserve, Uganda. *African Journal of Ecology*, **38**, 230-237.
- Baccini, A., Friedl, M., Woodcock, C. & Warbington, R. (2004) Forest biomass estimation over regional scales using multisource data. *Geophysical research letters*, **31**.
- Baccini, A., Goetz, S., Walker, W., Laporte, N., Sun, M., Sulla-Menashe, D., Hackler, J., Beck, P., Dubayah, R. & Friedl, M. (2012) Estimated carbon dioxide emissions from tropical deforestation improved by carbon-density maps. *Nature Climate Change*, **2**, 182.
- Baccini, A., Walker, W., Carvalho, L., Farina, M., Sulla-Menashe, D. & Houghton, R. (2017) Tropical forests are a net carbon source based on aboveground measurements of gain and loss. *Science*, **358**, 230-234.
- Baker, T.R., Phillips, O.L., Malhi, Y., Almeida, S., Arroyo, L., Di Fiore, A., Erwin, T., Higuchi, N., Killeen, T.J. & Laurance, S.G. (2004a) Increasing biomass in Amazonian forest plots. *Philosophical Transactions of the Royal Society of London B: Biological Sciences*, **359**, 353-365.
- Baker, T.R., Phillips, O.L., Malhi, Y., Almeida, S., Arroyo, L., Di Fiore, A., Erwin, T., Killeen, T.J., Laurance, S.G. & Laurance, W.F. (2004b) Variation in wood density determines spatial patterns in Amazonian forest biomass. *Global Change Biology*, **10**, 545-562.
- Baldeck, C.A., Asner, G.P., Martin, R.E., Anderson, C.B., Knapp, D.E., Kellner, J.R. & Wright, S.J. (2015) Operational tree species mapping in a diverse tropical forest with airborne imaging spectroscopy. *PLoS one*, **10**.
- Balfour, D. & Bond, W. (1993) Factors limiting climber distribution and abundance in a southern African forest. *Journal of Ecology*, 93-100.
- Banin, L., Feldpausch, T., Phillips, O., Baker, T., Lloyd, J., Affum-Baffoe, K., Arets, E., Berry, N., Bradford, M. & Brienen, R. (2012) What controls tropical forest architecture? Testing

- environmental, structural and floristic drivers. *Global Ecology and Biogeography*, **21**, 1179-1190.
- Barlow, J., Lennox, G.D., Ferreira, J., Berenguer, E., Lees, A.C., Mac Nally, R., Thomson, J.R., de Barros Ferraz, S.F., Louzada, J. & Oliveira, V.H.F. (2016) Anthropogenic disturbance in tropical forests can double biodiversity loss from deforestation. *Nature*, **535**, 144.
- Bastin, J.-F., Barbier, N., Couteron, P., Adams, B., Shapiro, A., Bogaert, J. & De Cannière, C. (2014) Aboveground biomass mapping of African forest mosaics using canopy texture analysis: toward a regional approach. *Ecological Applications*, **24**, 1984-2001.
- Bastin, J.F., Rutishauser, E., Kellner, J.R., Saatchi, S., Pélissier, R., Hérault, B., Slik, F., Bogaert, J., De Cannière, C. & Marshall, A.R. (2018) Pan-tropical prediction of forest structure from the largest trees. *Global Ecology and Biogeography*, **27**, 1366-1383.
- Bateson, A. & Curtiss, B. (1996) A method for manual endmember selection and spectral unmixing. *Remote Sensing of Environment*, **55**, 229-243.
- Bazezew, M.N., Hussin, Y.A. & Kloosterman, E. (2018) Integrating Airborne LiDAR and Terrestrial Laser Scanner forest parameters for accurate above-ground biomass/carbon estimation in Ayer Hitam tropical forest, Malaysia. *International Journal of Applied Earth Observation and Geoinformation*, **73**, 638-652.
- Beer, C., Reichstein, M., Tomelleri, E., Ciais, P., Jung, M., Carvalhais, N., Rödenbeck, C., Arain, M.A., Baldocchi, D. & Bonan, G.B. (2010) Terrestrial gross carbon dioxide uptake: global distribution and covariation with climate. *Science*, **329**, 834-838.
- Bell, S.A. (2001) A beginner's guide to uncertainty of measurement. *National Physical Laboratory*, **2**, <https://www.dit.ie/media/physics/documents/GPG11.pdf>.
- Belward, A. & Lambin, E. (1990) Limitations to the identification of spatial structures from AVHRR data. *International Journal of Remote Sensing*, **11**, 921-927.
- Benítez-Malvido, J. & Martínez-Ramos, M. (2003) Impact of forest fragmentation on understory plant species richness in Amazonia. *Conservation Biology*, **17**, 389-400.
- Berry, N.J., Phillips, O.L., Lewis, S.L., Hill, J.K., Edwards, D.P., Tawatao, N.B., Ahmad, N., Magintan, D., Khen, C.V. & Maryati, M. (2010) The high value of logged tropical forests: lessons from northern Borneo. *Biodiversity and Conservation*, **19**, 985-997.
- Bertault, J.-G. & Sist, P. (1997) An experimental comparison of different harvesting intensities with reduced-impact and conventional logging in East Kalimantan, Indonesia. *Forest Ecology and Management*, **94**, 209-218.
- Bicknell, J.E., Struebig, M.J., Edwards, D.P. & Davies, Z.G. (2014) Improved timber harvest techniques maintain biodiversity in tropical forests. *Current Biology*, **24**, R1119-R1120.
- Blaschke, T. (2010) Object based image analysis for remote sensing. *ISPRS journal of photogrammetry and remote sensing*, **65**, 2-16.
- Boisier, J.P., Ciais, P., Ducharne, A. & Guimberteau, M. (2015) Projected strengthening of Amazonian dry season by constrained climate model simulations. *Nature Climate Change*, **5**, 656-660.
- Bonal, D., Burban, B., Stahl, C., Wagner, F. & Hérault, B. (2016) The response of tropical rainforests to drought—lessons from recent research and future prospects. *Annals of Forest Science*, **73**, 27-44.
- Bongers, F., Ewango, C.E., van der Sande, M.T. & Poorter, L. (2020) Liana species decline in Congo basin contrasts with global patterns. *Ecology*, **101** (5), <https://doi.org/10.1002/ecy.3004>.
- Bongers, F., Poorter, L., Hawthorne, W.D. & Sheil, D. (2009) The intermediate disturbance hypothesis applies to tropical forests, but disturbance contributes little to tree diversity. *Ecology letters*, **12**, 798-805.
- Bongers, F., Schnitzer, S. & Traore, D. (2002) The importance of lianas and consequences for forest management in West Africa. *BioTerre, Special edition*, 59-70.
- Bowd, E.J., Banks, S.C., Strong, C.L. & Lindenmayer, D.B. (2019) Long-term impacts of wildfire and logging on forest soils. *Nature Geoscience*, **12**, 113-118.
- Boyd, D.S., Hill, R.A., Hopkinson, C. & Baker, T.R. (2013) Landscape-scale forest disturbance regimes in southern Peruvian Amazonia. *Ecological Applications*, **23**, 1588-1602.

- Bradford, M. & Murphy, H.T. (2019) The importance of large-diameter trees in the wet tropical rainforests of Australia. *PloS one*, **14** (5), e0208377.
- Bradshaw, C.J., Sodhi, N.S. & Brook, B.W. (2009) Tropical turmoil: a biodiversity tragedy in progress. *Frontiers in Ecology and the Environment*, **7**, 79-87.
- Brienen, R.J., Phillips, O., Feldpausch, T., Gloor, E., Baker, T., Lloyd, J., Lopez-Gonzalez, G., Monteagudo-Mendoza, A., Malhi, Y. & Lewis, S.L. (2015) Long-term decline of the Amazon carbon sink. *Nature*, **519**, 344-348.
- Brock, P.M., Fornace, K.M., Grigg, M.J., Anstey, N.M., William, T., Cox, J., Drakeley, C.J., Ferguson, H.M. & Kao, R.R. (2019) Predictive analysis across spatial scales links zoonotic malaria to deforestation. *Proceedings of the Royal Society B*, **286**, 20182351.
- Brokaw, N.V. & Scheiner, S.M. (1989) Species composition in gaps and structure of a tropical forest. *Ecology*, **70**, 538-541.
- Bunker, D.E., DeClerck, F., Bradford, J.C., Colwell, R.K., Perfecto, I., Phillips, O.L., Sankaran, M. & Naeem, S. (2005) Species loss and aboveground carbon storage in a tropical forest. *Science*, **310**, 1029-1031.
- Caballé, G. & Martin, A. (2001) Thirteen years of change in trees and lianas in a Gabonese rainforest. *Plant Ecology*, **152**, 167-173.
- Cai, Z.-Q., Schnitzer, S.A. & Bongers, F. (2009) Seasonal differences in leaf-level physiology give lianas a competitive advantage over trees in a tropical seasonal forest. *Oecologia*, **161**, 25-33.
- Campanello, P.I., Manzané, E., Villagra, M., Zhang, Y.-J., Panizza, A.M., di Francescantonio, D., Rodriguez, S.A., Chen, Y.-J., Santiago, L.S. & Goldstein, G. (2016) Carbon allocation and water relations of lianas versus trees. In *Tropical tree physiology*, pp. 103-124. Springer.
- Campbell, E. & Newbery, D.M. (1993) Ecological relationships between lianas and trees in lowland rain forest in Sabah, East Malaysia. *Journal of Tropical Ecology*, **9**, 469-490.
- Campbell, M.J., Edwards, W., Magrath, A., Alamgir, M., Porolak, G., Mohandass, D. & Laurance, W.F. (2018) Edge disturbance drives liana abundance increase and alteration of liana–host tree interactions in tropical forest fragments. *Ecology and evolution*, **8**, 4237-4251.
- Cannon, C.H., Peart, D.R. & Leighton, M. (1998) Tree species diversity in commercially logged Bornean rainforest. *Science*, **281**, 1366-1368.
- Cao, L., Coops, N., Hermosilla, T., Innes, J., Dai, J. & She, G. (2014) Using small-footprint discrete and full-waveform airborne LiDAR metrics to estimate total biomass and biomass components in subtropical forests. *Remote Sensing*, **6**, 7110-7135.
- Cao, L., Gao, S., Li, P., Yun, T., Shen, X. & Ruan, H. (2016) Aboveground biomass estimation of individual trees in a coastal planted forest using full-waveform airborne laser scanning data. *Remote Sensing*, **8**, 729.
- Carlson, K.M., Asner, G.P., Hughes, R.F., Ostertag, R. & Martin, R.E. (2007) Hyperspectral remote sensing of canopy biodiversity in Hawaiian lowland rainforests. *Ecosystems*, **10**, 536-549.
- Castro-Esau, K., Sánchez-Azofeifa, G. & Caelli, T. (2004) Discrimination of lianas and trees with leaf-level hyperspectral data. *Remote Sensing of Environment*, **90**, 353-372.
- Castro, K., Sanchez-Azofeifa, G.A. & Rivard, B. (2003) Monitoring secondary tropical forests using space-borne data: implications for Central America. *International Journal of Remote Sensing*, **24**, 1853-1894.
- Chang, H. & Yoon, W.S. (2003) Improving the classification of LANDSAT data using standardized principal components analysis. *KSCE Journal of Civil Engineering*, **7**, 469-474.
- Chapman, S., Syktus, J.I., Trancoso, R., Salazar, A., Thatcher, M.J., Watson, J.E., Meijaard, E., Sheil, D., Dargusch, P. & McAlpine, C.A. (2020) Compounding impact of deforestation on Borneo's climate during El Niño events. *Environmental Research Letters*. DOI: <https://doi.org/10.1088/1748-9326/ab86f5>
- Chauve, A., Vega, C., Durrieu, S., Bretar, F., Allouis, T., Pierrot Deseilligny, M. & Puech, W. (2009) Advanced full-waveform lidar data echo detection: Assessing quality of derived terrain and tree height models in an alpine coniferous forest. *International Journal of Remote Sensing*, **30**, 5211-5228.

- Chave, J., Condit, R., Aguilar, S., Hernandez, A., Lao, S. & Perez, R. (2004) Error propagation and scaling for tropical forest biomass estimates. *Philosophical Transactions of the Royal Society of London. Series B: Biological Sciences*, **359**, 409-420.
- Chave, J., Condit, R., Muller-Landau, H.C., Thomas, S.C., Ashton, P.S., Bunyavejchewin, S., Dattaraja, H.S., Davies, S.J., Esufali, S. & Ewango, C.E. (2008a) Assessing evidence for a pervasive alteration in tropical tree communities. *PLoS Biol*, **6**, e45.
- Chave, J., Coomes, D., Jansen, S., Lewis, S.L., Swenson, N.G. & Zanne, A.E. (2009) Towards a worldwide wood economics spectrum. *Ecology letters*, **12**, 351-366.
- Chave, J., Olivier, J., Bongers, F., Châtelet, P., Forget, P.-M., van der Meer, P., Norden, N., Riéra, B. & Charles-Dominique, P. (2008b) Above-ground biomass and productivity in a rain forest of eastern South America. *Journal of Tropical Ecology*, **24**, 355-366.
- Chave, J., Réjou-Méchain, M., Búrquez, A., Chidumayo, E., Colgan, M.S., Delitti, W.B., Duque, A., Eid, T., Fearnside, P.M. & Goodman, R.C. (2014) Improved allometric models to estimate the aboveground biomass of tropical trees. *Global Change Biology*, **20**, 3177-3190.
- Chave, J., Riéra, B. & Dubois, M.-A. (2001) Estimation of biomass in a neotropical forest of French Guiana: spatial and temporal variability. *Journal of Tropical Ecology*, **17**, 79-96.
- Chazdon, R.L. (2014) *Second growth: the promise of tropical forest regeneration in an age of deforestation*. University of Chicago Press.
- Chazdon, R.L. & Guariguata, M.R. (2016) Natural regeneration as a tool for large-scale forest restoration in the tropics: prospects and challenges. *Biotropica*, **48**, 716-730.
- Che, Z.-G., Chiang, T.-A. & Che, Z.-H. (2011) Feed-forward neural networks training: a comparison between genetic algorithm and back-propagation learning algorithm. *International journal of innovative computing, information and control*, **7**, 5839-5850.
- Chen, S., Cowan, C.F. & Grant, P.M. (1991) Orthogonal least squares learning algorithm for radial basis function networks. *IEEE Transactions on neural networks*, **2**, 302-309.
- Chen, Y., Zhou, Y.n., Ge, Y., An, R. & Chen, Y. (2018) Enhancing land cover mapping through integration of pixel-based and object-based classifications from remotely sensed imagery. *Remote Sensing*, **10**, 77.
- Chen, Y.J., Cao, K.F., Schnitzer, S.A., Fan, Z.X., Zhang, J.L. & Bongers, F. (2015) Water-use advantage for lianas over trees in tropical seasonal forests. *New Phytologist*, **205**, 128-136.
- Clark, D.B. & Clark, D.A. (1990) Distribution and effects on tree growth of lianas and woody hemiepiphytes in a Costa Rican tropical wet forest. *Journal of Tropical Ecology*, **6**, 321-331.
- Clark, M.L., Roberts, D.A. & Clark, D.B. (2005) Hyperspectral discrimination of tropical rain forest tree species at leaf to crown scales. *Remote Sensing of Environment*, **96**, 375-398.
- Clark, M.L., Roberts, D.A., Ewel, J.J. & Clark, D.B. (2011) Estimation of tropical rain forest aboveground biomass with small-footprint lidar and hyperspectral sensors. *Remote Sensing of Environment*, **115**, 2931-2942.
- Cliff, N. (2014) *Ordinal methods for behavioral data analysis*. Psychology Press.
- Cochrane, M. (2000) Using vegetation reflectance variability for species level classification of hyperspectral data. *International Journal of Remote Sensing*, **21**, 2075-2087.
- Cochrane, M.A. (2003) Fire science for rainforests. *Nature*, **421**, 913.
- Cochrane, M.A. & Schulze, M.D. (1999) Fire as a Recurrent Event in Tropical Forests of the Eastern Amazon: Effects on Forest Structure, Biomass, and Species Composition 1. *Biotropica*, **31**, 2-16.
- Cohen, W.B. & Spies, T.A. (1992) Estimating structural attributes of Douglas-fir/western hemlock forest stands from Landsat and SPOT imagery. *Remote Sensing of Environment*, **41**, 1-17.
- Condon, M., Sasek, T. & Strain, B. (1992) Allocation patterns in two tropical vines in response to increased atmospheric CO₂. *Functional Ecology*, **6**, 680-685, DOI: 10.2307/2389964.
- Connell, J.H. (1978) Diversity in tropical rain forests and coral reefs. *Science*, **199**, 1302-1310.
- Coomes, D.A., Dalponte, M., Jucker, T., Asner, G.P., Banin, L.F., Burslem, D.F., Lewis, S.L., Nilus, R., Phillips, O.L. & Phua, M.-H. (2017) Area-based vs tree-centric approaches to mapping forest

- carbon in Southeast Asian forests from airborne laser scanning data. *Remote Sensing of Environment*, **194**, 77-88.
- Costa, H., Foody, G.M. & Boyd, D.S. (2018) Supervised methods of image segmentation accuracy assessment in land cover mapping. *Remote Sensing of Environment*, **205**, 338-351.
- Cox, C.J., Edwards, W., Campbell, M.J., Laurance, W.F. & Laurance, S.G. (2019) Liana cover in the canopies of rainforest trees is not predicted by local ground-based measures. *Austral Ecology*, **44**, 759-767.
- Crespo-Peremarch, P. & Ruiz, L.A. (2020) A Full-Waveform Airborne Laser Scanning Metric Extraction Tool for Forest Structure Modelling. Do Scan Angle and Radiometric Correction Matter? *Remote Sensing*, **12**, 292.
- Crouzeilles, R., Ferreira, M.S., Chazdon, R.L., Lindenmayer, D.B., Sansevero, J.B., Monteiro, L., Iribarrem, A., Latawiec, A.E. & Strassburg, B.B. (2017) Ecological restoration success is higher for natural regeneration than for active restoration in tropical forests. *Science Advances*, **3**, e1701345.
- Currie, D.J., Pétrin, C. & Boucher-Lalonde, V. (2019) How perilous are broad-scale correlations with environmental variables? *Frontiers of Biogeography*, DOI: <http://dx.doi.org/10.21425/F5FBG44842>
- Cusack, D.F., Karpman, J., Ashdown, D., Cao, Q., Ciochina, M., Halterman, S., Lydon, S. & Neupane, A. (2016) Global change effects on humid tropical forests: Evidence for biogeochemical and biodiversity shifts at an ecosystem scale. *Reviews of Geophysics*, **54**, 523-610.
- Cushman, S.A., Macdonald, E.A., Landguth, E.L., Malhi, Y. & Macdonald, D.W. (2017) Multiple-scale prediction of forest loss risk across Borneo. *Landscape Ecology*, **32**, 1581-1598.
- Cutler, M., Boyd, D., Foody, G. & Vetrivel, A. (2012) Estimating tropical forest biomass with a combination of SAR image texture and Landsat TM data: An assessment of predictions between regions. *ISPRS journal of photogrammetry and remote sensing*, **70**, 66-77.
- Dalling, J.W., Schnitzer, S.A., Baldeck, C., Harms, K.E., John, R., Mangan, S.A., Lobo, E., Yavitt, J.B. & Hubbell, S.P. (2012) Resource-based habitat associations in a neotropical liana community. *Journal of Ecology*, **100**, 1174-1182.
- Dalponte, M., Ørka, H.O., Gobakken, T., Gianelle, D. & Næsset, E. (2012) Tree species classification in boreal forests with hyperspectral data. *IEEE Transactions on Geoscience and Remote Sensing*, **51**, 2632-2645.
- Davis, K.F., Koo, H.I., Dell'Angelo, J., D'Odorico, P., Estes, L., Kehoe, L.J., Kharratzadeh, M., Kuemmerle, T., Machava, D., Pais, A.d.J.R., Ribeiro, N., Rulli, M.C. & Tatlhego, M. (2020) Tropical forest loss enhanced by large-scale land acquisitions. *Nature Geoscience*, DOI: <https://doi.org/10.1038/s41561-020-0592-3>
- de Castilho, C.V., Magnusson, W.E., de Araújo, R.N.O., Luizao, R.C., Luizao, F.J., Lima, A.P. & Higuchi, N. (2006) Variation in aboveground tree live biomass in a central Amazonian Forest: Effects of soil and topography. *Forest Ecology and Management*, **234**, 85-96.
- Delegido, J., Verrelst, J., Rivera, J.P., Ruiz-Verdú, A. & Moreno, J. (2015) Brown and green LAI mapping through spectral indices. *International Journal of Applied Earth Observation and Geoinformation*, **35**, 350-358.
- Denslow, J.S. (1987) Tropical rainforest gaps and tree species diversity. *Annual Review of Ecology and Systematics*, **18**, 431-451.
- Denslow, J.S., Ellison, A.M. & Sanford, R.E. (1998) Treefall gap size effects on above-and below-ground processes in a tropical wet forest. *Journal of Ecology*, **86**, 597-609.
- DeWalt, S., Schnitzer, S. & Denslow, J. (2000) Density and Diversity of Lianas along a Chronosequence in a Central Panamanian Lowland Forest. *Journal of Tropical Ecology*, **16**, 1-19.
- DeWalt, S.J. & Chave, J. (2004) Structure and biomass of four lowland Neotropical forests. *Biotropica*, **36**, 7-19.
- DeWalt, S.J., Ickes, K., Nilus, R., Harms, K.E. & Burslem, D.F. (2006) Liana habitat associations and community structure in a Bornean lowland tropical forest. *Plant Ecology*, **186**, 203-216.

- DeWalt, S.J., Schnitzer, S.A., Chave, J., Bongers, F., Burnham, R.J., Cai, Z., Chuyong, G., Clark, D.B., Ewango, C.E. & Gerwing, J.J. (2010) Annual Rainfall and Seasonality Predict Pan-tropical Patterns of Liana Density and Basal Area. *Biotropica*, **42**, 309-317.
- di Porcia E Brugnera, M., Meunier, F., Longo, M., Krishna Moorthy, S.M., De Deurwaerder, H., Schnitzer, S.A., Bonal, D., Faybishenko, B. & Verbeeck, H. (2019) Modeling the impact of liana infestation on the demography and carbon cycle of tropical forests. *Global Change Biology*, **25**, 3767-3780.
- Di Vittorio, A.V., Negrón-Juárez, R.I., Higuchi, N. & Chambers, J.Q. (2014) Tropical forest carbon balance: effects of field-and satellite-based mortality regimes on the dynamics and the spatial structure of Central Amazon forest biomass. *Environmental Research Letters*, **9**, 034010.
- Dillenburg, L.R., Whigham, D.F., Teramura, A.H. & Forseth, I.N. (1993) Effects of vine competition on availability of light, water, and nitrogen to a tree host (*Liquidambar styraciflua*). *American journal of botany*, **80**, 244-252.
- Dirzo, R. & Raven, P.H. (2003) Global state of biodiversity and loss. *Annual review of Environment and Resources*, **28**.
- Convention on Biological Diversity (2015) Strategic Plan for Biodiversity 2011–2020, Aichi Biodiversity Targets. <https://www.cbd.int/sp/default.shtml>.
- Doughty, C.E., Metcalfe, D., Girardin, C., Amézquita, F.F., Cabrera, D.G., Huasco, W.H., Silva-Espejo, J., Araujo-Murakami, A., Da Costa, M. & Rocha, W. (2015) Drought impact on forest carbon dynamics and fluxes in Amazonia. *Nature*, **519**, 78-82.
- Drake, J.B., Dubayah, R.O., Clark, D.B., Knox, R.G., Blair, J.B., Hofton, M.A., Chazdon, R.L., Weishampel, J.F. & Prince, S. (2002) Estimation of tropical forest structural characteristics using large-footprint lidar. *Remote Sensing of Environment*, **79**, 305-319.
- Drake, J.B., Knox, R.G., Dubayah, R.O., Clark, D.B., Condit, R., Blair, J.B. & Hofton, M. (2003) Above-ground biomass estimation in closed canopy neotropical forests using lidar remote sensing: Factors affecting the generality of relationships. *Global Ecology and Biogeography*, **12**, 147-159.
- Durán, S.M. & Gianoli, E. (2013) Carbon stocks in tropical forests decrease with liana density. *Biology letters*, **9**, 20130301.
- Durán, S.M., Martin, R.E., Díaz, S., Maitner, B.S., Malhi, Y., Salinas, N., Shenkin, A., Silman, M.R., Wiczynski, D.J. & Asner, G.P. (2019) Informing trait-based ecology by assessing remotely sensed functional diversity across a broad tropical temperature gradient. *Science Advances*, **5** (12), DOI: 10.1126/sciadv.aaw8114
- Durán, S.M., Sánchez-Azofeifa, G.A., Rios, R.S. & Gianoli, E. (2015) The relative importance of climate, stand variables and liana abundance for carbon storage in tropical forests. *Global Ecology and Biogeography*, **24**, 939-949.
- Edwards, D.P., Tobias, J.A., Sheil, D., Meijaard, E. & Laurance, W.F. (2014) Maintaining ecosystem function and services in logged tropical forests. *Trends in Ecology & Evolution*, **29**, 511-520.
- Ellis, P.W., Gopalakrishna, T., Goodman, R.C., Putz, F.E., Roopsind, A., Umunay, P.M., Zalman, J., Ellis, E.A., Mo, K. & Gregoire, T.G. (2019) Reduced-impact logging for climate change mitigation (RIL-C) can halve selective logging emissions from tropical forests. *Forest Ecology and Management*, **438**, 255-266.
- Espírito-Santo, F.D., Gloor, M., Keller, M., Malhi, Y., Saatchi, S., Nelson, B., Junior, R.C.O., Pereira, C., Lloyd, J. & Frohking, S. (2014) Size and frequency of natural forest disturbances and the Amazon forest carbon balance. *Nature Communications*, **5**, 1-6.
- Esquivel-Muelbert, A., Baker, T.R., Dexter, K.G., Lewis, S.L., Brienen, R.J., Feldpausch, T.R., Lloyd, J., Monteagudo-Mendoza, A., Arroyo, L. & Álvarez-Dávila, E. (2019) Compositional response of Amazon forests to climate change. *Global Change Biology*, **25**, 39-56.
- Estrada-Villegas, S., Hall, J.S., van Breugel, M. & Schnitzer, S.A. (2020) Lianas reduce biomass accumulation in early successional tropical forests. *Ecology*, **101** (5), DOI: <https://doi.org/10.1002/ecy.2989>.

- Feeley, K.J., Davies, S.J., Perez, R., Hubbell, S.P. & Foster, R.B. (2011) Directional changes in the species composition of a tropical forest. *Ecology*, **92**, 871-882.
- Feldpausch, T.R., Jirka, S., Passos, C.A., Jasper, F. & Riha, S.J. (2005) When big trees fall: damage and carbon export by reduced impact logging in southern Amazonia. *Forest Ecology and Management*, **219**, 199-215.
- Feldpausch, T.R., Lloyd, J., Lewis, S.L., Brienen, R.J., Gloor, M., Monteagudo Mendoza, A., Lopez-Gonzalez, G., Banin, L., Abu Salim, K. & Affum-Baffoe, K. (2012) Tree height integrated into pantropical forest biomass estimates. *Biogeosciences*, **9**, 3381-3403, DOI: <https://doi.org/10.5194/bg-9-3381-2012>.
- Féret, J.-B. & Asner, G.P. (2012) Tree species discrimination in tropical forests using airborne imaging spectroscopy. *IEEE Transactions on Geoscience and Remote Sensing*, **51**, 73-84.
- Féret, J.-B. & Asner, G.P. (2014) Mapping tropical forest canopy diversity using high-fidelity imaging spectroscopy. *Ecological Applications*, **24**, 1289-1296.
- Ferreira, M.P., Grondona, A.E., Rolim, S.B.A. & Shimabukuro, Y.E. (2013) Analyzing the spectral variability of tropical tree species using hyperspectral feature selection and leaf optical modeling. *Journal of Applied Remote Sensing*, **7**, 073502.
- Ferreira, M.P., Zortea, M., Zanotta, D.C., Shimabukuro, Y.E. & de Souza Filho, C.R. (2016) Mapping tree species in tropical seasonal semi-deciduous forests with hyperspectral and multispectral data. *Remote Sensing of Environment*, **179**, 66-78.
- Ferry, B., Morneau, F., Bontemps, J.D., Blanc, L. & Freycon, V. (2010) Higher treefall rates on slopes and waterlogged soils result in lower stand biomass and productivity in a tropical rain forest. *Journal of Ecology*, **98**, 106-116.
- Field, C.B., Behrenfeld, M.J., Randerson, J.T. & Falkowski, P. (1998) Primary production of the biosphere: integrating terrestrial and oceanic components. *Science*, **281**, 237-240.
- Fine, T.L. (2006) *Feedforward neural network methodology*. Springer Science & Business Media.
- Flint, E. (1994) Changes in land use in South and Southeast Asia from 1880 to 1980: a data base prepared as part of a coordinated research program on carbon fluxes in the tropics. *Chemosphere*, **29**, 1015-1062.
- Foley, J.A., DeFries, R., Asner, G.P., Barford, C., Bonan, G., Carpenter, S.R., Chapin, F.S., Coe, M.T., Daily, G.C. & Gibbs, H.K. (2005) Global consequences of land use. *Science*, **309**, 570-574.
- Foody, G. (2002) Hard and soft classifications by a neural network with a non-exhaustively defined set of classes. *International Journal of Remote Sensing*, **23**, 3853-3864.
- Foody, G.M. (1996) Relating the land-cover composition of mixed pixels to artificial neural network classification output. *Photogrammetric engineering and remote sensing*, **62**, 491-498.
- Foody, G.M. (1997) Fully fuzzy supervised classification of land cover from remotely sensed imagery with an artificial neural network. *Neural Computing & Applications*, **5**, 238-247.
- Foody, G.M. (2000) Mapping land cover from remotely sensed data with a softened feedforward neural network classification. *Journal of Intelligent and Robotic Systems*, **29**, 433-449.
- Foody, G.M. (2003) Remote sensing of tropical forest environments: towards the monitoring of environmental resources for sustainable development. *International Journal of Remote Sensing*, **24**, 4035-4046.
- Foody, G.M. & Boyd, D.S. (1999) Fuzzy mapping of tropical land cover along an environmental gradient from remotely sensed data with an artificial neural network. *Journal of Geographical Systems*, **1**, 23-35.
- Foody, G.M., Boyd, D.S. & Cutler, M.E. (2003) Predictive relations of tropical forest biomass from Landsat TM data and their transferability between regions. *Remote Sensing of Environment*, **85**, 463-474.
- Foody, G.M. & Curran, P.J. (1994) Estimation of tropical forest extent and regenerative stage using remotely sensed data. *Journal of Biogeography*, **21** (3), 223-244.
- Foody, G.M. & Cutler, M.E. (2006) Mapping the species richness and composition of tropical forests from remotely sensed data with neural networks. *Ecological modelling*, **195**, 37-42.

- Foody, G.M., Cutler, M.E., McMorrow, J., Pelz, D., Tangki, H., Boyd, D.S. & Douglas, I. (2001) Mapping the biomass of Bornean tropical rain forest from remotely sensed data. *Global Ecology and Biogeography*, **10**, 379-387.
- Foody, G.M. & Doan, H. (2007) Variability in soft classification prediction and its implications for sub-pixel scale change detection and super resolution mapping. *Photogrammetric Engineering & Remote Sensing*, **73**, 923-933.
- Foster, J.R., Townsend, P.A. & Zganjar, C.E. (2008) Spatial and temporal patterns of gap dominance by low-canopy lianas detected using EO-1 Hyperion and Landsat Thematic Mapper. *Remote Sensing of Environment*, **112**, 2104-2117.
- Franklin, S., Hall, R., Moskal, L., Maudie, A. & Lavigne, M. (2000) Incorporating texture into classification of forest species composition from airborne multispectral images. *International Journal of Remote Sensing*, **21**, 61-79.
- Fréjaville, T. & Benito Garzón, M. (2018) The EuMedClim database: Yearly climate data (1901–2014) of 1 km resolution grids for Europe and the Mediterranean basin. *Frontiers in Ecology and Evolution*, **6**, 31.
- Face the Future. (2011) INFAPRO Rehabilitation of logged-over dipterocarp forest in Sabah, Malaysia. pp. 1–101.
- Garcia, B.N., Libonati, R. & Nunes, A. (2018) Extreme drought events over the amazon basin: the perspective from the reconstruction of South American hydroclimate. *Water*, **10**, 1594.
- García León, M.M., Martínez Izquierdo, L., Mello, F.N.A., Powers, J.S. & Schnitzer, S.A. (2018) Lianas reduce community-level canopy tree reproduction in a Panamanian forest. *Journal of Ecology*, **106**, 737-745.
- Gauch, H.G., Hwang, J.T. & Fick, G.W. (2003) Model evaluation by comparison of model-based predictions and measured values. *Agronomy Journal*, **95**, 1442-1446.
- Gaveau, D.L., Locatelli, B., Salim, M.A., Yaen, H., Pacheco, P. & Sheil, D. (2019) Rise and fall of forest loss and industrial plantations in Borneo (2000–2017). *Conservation Letters*, **12**, e12622.
- Geist, H.J. & Lambin, E.F. (2002) Proximate Causes and Underlying Driving Forces of Tropical Deforestation Tropical forests are disappearing as the result of many pressures, both local and regional, acting in various combinations in different geographical locations. *BioScience*, **52**, 143-150.
- Gentry, A. (1991) Distribution and evolution of climbing plants. *Biology of vines*, 3-49.
- Gerwing, J.J. (2006) The influence of reproductive traits on liana abundance 10 years after conventional and reduced-impacts logging in the eastern Brazilian Amazon. *Forest Ecology and Management*, **221**, 83-90.
- Gerwing, J.J. & Farias, D.L. (2000) Integrating liana abundance and forest stature into an estimate of total aboveground biomass for an eastern Amazonian forest. *Journal of Tropical Ecology*, **16**, 327-335.
- Gerwing, J.J. & Uhl, C. (2002) Pre-logging liana cutting reduces liana regeneration in logging gaps in the eastern Brazilian Amazon. *Ecological Applications*, **12**, 1642-1651.
- Gerwing, J.J. & Vidal, E. (2002) Changes in liana abundance and species diversity eight years after liana cutting and logging in an eastern Amazonian forest. *Conservation Biology*, **16**, 544-548.
- Ghazoul, J. (2016) *Dipterocarp biology, ecology, and conservation*. Oxford University Press.
- Giam, X. (2017) Global biodiversity loss from tropical deforestation. *Proceedings of the National Academy of Sciences*, **114**, 5775-5777.
- Gibson, L., Lee, T.M., Koh, L.P., Brook, B.W., Gardner, T.A., Barlow, J., Peres, C.A., Bradshaw, C.J., Laurance, W.F. & Lovejoy, T.E. (2011) Primary forests are irreplaceable for sustaining tropical biodiversity. *Nature*, **478**, 378-381.
- Gloor, M., Phillips, O.L., Lloyd, J., Lewis, S.L., Malhi, Y., Baker, T.R., LÓPEZ-GONZALEZ, G., Peacock, J., Almeida, S. & de Oliveira, A.A. (2009) Does the disturbance hypothesis explain the biomass increase in basin-wide Amazon forest plot data? *Global Change Biology*, **15**, 2418-2430.

- Gonzalez de Tanago, J., Lau, A., Bartholomeus, H., Herold, M., Avitabile, V., Raunonen, P., Martius, C., Goodman, R.C., Disney, M. & Manuri, S. (2018) Estimation of above-ground biomass of large tropical trees with terrestrial LiDAR. *Methods in Ecology and Evolution*, **9**, 223-234.
- Grace, J., Mitchard, E. & Gloor, E. (2014) Perturbations in the carbon budget of the tropics. *Global Change Biology*, **20**, 3238-3255.
- Granados, J. & Körner, C. (2002) In deep shade, elevated CO₂ increases the vigor of tropical climbing plants. *Global Change Biology*, **8**, 1109-1117.
- Grauel, W.T. & Putz, F.E. (2004) Effects of lianas on growth and regeneration of *Prioria copaifera* in Darien, Panama. *Forest Ecology and Management*, **190**, 99-108.
- Guanter, L., Kaufmann, H., Segl, K., Foerster, S., Rogass, C., Chabrillat, S., Kuester, T., Hollstein, A., Rossner, G. & Chlebek, C. (2015) The EnMAP spaceborne imaging spectroscopy mission for earth observation. *Remote Sensing*, **7**, 8830-8857.
- Guzmán, Q., Antonio, J., Sánchez-Azofeifa, G.A. & Rivard, B. (2018) Differences in leaf temperature between lianas and trees in the neotropical canopy. *Forests*, **9**, 307.
- Guzman, Q.J., Rivard, B. & Sánchez-Azofeifa, G.A. (2018) Discrimination of liana and tree leaves from a Neotropical Dry Forest using visible-near infrared and longwave infrared reflectance spectra. *Remote Sensing of Environment*, **219**, 135-144.
- Hansen, M.C., Potapov, P.V., Moore, R., Hancher, M., Turubanova, S., Tyukavina, A., Thau, D., Stehman, S., Goetz, S. & Loveland, T. (2013) High-resolution global maps of 21st-century forest cover change. *Science*, **342**, 850-853.
- Happel, B.L. & Murre, J.M. (1994) Design and evolution of modular neural network architectures. *Neural networks*, **7**, 985-1004.
- Harris, N.L., Brown, S., Hagen, S.C., Saatchi, S.S., Petrova, S., Salas, W., Hansen, M.C., Potapov, P.V. & Lutsch, A. (2012) Baseline map of carbon emissions from deforestation in tropical regions. *Science*, **336**, 1573-1576.
- Hasler, N., Werth, D. & Avissar, R. (2009) Effects of tropical deforestation on global hydroclimate: A multimodel ensemble analysis. *Journal of Climate*, **22**, 1124-1141.
- Heermann, P.D. & Khazenie, N. (1992) Classification of multispectral remote sensing data using a back-propagation neural network. *IEEE Transactions on Geoscience and Remote Sensing*, **30**, 81-88.
- Hegarty, E.E. & Cabelle, G. (1991) Distribution and abundance of vines in forest communities. In *The Biology of Vines* (eds Putz, F.E. & H.A. Mooney). Cambridge University Press, Cambridge, UK. pp. 313-335.
- Hernández-Stefanoni, J., Dupuy, J., Johnson, K., Birdsey, R., Tun-Dzul, F., Peduzzi, A., Caamal-Sosa, J., Sánchez-Santos, G. & López-Merlín, D. (2014) Improving species diversity and biomass estimates of tropical dry forests using airborne LiDAR. *Remote Sensing*, **6**, 4741-4763.
- Hesketh, M. & Sánchez-Azofeifa, G.A. (2012) The effect of seasonal spectral variation on species classification in the Panamanian tropical forest. *Remote Sensing of Environment*, **118**, 73-82.
- Higgins, M.A., Asner, G.P., Martin, R.E., Knapp, D.E., Anderson, C., Kennedy-Bowdoin, T., Saenz, R., Aguilar, A. & Wright, S.J. (2014) Linking imaging spectroscopy and LiDAR with floristic composition and forest structure in Panama. *Remote Sensing of Environment*, **154**, 358-367.
- Holl, K.D. & Aide, T.M. (2011) When and where to actively restore ecosystems? *Forest Ecology and Management*, **261**, 1558-1563.
- Hsu, W.-Y. (2012) Registration accuracy and quality of real-life images. *PloS one*, **7**, e40558.
- Hu, T., Su, Y., Xue, B., Liu, J., Zhao, X., Fang, J. & Guo, Q. (2016) Mapping global forest aboveground biomass with spaceborne LiDAR, optical imagery, and forest inventory data. *Remote Sensing*, **8**, 565.
- Huang, M. & Asner, G.P. (2010) Long-term carbon loss and recovery following selective logging in Amazon forests. *Global Biogeochemical Cycles*, **24** (3), DOI: <https://doi.org/10.1029/2009GB003727>.

- Hubau, W., Lewis, S.L., Phillips, O.L., Affum-Baffoe, K., Beeckman, H., Cuní-Sánchez, A., Daniels, A.K., Ewango, C.E., Fauset, S. & Mukinzi, J.M. (2020) Asynchronous carbon sink saturation in African and Amazonian tropical forests. *Nature*, **579**, 80-87.
- Hubbell, S.P. (1986) Canopy gaps and the dynamics of a neotropical forest. *Plant Ecology*, 77-96.
- Huete, A.R., Kim, Y., Ratana, P., Didan, K., Shimabukuro, Y.E. & Miura, T. (2008) Assessment of phenologic variability in Amazon tropical rainforests using hyperspectral Hyperion and MODIS satellite data. *Hyperspectral Remote Sensing of Tropical and Sub-Tropical Forests*, pp. 233-259. CRC Press.
- Hunter, M.O., Keller, M., Morton, D., Cook, B., Lefsky, M., Ducey, M., Saleska, S., de Oliveira Jr, R.C. & Schietti, J. (2015) Structural dynamics of tropical moist forest gaps. *PLoS one*, **10**, e0132144.
- Huntingford, C., Zelazowski, P., Galbraith, D., Mercado, L.M., Sitch, S., Fisher, R., Lomas, M., Walker, A.P., Jones, C.D. & Booth, B.B. (2013) Simulated resilience of tropical rainforests to CO₂-induced climate change. *Nature Geoscience*, **6**, 268-273.
- Immitzer, M., Atzberger, C. & Koukal, T. (2012) Tree species classification with random forest using very high spatial resolution 8-band WorldView-2 satellite data. *Remote Sensing*, **4**, 2661-2693.
- Ingwell, L.L., Joseph Wright, S., Becklund, K.K., Hubbell, S.P. & Schnitzer, S.A. (2010) The impact of lianas on 10 years of tree growth and mortality on Barro Colorado Island, Panama. *Journal of Ecology*, **98**, 879-887.
- IPCC, I. (2006) Guidelines for National Greenhouse Gas Inventories Volume 4: Agriculture, Forestry, and Other Landuse. OECD Press, Paris (2006).
- Isenburg, M. (2014) LAStools—Efficient LiDAR Processing Software. Available online: lastools.org (accessed on 10 October 2017).
- Jakubowski, M., Li, W., Guo, Q. & Kelly, M. (2013) Delineating individual trees from LiDAR data: A comparison of vector- and raster-based segmentation approaches. *Remote Sensing*, **5**, 4163-4186.
- Jetz, W., Cavender-Bares, J., Pavlick, R., Schimel, D., Davis, F.W., Asner, G.P., Guralnick, R., Kattge, J., Latimer, A.M. & Moorcroft, P. (2016) Monitoring plant functional diversity from space. *Nature plants*, **2**, 16024.
- Jha, C., Singhal, J., Reddy, C., Rajashekar, G., Maity, S., Patnaik, C., Das, A., Misra, A., Singh, C. & Mohapatra, J. (2019) Characterization of species diversity and forest health using AVIRIS-NG hyperspectral remote sensing data. *Current Science (00113891)*, **116** (7), 1124-1135.
- Jiang, Y., Wang, J., Zhang, L., Zhang, G., Li, X. & Wu, J. (2019) Geometric Processing and Accuracy Verification of Zhuhai-1 Hyperspectral Satellites. *Remote Sensing*, **11**, 996.
- Jiménez-Muñoz, J.C., Mattar, C., Barichivich, J., Santamaría-Artigas, A., Takahashi, K., Malhi, Y., Sobrino, J.A. & Van Der Schrier, G. (2016) Record-breaking warming and extreme drought in the Amazon rainforest during the course of El Niño 2015–2016. *Scientific Reports*, **6**, 33130.
- Jing, L., Hu, B., Li, H., Li, J. & Noland, T. (2014) Automated individual tree crown delineation from LIDAR data using morphological techniques. *IOP Conference Series: Earth and Environmental Science*, pp. 012152. IOP Publishing.
- John, R., Dalling, J.W., Harms, K.E., Yavitt, J.B., Stallard, R.F., Mirabello, M., Hubbell, S.P., Valencia, R., Navarrete, H. & Vallejo, M. (2007) Soil nutrients influence spatial distributions of tropical tree species. *Proceedings of the National Academy of Sciences*, **104**, 864-869.
- Jucker, T., Asner, G.P., Dalponte, M., Brodrick, P.G., Philipson, C.D., Vaughn, N.R., Teh, Y.A., Brelsford, C., Burslem, D.F. & Deere, N.J. (2018) Estimating aboveground carbon density and its uncertainty in Borneo's structurally complex tropical forests using airborne laser scanning. *Biogeosciences*, **15**, 3811-3830.
- Kalacska, M., Bohlman, S., Sanchez-Azofeifa, G.A., Castro-Esau, K. & Caelli, T. (2007) Hyperspectral discrimination of tropical dry forest lianas and trees: Comparative data reduction approaches at the leaf and canopy levels. *Remote Sensing of Environment*, **109**, 406-415.

- Kalácska, M., Calvo-Alvarado, J.C. & Sánchez-Azofeifa, G.A. (2005) Calibration and assessment of seasonal changes in leaf area index of a tropical dry forest in different stages of succession. *Tree Physiology*, **25**, 733-744.
- Kalchbrenner, N., Grefenstette, E. & Blunsom, P. (2014) A convolutional neural network for modelling sentences. Proceedings of the 52nd Annual Meeting of the Association for Computational Linguistics (Volume 1: Long Papers), DOI: 10.3115/v1/P14-1062
- Karsoliya, S. (2012) Approximating number of hidden layer neurons in multiple hidden layer BPNN architecture. *International Journal of Engineering Trends and Technology*, **3**, 714-717.
- Keith, H., Mackey, B.G. & Lindenmayer, D.B. (2009) Re-evaluation of forest biomass carbon stocks and lessons from the world's most carbon-dense forests. *Proceedings of the National Academy of Sciences*, **106**, 11635-11640.
- Kellner, J.R., Albert, L.P., Burley, J.T. & Cushman, K. (2019) The case for remote sensing of individual plants. *American journal of botany*, **106** (9), 1139-1142, DOI: 10.1002/ajb2.1347
- Kellner, J.R., Clark, D.B. & Hubbell, S.P. (2009) Pervasive canopy dynamics produce short-term stability in a tropical rain forest landscape. *Ecology letters*, **12**, 155-164.
- Kennard, D.K. (1998) Biomechanical properties of tree saplings and free-standing lianas as indicators of susceptibility to logging damage. *Forest Ecology and Management*, **102**, 179-191.
- Kent, R., Lindsell, J., Laurin, G., Valentini, R. & Coomes, D. (2015) Airborne LiDAR detects selectively logged tropical forest even in an advanced stage of recovery. *Remote Sensing*, **7**, 8348-8367.
- Keshava, N. & Mustard, J.F. (2002) Spectral unmixing. *IEEE signal processing magazine*, **19**, 44-57.
- Kettle, C.J., Maycock, C.R. & Burslem, D. (2012) New directions in dipterocarp biology and conservation: a synthesis. *Biotropica*, **44**, 658-660.
- Kooperman, G.J., Chen, Y., Hoffman, F.M., Koven, C.D., Lindsay, K., Pritchard, M.S., Swann, A.L. & Randerson, J.T. (2018) Forest response to rising CO₂ drives zonally asymmetric rainfall change over tropical land. *Nature Climate Change*, **8**, 434-440.
- Körner, C. (2007) The use of 'altitude' in ecological research. *Trends in Ecology & Evolution*, **22**, 569-574.
- Lamb, D. (2011) Natural regeneration and secondary forests. In *Regreening the bare hills: Tropical Forest Restoration in the Asia-Pacific Region*, pp. 157-209. Springer.
- Lamb, D., Erskine, P.D. & Parrotta, J.A. (2005) Restoration of degraded tropical forest landscapes. *Science*, **310**, 1628-1632.
- Larjavaara, M. & Muller-Landau, H.C. (2013) Measuring tree height: a quantitative comparison of two common field methods in a moist tropical forest. *Methods in Ecology and Evolution*, **4**, 793-801.
- Laurance, W. & Edwards, D. (2014) Saving logged tropical forests. *Frontiers in Ecology and the Environment*, **12**, 147-147.
- Laurance, W.F. (1999) Reflections on the tropical deforestation crisis. *Biological Conservation*, **91**, 109-117.
- Laurance, W.F., Andrade, A.S., Magrach, A., Camargo, J.L., Valsko, J.J., Campbell, M., Fearnside, P.M., Edwards, W., Lovejoy, T.E. & Laurance, S.G. (2014) Long-term changes in liana abundance and forest dynamics in undisturbed Amazonian forests. *Ecology*, **95**, 1604-1611.
- Laurance, W.F., Pérez-Salicrup, D., Delamônica, P., Fearnside, P.M., D'Angelo, S., Jerozolinski, A., Pohl, L. & Lovejoy, T.E. (2001) Rain forest fragmentation and the structure of Amazonian liana communities. *Ecology*, **82**, 105-116.
- Laurin, G.V., Chan, J.C.-W., Chen, Q., Lindsell, J.A., Coomes, D.A., Guerriero, L., Del Frate, F., Miglietta, F. & Valentini, R. (2014a) Biodiversity mapping in a tropical West African forest with airborne hyperspectral data. *PloS one*, **9**, e97910.
- Laurin, G.V., Chen, Q., Lindsell, J.A., Coomes, D.A., Del Frate, F., Guerriero, L., Pirotti, F. & Valentini, R. (2014b) Above ground biomass estimation in an African tropical forest with lidar and hyperspectral data. *ISPRS journal of photogrammetry and remote sensing*, **89**, 49-58.
- Lawson, S., Blundell, A., Cabarle, B., Basik, N., Jenkins, M. & Canby, K. (2014) Consumer goods and deforestation: An analysis of the extent and nature of illegality in forest conversion for

- agriculture and timber plantations. *Forest Trend Report Series*, **131**, DOI: <https://www.forest-trends.org/publications/consumer-goods-and-deforestation>
- Lean, J. & Warrilow, D.A. (1989) Simulation of the regional climatic impact of Amazon deforestation. *Nature*, **342**, 411-413.
- Lechner, A.M., Foody, G.M. & Boyd, D.S. (2020) Applications in Remote Sensing to Forest Ecology and Management. *One Earth*, **2**, 405-412.
- Ledo, A., Illian, J.B., Schnitzer, S.A., Wright, S.J., Dalling, J.W. & Burslem, D.F. (2016) Lianas and soil nutrients predict fine-scale distribution of above-ground biomass in a tropical moist forest. *Journal of Ecology*, **104**, 1819-1828.
- Ledo, A. & Schnitzer, S.A. (2014) Disturbance and clonal reproduction determine liana distribution and maintain liana diversity in a tropical forest. *Ecology*, **95**, 2169-2178.
- Lee, J., Cai, X., Lellmann, J., Dalponte, M., Malhi, Y., Butt, N., Morecroft, M., Schönlieb, C.-B. & Coomes, D.A. (2016) Individual tree species classification from airborne multisensor imagery using robust PCA. *IEEE Journal of Selected Topics in Applied Earth Observations and Remote Sensing*, **9**, 2554-2567.
- Lee, T. & McPhaden, M.J. (2010) Increasing intensity of El Niño in the central-equatorial Pacific. *Geophysical research letters*, **37** (14), DOI: <https://doi.org/10.1029/2010GL044007>.
- Lefsky, M.A. (2010) A global forest canopy height map from the Moderate Resolution Imaging Spectroradiometer and the Geoscience Laser Altimeter System. *Geophysical research letters*, **37** (15), DOI: <https://doi.org/10.1029/2010GL043622>.
- Lefsky, M.A., Harding, D.J., Keller, M., Cohen, W.B., Carabajal, C.C., Del Bom Espirito-Santo, F., Hunter, M.O. & de Oliveira Jr, R. (2005) Estimates of forest canopy height and aboveground biomass using ICESat. *Geophysical research letters*, **32** (22), DOI: <https://doi.org/10.1029/2005GL023971>.
- Lewis, S.L., Edwards, D.P. & Galbraith, D. (2015) Increasing human dominance of tropical forests. *Science*, **349**, 827-832.
- Lewis, S.L., Lopez-Gonzalez, G., Sonké, B., Affum-Baffoe, K., Baker, T.R., Ojo, L.O., Phillips, O.L., Reitsma, J.M., White, L. & Comiskey, J.A. (2009) Increasing carbon storage in intact African tropical forests. *Nature*, **457**, 1003-1006.
- Lewis, S.L., Phillips, O.L., Baker, T.R., Lloyd, J., Malhi, Y., Almeida, S., Higuchi, N., Laurance, W.F., Neill, D. & Silva, J. (2004a) Concerted changes in tropical forest structure and dynamics: evidence from 50 South American long-term plots. *Philosophical Transactions of the Royal Society of London B: Biological Sciences*, **359**, 421-436.
- Lewis, S.L., Phillips, O.L., Sheil, D., Vinceti, B., Baker, T.R., Brown, S., Graham, A.W., Higuchi, N., Hilbert, D.W. & Laurance, W.F. (2004b) Tropical forest tree mortality, recruitment and turnover rates: calculation, interpretation and comparison when census intervals vary. *Journal of Ecology*, **92**, 929-944.
- Li, W., Campos-Vargas, C., Marzahn, P. & Sanchez-Azofeifa, A. (2018) On the estimation of tree mortality and liana infestation using a deep self-encoding network. *International Journal of Applied Earth Observation and Geoinformation*, **73**, 1-13.
- Li, X. & Shao, G. (2014) Object-based land-cover mapping with high resolution aerial photography at a county scale in midwestern USA. *Remote Sensing*, **6**, 11372-11390.
- Lieberman, D., Lieberman, M., Peralta, R. & Hartshorn, G.S. (1985) Mortality patterns and stand turnover rates in a wet tropical forest in Costa Rica. *The Journal of Ecology*, 915-924.
- Lin, M., Lucas Jr, H.C. & Shmueli, G. (2013) Research commentary—too big to fail: large samples and the p-value problem. *Information Systems Research*, **24**, 906-917.
- Liu, D. & Xia, F. (2010) Assessing object-based classification: advantages and limitations. *Remote Sensing Letters*, **1**, 187-194.
- Londré, R.A. & Schnitzer, S.A. (2006) The distribution of lianas and their change in abundance in temperate forests over the past 45 years. *Ecology*, **87**, 2973-2978.

- Lopez-Gonzalez, G., Lewis, S.L., Burkitt, M. & Phillips, O.L. (2011) ForestPlots. net: a web application and research tool to manage and analyse tropical forest plot data. *Journal of Vegetation Science*, **22**, 610-613.
- Lu, D., Chen, Q., Wang, G., Moran, E., Batistella, M., Zhang, M., Vaglio Laurin, G. & Saah, D. (2012) Aboveground forest biomass estimation with Landsat and LiDAR data and uncertainty analysis of the estimates. *International Journal of Forestry Research*, **2012**, DOI: <https://doi.org/10.1155/2012/436537>
- Lu, L., Zeng, X., Wu, S. & Zhong, S. (2008) A Novel Ensemble Approach for Improving Generalization Ability of Neural Networks. *International Conference on Intelligent Data Engineering and Automated Learning*, pp. 164-171. Springer.
- Lucier, J.W. (2018) Automatic UAV image registration using feature detection and matching with satellite imagery. Massachusetts Institute of Technology. Accessed online: <http://hdl.handle.net/1721.1/119920>.
- Luo, S., Wang, C., Xi, X., Nie, S., Fan, X., Chen, H., Ma, D., Liu, J., Zou, J. & Lin, Y. (2019) Estimating forest aboveground biomass using small-footprint full-waveform airborne LiDAR data. *International Journal of Applied Earth Observation and Geoinformation*, **83**, 101922.
- Luyssaert, S., Schulze, E.-D., Börner, A., Knohl, A., Hessenmöller, D., Law, B.E., Ciais, P. & Grace, J. (2008) Old-growth forests as global carbon sinks. *Nature*, **455**, 213-215.
- Magrath, A., Senior, R.A., Rogers, A., Nurdin, D., Benedick, S., Laurance, W.F., Santamaria, L. & Edwards, D.P. (2016) Selective logging in tropical forests decreases the robustness of liana–tree interaction networks to the loss of host tree species. *Proceedings of the Royal Society B*, **283** (1826), 20153008, DOI: <http://doi.org/10.1098/rspb.2015.3008>
- Malhi, Y. (2010) The carbon balance of tropical forest regions, 1990–2005. *Current Opinion in Environmental Sustainability*, **2**, (4), 237-244.
- Malhi, Y., Adu-Bredu, S., Asare, R.A., Lewis, S.L. & Mayaux, P. (2013) African rainforests: past, present and future. *Philosophical Transactions of the Royal Society B: Biological Sciences*, **368** (1625), 20120312.
- Malhi, Y., Aragao, L.E.O., Metcalfe, D.B., Paiva, R., Quesada, C.A., Almeida, S., Anderson, L., Brando, P., Chambers, J.Q. & Da Costa, A.C. (2009) Comprehensive assessment of carbon productivity, allocation and storage in three Amazonian forests. *Global Change Biology*, **15**, 1255-1274.
- Malhi, Y., Baker, T.R., Phillips, O.L., Almeida, S., Alvarez, E., Arroyo, L., Chave, J., Czimczik, C.I., Fiore, A.D. & Higuchi, N. (2004) The above-ground coarse wood productivity of 104 Neotropical forest plots. *Global Change Biology*, **10**, 563-591.
- Malhi, Y. & Grace, J. (2000) Tropical forests and atmospheric carbon dioxide. *Trends in Ecology & Evolution*, **15**, 332-337.
- Malhi, Y. & Phillips, O.L. (2004) Tropical forests and global atmospheric change: a synthesis. *Philosophical Transactions of the Royal Society of London. Series B: Biological Sciences*, **359**, 549-555.
- Malhi, Y. & Wright, J. (2004) Spatial patterns and recent trends in the climate of tropical rainforest regions. *Philosophical Transactions of the Royal Society of London. Series B: Biological Sciences*, **359**, 311-329.
- Malhi, Y. & Wright, J. (2005) Late twentieth-century patterns and trends in the climate of tropical forest regions. In *Tropical forests and global atmospheric change* (Eds Malhi, Y & Phillips, O). Oxford Scholarship Online.
- Malizia, A. & Grau, H.R. (2006) Liana–host tree associations in a subtropical montane forest of north-western Argentina. *Journal of Tropical Ecology*, **22**, 331-339.
- Mangueira, J.R.S., D. Holl, K. & Rodrigues, R.R. (2019) Enrichment planting to restore degraded tropical forest fragments in Brazil. *Ecosystems and People*, **15**, 3-10.
- Marceau, D.J., Gratton, D.J., Fournier, R.A. & Fortin, J.-P. (1994) Remote sensing and the measurement of geographical entities in a forested environment. 2. The optimal spatial resolution. *Remote Sensing of Environment*, **49**, 105-117.

- Maréchaux, I., Bartlett, M.K., Iribar, A., Sack, L. & Chave, J. (2017) Stronger seasonal adjustment in leaf turgor loss point in lianas than trees in an Amazonian forest. *Biology letters*, **13**, 20160819.
- Marfo, P. & Okyere, G. (2019) The accuracy of effect-size estimates under normals and contaminated normals in meta-analysis. *Heliyon*, **5**, e01838.
- Marimon, B.S., Oliveira-Santos, C., Marimon-Junior, B.H., Elias, F., de Oliveira, E.A., Morandi, P.S., Prestes, N.C.d.S., Mariano, L.H., Pereira, O.R. & Feldpausch, T.R. (2020) Drought generates large, long-term changes in tree and liana regeneration in a monodominant Amazon forest. *Plant Ecology*, 1-15, DOI: <https://doi.org/10.1007/s11258-020-01047-8>
- Marsh, C.W. & Greer, A.G. (1992) Forest land-use in Sabah, Malaysia: an introduction to Danum Valley. *Philosophical Transactions of the Royal Society of London. Series B: Biological Sciences*, **335**, 331-339.
- Marshall, A.R., Coates, M.A., Archer, J., Kivambe, E., Mnendendo, H., Mtoka, S., Mwakisoma, R., Figueiredo, R.J. & Njilima, F.M. (2017) Liana cutting for restoring tropical forests: a rare palaeotropical trial. *African Journal of Ecology*, **55**, 282-297.
- Marshall, A.R., Platts, P.J., Chazdon, R.L., Seki, H., Campbell, M.J., Phillips, O.L., Gereau, R.E., Marchant, R., Liang, J. & Herbohn, J. (2020) Conceptualising the global forest response to liana proliferation. *Frontiers in Forests and Global Change*, **3**, 35.
- Martin, P.A., Newton, A.C., Pfeifer, M., Khoo, M. & Bullock, J.M. (2015) Impacts of tropical selective logging on carbon storage and tree species richness: A meta-analysis. *Forest Ecology and Management*, **356**, 224-233.
- Martin, P.H., Sherman, R.E. & Fahey, T.J. (2004) Forty years of tropical forest recovery from agriculture: structure and floristics of secondary and old-growth riparian forests in the Dominican Republic. *Biotropica*, **36**, 297-317.
- Martínez-Izquierdo, L., García, M.M., Powers, J.S. & Schnitzer, S.A. (2016) Lianas suppress seedling growth and survival of 14 tree species in a Panamanian tropical forest. *Ecology*, **97**, 215-224.
- Marvin, D.C., Asner, G.P. & Schnitzer, S.A. (2016) Liana canopy cover mapped throughout a tropical forest with high-fidelity imaging spectroscopy. *Remote Sensing of Environment*, **176**, 98-106.
- Maxwell, S.L., Evans, T., Watson, J.E., Morel, A., Grantham, H., Duncan, A., Harris, N., Potapov, P., Runting, R.K. & Venter, O. (2019) Degradation and forgone removals increase the carbon impact of intact forest loss by 626%. *Science Advances*, **5** (10), eaax2546.
- McAlpine, C.A., Johnson, A., Salazar, A., Syktus, J., Wilson, K., Meijaard, E., Seabrook, L., Dargusch, P., Nordin, H. & Sheil, D. (2018) Forest loss and Borneo's climate. *Environmental Research Letters*, **13**, 044009.
- McDowell, N.G., Allen, C.D., Anderson-Teixeira, K., Aukema, B.H., Bond-Lamberty, B., Chini, L., Clark, J.S., Dietze, M., Grossiord, C. & Hanbury-Brown, A. (2020) Pervasive shifts in forest dynamics in a changing world. *Science*, **368**.
- Medjibe, V., Putz, F.E. & Romero, C. (2013) Certified and uncertified logging concessions compared in Gabon: changes in stand structure, tree species, and biomass. *Environmental management*, **51**, 524-540.
- Meyer, L., Diniz-Filho, J.A.F., Lohmann, L.G., Hortal, J., Barreto, E., Rangel, T. & Kissling, W.D. (2019) Canopy height explains species richness in the largest clade of Neotropical lianas. *Global Ecology and Biogeography*, **29** (1), 26-37.
- Meyer, V., Saatchi, S., CLARCK, D., Keller, M., Vicent, G., Ferraz, A., Espírito-Santo, F., OLIVEIRA, M.d., Kaki, D. & Chave, J. (2018) Canopy area of large trees explains aboveground biomass variations across neotropical forest landscapes. *Biogeosciences*, **15**, 3377-3390, DOI: <https://doi.org/10.5194/bg-15-3377-2018>.
- Mielcarek, M., Stereńczak, K. & Khosravipour, A. (2018) Testing and evaluating different LiDAR-derived canopy height model generation methods for tree height estimation. *International Journal of Applied Earth Observation and Geoinformation*, **71**, 132-143.
- Muscarella, R., Kolyaie, S., Morton, D.C., Zimmerman, J.K. & Uriarte, M. (2020) Effects of topography on tropical forest structure depend on climate context. *Journal of Ecology*, **108**, 145-159.

- Mutanga, O., Adam, E. & Cho, M.A. (2012) High density biomass estimation for wetland vegetation using WorldView-2 imagery and random forest regression algorithm. *International Journal of Applied Earth Observation and Geoinformation*, **18**, 399-406.
- Myers, N., Mittermeier, R.A., Mittermeier, C.G., Da Fonseca, G.A. & Kent, J. (2000) Biodiversity hotspots for conservation priorities. *Nature*, **403**, 853.
- Nabe-Nielsen, J., Kollmann, J. & Peña-Claros, M. (2009) Effects of liana load, tree diameter and distances between conspecifics on seed production in tropical timber trees. *Forest Ecology and Management*, **257**, 987-993.
- Narasimha, P.L., Delashmit, W.H., Manry, M.T., Li, J. & Maldonado, F. (2008) An integrated growing-pruning method for feedforward network training. *Neurocomputing*, **71**, 2831-2847.
- Neary, D.G., Ice, G.G. & Jackson, C.R. (2009) Linkages between forest soils and water quality and quantity. *Forest Ecology and Management*, **258**, 2269-2281.
- Negri, A.J., Adler, R.F., Xu, L. & Surratt, J. (2004) The impact of Amazonian deforestation on dry season rainfall. *Journal of Climate*, **17**, 1306-1319.
- Ni-Meister, W., Lee, S., Strahler, A.H., Woodcock, C.E., Schaaf, C., Yao, T., Ranson, K.J., Sun, G. & Blair, J.B. (2010) Assessing general relationships between aboveground biomass and vegetation structure parameters for improved carbon estimate from lidar remote sensing. *Journal of Geophysical Research: Biogeosciences*, **115**.
- Nie, S., Wang, C., Zeng, H., Xi, X. & Li, G. (2017) Above-ground biomass estimation using airborne discrete-return and full-waveform LiDAR data in a coniferous forest. *Ecological Indicators*, **78**, 221-228.
- Numata, S., Yasuda, M., Okuda, T., Kachi, N. & Supardi, M.N. (2006) Canopy gap dynamics of two different forest stands in a Malaysian lowland rain forest. *Journal of Tropical Forest Science*, 109-116.
- Nunes, M., Ewers, R., Turner, E. & Coomes, D. (2017) Mapping aboveground carbon in oil palm plantations using LiDAR: A comparison of tree-centric versus area-based approaches. *Remote Sensing*, **9**, 816.
- Nunes, M.H., Both, S., Bongalov, B., Brelford, C., Khoury, S., Burslem, D.F., Philipson, C., Majalap, N., Riutta, T. & Coomes, D.A. (2019) Changes in leaf functional traits of rainforest canopy trees associated with an El Niño event in Borneo. *Environmental Research Letters*, **14**, 085005.
- O'Brien, M.J., Philipson, C.D., Reynolds, G., Dzulkipli, D., Snaddon, J.L., Ong, R. & Hector, A. (2019) Positive effects of liana cutting on seedlings are reduced during El Niño-induced drought. *Journal of Applied Ecology*, **56**, 891-901.
- Olofsson, P., Foody, G.M., Herold, M., Stehman, S.V., Woodcock, C.E. & Wulder, M.A. (2014) Good practices for estimating area and assessing accuracy of land change. *Remote Sensing of Environment*, **148**, 42-57.
- Olson, M., Wyner, A. & Berk, R. (2018) Modern neural networks generalize on small data sets. *Advances in Neural Information Processing Systems*, pp. 3619-3628.
- Osuri, A.M., Kasinathan, S., Siddhartha, M.K., Mudappa, D. & Raman, T.S. (2019) Effects of restoration on tree communities and carbon storage in rainforest fragments of the Western Ghats, India. *Ecosphere*, **10**.
- Palace, M., Keller, M., Asner, G.P., Hagen, S. & Braswell, B. (2008) Amazon forest structure from IKONOS satellite data and the automated characterization of forest canopy properties. *Biotropica*, **40**, 141-150.
- Palace, M., Sullivan, F.B., Ducey, M. & Herrick, C. (2016) Estimating tropical forest structure using a terrestrial lidar. *PloS one*, **11**, e0154115.
- Palmer, M., Wohlgemuth, T., Earls, P., Arévalo, J. & Thompson, S. (2000) Opportunities for long-term ecological research at the Tallgrass Prairie Preserve, Oklahoma. *Proceedings of the ILTER Regional Workshop: Cooperation in Long Term Ecological Research in Central and Eastern Europe, Budapest, Hungary*, pp. 123-128.

- Pan, Y., Birdsey, R.A., Fang, J., Houghton, R., Kauppi, P.E., Kurz, W.A., Phillips, O.L., Shvidenko, A., Lewis, S.L. & Canadell, J.G. (2011) A large and persistent carbon sink in the world's forests. *Science*, **333**, 988-993.
- Papeş, M., Tupayachi, R., Martinez, P., Peterson, A. & Powell, G. (2010) Using hyperspectral satellite imagery for regional inventories: a test with tropical emergent trees in the Amazon Basin. *Journal of Vegetation Science*, **21**, 342-354.
- Parolari, A.J., Paul, K., Griffing, A., Condit, R., Perez, R., Aguilar, S. & Schnitzer, S.A. (2020) Liana abundance and diversity increase with rainfall seasonality along a precipitation gradient in Panama. *Ecography*, **43**, 25-33.
- Parren, M. & Bongers, F. (2001) Does climber cutting reduce felling damage in southern Cameroon? *Forest Ecology and Management*, **141**, 175-188.
- Pearson, T.R., Brown, S. & Casarim, F.M. (2014) Carbon emissions from tropical forest degradation caused by logging. *Environmental Research Letters*, **9**, 034017.
- Pearson, T.R., Brown, S., Murray, L. & Sidman, G. (2017) Greenhouse gas emissions from tropical forest degradation: an underestimated source. *Carbon balance and management*, **12**, 3.
- Pereira Jr, R., Zweede, J., Asner, G.P. & Keller, M. (2002) Forest canopy damage and recovery in reduced-impact and conventional selective logging in eastern Para, Brazil. *Forest Ecology and Management*, **168**, 77-89.
- Peres, C.A., Barlow, J. & Laurance, W.F. (2006) Detecting anthropogenic disturbance in tropical forests. *Trends in Ecology & Evolution*, **21**, 227-229.
- Pérez-Salicrup, D.R. (2001) Effect of liana cutting on tree regeneration in a liana forest in Amazonian Bolivia. *Ecology*, **82**, 389-396.
- Pérez-Salicrup, D.R. & Barker, M.G. (2000) Effect of liana cutting on water potential and growth of adult *Senna multijuga* (Caesalpinioideae) trees in a Bolivian tropical forest. *Oecologia*, **124**, 469-475.
- Pérez-Salicrup, D.R., Sork, V.L. & Putz, F.E. (2001) Lianas and Trees in a Liana Forest of Amazonian Bolivia. *Biotropica*, **33**, 34-47.
- Pettorelli, N., Vik, J.O., Mysterud, A., Gaillard, J.-M., Tucker, C.J. & Stenseth, N.C. (2005) Using the satellite-derived NDVI to assess ecological responses to environmental change. *Trends in Ecology & Evolution*, **20**, 503-510.
- Pfeifer, M., Kor, L., Nilus, R., Turner, E., Cusack, J., Lysenko, I., Khoo, M., Chey, V., Chung, A. & Ewers, R. (2016) Mapping the structure of Borneo's tropical forests across a degradation gradient. *Remote Sensing of Environment*, **176**, 84-97.
- Pfeifer, M., Lefebvre, V., Turner, E., Cusack, J., Khoo, M., Chey, V.K., Peni, M. & Ewers, R.M. (2015) Deadwood biomass: an underestimated carbon stock in degraded tropical forests? *Environmental Research Letters*, **10**, 044019.
- Phillips, O.L. (1996) Long-term environmental change in tropical forests: increasing tree turnover. *Environmental Conservation*, **23** (3), 235-248.
- Phillips, O.L., Aragão, L.E., Lewis, S.L., Fisher, J.B., Lloyd, J., López-González, G., Malhi, Y., Monteagudo, A., Peacock, J. & Quesada, C.A. (2009) Drought sensitivity of the Amazon rainforest. *Science*, **323**, 1344-1347.
- Phillips, O.L., Baker, T.R., Arroyo, L., Higuchi, N., Killeen, T.J., Laurance, W.F., Lewis, S.L., Lloyd, J., Malhi, Y. & Monteagudo, A. (2004) Pattern and process in Amazon tree turnover, 1976–2001. *Philosophical Transactions of the Royal Society of London. Series B: Biological Sciences*, **359**, 381-407.
- Phillips, O.L. & Gentry, A.H. (1994) Increasing turnover through time in tropical forests. *Science*, **263**, 954-958.
- Phillips, O.L., Hall, P., Gentry, A.H., Sawyer, S. & Vasquez, R. (1994) Dynamics and species richness of tropical rain forests. *Proceedings of the National Academy of Sciences*, **91**, 2805-2809.
- Phillips, O.L., Lewis, S.L., Baker, T.R., Chao, K.-J. & Higuchi, N. (2008) The changing Amazon forest. *Philosophical Transactions of the Royal Society B: Biological Sciences*, **363**, 1819-1827.

- Phillips, O.L., Malhi, Y., Higuchi, N., Laurance, W.F., Núñez, P.V., Vásquez, R.M., Laurance, S.G., Ferreira, L.V., Stern, M. & Brown, S. (1998) Changes in the carbon balance of tropical forests: evidence from long-term plots. *Science*, **282**, 439-442.
- Phillips, O.L., Martínez, R.V., Arroyo, L., Baker, T.R., Killeen, T., Lewis, S.L., ... & Vargas, P.N. (2002) Increasing dominance of large lianas in Amazonian forests. *Nature*, **418**, 770-774.
- Phillips, O.L., Sullivan, M.J., Baker, T.R., Mendoza, A.M., Vargas, P.N. & Vásquez, R. (2019) Species matter: wood density influences tropical forest biomass at multiple scales. *Surveys in geophysics*, **40**, 913-935.
- Phillips, O.L., Vásquez Martínez, R., Monteagudo Mendoza, A., Baker, T.R. & Núñez Vargas, P. (2005) Large lianas as hyperdynamic elements of the tropical forest canopy. *Ecology*, **86**, 1250-1258.
- Pimm, S.L. & Raven, P. (2000) Biodiversity: extinction by numbers. *Nature*, **403**, 843.
- Pinard, M.A. & Putz, F.E. (1996) Retaining forest biomass by reducing logging damage. *Biotropica*, **278-295**.
- Pinard, M.A., Putz, F.E. & Tay, J. (2000) Lessons learned from the implementation of reduced-impact logging in hilly terrain in Sabah, Malaysia. *The international forestry review*, **2** (1), 33-39.
- Piñeiro, G., Perelman, S., Guerschman, J.P. & Paruelo, J.M. (2008) How to evaluate models: observed vs. predicted or predicted vs. observed? *Ecological modelling*, **216**, 316-322.
- Pinter Jr, P.J., Jackson, R.D., Elaine Ezra, C. & Gausman, H.W. (1985) Sun-angle and canopy-architecture effects on the spectral reflectance of six wheat cultivars. *International Journal of Remote Sensing*, **6**, 1813-1825.
- Plaza, J., Hendrix, E.M., García, I., Martín, G. & Plaza, A. (2012) On endmember identification in hyperspectral images without pure pixels: A comparison of algorithms. *Journal of Mathematical Imaging and Vision*, **42**, 163-175.
- Popescu, S.C., Zhao, K., Neuenschwander, A. & Lin, C. (2011) Satellite lidar vs. small footprint airborne lidar: Comparing the accuracy of aboveground biomass estimates and forest structure metrics at footprint level. *Remote Sensing of Environment*, **115**, 2786-2797.
- Poulsen, J.R., Koerner, S.E., Miao, Z., Medjibe, V.P., Banak, L.N. & White, L. (2017) Forest structure determines the abundance and distribution of large lianas in Gabon. *Global Ecology and Biogeography*, **26**, 472-485.
- Powers, J.S., Corre, M.D., Twine, T.E. & Veldkamp, E. (2011) Geographic bias of field observations of soil carbon stocks with tropical land-use changes precludes spatial extrapolation. *Proceedings of the National Academy of Sciences*, **108**, 6318-6322.
- Price, J.C. (1994) How unique are spectral signatures? *Remote Sensing of Environment*, **49**, 181-186.
- Proctor, J., Anderson, J., Chai, P. & Vallack, H. (1983) Ecological studies in four contrasting lowland rain forests in Gunung Mulu National Park, Sarawak: I. Forest environment, structure and floristics. *The Journal of Ecology*, **71**, 237-260.
- Pu, R., Landry, S. & Yu, Q. (2011) Object-based urban detailed land cover classification with high spatial resolution IKONOS imagery. *International Journal of Remote Sensing*, **32**, 3285-3308.
- Putz, F.E. (1991) Silvicultural effects of lianas. In *The biology of vines* (Eds Putz, F.E & H.A Mooney). Cambridge University Press, Cambridge. pp. 493-501.
- Putz, F.E. (1983) Liana biomass and leaf area of a "tierra firme" forest in the Rio Negro Basin, Venezuela. *Biotropica*, **15**, 185-189.
- Putz, F.E. (1984) The natural history of lianas on Barro Colorado Island, Panama. *Ecology*, **65**, 1713-1724.
- Putz, F.E., Baker, T., Griscom, B.W., Gopalakrishna, T., Roopsind, A., Umunay, P.M., Zalman, J., Ellis, E.A. & Ellis, P.W. (2019) Intact forest in selective logging landscapes in the tropics. *Frontiers in Forests and Global Change*, **2**, 30.
- Putz, F.E. & Chai, P. (1987) Ecological studies of lianas in Lambir National Park, Sarawak, Malaysia. *Journal of Ecology*, **75**, 523-531.
- Putz, F.E., Sist, P., Fredericksen, T. & Dykstra, D. (2008a) Reduced-impact logging: challenges and opportunities. *Forest Ecology and Management*, **256**, 1427-1433.

- Putz, F.E., Zuidema, P.A., Pinard, M.A., Boot, R.G., Sayer, J.A., Sheil, D., Sist, P. & Vanclay, J.K. (2008b) Improved tropical forest management for carbon retention. *PLoS biology*, **6**, e166.
- Putz, F.E., Zuidema, P.A., Synnott, T., Peña-Claros, M., Pinard, M.A., Sheil, D., Vanclay, J.K., Sist, P., Gourlet-Fleury, S. & Griscom, B. (2012) Sustaining conservation values in selectively logged tropical forests: the attained and the attainable. *Conservation Letters*, **5**, 296-303.
- QGIS Development Team (2018) QGIS geographic information system. *Open Source Geospatial Foundation Project*.
- Qie, L., Lewis, S.L., Sullivan, M.J., Lopez-Gonzalez, G., Pickavance, G.C., Sunderland, T., Ashton, P., Hubau, W., Salim, K.A. & Aiba, S.-I. (2017) Long-term carbon sink in Borneo's forests halted by drought and vulnerable to edge effects. *Nature Communications*, **8**, 1966.
- Quesada, C., Phillips, O., Schwarz, M., Czimczik, C., Baker, T., Patiño, S., Fyllas, N., Hodnett, M., Herrera, R. & Almeida, S. (2012) Basin-wide variations in Amazon forest structure and function are mediated by both soils and climate. *Biogeosciences*, **9**, 2203-2246.
- R Core Team (2019) R: A language and environment for statistical computing. R Foundation for Statistical Computing, Vienna, Austria. URL: <https://www.R-project.org/>.
- Reiche, J., Lucas, R., Mitchell, A.L., Verbesselt, J., Hoekman, D.H., Haarpaintner, J., Kellndorfer, J.M., Rosenqvist, A., Lehmann, E.A. & Woodcock, C.E. (2016) Combining satellite data for better tropical forest monitoring. *Nature Climate Change*, **6**, 120-122.
- Rejou-Mechain, M., Muller-Landau, H.C., Detto, M., Thomas, S., Toan, T.L., Saatchi, S., Barreto-Silvia, J., Bourg, N., Bunyavejchewin, S. & Butt, N. (2014) Local spatial structure of forest biomass and its consequences for remote sensing of carbon stocks. *Biogeosciences Discussions*, **11**, 5711.
- Réjou-Méchain, M., Tanguy, A., Piponiot, C., Chave, J. & Hérault, B. (2017) biomass: an r package for estimating above-ground biomass and its uncertainty in tropical forests. *Methods in Ecology and Evolution*, **8**, 1163-1167.
- Reynolds, G., Payne, J., Sinun, W., Mosigil, G. & Walsh, R.P. (2011) Changes in forest land use and management in Sabah, Malaysian Borneo, 1990–2010, with a focus on the Danum Valley region. *Philosophical Transactions of the Royal Society B: Biological Sciences*, **366**, 3168-3176.
- Riedmiller, M. & Rprop, I. (1994) Rprop-description and implementation details. Technical Report. Accessed online: <http://www.inf.fu-berlin.de/lehre/WS06/Mustererkennung/Paper/rprop.pdf>
- Rocchini, D., Balkenhol, N., Carter, G.A., Foody, G.M., Gillespie, T.W., He, K.S., Kark, S., Levin, N., Lucas, K. & Luoto, M. (2010) Remotely sensed spectral heterogeneity as a proxy of species diversity: recent advances and open challenges. *Ecological Informatics*, **5**, 318-329.
- Rocchini, D., Boyd, D.S., Féret, J.B., Foody, G.M., He, K.S., Lausch, A., Nagendra, H., Wegmann, M. & Pettorelli, N. (2016) Satellite remote sensing to monitor species diversity: Potential and pitfalls. *Remote Sensing in Ecology and Conservation*, **2**, 25-36.
- Rocchini, D., Chiarucci, A. & Loiselle, S.A. (2004) Testing the spectral variation hypothesis by using satellite multispectral images. *Acta Oecologica*, **26**, 117-120.
- Rocha, E., Schiatti, J., Gerolamo, C., Burnham, R. & Nogueira, A. (2020) Higher rates of liana regeneration after canopy fall drives species abundance patterns in central Amazonia. *Journal of Ecology*, **108** (4). DOI: <https://doi.org/10.1111/1365-2745.13345>
- Rodríguez-Ronderos, M.E., Bohrer, G., Sanchez-Azofeifa, A., Powers, J.S. & Schnitzer, S.A. (2016) Contribution of lianas to plant area index and canopy structure in a Panamanian forest. *Ecology*, **97**, 3271-3277.
- Romano, J., Kromrey, J.D., Coraggio, J. & Skowronek, J. (2006) Appropriate statistics for ordinal level data: Should we really be using t-test and Cohen's d for evaluating group differences on the NSSE and other surveys. In *Annual meeting of the Florida Association of Institutional Research*, pp. 1-33.
- Rosa, I.M., Smith, M.J., Wearn, O.R., Purves, D. & Ewers, R.M. (2016) The environmental legacy of modern tropical deforestation. *Current Biology*, **26**, 2161-2166.

- Rosette, J., North, P. & Suarez, J. (2008) Vegetation height estimates for a mixed temperate forest using satellite laser altimetry. *International Journal of Remote Sensing*, **29**, 1475-1493.
- Russo, S.E., Davies, S.J., King, D.A. & Tan, S. (2005) Soil-related performance variation and distributions of tree species in a Bornean rain forest. *Journal of Ecology*, **93**, 879-889.
- Saatchi, S.S., Asefi-Najafabady, S., Malhi, Y., Aragão, L.E., Anderson, L.O., Myneni, R.B. & Nemani, R. (2013) Persistent effects of a severe drought on Amazonian forest canopy. *Proceedings of the National Academy of Sciences*, **110**, 565-570.
- Saatchi, S.S., Harris, N.L., Brown, S., Lefsky, M., Mitchard, E.T., Salas, W., Zutta, B.R., Buermann, W., Lewis, S.L. & Hagen, S. (2011) Benchmark map of forest carbon stocks in tropical regions across three continents. *Proceedings of the National Academy of Sciences*, **108**, 9899-9904.
- Saatchi, S.S., Houghton, R., Dos Santos Alvala, R., Soares, J.V. & Yu, Y. (2007) Distribution of aboveground live biomass in the Amazon basin. *Global Change Biology*, **13**, 816-837.
- Saleska, S.R., Didan, K., Huete, A.R. & Da Rocha, H.R. (2007) Amazon forests green-up during 2005 drought. *Science*, **318**, 612-612.
- Sanchez-Azofeifa, A., Rankine, C., do Espirito Santo, M.M., Fatland, R. & Garcia, M. (2011) Wireless sensing networks for environmental monitoring: Two case studies from tropical forests. *2011 IEEE Seventh International Conference on eScience*, pp. 70-76. IEEE.
- Sánchez-Azofeifa, G.A., Castro, K., Wright, S.J., Gamon, J., Kalacska, M., Rivard, B., Schnitzer, S.A. & Feng, J.L. (2009) Differences in leaf traits, leaf internal structure, and spectral reflectance between two communities of lianas and trees: implications for remote sensing in tropical environments. *Remote Sensing of Environment*, **113**, 2076-2088.
- Sánchez-Azofeifa, G. & Castro-Esau, K. (2006) Canopy observations on the hyperspectral properties of a community of tropical dry forest lianas and their host trees. *International Journal of Remote Sensing*, **27**, 2101-2109.
- Sankey, T.T., McVay, J., Swetnam, T.L., McClaran, M.P., Heilman, P. & Nichols, M. (2018) UAV hyperspectral and lidar data and their fusion for arid and semi-arid land vegetation monitoring. *Remote Sensing in Ecology and Conservation*, **4**, 20-33.
- Schlerf, M. & Atzberger, C. (2006) Inversion of a forest reflectance model to estimate structural canopy variables from hyperspectral remote sensing data. *Remote Sensing of Environment*, **100**, 281-294.
- Schnitzer, S.A. & Bongers, F. (2005) Lianas and gap-phase regeneration: implications for forest dynamics and species diversity. In *Forest Climbing Plants of West Africa: Diversity, Ecology and Management* (Eds Bongers, F., Parren, M & Traore, D.). CABI Publishing, UK. pp. 59-72.
- Schnitzer, S.A., Bongers, F., Burnham, R.J. & Putz, F.E. (2014a) *Ecology of lianas*. John Wiley & Sons.
- Schnitzer, S.A. (2005) A mechanistic explanation for global patterns of liana abundance and distribution. *The American Naturalist*, **166**, 262-276.
- Schnitzer, S.A. & Bongers, F. (2002) The ecology of lianas and their role in forests. *Trends in Ecology & Evolution*, **17**, 223-230.
- Schnitzer, S.A. & Bongers, F. (2011) Increasing liana abundance and biomass in tropical forests: emerging patterns and putative mechanisms. *Ecology letters*, **14**, 397-406.
- Schnitzer, S.A. & Carson, W.P. (2001) Treefall gaps and the maintenance of species diversity in a tropical forest. *Ecology*, **82**, 913-919.
- Schnitzer, S.A. & Carson, W.P. (2010) Lianas suppress tree regeneration and diversity in treefall gaps. *Ecology letters*, **13**, 849-857.
- Schnitzer, S.A., Dalling, J.W. & Carson, W.P. (2000) The impact of lianas on tree regeneration in tropical forest canopy gaps: evidence for an alternative pathway of gap-phase regeneration. *Journal of Ecology*, **88**, 655-666.
- Schnitzer, S.A., Kuzee, M.E. & Bongers, F. (2005) Disentangling above-and below-ground competition between lianas and trees in a tropical forest. *Journal of Ecology*, **93**, 1115-1125.
- Schnitzer, S.A., Mangan, S.A., Dalling, J.W., Baldeck, C.A., Hubbell, S.P., Ledo, A., Muller-Landau, H., Tobin, M.F., Aguilar, S. & Brassfield, D. (2012) Liana abundance, diversity, and distribution on Barro Colorado Island, Panama. *PLoS one*, **7**, e52114.

- Schnitzer, S.A., Parren, M.P. & Bongers, F. (2004) Recruitment of lianas into logging gaps and the effects of pre-harvest climber cutting in a lowland forest in Cameroon. *Forest Ecology and Management*, **190**, 87-98.
- Schnitzer, S.A., van der Heijden, G., Mascaró, J. & Carson, W.P. (2014b) Lianas in gaps reduce carbon accumulation in a tropical forest. *Ecology*, **95**, 3008-3017.
- Schnitzer, S.A. & van der Heijden, G.M. (2019) Lianas have a seasonal growth advantage over co-occurring trees. *Ecology*, **100**, e02655.
- Sfair, J.C., Rochelle, A.L.C., Rezende, A.A. & Martins, R. (2016) Liana avoidance strategies in trees: combined attributes increase efficiency. *Tropical Ecology*, **57**, 559-566.
- Shao, Y. & Lan, J. (2019) A Spectral Unmixing Method by Maximum Margin Criterion and Derivative Weights to Address Spectral Variability in Hyperspectral Imagery. *Remote Sensing*, **11**, 1045.
- Shen, X. & Cao, L. (2017) Tree-species classification in subtropical forests using airborne hyperspectral and LiDAR data. *Remote Sensing*, **9**, 1180.
- Shen, X., Cao, L., Chen, D., Sun, Y., Wang, G. & Ruan, H. (2018) Prediction of forest structural parameters using airborne full-waveform LiDAR and hyperspectral data in subtropical forests. *Remote Sensing*, **10**, 1729.
- Shenkin, A., Chandler, C.J., Boyd, D.S., Jackson, T., Disney, M., Majalap.... & Malhi, Y. (2019) The world's tallest tropical tree in three dimensions. *Frontiers in Forests and Global Change*, **2**, 32.
- Shimamoto, C.Y., Padial, A.A., da Rosa, C.M. & Marques, M.C. (2018) Restoration of ecosystem services in tropical forests: A global meta-analysis. *PloS one*, **13**, e0208523.
- Shono, K., Cadaweng, E.A. & Durst, P.B. (2007) Application of assisted natural regeneration to restore degraded tropical forestlands. *Restoration Ecology*, **15**, 620-626.
- Shukla, J., Nobre, C. & Sellers, P. (1990) Amazon deforestation and climate change. *Science*, **247**, 1322-1325.
- Silva, C.A., Valbuena, R., Pinagé, E.R., Mohan, M., de Almeida, D.R., North Broadbent, E., Jaafar, W.S.W.M., de Almeida Papa, D., Cardil, A. & Klauberg, C. (2019) ForestGapR: An r Package for forest gap analysis from canopy height models. *Methods in Ecology and Evolution*, **10**, 1347-1356.
- Simard, M., Pinto, N., Fisher, J.B. & Baccini, A. (2011) Mapping forest canopy height globally with spaceborne lidar. *Journal of Geophysical Research: Biogeosciences*, **116** (G4). DOI: <https://doi.org/10.1029/2011JG001708>
- Sims, D.A. & Gamon, J.A. (2002) Relationships between leaf pigment content and spectral reflectance across a wide range of species, leaf structures and developmental stages. *Remote Sensing of Environment*, **81**, 337-354.
- Singh, M., Malhi, Y. & Bhagwat, S. (2014) Biomass estimation of mixed forest landscape using a Fourier transform texture-based approach on very-high-resolution optical satellite imagery. *International Journal of Remote Sensing*, **35**, 3331-3349.
- Sist, P., Nolan, T., Bertault, J.-G. & Dykstra, D. (1998) Harvesting intensity versus sustainability in Indonesia. *Forest Ecology and Management*, **108**, 251-260.
- Slik, J., Aiba, S.I., Brearley, F.Q., Cannon, C.H., Forshed, O., Kitayama, K., Nagamasu, H., Nilus, R., Payne, J. & Paoli, G. (2010) Environmental correlates of tree biomass, basal area, wood specific gravity and stem density gradients in Borneo's tropical forests. *Global Ecology and Biogeography*, **19**, 50-60.
- Slik, J., Paoli, G., McGuire, K., Amaral, I., Barroso, J., Bastian, M., Blanc, L., Bongers, F., Boundja, P. & Clark, C. (2013) Large trees drive forest aboveground biomass variation in moist lowland forests across the tropics. *Global Ecology and Biogeography*, **22**, 1261-1271.
- Smith-Martin, C.M., Bastos, C.L., Lopez, O.R., Powers, J.S. & Schnitzer, S.A. (2019) Effects of dry-season irrigation on leaf physiology and biomass allocation in tropical lianas and trees. *Ecology*, **100**, e02827.
- Sodhi, N.S., Koh, L.P., Brook, B.W. & Ng, P.K. (2004) Southeast Asian biodiversity: an impending disaster. *Trends in Ecology & Evolution*, **19**, 654-660.

- Spanner, M.A., Pierce, L.L., Peterson, D.L. & Running, S.W. (1990) Remote sensing of temperate coniferous forest leaf area index The influence of canopy closure, understory vegetation and background reflectance. *International Journal of Remote Sensing*, **11**, 95-111.
- Spracklen, D.V. & Garcia-Carreras, L. (2015) The impact of Amazonian deforestation on Amazon basin rainfall. *Geophysical research letters*, **42**, 9546-9552.
- Spracklen, D.V., Arnold, S.R. & Taylor, C. (2012) Observations of increased tropical rainfall preceded by air passage over forests. *Nature*, **489**, 282-285.
- Stehman, S.V. & Foody, G.M. (2019) Key issues in rigorous accuracy assessment of land cover products. *Remote Sensing of Environment*, **231**, 111199.
- Steininger, M. (2000) Satellite estimation of tropical secondary forest above-ground biomass: data from Brazil and Bolivia. *International Journal of Remote Sensing*, **21**, 1139-1157.
- Stevens, G.C. (1987) Lianas as structural parasites: the *Bursera simaruba* example. *Ecology*, **68**, 77-81.
- Sullivan, M.J.P., Lewis, S.L., Affum-Baffoe, K., Castilho, C., Costa, F., Sanchez, A.C.... & Phillips, O.L. (2020) Long-term thermal sensitivity of Earth's tropical forests. *Science*, **368**, 869-874.
- Sullivan, M.J.P., Talbot, J., Lewis, S.L., Phillips, O.L., Qie, L., Begne, S.K....& Zemagho, L. (2017) Diversity and carbon storage across the tropical forest biome. *Scientific Reports*, **7**, 39102.
- Sun, G., Ranson, K., Kimes, D., Blair, J. & Kovacs, K. (2008) Forest vertical structure from GLAS: An evaluation using LVIS and SRTM data. *Remote Sensing of Environment*, **112**, 107-117.
- Swinfield, T., Both, S., Riutta, T., Bongalov, B., Elias, D., Majalap-Lee, N., Ostle, N., Svátek, M., Kvasnica, J. & Milodowski, D. (2020) Imaging spectroscopy reveals the effects of topography and logging on the leaf chemistry of tropical forest canopy trees. *Global Change Biology*, **26**, 989-1002.
- Tangki, H. & Chappell, N.A. (2008) Biomass variation across selectively logged forest within a 225-km² region of Borneo and its prediction by Landsat TM. *Forest Ecology and Management*, **256**, 1960-1970.
- Taylor (2001) Strategies for overcoming problems when mosaicking airborne scanner images. *Earth Observation Magazine*, **10**, 26-31.
- Taylor, P., Asner, G., Dahlin, K., Anderson, C., Knapp, D., Martin, R., Mascaro, J., Chazdon, R., Cole, R. & Wanek, W. (2015) Landscape-scale controls on aboveground forest carbon stocks on the Osa Peninsula, Costa Rica. *PloS one*, **10** (6): e0126748.
- Ter Steege, H., Pitman, N., Sabatier, D., Castellanos, H., Van Der Hout, P., Daly, D.C., Silveira, M., Phillips, O., Vasquez, R. & Van Andel, T. (2003) A spatial model of tree α -diversity and tree density for the Amazon. *Biodiversity & Conservation*, **12**, 2255-2277.
- Thirumalai, K., DiNezio, P.N., Okumura, Y. & Deser, C. (2017) Extreme temperatures in Southeast Asia caused by El Niño and worsened by global warming. *Nature Communications*, **8**, 1-8.
- Thompson, J., Proctor, J., Scott, D., Fraser, P., Marrs, R., Miller, R. & Viana, V. (1998) Rain forest on Maraca Island, Roraima, Brazil: artificial gaps and plant response to them. *Forest Ecology and Management*, **102**, 305-321.
- Thomson, E.R., Malhi, Y., Bartholomeus, H., Oliveras, I., Gvozdevaite, A., Peprah, T., Suomalainen, J., Quansah, J., Seidu, J. & Adonteng, C. (2018) Mapping the leaf economic spectrum across west African tropical forests using UAV-acquired hyperspectral imagery. *Remote Sensing*, **10**, 1532.
- Tilman, D., Fargione, J., Wolff, B., D'antonio, C., Dobson, A., Howarth, R., Schindler, D., Schlesinger, W.H., Simberloff, D. & Swackhamer, D. (2001) Forecasting agriculturally driven global environmental change. *Science*, **292**, 281-284.
- Tobin, M.F., Wright, A.J., Mangan, S.A. & Schnitzer, S.A. (2012) Lianas have a greater competitive effect than trees of similar biomass on tropical canopy trees. *Ecosphere*, **3**, 1-11.
- Toledo-Aceves, T. & Swaine, M. (2008) Effect of lianas on tree regeneration in gaps and forest understorey in a tropical forest in Ghana. *Journal of Vegetation Science*, **19**, 717-728.
- Torchiano, M. (2017) effsize: Efficient effect size computation. *R package version 0.7*, **1**.
- Turner, W. (2013) Satellites: make data freely accessible. *Nature*, **498**, 37-37.

- Tymen, B., Réjou-Méchain, M., Dalling, J.W., Fauset, S., Feldpausch, T.R., Norden, N., Phillips, O.L., Turner, B.L., Viers, J. & Chave, J. (2016) Evidence for arrested succession in a liana-infested Amazonian forest. *Journal of Ecology*, **104**, 149-159.
- Umaña, M.N., Manzané-Pinzón, E. & Comita, L.S. (2020) Long-term dynamics of liana seedlings suggest decelerating increases in liana relative abundance over time. *Journal of Ecology*, **108**, 460-469.
- Unger, M., Homeier, J. & Leuschner, C. (2012) Effects of soil chemistry on tropical forest biomass and productivity at different elevations in the equatorial Andes. *Oecologia*, **170**, 263-274.
- Urbazaez, M., Thiel, C., Cremer, F., Dubayah, R., Migliavacca, M., Reichstein, M. & Schimmler, C. (2018) Estimation of forest aboveground biomass and uncertainties by integration of field measurements, airborne LiDAR, and SAR and optical satellite data in Mexico. *Carbon balance and management*, **13**, 5.
- van der Heijden, G.M & Phillips, O.L (2009) Liana infestation impacts tree growth in a lowland tropical moist forest. *Biogeosciences*, **6**, 2217-2226.
- van der Heijden, G.M., Healey, J.R. & Phillips, O.L. (2008) Infestation of trees by lianas in a tropical forest in Amazonian Peru. *Journal of Vegetation Science*, **19**, 747-756.
- van der Heijden, G.M. & Phillips, O.L. (2008) What controls liana success in Neotropical forests? *Global Ecology and Biogeography*, **17**, 372-383.
- van der Heijden, G.M., Powers, J.S. & Schnitzer, S.A. (2015) Lianas reduce carbon accumulation and storage in tropical forests. *Proceedings of the National Academy of Sciences*, **112**, 13267-13271.
- van der Heijden, G.M., Powers, J.S. & Schnitzer, S.A. (2019) Effect of lianas on forest-level tree carbon accumulation does not differ between seasons: Results from a liana removal experiment in Panama. *Journal of Ecology*, **107**, 1890-1900.
- van der Heijden, G.M., Schnitzer, S.A., Powers, J.S. & Phillips, O.L. (2013) Liana impacts on carbon cycling, storage and sequestration in tropical forests. *Biotropica*, **45**, 682-692.
- van der Meer, P., Bongers, F., Chatrou, L. & Riéra, B. (1994) Defining canopy gaps in a tropical rain forest: effects on gap size and turnover time. *Acta Oecologia*, **15**, 701-714.
- van der Sande, M.T., Poorter, L., Schnitzer, S.A., Engelbrecht, B.M. & Markesteijn, L. (2019) The hydraulic efficiency–safety trade-off differs between lianas and trees. *Ecology*, **100**, e02666.
- Venter, O., Sanderson, E.W., Magrath, A., Allan, J.R., Beher, J., Jones, K.R., Possingham, H.P., Laurance, W.F., Wood, P. & Fekete, B.M. (2016) Sixteen years of change in the global terrestrial human footprint and implications for biodiversity conservation. *Nature Communications*, **7**, 12558.
- Vicca, S., Luysaert, S., Peñuelas, J., Campioli, M., Chapin III, F., Ciais, P., Heinemeyer, A., Höglberg, P., Kutsch, W. & Law, B.E. (2012) Fertile forests produce biomass more efficiently. *Ecology letters*, **15**, 520-526.
- Visser, M.D., Muller-Landau, H.C., Schnitzer, S.A., de Kroon, H., Jongejans, E. & Wright, S.J. (2018a) A host–parasite model explains variation in liana infestation among co-occurring tree species. *Journal of Ecology*, **106**, 2435-2445.
- Visser, M.D., Schnitzer, S.A., Muller-Landau, H.C., Jongejans, E., de Kroon, H., Comita, L.S., Hubbell, S.P. & Wright, S.J. (2018b) Tree species vary widely in their tolerance for liana infestation: A case study of differential host response to generalist parasites. *Journal of Ecology*, **106**, 781-794.
- Voss, M. & Sugumaran, R. (2008) Seasonal effect on tree species classification in an urban environment using hyperspectral data, LiDAR, and an object-oriented approach. *Sensors*, **8**, 3020-3036.
- Waite, C.E., van der Heijden, G.M., Field, R. & Boyd, D.S. (2019) A view from above: Unmanned aerial vehicles (UAVs) provide a new tool for assessing liana infestation in tropical forest canopies. *Journal of Applied Ecology*.
- Walsh, R. (1990) Climatic data for Danum Valley. *Unpublished Danum Valley Field Centre report*.

- Walsh, R. & Newbery, D. (1999) The ecoclimatology of Danum, Sabah, in the context of the world's rainforest regions, with particular reference to dry periods and their impact. *Philosophical Transactions of the Royal Society of London. Series B: Biological Sciences*, **354**, 1869-1883.
- Warner, T.A., McGraw, J.B. & Landenberger, R. (2006) Segmentation and classification of high resolution imagery for mapping individual species in a closed canopy, deciduous forest. *Science in China Series E: Technological Sciences*, **49**, 128-139.
- Watanabe, E. & Shimizu, H. (1993) Algorithm for pruning hidden units in multilayered neural network for binary pattern classification problem. *Proceedings of 1993 International Conference on Neural Networks (IJCNN-93-Nagoya, Japan)*, Nagoya, Japan, 1993, pp. 327-330 vol.1, doi: 10.1109/IJCNN.1993.713923.
- Watson, J.E., Evans, T., Venter, O., Williams, B., Tulloch, A., Stewart, C., Thompson, I., Ray, J.C., Murray, K. & Salazar, A. (2018) The exceptional value of intact forest ecosystems. *Nature ecology & evolution*, **2**, 599-610.
- West, T.A., Vidal, E. & Putz, F.E. (2014) Forest biomass recovery after conventional and reduced-impact logging in Amazonian Brazil. *Forest Ecology and Management*, **314**, 59-63.
- Whitmore, T. (1984) *Tropical rain forests of the Far East*, 2nd edn. Clarendon. Oxford.
- Woebbecke, D.M., Meyer, G.E., Von Bargen, K. & Mortensen, D. (1995) Color indices for weed identification under various soil, residue, and lighting conditions. *Transactions of the ASAE*, **38**, 259-269.
- Wright, S.J. (2010) The future of tropical forests. *Annals of the New York Academy of Sciences*, **1195**, 1-27. DOI: 10.1111/j.1749-6632.2010.05455.x.
- Wright, S.J. & Calderón, O. (2006) Seasonal, El Niño and longer term changes in flower and seed production in a moist tropical forest. *Ecology letters*, **9**, 35-44.
- Wright, S.J., Calderón, O., Hernández, A. & Paton, S. (2004) Are lianas increasing in importance in tropical forests? A 17-year record from Panama. *Ecology*, **85**, 484-489.
- Wright, S.J., Sun, I., Pickering, M., Fletcher, C.D. & Chen, Y.-Y. (2015) Long-term changes in liana loads and tree dynamics in a Malaysian forest. *Ecology*, **96**, 2748-2757.
- Wu, J., Chen, B., Reynolds, G., Xie, J., Liang, S., O'Brien, M.J. & Hector, A. (2020) Monitoring tropical forest degradation and restoration with satellite remote sensing: A test using Sabah Biodiversity Experiment. *Advances in Ecological Research*, **62**, 117-146.
- Xie, T., Yu, H. & Wilamowski, B. (2011) Comparison between traditional neural networks and radial basis function networks. *2011 IEEE International Symposium on Industrial Electronics*, pp. 1194-1199. IEEE.
- Yan, G., Mas, J.F., Maathuis, B., Xiangmin, Z. & Van Dijk, P. (2006) Comparison of pixel-based and object-oriented image classification approaches—a case study in a coal fire area, Wuda, Inner Mongolia, China. *International Journal of Remote Sensing*, **27**, 4039-4055.
- Yang, J., He, Y., Caspersen, J. & Jones, T. (2015) A discrepancy measure for segmentation evaluation from the perspective of object recognition. *ISPRS journal of photogrammetry and remote sensing*, **101**, 186-192.
- Yee, A.T., Lai, H.R., Chong, K.Y., Neo, L., Koh, C.Y., Tan, S.Y., Seah, W.W., Loh, J.W., Lim, R.C. & van Breugel, M. (2019) Short-term responses in a secondary tropical forest after a severe windstorm event. *Journal of Vegetation Science*, **30**, 720-731.
- Yorke, S.R., Schnitzer, S.A., Mascaro, J., Letcher, S.G. & Carson, W.P. (2013) Increasing liana abundance and basal area in a tropical forest: the contribution of long-distance clonal colonization. *Biotropica*, **45**, 317-324.
- Yu, C.-C. & Liu, B.-D. (2002) A backpropagation algorithm with adaptive learning rate and momentum coefficient. *Proceedings of the 2002 International Joint Conference on Neural Networks. IJCNN'02 (Cat. No. 02CH37290)*, pp. 1218-1223. IEEE.
- Yu, Q., Gong, P., Clinton, N., Biging, G., Kelly, M. & Schirokauer, D. (2006) Object-based detailed vegetation classification with airborne high spatial resolution remote sensing imagery. *Photogrammetric Engineering & Remote Sensing*, **72**, 799-811.

Chapter 6: References

- Yuan, X., Laakso, K., Marzahn, P. & Sanchez-Azofeifa, G.A. (2019) Canopy Temperature Differences between Liana-Infested and Non-Liana-infested Areas in a Neotropical Dry Forest. *Forests*, **10**, 890.
- Zanne, A.E., Lopez-Gonzalez, G., Coomes, D.A., Ilic, J., Jansen, S., Lewis, S.L., Miller, R.B., Swenson, N.G., Wiemann, M.C. & Chave, J. (2009) Data from: Towards a worldwide wood economics spectrum, v2, Dryad, Dataset, <https://doi.org/10.5061/dryad.234>.
- Zelazowski, P., Malhi, Y., Huntingford, C., Sitch, S. & Fisher, J.B. (2011) Changes in the potential distribution of humid tropical forests on a warmer planet. *Philosophical Transactions of the Royal Society A: Mathematical, Physical and Engineering Sciences*, **369**, 137-160.
- Zhang, J., Rivard, B., Sánchez-Azofeifa, A. & Castro-Esau, K. (2006) Intra-and inter-class spectral variability of tropical tree species at La Selva, Costa Rica: Implications for species identification using HYDICE imagery. *Remote Sensing of Environment*, **105**, 129-141.
- Zhang, L., Sun, X., Wu, T. & Zhang, H. (2015) An analysis of shadow effects on spectral vegetation indexes using a ground-based imaging spectrometer. *IEEE Geoscience and Remote Sensing Letters*, **12**, 2188-2192.
- Zhang, Z., Kazakova, A., Moskal, L.M. & Styers, D.M. (2016) Object-based tree species classification in urban ecosystems using LiDAR and hyperspectral data. *Forests*, **7**, 122.
- Zolkos, S., Goetz, S. & Dubayah, R. (2013) A meta-analysis of terrestrial aboveground biomass estimation using lidar remote sensing. *Remote Sensing of Environment*, **128**, 289-298.
- Zotz, G., Cueni, N. & Körner, C. (2006) In situ growth stimulation of a temperate zone liana (*Hedera helix*) in elevated CO₂. *Functional Ecology*, **20**, 763-769.

Appendix 1: Paper 1

1.1. Tree crown segmentation

A grid search was performed using four different values for each of the three parameters: Scale, Radius and Threshold. Scale refers to the spatial radius of the neighbour, Radius refers to the radius (expressed in radiometry unit) in the hyperspectral space and threshold refers to a value at which the algorithm will finish if the mean-shift vector is below a threshold. Following the first grid search, the values for each parameter were refined and a second grid search was performed. The values given to each parameter are shown in Table S1.1. Every combination of values for the first (64 combinations, Table S1.2) and second (26 combinations, Table S1.3) grid searches were used and evaluated using the Segmentation Evaluation Index (Yang *et al.* 2015).

Table S1.1 The first and second grid searches with meanshift parameters.

	Scale	Radius	Threshold
First grid search			
	5	3	0.005
	10	5	0.01
	15	10	0.1
	20	15	1
Second grid search			
	14	4	0.004
	15	5	0.005
	16	6	0.006

Appendices

Table S1.2 All parameter combinations ($n=64$) within the first grid search and corresponding Segmentation Evaluation Index (SEI). The segmentation highlighted in orange was the optimal segmentation for the first grid search.

File	Scale	Radius	Threshold	SEI
meanshift_S05R03T0.005	5	3	0.005	0.557
meanshift_S05R03T0.01	5	3	0.01	0.537
meanshift_S05R03T0.1	5	3	0.1	0.473
meanshift_S05R03T1.0	5	3	1	0.336
meanshift_S05R05T0.005	5	5	0.005	0.390
meanshift_S05R05T0.01	5	5	0.01	0.379
meanshift_S05R05T0.1	5	5	0.1	0.355
meanshift_S05R05T1.0	5	5	1	0.380
meanshift_S05R10T0.005	5	10	0.005	0.499
meanshift_S05R10T0.01	5	10	0.01	0.510
meanshift_S05R10T0.1	5	10	0.1	0.545
meanshift_S05R10T1.0	5	10	1	0.632
meanshift_S05R15T0.005	5	15	0.005	0.628
meanshift_S05R15T0.01	5	15	0.01	0.649
meanshift_S05R15T0.1	5	15	0.1	0.727
meanshift_S05R15T1.0	5	15	1	0.818
meanshift_S10R03T0.005	10	3	0.005	0.456
meanshift_S10R03T0.01	10	3	0.01	0.462
meanshift_S10R03T0.1	10	3	0.1	0.446
meanshift_S10R03T1.0	10	3	1	0.438
meanshift_S10R05T0.005	10	5	0.005	0.332
meanshift_S10R05T0.01	10	5	0.01	0.327
meanshift_S10R05T0.1	10	5	0.1	0.334
meanshift_S10R05T1.0	10	5	1	0.377
meanshift_S10R10T0.005	10	10	0.005	0.404
meanshift_S10R10T0.01	10	10	0.01	0.418
meanshift_S10R10T0.1	10	10	0.1	0.545
meanshift_S10R10T1.0	10	10	1	0.594
meanshift_S10R15T0.005	10	15	0.005	0.558
meanshift_S10R15T0.01	10	15	0.01	0.596
meanshift_S10R15T0.1	10	15	0.1	0.660
meanshift_S10R15T1.0	10	15	1	0.748
meanshift_S15R03T0.005	15	3	0.005	0.357
meanshift_S15R03T0.01	15	3	0.01	0.368
meanshift_S15R03T0.1	15	3	0.1	0.366
meanshift_S15R03T1.0	15	3	1	0.370
meanshift_S15R05T0.005	15	5	0.005	0.276
meanshift_S15R05T0.01	15	5	0.01	0.291
meanshift_S15R05T0.1	15	5	0.1	0.300
meanshift_S15R05T1.0	15	5	1	0.325

Appendices

meanshift_S15R10T0.005	15	10	0.005	0.450
meanshift_S15R10T0.01	15	10	0.01	0.455
meanshift_S15R10T0.1	15	10	0.1	0.494
meanshift_S15R10T1.0	15	10	1	0.557
meanshift_S15R15T0.005	15	15	0.005	0.628
meanshift_S15R15T0.01	15	15	0.01	0.628
meanshift_S15R15T0.1	15	15	0.1	0.676
meanshift_S15R15T1.0	15	15	1	0.743
meanshift_S20R03T0.005	20	3	0.005	0.363
meanshift_S20R03T0.01	20	3	0.01	0.363
meanshift_S20R03T0.1	20	3	0.1	0.344
meanshift_S20R03T1.0	20	3	1	0.348
meanshift_S20R05T0.005	20	5	0.005	0.309
meanshift_S20R05T0.01	20	5	0.01	0.315
meanshift_S20R05T0.1	20	5	0.1	0.312
meanshift_S20R05T1.0	20	5	1	0.347
meanshift_S20R10T0.005	20	10	0.005	0.493
meanshift_S20R10T0.01	20	10	0.01	0.593
meanshift_S20R10T0.1	20	10	0.1	0.524
meanshift_S20R10T1.0	20	10	1	0.593
meanshift_S20R15T0.005	20	15	0.005	0.684
meanshift_S20R15T0.01	20	15	0.01	0.676
meanshift_S20R15T0.1	20	15	0.1	0.713
meanshift_S20R15T1.0	20	15	1	0.710

Table S1.3 All parameter combinations ($n=27$) within the second grid search and corresponding Segmentation Evaluation Index (SEI). The segmentation highlighted in orange was the optimal segmentation for the second grid search, which did not differ from the first grid search.

File	Scale	Radius	Threshold	SEI
meanshift_S14R04T0.004	14	4	0.004	0.297
meanshift_S14R04T0.005	14	4	0.005	0.291
meanshift_S14R04T0.006	14	4	0.006	0.298
meanshift_S14R05T0.004	14	5	0.004	0.279
meanshift_S14R05T0.005	14	5	0.005	0.279
meanshift_S14R05T0.006	14	5	0.006	0.285
meanshift_S14R06T0.004	14	6	0.004	0.322
meanshift_S14R06T0.005	14	6	0.005	0.322
meanshift_S14R06T0.006	14	6	0.006	0.322
meanshift_S15R04T0.004	15	4	0.004	0.283
meanshift_S15R04T0.005	15	4	0.005	0.283
meanshift_S15R04T0.006	15	4	0.006	0.283
meanshift_S15R05T0.004	15	5	0.004	0.284
meanshift_S15R05T0.005	15	5	0.005	0.276
meanshift_S15R05T0.006	15	5	0.006	0.277
meanshift_S15R06T0.004	15	6	0.004	0.309
meanshift_S15R06T0.005	15	6	0.005	0.309
meanshift_S15R06T0.006	15	6	0.006	0.309
meanshift_S16R04T0.004	16	4	0.004	0.304
meanshift_S16R04T0.005	16	4	0.005	0.297
meanshift_S16R04T0.006	16	4	0.006	0.297
meanshift_S16R05T0.004	16	5	0.004	0.285
meanshift_S16R05T0.005	16	5	0.005	0.276
meanshift_S16R05T0.006	16	5	0.006	0.277
meanshift_S16R06T0.004	16	6	0.004	0.321
meanshift_S16R06T0.005	16	6	0.005	0.321
meanshift_S16R06T0.006	16	6	0.006	0.321

1.2. Neural network model parametrisation

I ran neural network models with the number of neurons ranging between 1 and 7 and two different error threshold values. The threshold specifies a value for the partial derivatives of the error function as a stopping criteria. Thus, the model will continue to iterate until it reaches a point where the overall error of the model is not reducing by more than the given threshold value, *i.e.* with a threshold of 0.01, a change in error of less than 1% will stop further model optimization. Results showed no decrease in classification accuracy, whilst also reducing convergence time, using a threshold of 0.05 in comparison to a lower threshold of 0.01. Models that exceeded 1000 seconds for convergence were excluded. Using a threshold of 0.05, I identified hidden neurons ranging between 2 and 5 as optimal in terms of accuracy and convergence time (Table S1.4). Using these parameters I ran a 10 fold cross validation for each model. Metrics used for model accuracy highlighted the model with four hidden neurons to have the best performance (Table S1.4).

Table S1.4 Neural network model parametrisation and assessment of best performing model. Models highlighted in orange correspond to models with best performance. Models that required longer than 1000 seconds to converge were removed (highlighted in grey).

Hidden neurons	Threshold	Accuracy	CI	Sensitivity	Specificity	F1	Convergence Time
7	0.05	0.788	(0.7441, 0.8266)	0.82	0.755	0.7942	440.4
6	0.05	0.786	(0.7441, 0.8266)	0.84	0.735	0.7981	160.6
5	0.05	0.7875	(0.7441, 0.8266)	0.86	0.715	0.8019	94.5
4	0.05	0.785	(0.7415, 0.8243)	0.845	0.725	0.7972	86.3
3	0.05	0.788	(0.7441, 0.8266)	0.845	0.73	0.7991	31.63
2	0.05	0.793	(0.7494, 0.8312)	0.845	0.74	0.8029	25.98
1	0.05	0.7825	(0.7388, 0.822)	0.83	0.735	0.7924	9
7	0.01						>1000
6	0.01						>1000
5	0.01						>1000
4	0.01	0.788	(0.7441, 0.8266)	0.84	0.735	0.7981	748.05
3	0.01	0.783	(0.7388, 0.822)	0.82	0.745	0.7904	457.2
2	0.01	0.788	(0.7441, 0.8266)	0.825	0.75	0.7952	163.8
1	0.01	0.79	(0.7468, 0.8289)	0.83	0.75	0.7981	23.5
Cross-Validation (10-fold)							
5	0.05	0.787	0.779-0.799	0.805	0.769	0.79	
4	0.05	0.802	0.79-0.816	0.824	0.78	0.806	
3	0.05	0.794	0.78-0.812	0.821	0.768	0.799	
2	0.05	0.787	0.774-0.802	0.812	0.762	0.792	

1.3. Relationship between liana canopy cover and canopy height

Liana canopy cover data were collected in the field using a tablet computer with a Canopy Height Model pre-loaded. As such, estimates of liana canopy cover could be directly related to tree height. I found an increase in liana infestation corresponded to a decrease in canopy height for both the pixel- (Figure S1.1a) and object-based (Figure S1.1b) data. This pattern is also apparent in the predicted liana infestation map whereby low canopy heights are often associated with severe ($\geq 75\%$) liana infestation.

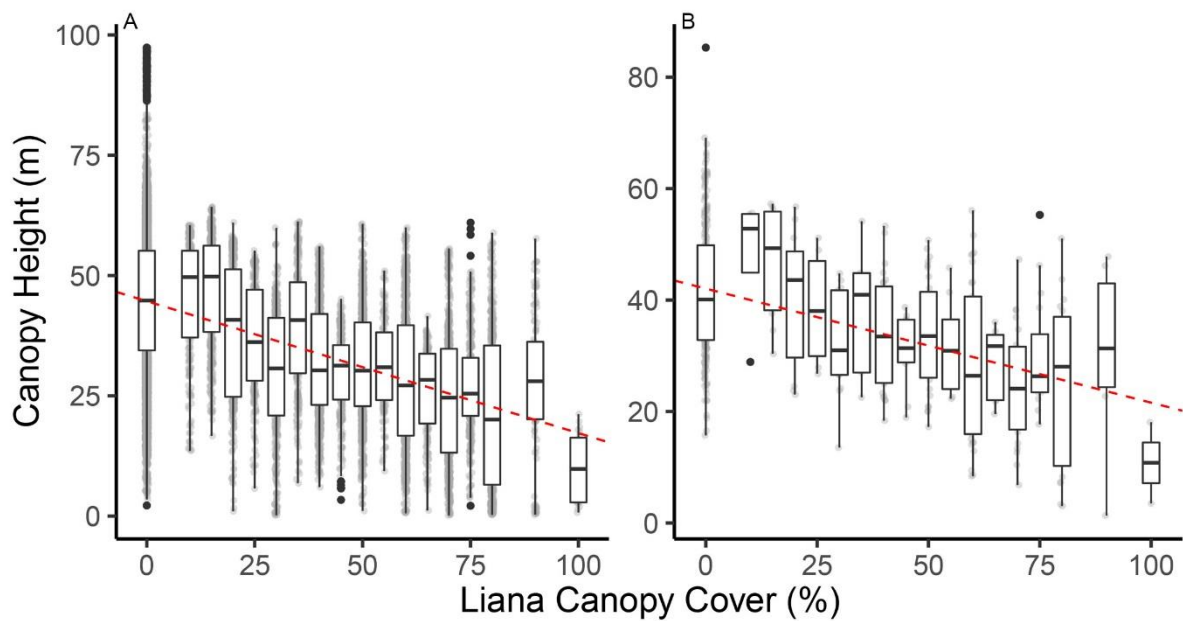


Figure S1.1 Relationship between liana canopy cover (%) and canopy height (m) for **a)** pixel- and **b)** object-based data. Red dashed lines correspond to fitted linear regression models.

1.4. Predicted and observed liana canopy cover

The relationship between observed and predicted liana infestation revealed a better fit with a pixel-based approach in comparison to an object-based approach, as shown by the deviation of points with respect to the 1:1 line (Figure 2.3). However, fitting a linear regression to the observed and predicted liana infestation data allows a visualisation of the overall relationship between predicted and observed values with respect to the 1:1 line. I found a stronger relationship between predicted and observed liana infestation when using a pixel-based approach ($R^2=0.79$) in comparison to an object-based approach ($R^2=0.64$). A test of non-inferiority showed that there was a significant difference between the correlations of both pixel- and object-based predictions with observed values (Hotelling's $t(165) = 10.96, p < 0.001$) suggesting that a pixel-based approach is significantly more accurate.

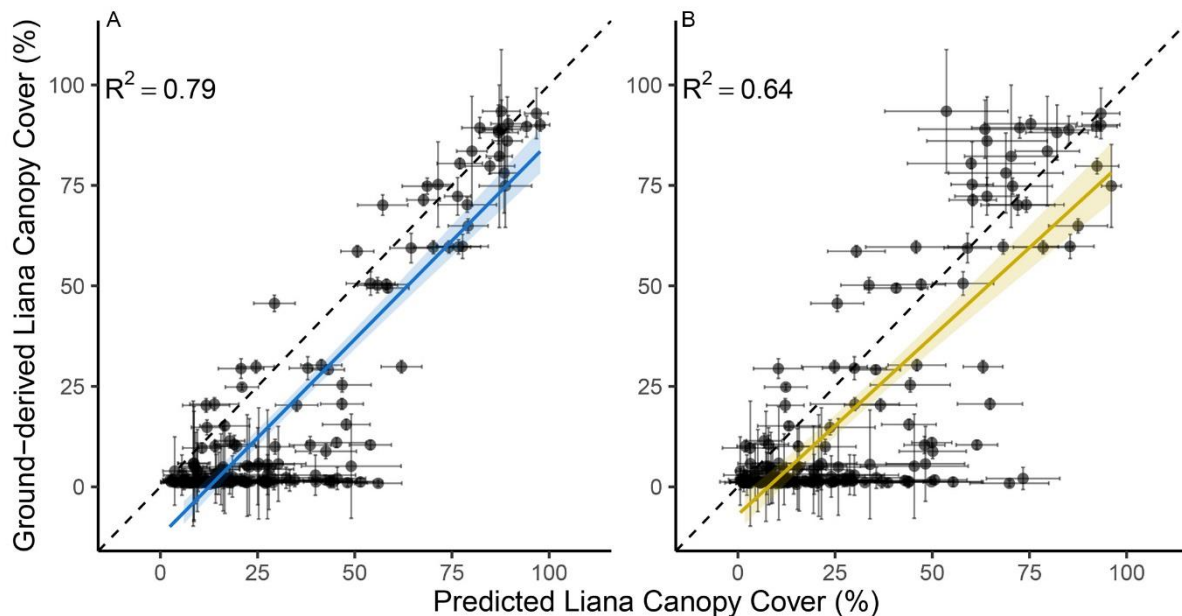


Figure S1.2 Relationship between predicted and ground reference liana canopy cover for **a)** a pixel-based approach and **b)** an object-based approach on a continuous scale. Black dashed line represents a 1:1 line, solid line corresponds to a linear regression line. Points with darker shades indicate multiple overlapping points. Horizontal error bars represent the standard deviation of 100 predicted values generated from multiple iterations of the neural network model. Vertical error bars represent the standard deviation of 100 randomly generated liana canopy cover values using Monte Carlo simulations.

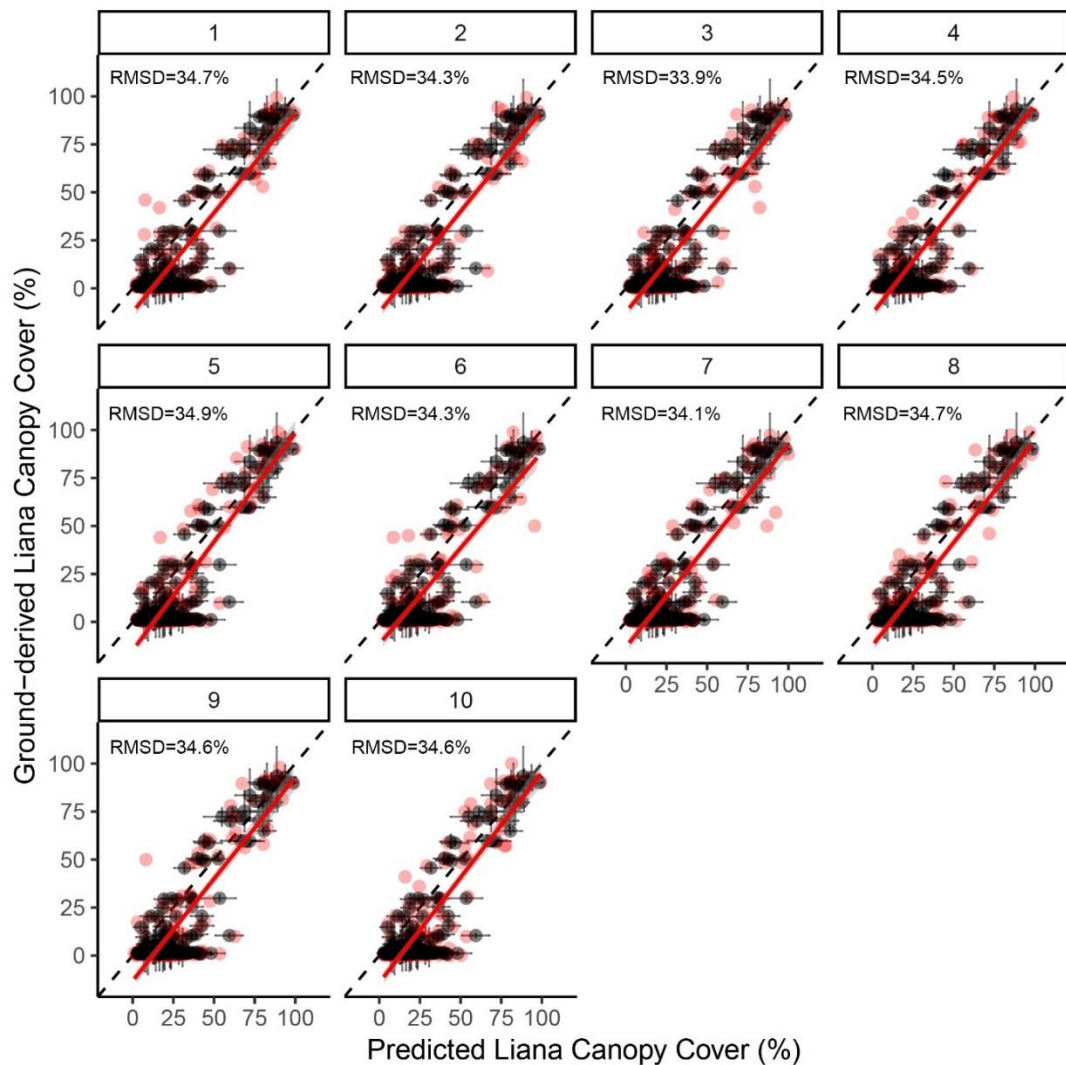


Figure S1.3 Relationship between predicted and ground reference liana canopy cover for 168 trees inside the 50 ha plot for the first 10 of the 100 iterations of the modelling process. Black points represent the mean values over 100 iterations. Red points correspond to predicted and ground-reference data that have changed with each iteration. Red solid line represents a linear model fitted to the data that has changed with each iteration (red points). During the training of the model I permuted 47 pixels into an incorrect class to represent temporal change (3.5 years) between ground and airborne data collection. I accounted for error in ground reference data associated with observational uncertainty and temporal change. Firstly, I quantified observational error such that 90% of trees contained a small error of 5% and 4% of trees contained a large error of 30%. Error derived from temporal change was also applied whereby 6% of trees had an error of 50%. Root mean squared deviation (RMSD) was calculated for each iteration.

Appendices

To assess whether the relationship between predicted and ground reference liana canopy cover for each iteration were significantly different (Figure S1.3), I compared the slopes of each linear model. To test for significant differences between slope coefficients I used a pairwise comparison (Table S1.5). A comparison of slopes indicated no significant differences between slopes. This suggests that error which may have occurred due to the time lag between ground and airborne data collection did not affect the overall relationship between predicted and observed liana canopy cover.

Table S1.5 Pairwise comparison of linear regression slope coefficients in Figure S1.3.

contrast	estimate	SE	df	t.ratio	p.value
1-2	-2.14983	5.842717	1660	-0.36795	0.999998
1-3	-2.3617	5.819776	1660	-0.40581	0.999995
1-4	-1.51804	5.803489	1660	-0.26157	1
1-5	0.46969	5.664691	1660	0.082915	1
1-6	2.147815	5.767518	1660	0.372398	0.999998
1-7	0.697156	5.804069	1660	0.120115	1
1-8	-5.8534	5.943731	1660	-0.9848	0.993113
1-9	-0.49299	5.791518	1660	-0.08512	1
1-10	-2.59642	5.867027	1660	-0.44254	0.99999
2-3	-0.21187	5.869917	1660	-0.03609	1
2-4	0.631792	5.853769	1660	0.107929	1
2-5	2.619519	5.716193	1660	0.458263	0.999986
2-6	4.297644	5.818109	1660	0.738667	0.999255
2-7	2.846985	5.854344	1660	0.486303	0.999977
2-8	-3.70357	5.992834	1660	-0.618	0.999827
2-9	1.656839	5.841901	1660	0.283613	1
2-10	-0.44659	5.916767	1660	-0.07548	1
3-4	0.843662	5.830872	1660	0.144689	1
3-5	2.83139	5.692742	1660	0.497368	0.999972
3-6	4.509514	5.795071	1660	0.778164	0.998869
3-7	3.058856	5.831449	1660	0.524545	0.999957
3-8	-3.4917	5.97047	1660	-0.58483	0.999891
3-9	1.86871	5.818958	1660	0.321142	0.999999
3-10	-0.23472	5.894115	1660	-0.03982	1
4-5	1.987728	5.67609	1660	0.350193	0.999999
4-6	3.665852	5.778713	1660	0.634372	0.999785
4-7	2.215193	5.815194	1660	0.380932	0.999997
4-8	-4.33536	5.954595	1660	-0.72807	0.999337
4-9	1.025047	5.802667	1660	0.176651	1
4-10	-1.07838	5.878033	1660	-0.18346	1
5-6	1.678124	5.639306	1660	0.297576	1
5-7	0.227466	5.676683	1660	0.04007	1
5-8	-6.32309	5.819403	1660	-1.08655	0.986027

Appendices

5-9	-0.96268	5.66385	1660	-0.16997	1
5-10	-3.06611	5.741038	1660	-0.53407	0.999949
6-7	-1.45066	5.779296	1660	-0.25101	1
6-8	-8.00122	5.919542	1660	-1.35166	0.941219
6-9	-2.6408	5.766691	1660	-0.45794	0.999986
6-10	-4.74423	5.842521	1660	-0.81202	0.998417
7-8	-6.55056	5.95516	1660	-1.09998	0.984772
7-9	-1.19015	5.803248	1660	-0.20508	1
7-10	-3.29357	5.878606	1660	-0.56026	0.999924
8-9	5.360412	5.942929	1660	0.901981	0.996431
8-10	3.256985	6.016538	1660	0.541339	0.999943
9-10	-2.10343	5.866215	1660	-0.35857	0.999998

Appendix 2: Paper 2

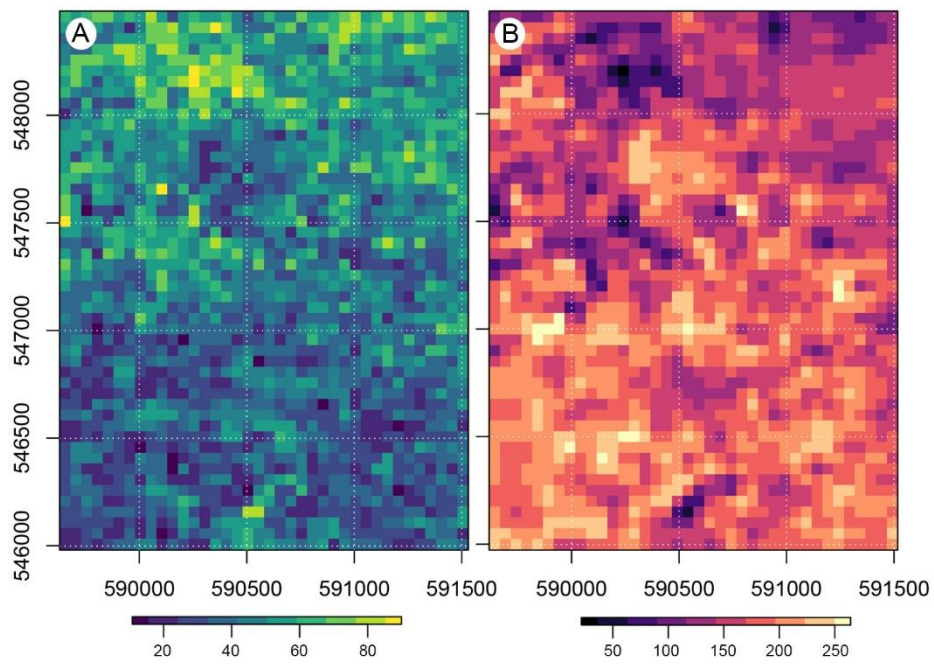


Figure S2.1 An extract from predicted **a)** liana infestation and **b)** aboveground carbon stocks in Mg C ha⁻¹. Spatial resolution for both maps is 2500 m².

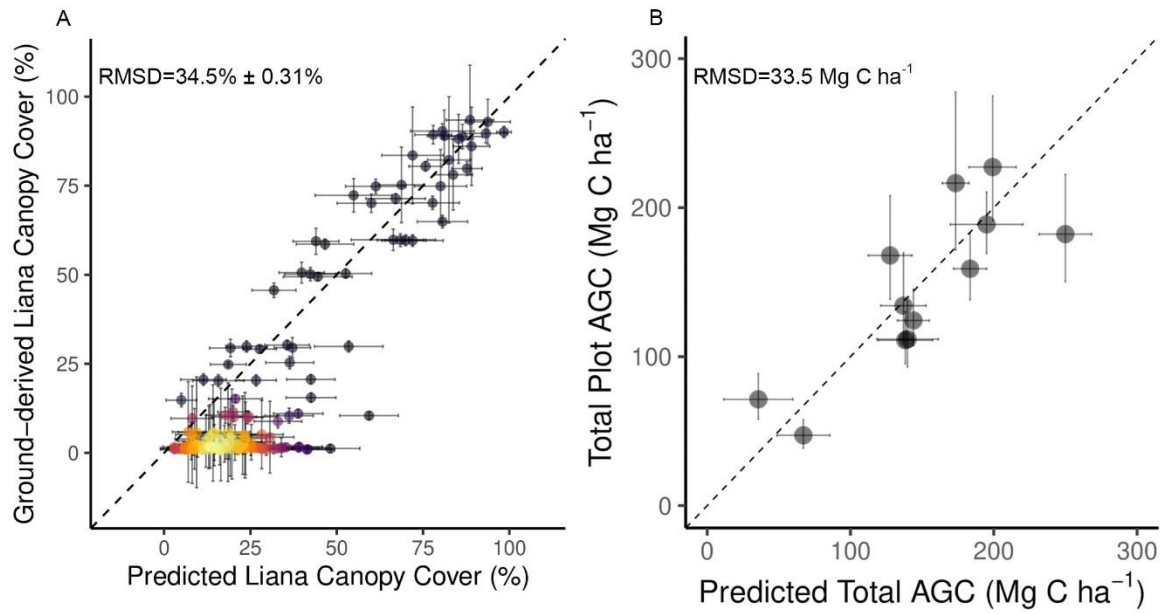


Figure S2.2 Relationship between predicted and ground reference **a)** liana canopy cover and **b)** aboveground carbon stocks (Mg C ha^{-1}). I accounted for error at all stages of the mapping of both liana infestation and AGC and propagated these errors to obtain a robust level of uncertainty around predictions. Error bars in **(a)** represent standard deviation. Error bars in **(b)** represent 95% confidence intervals following error propagation. Coloured points correspond to the density of overlapping points from black to yellow. Dashed line represents the 1:1 line.

Table S2.1 Accuracy assessment for predicted liana infestation in three and two classes. 95%CI, 95% confidence intervals for accuracy; Bal. Acc., Balanced Accuracy = $(sensitivity + specificity)/2$; F₁, F₁ score or F-measure; AUC, Area under the curve.

	Accuracy	95%CI	Sensitivity	Specificity	Bal. Acc.	F ₁	AUC
3 Class: Low [0-25%], Medium/High [25-75%], Severe [75-100%]							
3 Class	0.84	0.77-0.89					0.91
Class: L			0.85	1	0.92	0.92	
Class: M/H			0.85	0.84	0.84	0.45	
Class: S			0.77	0.99	0.88	0.83	
2 Class: Low [0-25%], Severe [75-100%]							
2 Class	1	0.97-1	1	1	1	1	1

The inclusion of height within allometric models is an essential parameter for accurate estimates of carbon stocks as variation in tropical forest tree height varies significantly across plots, regions and continents for a given diameter (Banin *et al.* 2012). However tree height can be extremely difficult to measure in dense closed-canopy forests and even laser rangefinder measurements can have large uncertainties (Larjavaara & Muller-Landau 2013). Therefore, H estimates from regional $H:D$ models can provide an efficient way to improve aboveground biomass estimates. Feldpausch *et al.* (2012) recommended the use of the region-specific Weibull- H model as it had the lowest error in biomass estimation. However, the power function (log 1) showed a better relationship with 50 trees ($D > 140$ cm) of known D and H (Figure S2.3). I also show the location of the world's current tallest tropical tree 'Menara' at 98.9m (Shenkin *et al.* 2019), which I suggest is not an outlier as multiple trees (canopy height > 90 m) were observed in ALS data in the surrounding area.

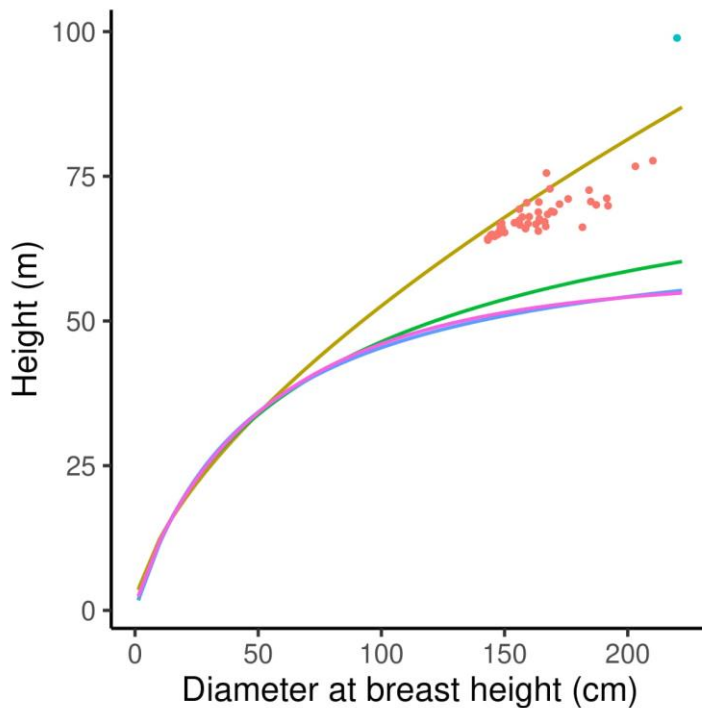


Figure S2.3 Height – Diameter models and their relationship with 50 trees ($D > 140$ cm) of known D and H as well as 'Menara' the World's tallest tropical tree at 98.9m. Models used to estimate height include: weibull: $H = a * (1 - \exp(-(D/b)^c))$, which is the same as the region-specific model used to estimate H ; log 1, $(\log(H) = a + b * \log(D))$ (equivalent to a power model); log 2, $(\log(H) = a + b * \log(D) + c * \log(D)^2)$ and michaelis: $H = (A * D)/(B + D)$.

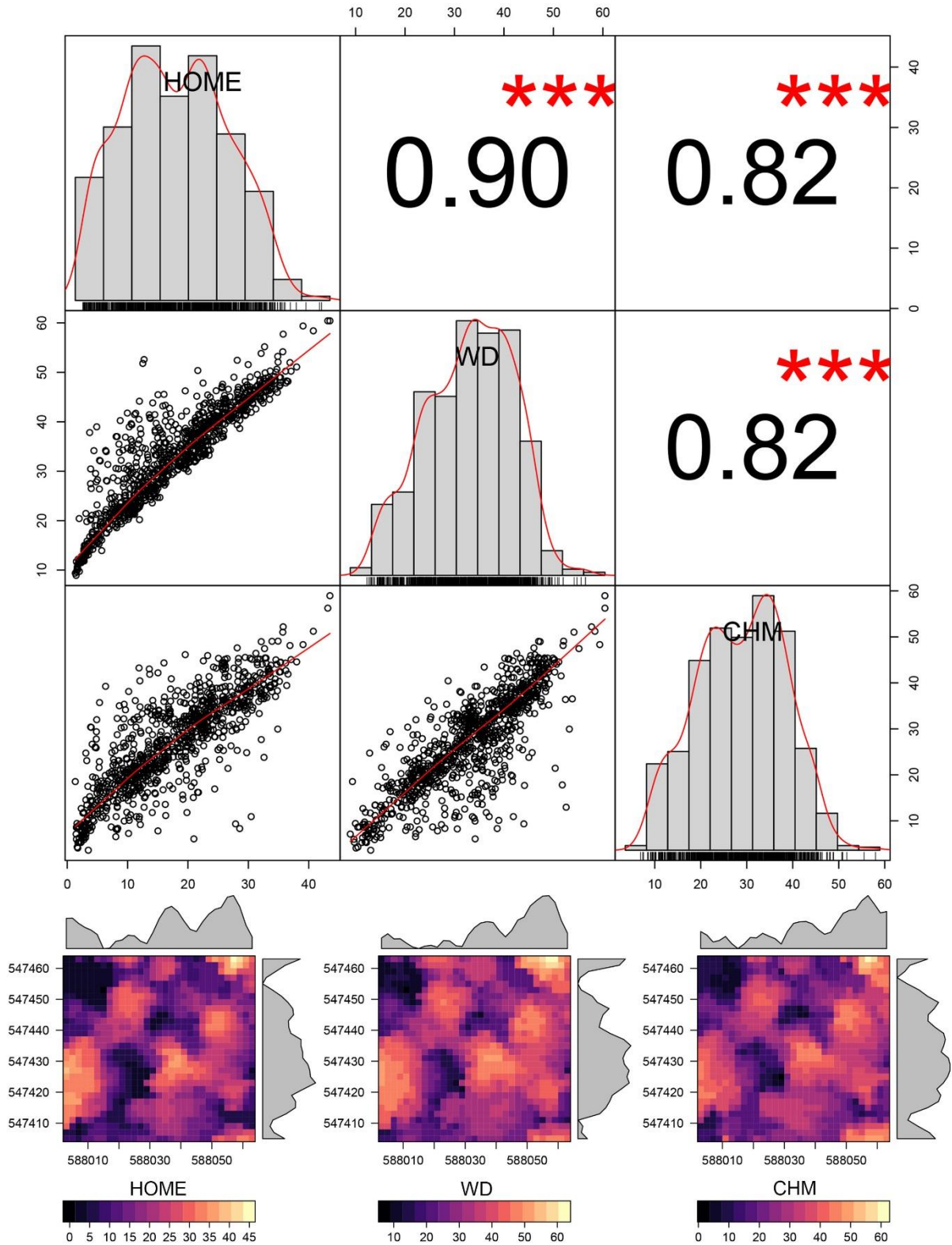


Figure S2.4 Relationship between three airborne laser scanning (ALS)-derived metrics: 1) height of median energy (HOME), 2) waveform distance (WFD) and 3) the top-of-canopy height derived from the canopy height model (CHM).

Table S2.2 Results from a ten-fold cross validation to identify the best model for the prediction of aboveground carbon stocks (AGC). The model with the highest R^2 is highlighted in green.

Run	Var1	Var2	Var3	R^2
1	CHMmed	CHMmin		0.426
2	CHMmed	CHMmin	WFDmin	0.404
3	CHMmean	WFDcover ₂₀	HOMEcover ₂₀	0.463
4	CHMmed	CHMmin	WFDcover ₂₀	0.448
5	CHMmed	WFDcover ₂₀	CHMcover ₂₀	0.494
6	CHMmed	CHMmin	WFDcover ₂₀	0.454
7	CHMmin	WFDcover ₂₀	HOMEmed	0.421
8	CHMmed	WFDcover ₂₀	HOMEmin	0.475
9	CHMmean	CHMmin	WFDcover ₂₀	0.454
10	CHMmed	WFDcover ₂₀	HOMEcover ₂₀	0.468

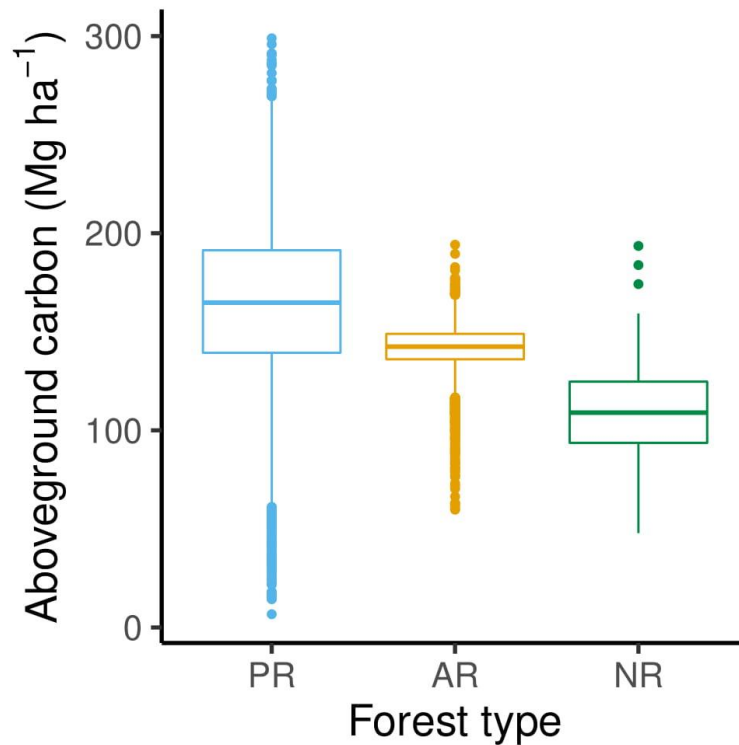


Figure S2.5 Predicted aboveground carbon stocks (Mg C ha⁻¹) within the three forest types. Values correspond to pixels with a spatial resolution of 50 m. PR, primary; AR, actively restored and NR, naturally regenerating forest.

Table S2.3 Tukey Honest Significant Differences between predicted levels of aboveground carbon (AGC) in the primary (PR), actively restored (AR) and naturally regenerating (NR) forests. Mean levels of AGC were 164.2 Mg C ha⁻¹, 141.6 Mg C ha⁻¹ and 108.3 Mg C ha⁻¹ for the primary, actively restored and naturally regenerating forests, respectively. Cliff's *delta* is a measure of effect size to indicate the magnitude of difference between levels of AGC.

Comparison	Difference	Upper 95% CI	Lower 95% CI	<i>p</i> value	Cliff's <i>delta</i>
PR – AR	22.6	23.8	21.4	<0.0001	0.44
PR – NR	55.9	59.2	52.6	<0.0001	0.78
NR – AR	- 33.3	- 30	- 36.7	<0.0001	0.83

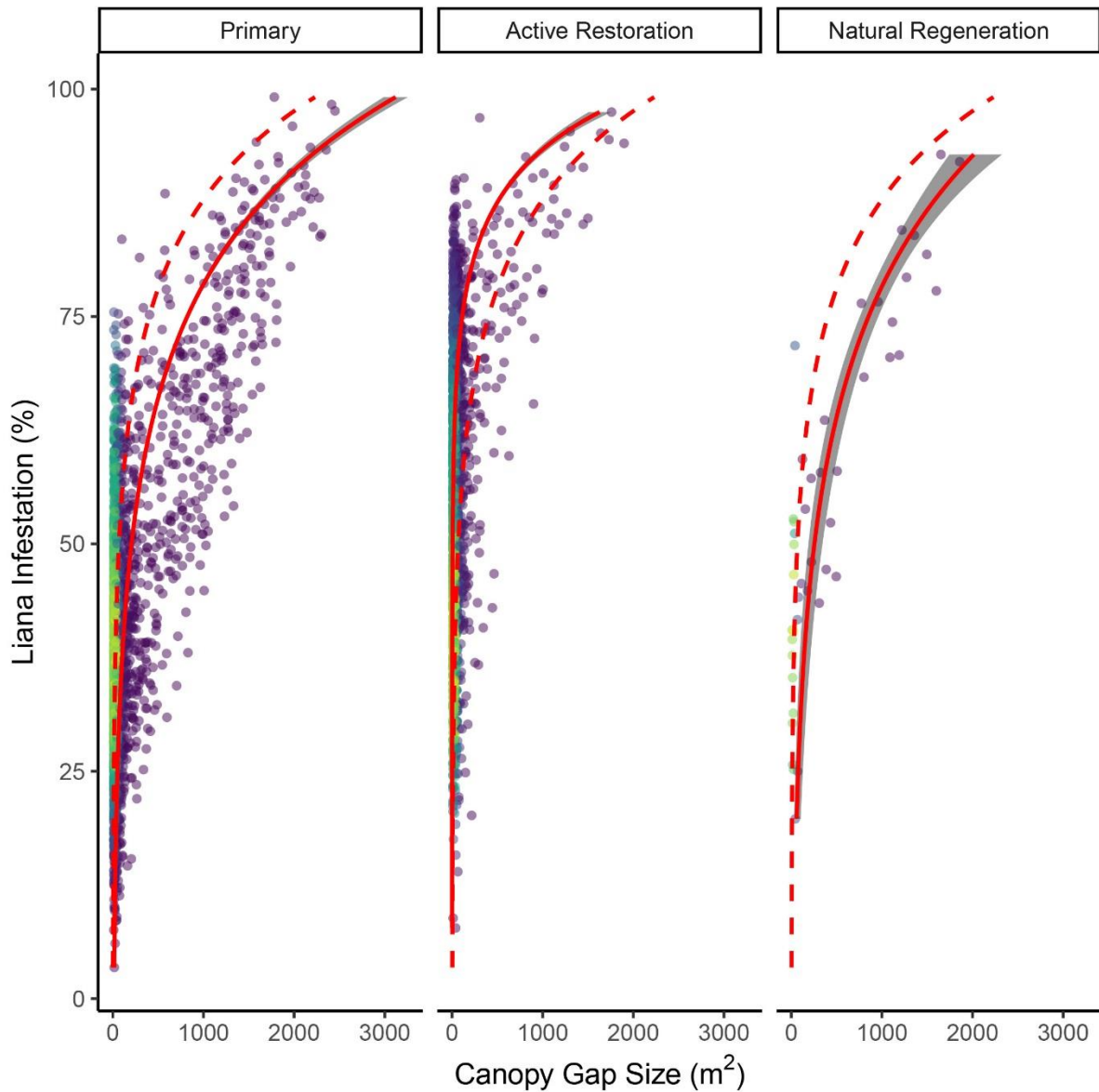


Figure S2.6 Relationship between canopy gap size and liana infestation. On average, a gap size of $\sim 400\text{m}^2$ was the size at which a gap was likely to be severely ($\geq 75\%$) liana-infested. Red solid lines represents individual models fit to data for each forest type. The red dashed lines represent a model fit across all forest types. The colour of points correspond to the density of overlapping points ranging from purple to yellow with increasing density.

The parameters used to define canopy gaps vary considerably depending on the location and the study interest. For example, small gaps (2-4m²) have been detected in Neotropical. However, in South-east Asian forests, which have a high proportion of tall, emergent dipterocarp trees, canopy gaps may be larger. Here, I defined a canopy gap as having a maximum canopy height of 10 m and a minimum size of 10 m², the same definition applied by Hunter *et al.* (2015). However, I also identified canopy gaps using a set of different parameters (Table S2.4, Figure. S2.7) to assess the effect of how gaps are defined on the relationship between liana infestation and aboveground carbon stocks. I found that parameter combination 2 and 3 (a change in canopy height) did not result in substantially different λ -values in comparison to parameter combination 1 (Table S2.4, Figure S2.7). However λ -values derived from parameter combinations 4 and 5 (a change in canopy gap size) were noticeably different to parameter combination 1 (Table S2.4, Figure S2.7).

Table S2.4 Different parameter combinations used for the detection of canopy gaps and the resulting power-law exponent (λ -value) representing the gap size frequency distribution.

Par. Comb.	Forest	GapSize	CanopyHeight	λ	N
1	Primary	10	10	1.235	26770
1	Active Restoration	10	10	1.241	13204
1	Natural Regeneration	10	10	1.224	2554
2	Primary	10	5	1.244	17430
2	Active Restoration	10	5	1.25	7786
2	Natural Regeneration	10	5	1.233	2742
3	Primary	10	2	1.251	10879
3	Active Restoration	10	2	1.26	4635
3	Natural Regeneration	10	2	1.253	1965
4	Primary	5	10	1.27	37685
4	Active Restoration	5	10	1.28	18996
4	Natural Regeneration	5	10	1.256	3481
5	Primary	2	10	1.336	56013
5	Active Restoration	2	10	1.35	29031
5	Natural Regeneration	2	10	1.32	5127

Par. Comb.: Parameter Combination; Gap size in m²; Canopy height in m; N, number of gaps

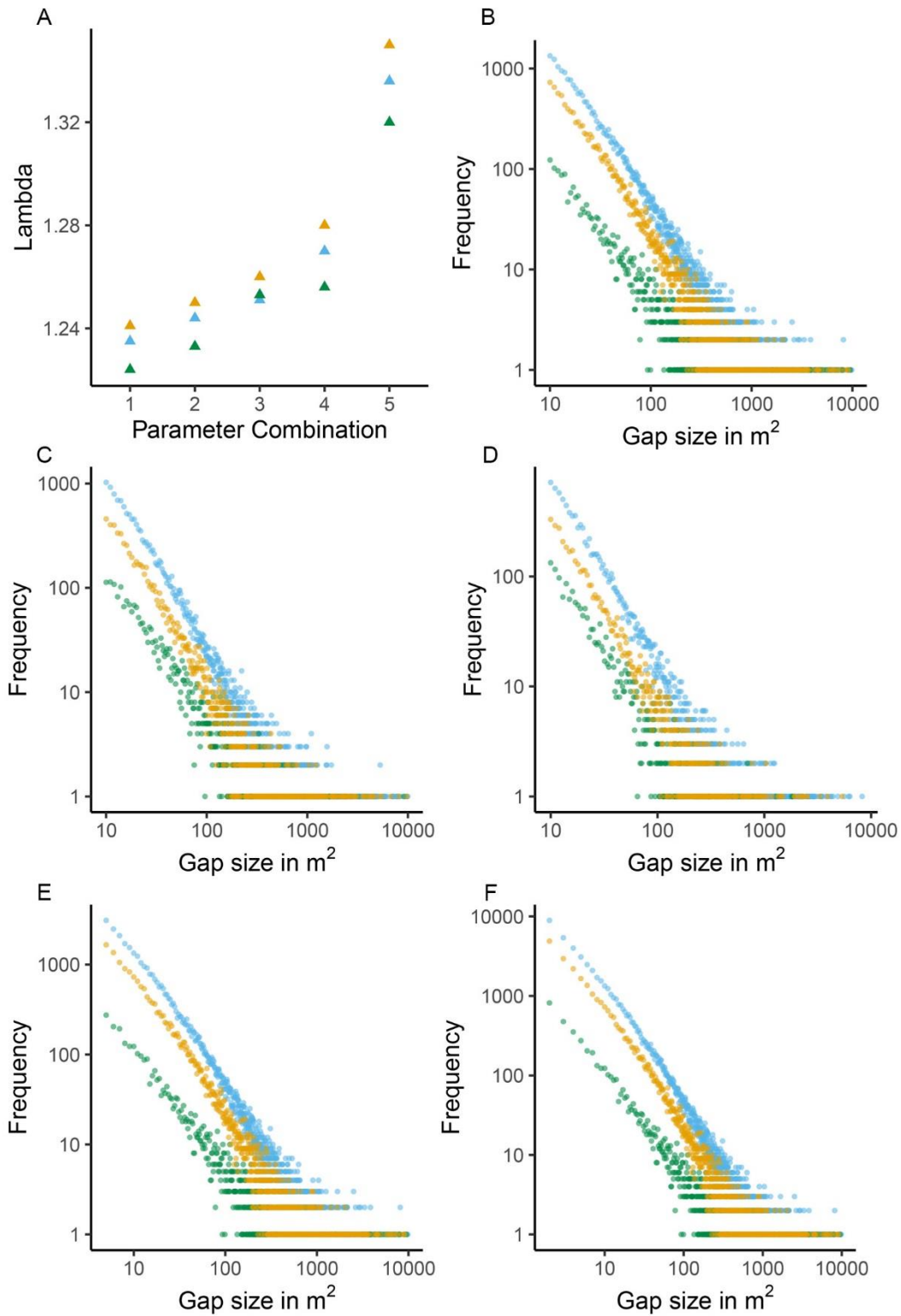


Figure S2.7 The gap-size frequency distributions represented by the power-law exponent (λ) within the primary (blue), actively restored (orange) and naturally regenerating (green) forests using **a)** five different parameter combinations **b) 1, c) 2, d) 3, e) 4 and f) 5**. Parameter combination values correspond with Table S2.4.

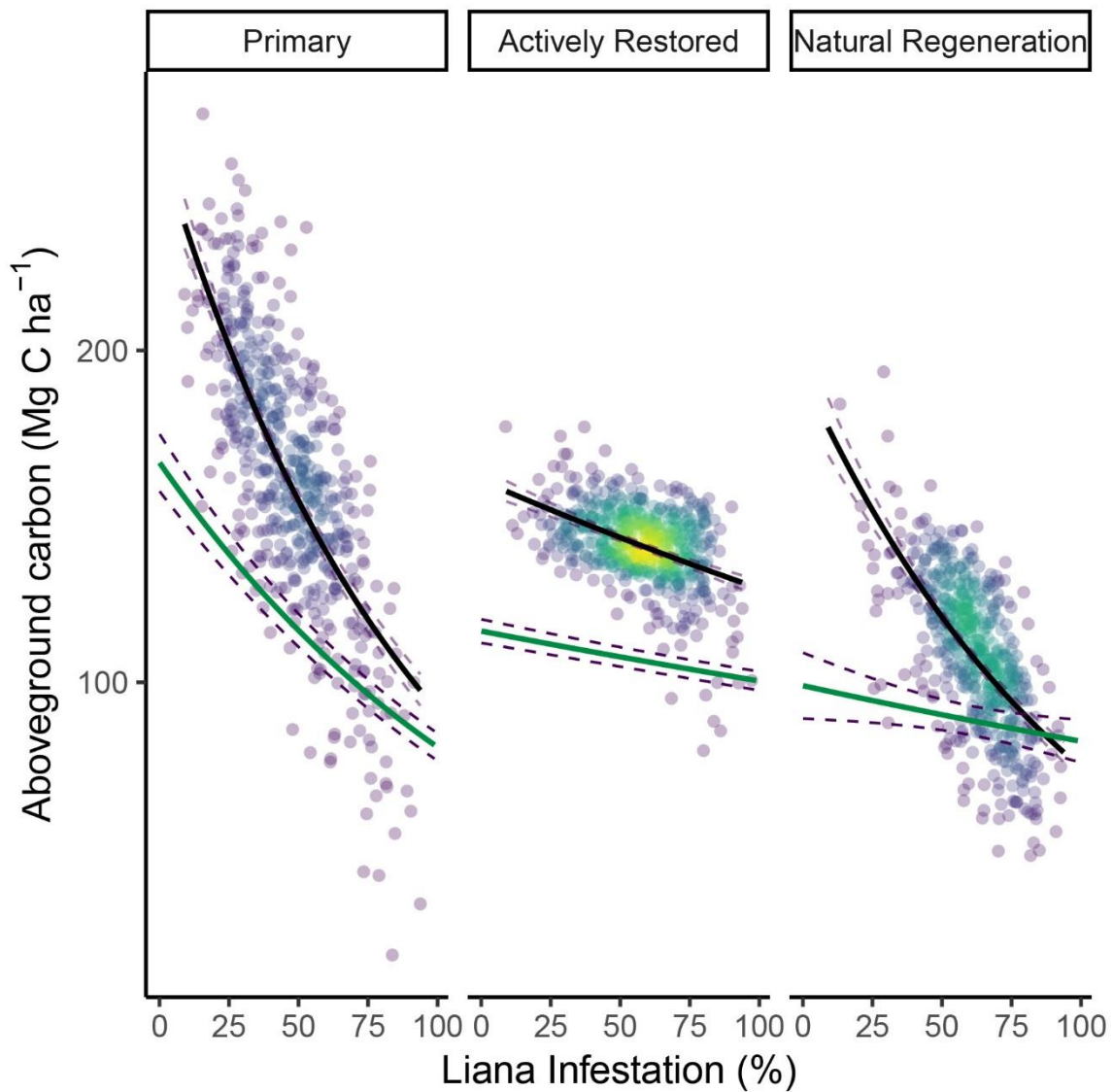


Figure S2.8 Relationship between liana infestation and aboveground carbon stocks (Mg C ha⁻¹) within each forest type. The black solid line shows the generalised linear model fit to the data. The green line corresponds to same model after accounting for the effect of canopy gaps and topography. Dashed lines represent 95% confidence intervals. The colour of points correspond to the density of overlapping points ranging from purple to yellow with increasing density.

Table S2.5 Summary table showing the coefficients (log scale) from multiple regressions using a generalised linear model for each forest type and for all forests combined.

	Estimate	Std. Error	t value	Pr (> t)	Sig
Primary, n=7791					
	5.454				
Intercept (exp)	(233.6)	1.383e-02	394.205	< 2e-16	***
Liana Infestation	-8.185e-03	1.602e-04	-51.088	< 2e-16	***
Elevation	1.967e-04	3.714e-05	5.296	1.22e-07	***
Slope	1.306e-03	2.923e-04	4.467	8.04e-06	***
Aspect	-7.553e-05	2.951e-05	-2.560	0.0105	*
Gap Area	-4.591e-03	4.055e-04	-11.322	< 2e-16	***
Gap Freq.	2.307e-04	2.191e-04	1.053	0.2924	
Gap Area*Gap Freq.	-8.043e-05	1.622e-05	-4.960	7.20e-07	***
Active Restoration, n=3714					
	5.054				
Intercept (exp)	(156.6)	9.972e-03	506.788	< 2e-16	***
Liana Infestation	-1.48e-03	9.268e-05	-15.968	< 2e-16	***
Elevation	-1.808e-05	2.483e-05	-0.728	0.4667	
Slope	2.043e-04	2.256e-04	0.905	0.3654	
Aspect	2.172e-05	1.969e-05	1.103	0.2700	
Gap Area	-5.216e-03	3.943e-04	-13.230	< 2e-16	***
Gap Freq.	3.813e-04	1.698e-04	2.246	0.0248	*
Gap Area*Gap Freq.	-7.095e-05	1.596e-05	-4.445	9.05e-06	***
Natural Regeneration, n=524					
	5.400				
Intercept (exp)	(221.3)	6.775e-02	79.696	< 2e-16	***
Liana Infestation	-3.471e-03	5.836e-04	-5.948	5.00e-09	***
Elevation	-1.397e-03	1.866e-04	-7.489	3.04e-13	***
Slope	4.979e-03	1.196e-03	4.161	3.71e-05	***
Aspect	-9.561e-05	1.226e-04	-0.780	0.436	
Gap Area	-7.220e-03	1.167e-03	-6.187	1.25e-09	***
Gap Freq.	-7.686e-04	6.500e-04	-1.182	0.238	
Gap Area*Gap Freq.	-3.355e-05	3.656e-05	-0.918	0.359	
All, n=12029					
	5.336				
Intercept (exp)	(207.8)	1.127e-02	473.334	< 2e-16	***
Liana Infestation	-7.467e-03	1.038e-04	-71.933	< 2e-16	***
Elevation	1.466e-04	2.915e-05	5.029	5.00e-07	***
Slope	2.849e-03	2.340e-04	12.175	< 2e-16	***
Aspect	3.507e-05	2.362e-05	1.485	0.138	

Appendices

Gap Area	-3.132e-03	3.286e-04	-9.531	< 2e-16	***
Gap Freq.	1.124e-03	1.748e-04	6.430	1.32e-10	***
Gap Area*Gap Freq.	-1.405e-04	1.343e-05	-10.464	< 2e-16	***

Sig, significance: . $p < 0.05$; * $p < 0.01$; ** $p < 0.001$; *** $p = 0$

It is expected that the gap size frequency distribution (GSFD) will change with different parameters for gap detection (*i.e.* canopy height and gap size). However, it is not clear how a change in GSFD may affect the relationship between liana infestation and AGC. I assessed the relationship of liana infestation and AGC accounting for canopy gaps detected using all parameter combinations. I found no significant differences in the amount of carbon reduction associated with an increase in liana infestation (Figure S2.9).

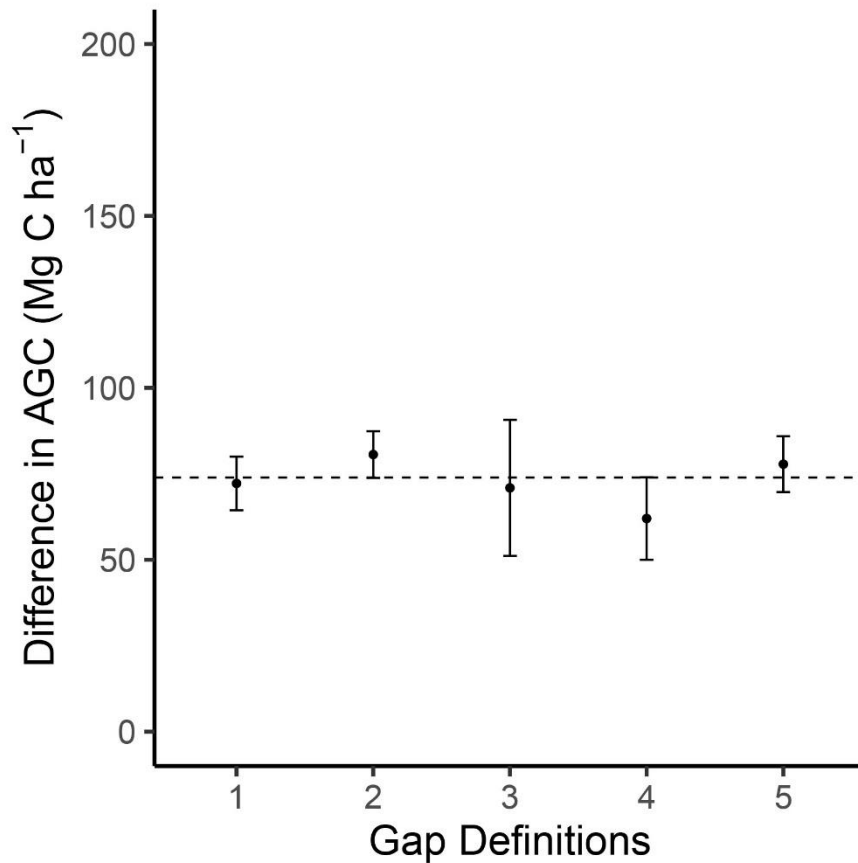


Figure S2.9 The effect of different gap definitions on the change in aboveground carbon stocks in relation to areas that were completely liana-infested or liana-free. Error bars corresponds to the 95% confidence intervals. Gap definitions refer to the five parameter combinations in Table S2.4.

Appendix 3: Paper 3

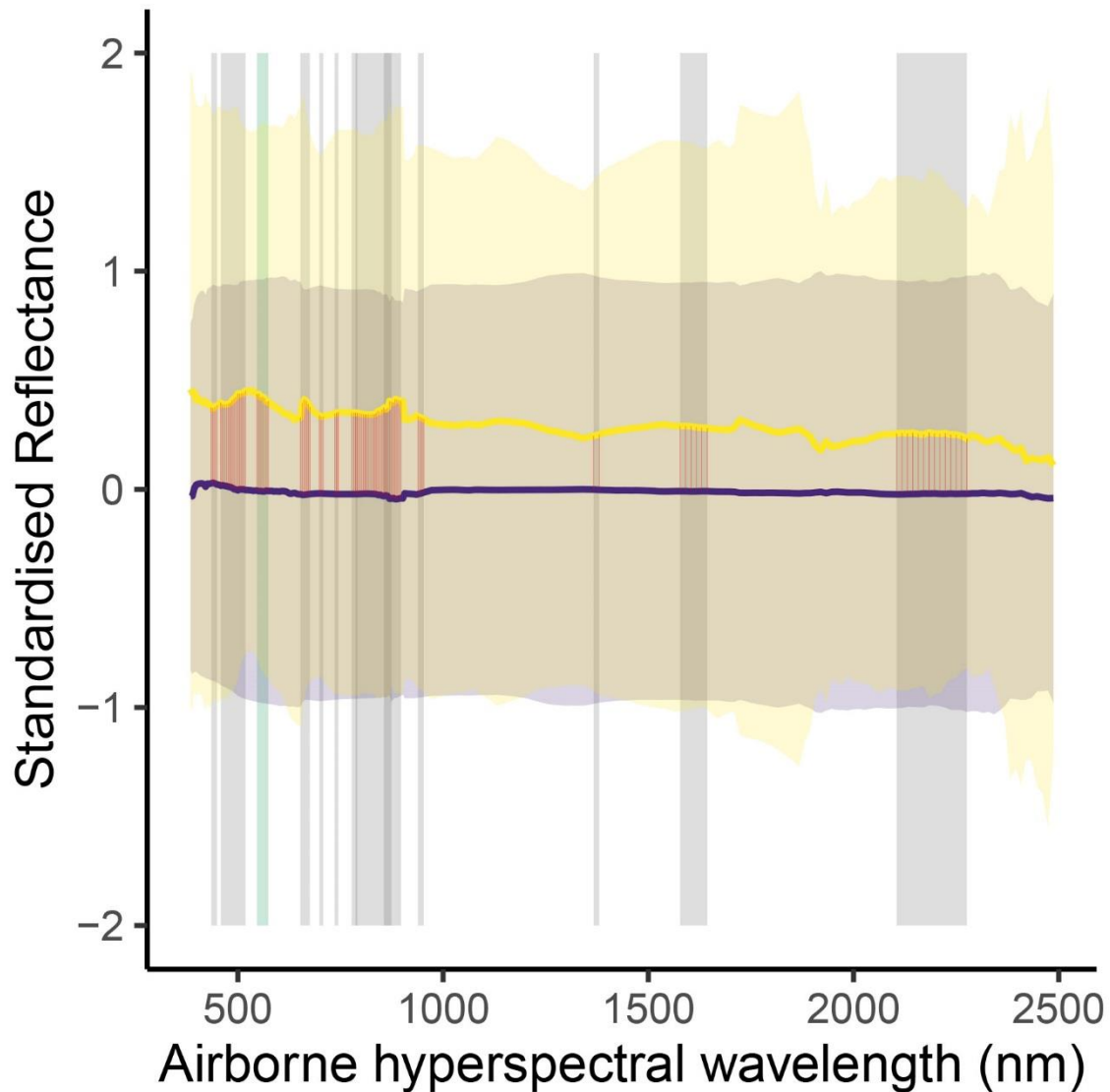


Figure S3.1 Airborne-derived standardised ($\mu = 0$, $\sigma = 1$) hyperspectral reflectance of liana-free trees and trees severely infested with liana leaves. Lines are mean reflectance values for all trees (shading ± 1 SD). Blue lines represent liana-free trees ($n_{\text{trees}} = 226$, $n_{\text{pixels}} = 7826$), yellow lines represent trees highly infested with liana leaves ($n_{\text{trees}} = 41$, $n_{\text{pixels}} = 1001$). Grey vertical bars represent the position of Sentinel-2 bands. Red vertical lines correspond to airborne hyperspectral bands that are within Sentinel-2 bands. The green vertical bar indicates the green region of the spectra that shows the greatest difference between liana-free and liana-infested trees.

Table S3.1 Comparison of vegetation indices for the separation of low ($\leq 25\%$) and severe ($\geq 75\%$) liana infestation classes within the primary and logged forests and across the full landscape for each of the four satellite-derived images (2016-2019). Values correspond to Cliff's *delta* effect sizes. Overall average corresponds to the average of the 4-year average for all locations.

Year	Metric	All	Primary	Logged	Overall Average
2016	Green	0.43	0.32	0.09	
2017	Green	0.27	0.14	0.1	
2018	Green	0.2	0.11	0.27	
2019	Green	0.07	0.15	0.08	
Average	Green	0.2425	0.18	0.135	0.185833
2016	Greenness	0.39	0.41	0.27	
2017	Greenness	0.32	0.26	0.4	
2018	Greenness	0.22	0.15	0.32	
2019	Greenness	0.3	0.22	0.3	
Average	Greenness	0.3075	0.26	0.3225	0.296667
2016	CLG	0.05	0.13	0.02	
2017	CLG	0.07	0.07	0.17	
2018	CLG	0.09	0.03	0.08	
2019	CLG	0.34	0.33	0.27	
Average	CLG	0.1375	0.14	0.135	0.1375
2016	CLRE	0.13	0.08	0.03	
2017	CLRE	0.21	0.1	0.13	
2018	CLRE	0.05	0.03	0.13	
2019	CLRE	0.22	0.28	0.23	
Average	CLRE	0.1525	0.1225	0.13	0.135
2016	CTVI	0.23	0.37	0.21	
2017	CTVI	0.12	0.12	0.37	
2018	CTVI	0.21	0.16	0.3	
2019	CTVI	0.39	0.36	0.37	
Average	CTVI	0.2375	0.2525	0.3125	0.2675
2016	EVI	0.37	0.39	0.15	
2017	EVI	0.17	0.09	0.25	
2018	EVI	0.22	0.14	0.31	
2019	EVI	0.23	0.14	0.31	
Average	EVI	0.2475	0.19	0.255	0.230833
2016	GEMI	0.36	0.36	0.15	
2017	GEMI	0.16	0.08	0.26	
2018	GEMI	0.21	0.13	0.31	
2019	GEMI	0.18	0.1	0.28	
Average	GEMI	0.2275	0.1675	0.25	0.215
2016	GNDVI	0.21	0.3	0.14	
2017	GNDVI	0.04	0.01	0.27	

Appendices

2018	GNDVI	0.18	0.11	0.26	
2019	GNDVI	0.25	0.21	0.3	
Average	GNDVI	0.17	0.1575	0.2425	0.19
2016	MNDWI	0.08	0.1	0.02	
2017	MNDWI	0.19	0.2	0.06	
2018	MNDWI	0.24	0.25	0.04	
2019	MNDWI	0.49	0.52	0.25	
Average	MNDWI	0.25	0.2675	0.0925	0.203333
2016	MSAVI	0.32	0.37	0.18	
2017	MSAVI	0.15	0.09	0.3	
2018	MSAVI	0.22	0.14	0.32	
2019	MSAVI	0.27	0.21	0.33	
Average	MSAVI	0.24	0.2025	0.2825	0.241667
2016	MSAVI2	0.35	0.37	0.16	
2017	MSAVI2	0.16	0.09	0.28	
2018	MSAVI2	0.22	0.13	0.31	
2019	MSAVI2	0.22	0.15	0.3	
Average	MSAVI2	0.2375	0.185	0.2625	0.228333
2016	MTCI	0.31	0.18	0.13	
2017	MTCI	0.42	0.32	0.2	
2018	MTCI	0.17	0.03	0.06	
2019	MTCI	0.22	0.14	0.07	
Average	MTCI	0.28	0.1675	0.115	0.1875
2016	NBRI	0.04	0.12	0.12	
2017	NBRI	0.14	0.21	0.25	
2018	NBRI	0.11	0.18	0.19	
2019	NBRI	0.18	0.25	0.03	
Average	NBRI	0.1175	0.19	0.1475	0.151667
2016	NDREI	0.08	0.13	0.01	
2017	NDREI	0.13	0.02	0.19	
2018	NDREI	0.02	0.07	0.16	
2019	NDREI	0.24	0.31	0.24	
Average	NDREI	0.1175	0.1325	0.15	0.133333
2016	NDREI2	0.13	0.08	0.03	
2017	NDREI2	0.21	0.1	0.13	
2018	NDREI2	0.05	0.03	0.13	
2019	NDREI2	0.22	0.28	0.23	
Average	NDREI2	0.1525	0.1225	0.13	0.135
2016	NDVI	0.23	0.37	0.21	
2017	NDVI	0.12	0.12	0.37	
2018	NDVI	0.21	0.16	0.3	
2019	NDVI	0.39	0.36	0.37	
Average	NDVI	0.2375	0.2525	0.3125	0.2675
2016	NDWI	0.21	0.3	0.14	
2017	NDWI	0.04	0.01	0.27	

Appendices

2018	NDWI	0.18	0.11	0.26	
2019	NDWI	0.25	0.21	0.3	
Average	NDWI	0.17	0.1575	0.2425	0.19
2016	NDWI2	0.13	0.2	0.14	
2017	NDWI2	0.11	0.16	0.21	
2018	NDWI2	0.05	0.1	0.24	
2019	NDWI2	0.21	0.26	0.06	
Average	NDWI2	0.125	0.18	0.1625	0.155833
2016	NRVI	0.23	0.37	0.21	
2017	NRVI	0.12	0.12	0.37	
2018	NRVI	0.21	0.16	0.3	
2019	NRVI	0.39	0.36	0.37	
Average	NRVI	0.2375	0.2525	0.3125	0.2675
2016	REIP	0.02	0.21	0.07	
2017	REIP	0.04	0.11	0.24	
2018	REIP	0.05	0.11	0.12	
2019	REIP	0.27	0.32	0.21	
Average	REIP	0.095	0.1875	0.16	0.1475
2016	RVI	0.23	0.37	0.21	
2017	RVI	0.12	0.12	0.37	
2018	RVI	0.21	0.16	0.3	
2019	RVI	0.39	0.36	0.37	
Average	RVI	0.2375	0.2525	0.3125	0.2675
2016	SLAVI	0.17	0.26	0.17	
2017	SLAVI	0.05	0.08	0.28	
2018	SLAVI	0.007	0.05	0.26	
2019	SLAVI	0.02	0.07	0.16	
Average	SLAVI	0.06175	0.115	0.2175	0.131417
2016	SR	0.23	0.37	0.21	
2017	SR	0.12	0.12	0.37	
2018	SR	0.21	0.16	0.3	
2019	SR	0.39	0.36	0.37	
Average	SR	0.2375	0.2525	0.3125	0.2675
2016	TTVI	0.23	0.37	0.21	
2017	TTVI	0.12	0.12	0.37	
2018	TTVI	0.21	0.16	0.3	
2019	TTVI	0.39	0.36	0.37	
Average	TTVI	0.2375	0.2525	0.3125	0.2675
2016	TVI	0.23	0.37	0.21	
2017	TVI	0.12	0.12	0.37	
2018	TVI	0.21	0.16	0.3	
2019	TVI	0.39	0.36	0.37	
Average	TVI	0.2375	0.2525	0.3125	0.2675

Green, Green reflectance; **Greenness**, Greenness Index; **CLG**, Green-band Chlorophyll Index; **CLRE**, Red-edge-band Chlorophyll Index; **CTVI**, Corrected transformed vegetation index; **EVI**, Enhanced

Appendices

vegetation index; **GEMI**, Global environmental monitoring index; **GNDVI**, Green normalised difference vegetation index; **MNDWI**, modified normalised difference water index; **MSAVI**, modified soil adjusted vegetation index; **MSAVI2**, modified soil adjusted vegetation index 2; **MTCI**, MERIS terrestrial chlorophyll index; **NBRI**, normalised burn ratio index; **NDREI1**, normalised difference red edge index1; **NDREI2**, normalised difference red edge index2; **NDVI**, normalised difference vegetation index; **NDWI**, normalised difference water index; **NDWI2**, normalised difference water index2; **NRVI**, normalised ration vegetation index; **REIP**, red edge inflection point; **RVI**, ratio vegetation index; **SLAVI**, specific leaf area vegetation index; **SR**, simple ratio vegetation index; **TTVI**, Thiam's transformed vegetation index; **TVI**, transformed vegetation index.

Table S3.2 Accuracy assessment for predicted liana infestation in satellite-based multispectral imagery using three different sets of input variables: **1)** all Sentinel 2-bands, **2)** Greenness Index **3)** all Sentinel 2-bands and Greenness Index within the primary and selectively logged forests. 95%CI, 95% confidence intervals for accuracy; Bal. Acc., Balanced Accuracy = $(sensitivity + specificity)/2$; F_1 , F_1 score or F-measure; AUC, Area under the curve.

Class	Accuracy	95% CI	Sensitivity	Specificity	Bal. Acc	F1	AUC
1) All Sentinel-2 bands							
<i>Primary</i>							
2 classes: [0-25], [75-100]							
	0.99	0.976-1	1	0.97	0.98	0.99	0.98
4 Classes: [0-25], [25-50], [50-75], [75-100]							
	0.45	0.44-0.462					0.76
Class: L			0.56	0.78	0.67	0.3	
Class: M			0.55	0.53	0.54	0.54	
Class: H			0.32	0.87	0.6	0.42	
Class: S			0.24	0.98	0.61	0.32	
<i>Secondary</i>							
2 classes: [0-25], [75-100]							
	0.84	0.802-0.875	1	0.82	0.91	0.61	0.91
4 Classes: [0-25], [25-50], [50-75], [75-100]							
	0.35	0.34-0.361					0.7
Class: L			0.38	0.86	0.62	0.08	
Class: M			0.59	0.51	0.55	0.41	
Class: H			0.28	0.75	0.51	0.37	
Class: S			0.2	0.96	0.58	0.29	
2) Greenness Index							
<i>Primary</i>							
2 classes: [0-25], [75-100]							
	0.86	0.798-0.908	0.97	0.69	0.83	0.89	0.83
4 Classes: [0-25], [25-50], [50-75], [75-100]							
	0.45	0.442-0.464					0.61
Class: L			0.14	0.89	0.52	0.13	
Class: M			0.73	0.32	0.52	0.6	
Class: H			0.21	0.85	0.53	0.29	

Appendices

Class: S	0.1	0.99	0.55	0.16
----------	-----	------	------	------

Secondary

2 classes: [0-25], [75-100]

0.25	0.03-0.65	0	0.33	0.17	0	0
------	-----------	---	------	------	---	---

4 Classes: [0-25], [25-50], [50-75], [75-100]

0.39	0.38-0.401					0.59
------	------------	--	--	--	--	------

Class: L	0	1	0.5	0
Class: M	0.68	0.43	0.55	0.41
Class: H	0.4	0.6	0.5	0.46
Class: S	0	1	0.5	0

3) All Sentinel-2 bands + Greenness Index

Primary

2 classes: [0-25], [75-100]

0.99	0.978-0.996	1	0.98	0.99	0.99	0.99
------	-------------	---	------	------	------	------

4 Classes: [0-25], [25-50], [50-75], [75-100]

0.48	0.473-0.495					0.8
------	-------------	--	--	--	--	-----

Class: L	0.61	0.79	0.7	0.32
Class: M	0.51	0.64	0.58	0.54
Class: H	0.43	0.84	0.64	0.5
Class: S	0.39	0.96	0.68	0.4

Secondary

2 classes: [0-25], [75-100]

0.88	0.849-0.914	0.947	0.874	0.91	0.7	0.91
------	-------------	-------	-------	------	-----	------

4 Classes: [0-25], [25-50], [50-75], [75-100]

0.37	0.359-0.38					0.71
------	------------	--	--	--	--	------

Class: L	0.36	0.86	0.61	0.08
Class: M	0.58	0.52	0.55	0.41
Class: H	0.32	0.75	0.53	0.41
Class: S	0.21	0.97	0.59	0.3

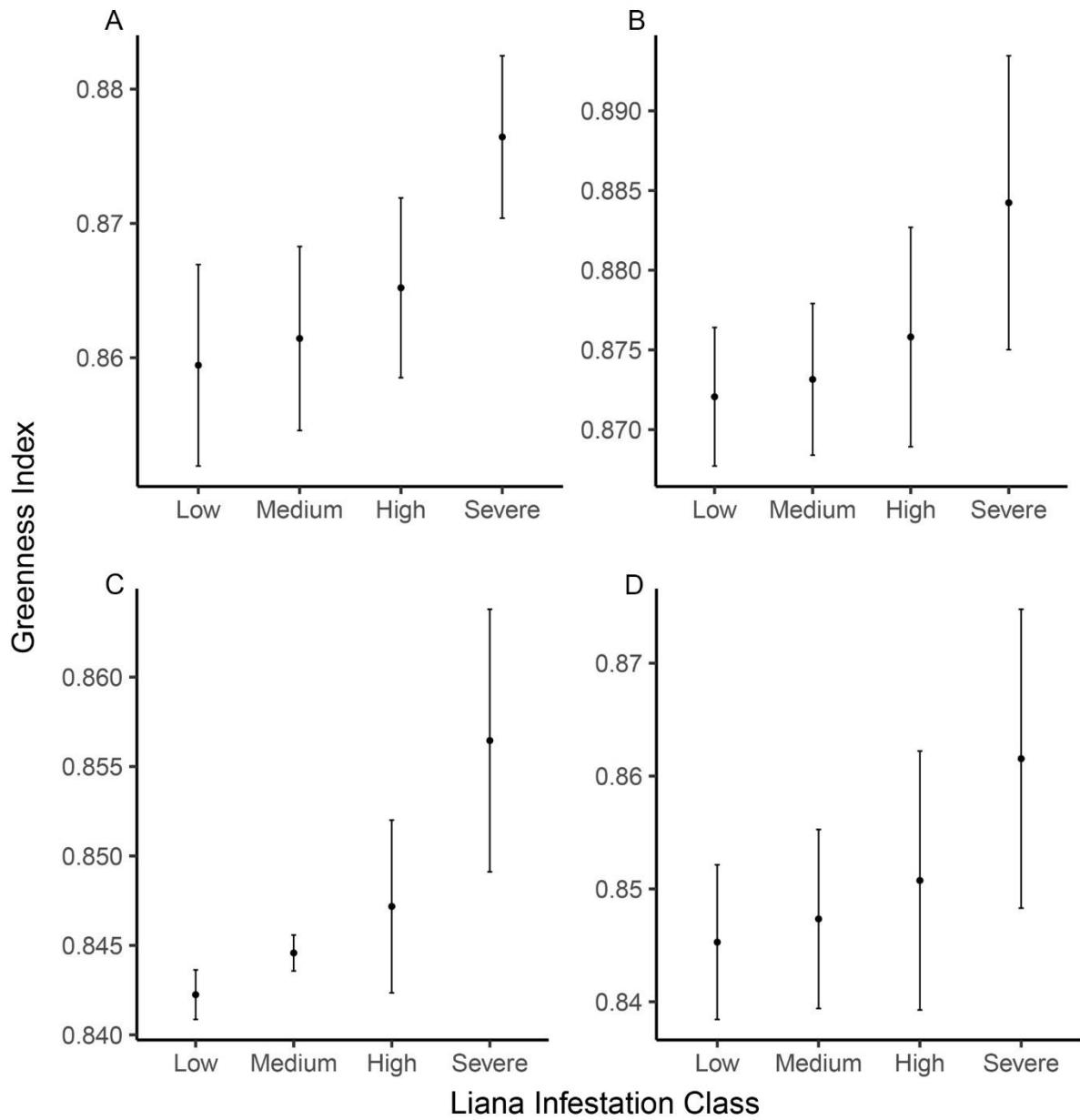


Figure S3.2 Satellite-derived predicted mean greenness in response to airborne-derived liana infestation classes for **a)** 2016, **b)** 2017, **c)** 2018 and **d)** 2019. Liana infestation classes are defined as: Low [$\leq 25\%$], Medium [26-50%], High [51-74%] and Severe [$\geq 75\%$]. Error bars are 95% confidence intervals based on error in model fit as well as uncertainty derived from error in airborne-derived liana infestation estimates.

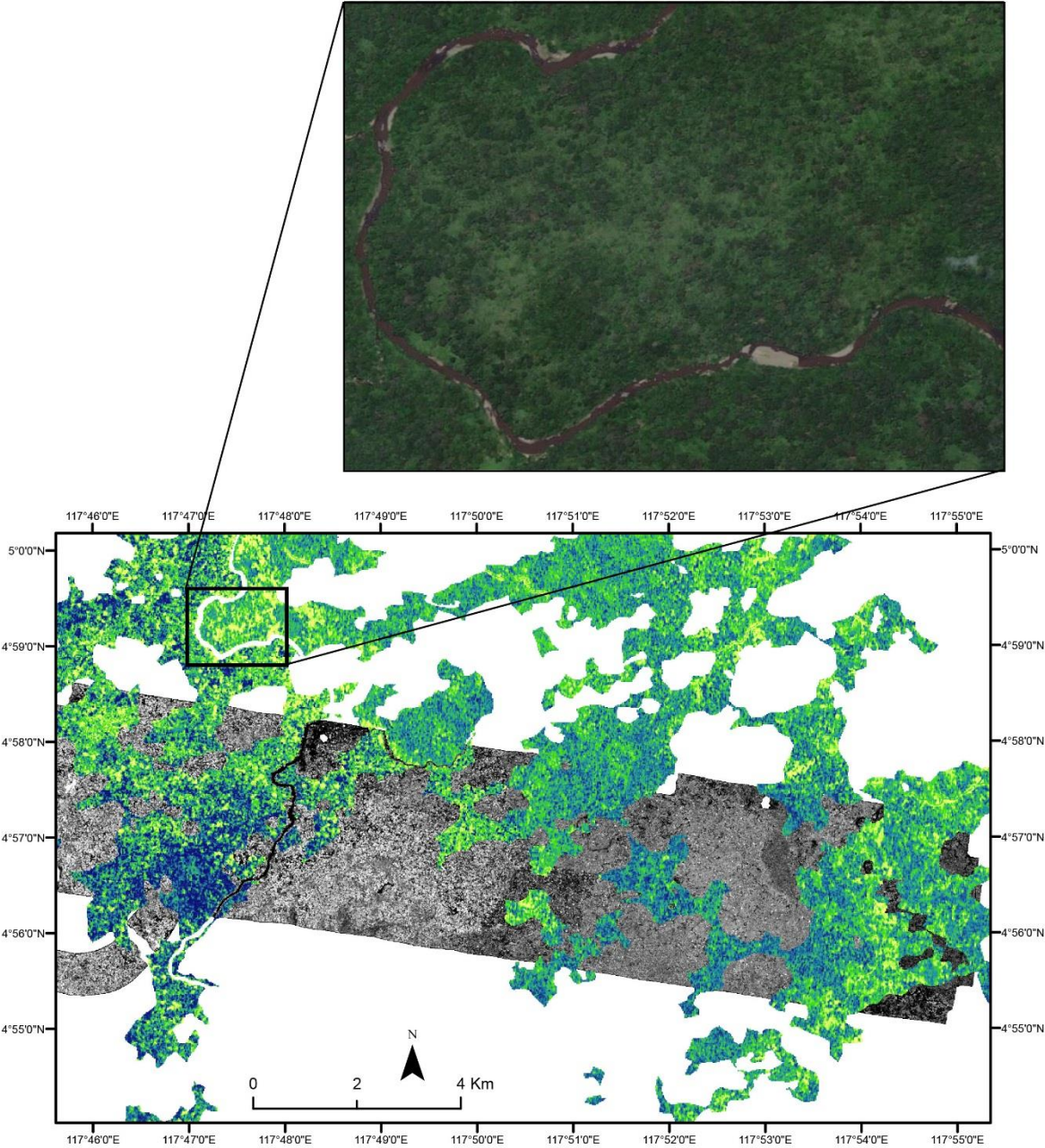


Figure S3.3 Predicted liana infestation across primary and selectively logged forests, showing the extent of the predictions in relation to the airborne lidar data (greyscaled). Missing values correspond to areas which were cloud covered. Inset shows an area with an open canopy structure as a result of selective logging and therefore a high coverage of severe liana infestation.

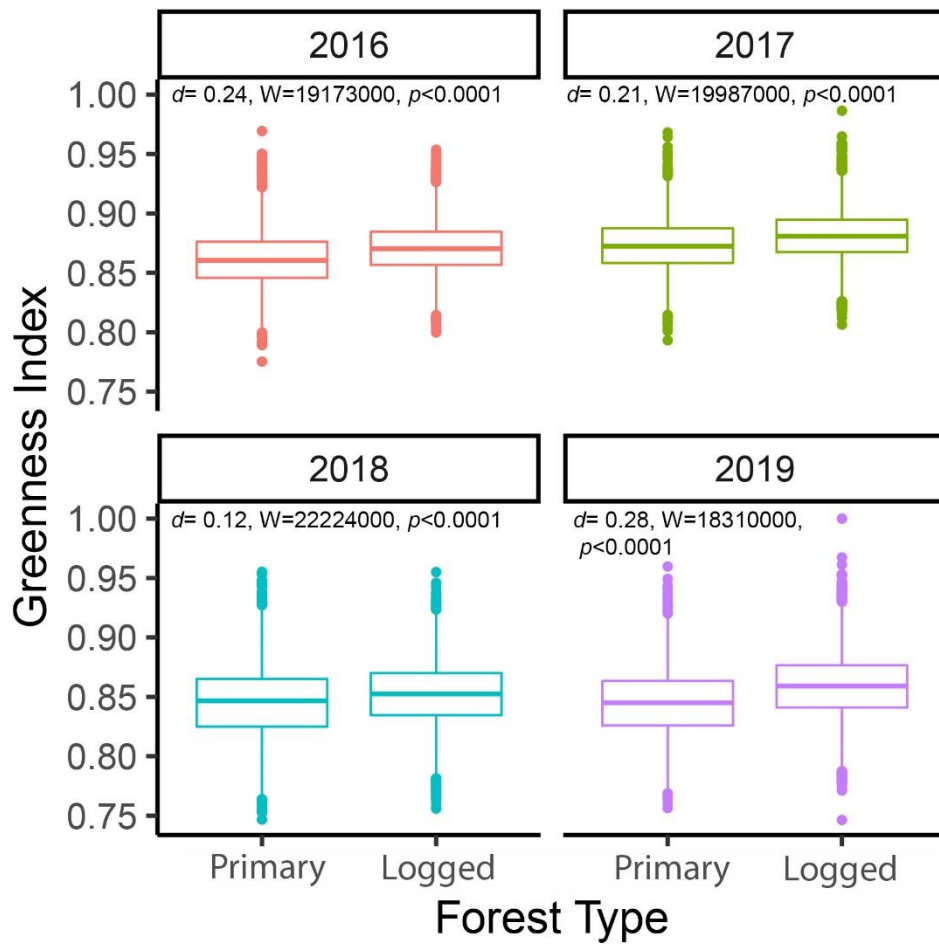


Figure S3.4 Difference in greenness between the primary and logged forest for imagery collected from 2016 to 2019. Statistically significant differences in greenness values between primary and logged forests are indicated with Cliff's *delta* (*d*), as a measure of effect size, and a 2 sample Wilcoxon test.

Table S3.3 Change in the percentage of pixels classified as having low ($\leq 25\%$) and severe ($\geq 75\%$) liana infestation from 2016 to 2019 in the primary forest, Danum Valley.

Year comparison		Diff.	Lower CI	Upper CI	<i>p</i> value	Group	% infested	Tukey	B.
<i>Change in low ($\leq 25\%$) liana infestation</i>									
2017	2016	-4.72	-11.2561	1.8158	0.2255	2016	35.4% \pm 9.4	a	a
2018	2016	-0.518	-7.054	6.0175	0.9964	2017	30.9% \pm 8.1	a	a
2019	2016	-1.9232	-8.4592	4.6127	0.85515	2018	35.4% \pm 7.9	a	a
2018	2017	4.2017	-2.334	10.737	0.3196	2019	33.6% \pm 8	a	a
2019	2017	2.7969	-3.739	9.33294	0.65617				
2019	2018	-1.4047	-7.9407	5.1312	0.9366				
<i>Change in severe ($\geq 75\%$) liana infestation</i>									
2017	2016	0.997	-2.21724	4.2113	0.83726	2016	12.9% \pm 1	a	a
2018	2016	3.209	-0.00508	6.4235	0.0504	2017	13.1% \pm 3.6	ab	a
2019	2016	5.467	2.2534	8.682	0.0003	2018	15.4% \pm 2	bc	ab
2018	2017	2.2121	-1.00214	5.426	0.2658	2019	17.3% \pm 3.3	c	b
2019	2017	4.47072	1.2564	7.685	0.0033				
2019	2018	2.25857	-0.95572	5.472	0.24921				

Diff., Difference in the percentage of pixels between years; Lower CI, Lower 95% confidence interval; Upper CI, Upper 95% confidence interval; % infested, the percentage of pixels classified as low or severe liana infestation; Tukey, Tukey's test for post-hoc analysis; B., least significant difference test with Bonferroni adjusted *p* values. Tukey and B. show significant differences between groups as indicated by letters.

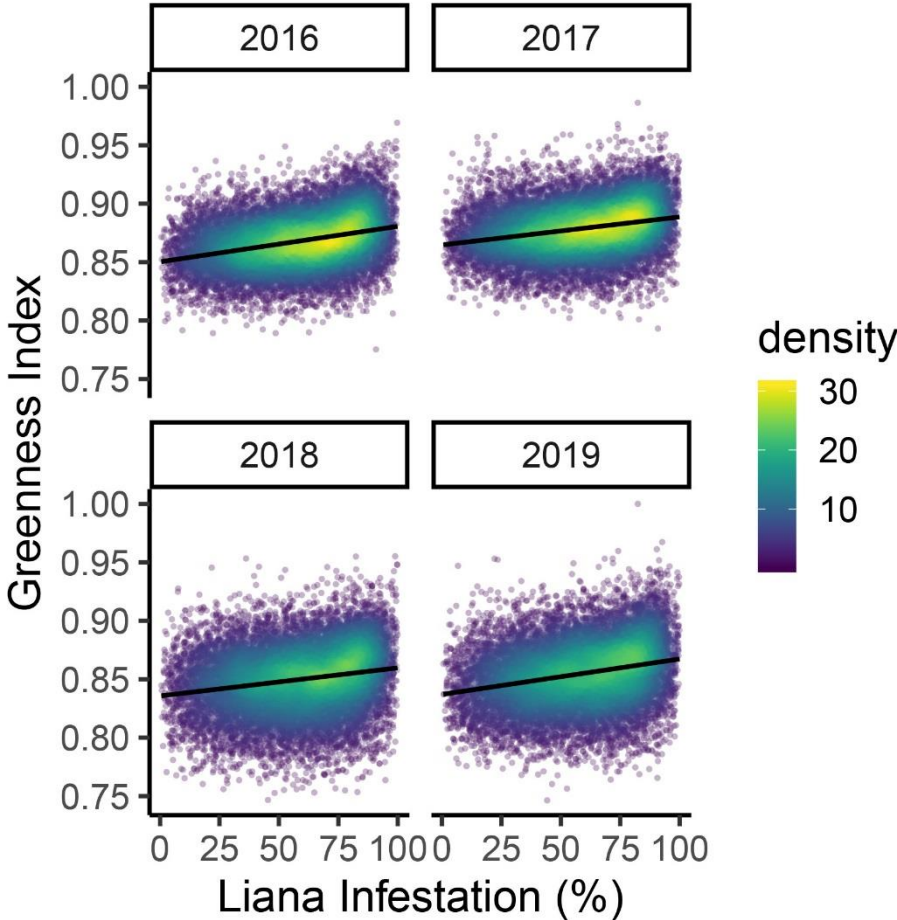


Figure S3.5 Predicted greenness in response to liana infestation for each year (2016-2019) showing the distribution of data points. Linear lines are the same as shown in Figure 4.2.

Appendix 4

4.1. Introduction

An artificial neural network (ANN) is a type of machine learning inspired by the human brain, which, via a set of algorithms, is able to learn patterns and generalise. ANNs have considerable potential for supervised classifications in remote sensing (Heermann & Khazenie 1992; Foody 1997; Foody & Boyd 1999; Foody 2002). While a range of network types and constructions have been used, most common are simple layered feedforward network architecture (Foody 2000; Fine 2006). Other network types have also been employed, for example; Radial basis function (Chen, Cowan & Grant 1991), Modular (Happel & Murre 1994) and Convolutional (Kalchbrenner, Grefenstette & Blunsom 2014). However, often simple feedforward networks can achieve better classification results (Xie, Yu & Wilamowski 2011).

4.2. Model architecture

Such architectures can be visualised as units arranged in layers, which relate to the nature of the remotely sensed data and the desired classification. For example, there is usually an input layer with units that correspond to each discriminating variable (*e.g.* spectral bands in remotely sensed data) and an output layer with units that relate to each land cover class to be mapped (Figure S4.1). The number of hidden layers and units are defined subjectively based on trial runs and the models performance with a verification dataset. In general, the larger the network (*i.e.* more hidden layers and units) the more able the network is to recognise patterns in the training data, however at risk of overfitting and therefore reducing the capacity of the model to generalise.

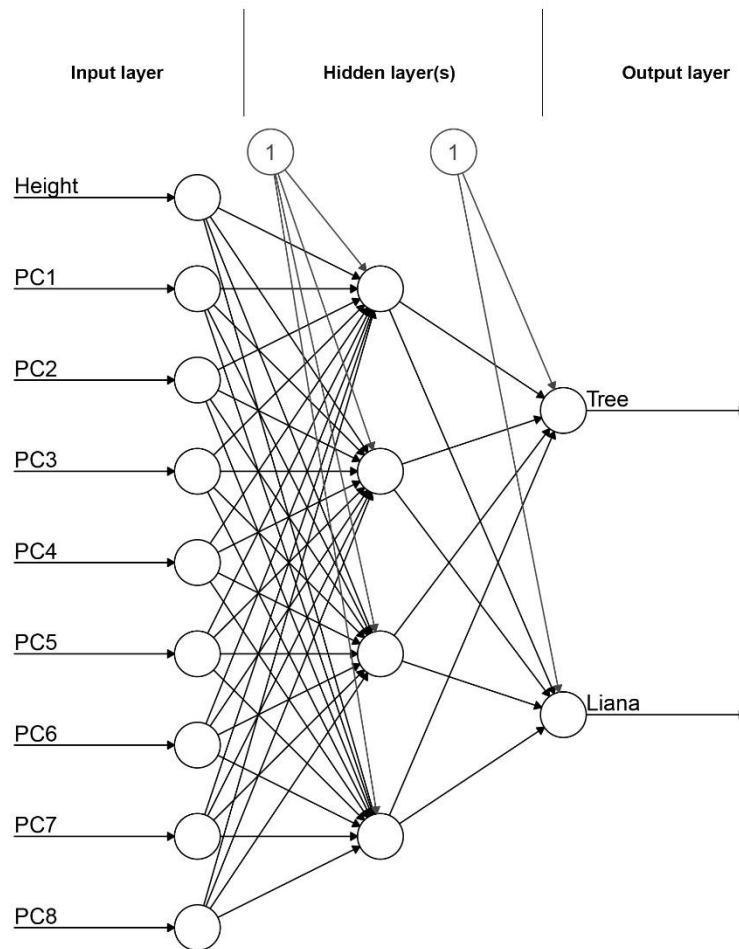


Figure S4.1 Neural network architecture showing the input layer with nine variables, one hidden layer with four neurons and one output layer corresponding to each class to be predicted.

Methods include starting with a small network and sequentially add additional hidden units and visualise the change in error until the point where adding an additional unit has no significant effect on error (Narasimha *et al.* 2008). Alternatively, the size of hidden layers can be achieved through pruning whereby a large network is trained and then units are removed while maintaining the networks accuracy (Watanabe & Shimizu 1993; Babaeizadeh, Smaragdis & Campbell 2016). Others suggest, as a rule of thumb, that the number of hidden units can be defined as:

$$\frac{2}{3} (\#input\ units + \#output\ units) \text{ (see, Karsoliya 2012).}$$

4.3. Model process

In the process of training a neural network, data are fed into the neurons in the input layer. Each neuron performs a linear transformation by first computing the weighted sum of the input data then adding a bias (constant):

$$Y = \sum (\text{weight} * \text{input}) + \text{bias}$$

The computed value (Y) is then fed into an activation function. Activation functions decide whether a neuron should be activated or not and then moves it to the next hidden layer where the process is repeated. This forward movement is known as forward propagation. Typically non-linear activation functions are used that allow the network to learn complex, non-linear data. Furthermore, non-linear activation functions allow the use of backpropagation, which means the training process can move back through the network and adjust weights and biases in order to decrease the error function (*i.e.* the difference between the actual output and desired output) (Che, Chiang & Che 2011). Backpropagation using a linear activation function is not possible as the derivative of the function is a constant and has no relation to the input. Whereas non-linear activation functions have derivative functions which relate to the inputs. For example, the widely used sigmoid activation function, $\sigma(x) = \frac{1}{1+e^{-x}}$ has the derivative, $\frac{d}{dx} = \frac{e^{-x}}{(1+e^{-x})^2}$ which can be visualised (Figure S4.2).

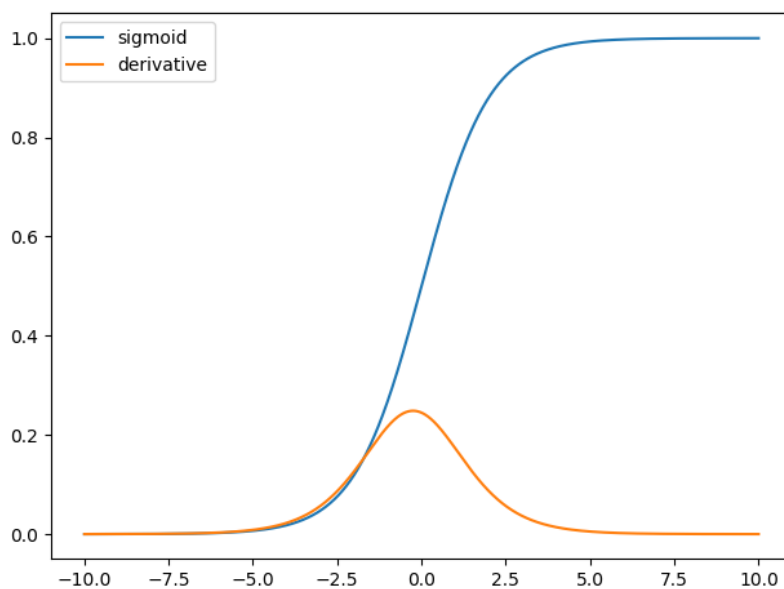


Figure S4.2 A sigmoid function (blue) and its derivative (orange).

Unlike other activation functions, the outputs of the logistic sigmoid function will be normalised and always within a range between 0 and 1, *i.e.* $\sigma(x) \in (0, 1)$. Therefore, it can be particularly useful for models that want to predict probability as an output. Additionally, I used a resilient backpropagation with weight backtracking, *algorithm='RPROP+'*, as oppose to the more traditional (regular) backpropagation (Riedmiller & Rprop 1994). Regular backpropagation uses the magnitudes of the partial derivatives (gradient) to determine how much to adjust a weight value. However, this can result in weight values being wildly adjusted in different directions and taking a long time, or never being able, to find the weight with the minimum error. To overcome this, a small learning rate can be set to gradually change weights. This means the process is unlikely to overshoot the optimal value, however training will be very slow. The use of Rprop, on the other hand, does not use the magnitude of the gradient to determine a weight but instead uses the sign of the gradient and modifies the learning rate throughout the training process (Riedmiller & Rprop 1994). Via this approach, Rprop is often faster than regular backpropagation and doesn't require parameters such as learning rate to be specified (Yu & Liu 2002).

4.4. Over-fitting

To avoid overfitting a neural network to the training data, additional arguments can be defined. For example, a threshold for the partial derivatives of the error function can be given as a stopping criteria. Therefore, the model will continue to train and find the best solution (*i.e.* ideal weight contributions from different variables) until it reaches a point where the overall error of the model is not reducing by more than a defined threshold. For example, a threshold set at 0.05, will continue to run until a change in error is less than 5%. Furthermore, by assessing the model using a verification data set (*i.e.* 20% of the training data), the accuracy can be assessed based on data not used to train the model. This verification dataset is also completely independent to the final validation data set.

4.5. Output from a neural network

In this thesis, the output from the neural network classification was made up of two classes, either 'liana' or 'tree'. For a single pixel an output (membership) value is given for each class and, as a sigmoid activation function is used, the combined value for both classes will have a value of 1. In a case where a pixel may correspond to 50% liana leaves and 50% tree leaves the spectral reflectance is mixed and will not strongly relate to either class, therefore a membership value will be given to

Appendices

each class. The output class with the greatest membership value can be chosen as the predicted class, or, a soft classification can be applied which uses the membership value as the final output. Therefore, the membership value for the liana class can be view as a proportion of liana infestation from 0 to 100%. For example, in Table S4.1, membership values are produced for each pixel. For pixel number four the model has strongly predicted the output as a tree. However, in pixel number five, the output is not clearly a liana or tree in which case a liana infestation value of 52% can be derived from a soft classification.

Table S4.1 Example of neural network output conducting a hard or soft classification

Pixel	Tree	Liana	Hard	Soft
1	0.4	0.6	liana	60%
2	0.02	0.98	liana	98%
3	0.1	0.9	liana	90%
4	1	0	tree	0%
5	0.48	0.52	liana	52%
6	0.3	0.7	liana	70%
7	0.8	0.2	tree	20%